University of Turin
Department of Chemistry

Tech4Culture:
PhD Technology Driven Sciences:
Technologies for Cultural Heritage

Identification of Rammed Earth Fracture Parameters

Candidate: Mahshid Zeighami Moghaddam
Tutor: Prof. Monica Gulmini
Co-tutor: Prof. Anna Maria Ferrero

This project has received funding from the European Union's Horizon 2020 research and innovation programme under the Marie Skłodowska-Curie grant agreement No 754511

Especial gratitude to

Prof. Monica Gulmini
Prof. Anna Maria Ferrero
Tech4Culture group

&

Prof. Cesare Comina
Dr. Federico Vagnon
Dr. Gessica Umili

&

Prof. Nicola Moraci
Prof. Maria Migliazza

To address key challenges for conservation of cultural heritage, which lies at the intersection of many different disciplines, this dissertation makes an attempt to portray many gaps in relation to the intersection between practical science of conservation and interdisciplinary engineering knowledge. Hope this approach will help in advancing research in the field, with the sole purpose of translating practical and laboratory observations and experience into a usable form for conservative practices on inherently complex rammed earth architectural heritage buildings

Table of contents

Preface

Since early times, a long history of human settlements has been formed under influence of many factors such as natural environmental and geographical features of territories. One type of the ancient and natural way by which communities have been housing themselves is the earthen vernacular buildings. As attractive product of a society and a history, an ancient building can be considered as fundamental expression of the cultural identity of its creators and the historical and social evolution of a society over the course of many generations, manifested in constant recreation by adapting the structures to the changing environmental and climatic conditions and changing historical and time dependent needs of life, where inhabitants use available resources to cope with natural and environmental conditions, the environmental and cultural conditions of its territory, giving rise to interconnectivity of traditions and values in shaping architectural features base on natural environmental and climatic conditions, local materials and available resources and living cultures of its territory.

Earthen vernacular dwellings have been facing dramatic threat. As a result of changes in inhabitants' perspectives to move away from their old villages and towns, earthen houses have been abandoned to deteriorate. As a result of tendency of inhabitants to adopt a modern lifestyle in some parts of the world, earthen architecture have been demolished and replaced with modern buildings constructed with industrialized building material. However, the change in the appreciation of traditional values greatly endanger the continued existence of earthen vernacular architecture and the inherited values of these regional dwellings

The survival of these construction tradition is under threat either from changing social and economical living standards often seen as the paradigm of development, and the impact of urban culture on inhabitants of rural areas, either from environmental factors such as natural disasters including floods or earthquakes, leading to decline or disappearance of not only these traditional architectural heritage, but also knowledge, skills, techniques and methods of the practitioners and traditions behind the creation and adoption of such vernacular buildings. These existing and remaining earthen vernacular dwellings make up a significant portion of the human heritage. This highlights the need for taking actions to prolong the life of these architectural heritage to preserve these architectures and associated cultural values in order to ensure that human messages are continuously handed down from one generation to the next.

The conservation of architectural heritage buildings, where cracks and damages play controlling factor in terms of stability, have mostly concentrated on assessing the state of stress relative to the state of intact material. For the conservation of these tangible and intangible cultural heritage, the documentation and analyzing the potential role of different destructive and non-destructive testing methods and digital tools is the most significant requirement. Various scientists and researchers with different disciplinary backgrounds and conservation professionals working in the field of conservation of earthen heritage buildings have significantly contributed to advance the knowledge in the field. However, those contributions explicitly on an integrating and interpretation of practical and laboratory observations and experience in its various forms and in relation to engineering science of

conservation remain limited. Related researches and information are therefore fragmented, leaving many gaps and considerable room for further research potentially aimed at advancing basic knowledge in the field.

This thesis aims at portraying the above-mentioned gap in relation to the intersection between practical science of conservation and interdisciplinary engineering knowledge with the sole purpose of translating such practical and laboratory observations and experience into a usable form for conservative practices on inherently complex rammed earth architectural heritage buildings constructed of multiphase material with texture dependent behaviors. The work described in this thesis evaluates the use and development of different rigorous techniques for different geotechnical engineering tasks. These methodologies are used to characterize and interpret the processes and mechanisms responsible for observed behaviour of rammed earth material. The research performed and reported in this thesis has been organized as follow:

Chapter 1 provides an account of different construction technologies implemented around the world. This section focuses on underlying soil properties of rammed earth, which have been addressed by geotechnical studies of rammed earth heritage. Moreover, recommendations of literature on properties of rammed earth material have been discussed.

Chapter 2 corresponds to the published journal article (Moghaddam et al. (2020)) and investigates fundamental problems in object recognition in earthen heritage and addresses the possibility of an automatic crack detection method for rammed earth images. We propose and validate a simple, straightforward and flexible support vector machine (SVM)-based bidirectional morphological approach to automatically generate crack and texture line maps. This automatic algorithmic approach, which couples bidirectional local gradient and geometrical characteristics to a powerful, simple and straightforward framework, comprises of four major elements, including: (1) bidirectional edge maps, (2) bidirectional equivalent connected component maps, (3) machine learning SVM-based classifier and (4) crack and architectural line feature map generation. Alongside, a detailed description of each stage and difficulties that may appear when trying to shape the above-mentioned framework have been reported in each section. Finally, the proposed algorithm are verified through comparative experiments in a set of simulations on surface images of rammed earth with different crack patterns, through which predicted data has been demonstrated to be satisfactorily conforming to labeled data provided manually for images.

Chapter 3 deals with the quantification of size effect on mechanical strength characteristics of compacted earth material. The role of water content is also discussed. The aim of this work is to provide a simple and useful framework to improve the analysis and interpretation of uniaxial compressive strength for the characterization of earth building materials. Motivated by the difficulty in comparing the uniaxial compressive strength (UCS) of rammed earth specimens in a great variety of geometrical characteristics in literature, this study attempts to extend the current understanding of the size effect on compressive strength of compacted earth. This research focuses on two different areas: 1) the behaviour of soils during the uniaxial compression loading is investigated and experimental data for size effect modelling is obtained from the literature; 2) an analytical approach is developed for the establishment of the compressive strength–size relationship for rammed earth specimens. The present research is the very first analytical approach to size effect in characterization of mechanical strength in rammed earth materials. This data and approach will help in advancing research in the field.

Chapter 4 reports the work aiming at contributing to the development of the limited knowledge and clear understanding on properties of rammed earth. The aim of the experimental work is to reproduce rammed earth in a controlled way in the lab and to analyse the influence of different constitutive components. The soil material, which is the constituent of rammed earth buildings, is the main subject of geotechnical studies. Therefore,

in the framework of Tech4Culture, Technologies for Cultural Heritage - T4C, program, an experimental program has been defined and carried out at the department of earth science of UNITO based on geotechnical and geophysical tests. Rammed earth specimens have been reconstructed in laboratory and an investigation was performed on characteristics of rammed earth material, involving characterization of compaction curves and uniaxial compression test and digital image correlation (DIC) analysis. This section addresses the work performed on characterization of rammed earth specimens and uniaxial compression test. It is obvious that such a narrow range of mixture characteristics cannot cover the wide variation of material property, which might be encountered in the numerous types of rammed earth structures found in cultural heritage. However, they provide an enhanced understanding of the behaviour of rammed earth material for advancement of research in this field. Another important fact is that numerous influencing factors lead to the uncertainties and the variabilities of parameters considering only one type of granulometric property and experimental data which do not include all of the controlling parameters, involved in structural characterizations of material, can not be necessarily comparable. Therefore, due to the inherent variability of controlling parameters for different types of rammed earth material, the results of such experiments can not be extrapolated over a wider range outside of the range investigated.

Chapter 5 reports the results of a research to evaluate and develop the application of ultrasonic pulse velocity test in investigating the rammed earth physical and mechanical-related properties. To that aim, we have combined non-destructive UPV and destructive uniaxial compression testing measurements for rammed earth specimens, which are described in detail in this chapter. This experimental investigation has provided data whose analysis produces evidence on the material behaviour under varying conditions. Cylindrical specimens (51 mm diameter and 102 mm height) of rammed earth were produced to perform a series of uniaxial compression test and ultrasonic pulse velocity measurements.
The main objective of this chapter is to investigate the ultrasonic pulse velocity, compression and shear wave velocities of rammed earth specimens for four different granulometric distributions, to attempt evaluating the relationship between the UPV and mechanical properties - also evaluated through destructive uniaxial compression testing - and the effects of different parameters of rammed earth material on measured ultrasonic pulse velocity. This chapter discusses the behaviour of UPV through rammed earth with respect to compactive effort, grain-size distribution, water content, density, void ratio and saturation degree, and resulting modulus of elasticity. It was observed that variation in ultrasonic velocities is a comprehensive result of variation in physical and mechanical characteristics of material, will all the above-mentioned material characteristics.

Chapter 6 focuses on the mechanics of crack development and failure of rammed earth material under uniaxial compression stress condition. Therefore, aiming at contributing to advance the understanding of crack propagation in rammed earth specimens, by using uniaxial compression testing and digital image correlation technique, an experimental campaign was conducted on cylindrical specimens of clay-sand, as described in chapter 5. Beginning with this experimental investigation, a more theoretical analysis of different pattern of cracking and possible driver of crack propagation for different material texture is now further investigated.

Chapter 7 evaluates the effectiveness of back analysis in parameter identification of rammed earth material using finite element analysis and laboratory examination results. Motivated by the complexity of the shape of stress-strain curve, which is inherent to each soil structure, and the consequent difficulty in the selection of appropriate Young's modulus of rammed earth specimens, a general equalization is applied which describes the behaviour of a wide range of rammed earth material by a single framework. Based on this semi-inverse analytical approach, in order to simplifying the curve into a uniform form, a generalized

equivalent stress-strain curve is defined, upon which the inverse analysis is mainly employed. This equivalent stress-strain curve provides useful equivalent parameters by which to interpret the behaviour of various rammed earth composition observed in laboratory testing. Whether the analytical procedure examined in this study can be extended to include more comprehensively important aspects associated with the behaviour of rammed earth material will be an issue requiring further examination. The present research is the very first analytical approach to back analysis of rammed earth specimens and therefore it is, to a certain extent, bound to further investigation. In view of the very limited experimental data, in which important material characteristics have not been investigated, there is a clear need for further laboratory work on characterization of rammed earth material. However, in light of future research, it may be possible to develop a more efficient approach for prediction of parameters.

Chapter 8 provides a summary and presents major conclusions of the work performed in this thesis with final remarks on perspective studies on this topic.

CHAPTER 1

Rammed earth heritage around the world and Decay of rammed earth constructions

1.1. Rammed earth

It is acknowledged that traditional buildings and structures represent an important part of cultural heritage. Earth is considered to be one of the simplest, oldest and the most widely used construction materials, with traditional earthen buildings widely distributed all over the world. A high number of architectural cultural heritage in the world has been constructed with raw earth. Earthen buildings, depending on their location involve different construction technologies implemented around the world. Concurrently, Rammed earth buildings are an important part of heritage building spread worldwide and possess a great value for the society as their importance is acknowledged as unique products of historical, cultural, artistic and architectonic values of their time and place.

1.2. History of constructions, distribution and composition of materials around the world

Rammed earth construction has been practiced in different regions around the world, also known as “taipa”, “taipa de pilão” “tapial”, “pise de terre”, “pisé” or “stampflehm”. The common traditional technique of constructing a rammed earth wall is composed of compacting layers of moistened earth between formwork. The formwork, which is a temporary wooden support structure, is made of two panels and several long bolts in the middle, which holds the soil in place during ramming process. In the past soil was compacted manually utilizing a wooden rammer. To build a rammed earth wall, soil mixture is poured into formwork and is then compacted to a very high density. Successive layer of mixture is then poured on top of compacted layer and is then compacted. This process, which is repeated layer by layer until reaching a full-height wall, results in a distinctive layered appearance, often seen as feature of the rammed earth architecture.
According to Martín-del-Rio et al. (2018), depending on the construction system, two main groups of rammed earth walls can be identified: (1) Monolithic rammed earth walls, a homogeneous mass of equal strength earth material. (2) Mixed rammed earth walls, in which specific points in the wall rammed earth are mixed with brick and mortar in the construction of walls.

In Spain, the traditional rammed earth construction technique has involved pouring the material in layers with thickness about 10–15 cm into a formwork composed of boards 3m wide and 0.90 m high and varying thickness (Cuchí i Burgos (1996)). Furthermore, Sebastián et al. (2010) have addressed the construction system of two historical buildings, the Palacio de los Abencerrajes and Silla del Moro, also known as Castillo de Santa Elena, situated inside the Alhambra complex. According to Sebastián et al. (2010), the tower known as La Silla del Moro

features the application of a strip of mortar containing a higher proportion of lime to the outside of the wall followed by the subsequent compaction of the earth, resulting in the lime mortar being indented in the wall, forming a crust on the surface of the wall, which protect the wall from the erosion.

This section addresses a brief description of rammed earth heritage in different regions, the purpose of which is to allow a greater knowledge of this type of historical constructions, and therefore to potentially help to identify and preserve historical values of rammed earth heritage around the world.

1.2.1. Rammed earth in Europe

In Europe, the rammed earth heritage has been reported by several studies. In France, the Rhône-Alpes region is a rich center of historical rammed earth buildings (Alex (2018)). The Alhambra of Granada has been reported as one of the most striking example of rammed-earth in Spain (Sebastián and Cultrone (2010)). In Spain, there is a wealth of important historical forts, city walls, and towers dating back to the 11th century onwards and churches with historical significance built after the conquest of the city by the Christians in 1492, with an excellent example being Church of San Juan de los Reyes in the Albaicín quarter of Granada. (Sebastián and Cultrone (2010))

In Spain, the rammed earth material is characterized by the presence of a varying amount of thick aggregate (Sebastián and Cultrone (2010)), and in some special cases such as Spanish Muslim buildings, by the presence of lime having been used to hold the mass of material together (Valverde Espinosa et al. (1997); Sebastián Pardo et al. (2000)). The rammed-earth buildings built by the Arabs, such as Alcazaba Cadima of Granada, or the Alcazaba of the Alhambra, have been characterized by the material being a mixture of lime with sand and thick aggregate, a technique that was normally used for construction of the foundations of large defensive buildings (Sebastián and Cultrone (2010)). Puerta de las Pesas in the Albaicín, Granada features a series of 100% lime layers having thicknes of about 2–5 cm, and other layers of earth featuring no lime (Sebastián and Cultrone (2010)). Some constructions dating back to the 12th and part of the 13th century, such as Arch of the Puerta Elvira in Granada, have been reported to be composed of earth layers about 60–80 cm thick and pure lime layers about 8–12 cm thick at the ceiling and at the base (Sebastián and Cultrone (2010)). Some constructions dating back to the end of the 13th century and the 14th century, such as the Arrabal in the Albayzin and other buildings from the Nasrid period in Granada, have involved the application of a strip of mortar featuring a higher proportion of lime to the outside of the wall followed by the subsequent compaction of the earth, resulting in the lime mortar being indented in the wall (Ontiveros Ortega et al. (1999); Sebastián Pardo (2001)), forming a crust on the surface of the wall, which protect the wall from the erosion (Sebastián and Cultrone (2010)).

In Portugal, traditional rammed earth construction, known as taipa, is mainly concentrated in the southern region (Gomes et al. (2019)). Gomes et al. (2014) has reported some of these historical buildings, including a rural house located in Monte das Covas, Valongo, Avis, being built in 1933, a rural house located in Monte Pá Danado, Taliscas, Odemira, dating back to the late nineteenth century, with the soil featuring strong reddish color and a significant amount of gravel, a rural house located in Monte Vale Chaim, Taliscas, Odemira, dating back to 1940, featuring brown gray colour and large sized aggregates, a rural storehouse located in Monte se Deus Quiser, Corte Zorrinha, Almodôvar, originally built in 1930. This house was reported to be one of the few examples of rammed earth in this region, with brown color and large size aggregates. Another historical house reported by Gomes et al. (2014) is a rural house, Barranco do Cai Logo, Colos, Ourique, built in 1947/48, featuring

brown color and presence of gravel. Another example is a 200-year-old urban house in Arraiolos, featuring dark brown color with a high percentage of organic matter.

1.2.2. Rammed earth in Asia

In South Korea, rammed earth ramparts have been reported in literature (Jo et al. (2018)). The Great Wall of China is perhaps one of the most striking example of rammed-earth in China (Sebastián and Cultrone (2010)). Historical architectural relics made from rammed earth can be found in China. These rammed earth structures have been made during successive Chinese dynasties, including the Qin, Han, Tang, Song, Ming and Qing dynasties, in northwest China (Cui et al. (2019)).

1.2.3. Rammed earth in America

In Brazil, the 19th century rammed earth buildings located in the middle valley of the Paraíba do Sul River, South-East Brazil, has been reported by Cavicchioli et al. (2018).
Historical rammed earth construction can be found in Nepal, at the western end of the Annapurna region of the Himalaya. Kag Chode Thupten Samphel Ling established in 1429 has been reported as an example of rammed earth structure in Nepal (Jaquin (2011)).
The vernacular construction rammed earth technique can be found in Bhutan, at the eastern end of the Himalayas. An example of such buildings in Buthan is rammed earth section of Kyichu Lhakhang monastery, built around 1700 (Jaquin (2011)). Jaquin (2011) reports a section of the wall of Rabtan Lhartsekhar Castle at basgo, the capital of Ladakh before 1357 and Leh fort, constructed around 1555.

In Peru, an important example of structures from pre-Incaican periods can be found, exclusively in rammed earth, but also mixed with other techniques (Soria et al. (2011)) .

In Mexico historic and traditional rammed earth architecture can be found is an area between the states of Puebla, Tlaxcala, and Veracruz (Soria et al. (2011)). External perimeter walls of houses in this area were basically constructed by rammed earth. On one hand, the emergence of rammed earth technique in this region is linked to the hypothesis that, after the 16th century, this technique was practised in this area by the settlers that came from Spanish provinces where this technique was used (Soria et al. (2011)). On the other hand, it is also hypothesized that in Mexico rammed earth was introduced by architectural influences from France (Soria et al. (2011)).

1.2.4. Rammed earth in North Africa

In Morocco, the rammed earth heritage can be found in the southern regions, in Tiznit, Ouarzazate and Marrakech (Kourdou and Cherradi (2016)). The walls of the XVIth century Badii Palace, one of the most prestigious monuments of the Islamic tradition, has been entirely constructed by rammed earth (Daoudi et al. (2018)). The Drâa valley, in the south-east of Morocco, is characterized by rammed earth heritage (Baglioni et al. (2016)). In Morocco, the Atlas mountain range is considered to divide the architectural heritage into two sides. In south east of Morocco near the Sahara Desert, the Drâa valley, which cut the Anti Atlas up to the narrow passage of Beni Slimane, separates the Eastern Anti Atlas by the Western Anti Atlas. The Drâa valley of southern Morocco, known as one of the greatest earthen architecture heritage, ksur and kasbah, is characterized by more than 300 ksur among palm forests. The kasbah of the Draa Valley is another example of traditional architectural

heritage worldwide. These big fortified houses, belonging to wealthy families of villages, and later to the administrators of the territory, have been constructed entirely with earth (Baglioni et al. (2016)). In Morroco, in Marrakech, there is evidence of the existence of the load bearing walls, where rammed earh technique has been mixed with brick and mortar. As reported the walls are composed of traditional solid brick joined by a traditional lime mortar resting on a base of rammed earth (Benkmil et al. (2018)). The thickness of the walls was reported to vary between 30 cm and 1 m.

1.2.5. Rammed earth in South Asia

In Bhutan, as reported by Wangmo et al. (2019), the traditional technique for construction practices of rammed earth involves the use of locally available soils nearby the construction site, selected based on visual inspection, poured inside the wooden formworks, followed by compaction using special ramming tools. It worth mentioning that DOC (2017), considers the reddish white soil with small pebbles as the best earth, while black, yellow or sandy earth is not considered to be suitable for building construction (Wangmo et al. (2019)).

The formwork is made of shutter planks on both sides, horizontal members on top and bottom to hold panels together, and vertical members and wedges between the vertical members and shutter planks for providing support for stability of formwork. After placement of formwork, soil is poured into the formwork and compacted using special ramming tools. The ramming lasts from 30 min to 1 hr until the compacted layer of soil reaches sufficient hardness and smoothness. Next, a new layer of soil is poured over the hardened layer, and ramming process is performed for this new layer. The process is repeated for 5 layers until reaching a height of 60–70 cm, which gives a rammed earth section with length of around 250 cm, height of 60–70 cm and thickness of 60 cm. Following completion of one section of rammed earth, the formwork is moved immediately to next section of wall. (Wangmo et al. (2019))

The granulometry characteristics of above-mentioned rammed earth heritage have been reported by several studies, Wangmo et al. (2019), Jo et al. (2018), Daoudi et al. (2018), Baglioni et al. (2016), Benkmil et al. (2018), Ruiz et al. (2014), Martín-del-Rio et al. (2018), Gomes et al. (2019), and Gomes et al. (2014)), as illustrated in Figure 1.1.

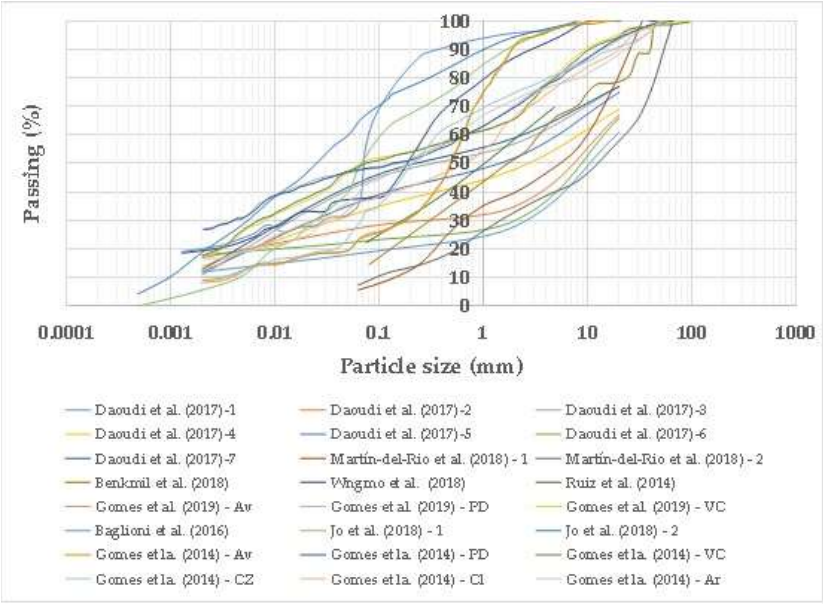

Figure 1.1. Granulometry properties of historical rammed earth in literature

1.3. Decay of rammed earth constructions

Unfortunately, several factors put the rammed earth heritage at high risk of being damaged or collapsed. Damages and the subsequent serious durability problems to these constructions is basically caused by a variety of different reasons and mechanisms. Engineering-related, water-related, and mechanical properties are major factors causing the deterioration of rammed earth heritage.

Due to their long-term exposure to the combined effects of environment, severely damaged or collapsed houses can be commonly found worldwide. Rammed earth structures are acknowledged by an intrinsic weaknesses to some external agents and natural disasters, such as rainfall, wind, solar radiation, rising damp, temperature oscillations, freeze-and-thaw cycles, environmental chemicals (e.g. salts and acid rain), soil settlements, earthquakes and floods.

One of the main issues causing deterioration of historical buildings can be mainly attributed to seismic events. Natural disasters as earthquakes can lead to an advanced level of damage and in the worst scenario to the complete collapse of the structure. Catastrophic effect of disaster on rammed earth structures are huge compared with the impact of other earthquakes of similar magnitudes and seismic intensity on contemporary structures.

Severely damaged or collapsed houses can be commonly found in earthquake-prone places with an important seismic hazard with moderate to high seismic hazard and less developed rural areas around the world, where the frequent earthquakes in the regions have resulted in significant damages to the majority of the existing rammed earth rural homes and historical residential buildings.

This can be a consequence of poor mechanical properties, low strength and high dead-weight, deficiencies of the wall and poor connections between structural elements, which have usually made rammed earth structures highly vulnerable to earthquake forces, putting at risk the rammed earth built heritage itself and the life of inhabitants, by causing severe injuries and deaths, as well as property losses.

Water, erosion and deficiencies are acknowledged to be the key factors having significant negative impact on the structural performance and deterioration of rammed earth structures, resulting in some kinds of structural failure, material failure and surface failure in these buildings.

Typical mode of structural damage found in existing rammed-earth structures are damage to the walls, in the form of cracking, vertical cracking often forming around the corners of the buildings and at loading points, reduction of the bearing cross sections and substantial reduction of the mechanical properties of the materials, their bearing capacity and stiffness.

Various pathologies in the form of cracks and fissures can form due to mechanical stresses, which destroy the original integrity of wall surface and provide preferential paths for accelerating the deeper infiltration of water, gas and solutes into the wall and, consequently increases the further deterioration of the building, threatening stability and existence of rammed earth heritage.

The layered structure of rammed earth due to the compaction process of earth in a formwork may influence the crack mechanisms, since horizontal joints between layers usually mean a discontinuity, which constitute the weak points contributing to local sliding failure tending to occur along the interfaces in some cases.

Lack of additional element such as perimeter beams for transmission of roof load lead elements of the roof transmit load directly on the rammed earth wall, which compromise seriously the durability of rammed earth constructions as the concentrated forces at the loading points, where roof elements directly sit on the wall, often contribute to the initial degradation of the wall by causing local crushing and cracking tending to extend vertically.

The combination of external circumstances, such as wind, variations in temperature and water, contributes to the removal of fine particles from the material and produces a very rough surface resulting from erosion. Erosion may be consequence of water gathered in joints and holes or water run-off and weathering.

Material failures is also linked to deterioration directly related to mass cohesion which, depending on the level of damage, may occur in the form of slight loss of the mass that surface chunks of material may come off easily or high percentage of mass loss in which the thickness of wall may be affected, disintegration, resulting in an increase in porosity, as a consequence of which a huge amount of earth material containing coarse particles may easily be brushed away. In the worst scenario, material failure may occur in the form of a total lack of cohesion and a greater material loss.

Although the impact of weathering by several weathering agents, substantially affecting façades, might be relatively low in short term, it can be considered as a critical cause of surface damage for RE under service conditions, which accompanied by lack of maintenance in the long term may lead the wall to an advanced state of decay, considerably disturbing the integrity of constructions and increasing the risk of further deteriorations.

Damage assessment remarks an essential step in the context of conservation of heritage buildings, being a major source of information in order to achieve a proper technical knowledge for decision making in heritage conservation. A review of literature reveals that the field work for damage assessment of rammed earth heritage has been carried out and reported by some research studies, including Gamrani (2014), Daoudi et al. (2018), Ruiz et al. (2014) and Kourdou and Cherradi (2016).

Based on damage assessment of the Badii Palace several degradation processes have been identified, including cracking, salt efflorescence, plaster detachment, damage from the action of capillary rise, detachment of the plaster, salt efflorescence, human actions and the chemically destructive action of bird droppings (Gamrani (2014), Daoudi et al. (2018)).

According to the field work for damage assessment of Sixteenth- and Seventeenth-Century Rammed Earth Churches, Ruiz et al. (2014) has linked the most common problem regarding rammed earth buildings to structural issues such as subsidence of foundation, deficiencies in structural cohesion, and damage caused by the roof structure (Ruiz et al. (2014)). Ruiz et al. (2014) observed that the most prevalent issues were the presence of moisture. Inadequate reinforcement of the wooden structure was reported as the frequent problem affecting the roofs. In some examples, moisture stains and disintegration of the plaster finish were also observed. Deficiencies in structural cohesion make structures susceptible to erosion or disintegration caused by excess of moisture in the walls due to rainfall or water infiltration from groundwater (Ruiz et al. (2014)). These cohesion deficiencies can be mainly attributable to a lack of sufficient anchorage between the walls and floors and between the walls, the low tension and shear strength of the earth materials (Ruiz et al. (2014)). Ruiz et al. (2014) has reported some evidences of deterioration caused by moisture in discoloration and disintegration of the wall surface, as well as stains on the base of the walls, although water table was relatively far from the surface at the sites of the churches.

Aiming at the restoration and the preservation of the Medina of Tiznit, an on-field investigation of disorders affecting the structure, and therefore the state of Medina, has been conducted by Kourdou and Cherradi (2016) in the medina of Tiznit, one of the southern regions of Morocco, whose built heritage has been ranked as a national heritage since 1932 (Kourdou and Cherradi (2016)). As reported, the medina has suffered extensive disorders and deterioration in materials caused by the rains following the floods of November 2014. Kourdou and Cherradi (2016) have reported the lack of maintenance as the major source of problems behind the loss and damage incurred during the floods. As reported there is also evidence of abnormal presence of moisture, namely saltpeter and coating discoloration at the base of the walls, which can be attributed to infiltration of water close to the wall as reported

in the case of the Medina of Tiznit during floods (Kourdou and Cherradi (2016)). The majority of the sensitive points for developing the erosion phenomenon has been reported to be located at the top and bottom of the walls, where are not usually well protected and well designed (Kourdou and Cherradi (2016)).

Structural issues affecting the supporting structure of the rammed earth heritage may arise from an error in the design stage of building, the execution of construction, or the assessment of environmental issues such as foundation or diverse natural and accidental actions during the life time of a building. Degradations caused by the natural actions, where water is one of the main agent, result mainly from exposure of the structure to weathering agents and capillary rise. Gomes et al. (2019) has reported capillary rise on the base of the earth walls as major agent contributing to issues, such as loss of cohesion and erosion.

The erosion in rammed earth walls can be a consequence of capillary rise on the base of the earth walls (Gomes et al. (2019)), or the action of rainfall and wind (Gomes et al. (2019)), resulted from exposure of the façades to these weathering conditions.

Abnormal presence of water, which may have dangerous consequences on a structure, may be manifested in different forms including, erosion, humidity due to capillary rise, humidity due to rainfall, as well as humidity due to the occurrence of infiltrations caused by poor drainage of water from the roof through direct rain, deficiencies in coverage or existing cracks or rupture of plumbing (Gomes et al. (2019)). In case of water infiltration phenomenon, the presence of structural cracks in walls, may constitute a path for further propagation of damage. Erosion starts with localized crumbling of the material, which then gradually grow further to significant depth, threatening the integrity of the wall.

1.4. Geotechnical investigations of rammed earth

Under service conditions, the capacity of rammed earth heritage is highly subjective on the underlying soil properties. This section focuses on these properties, which have been addressed by geotechnical studies of rammed earth heritage. Moreover, recommendations of literature on properties of rammed earth material have been discussed.

1.4.1. Geotechnical properties

1.4.1.1. Grain-size distribution

Soils are mainly classified according to size of their components. The five major constituent of soil are: gravel, sand, silt, clay, and organic matter. The sizes of components that constitute soil vary over a wide range, with grains constituting the skeleton and clay playing the role of a binder between them. In order to describe soils by their particle size distribution (PSD), particle size classification has been developed by International Organization for Standardization, 2002, as: gravel (2 mm to 63 mm), sand (0.063 mm to 2 mm), silt: (0.002 mm to 0.063 mm) and clay (less than 0.002 mm).

Generally, gravels are unstable and unworkable grains playing major role in providing bearing capacity of the soil. The addition of sand and clay increases stability and workability of soil. Granular elements of soil provide good internal friction, which contributes in preventing slides, and good bearing capacity. The presence of clay acts as a binder making the mixture easy to work.

Organic material is generated when living matters such as vegetables are partly decomposed. This constituent of soil is generally characterized by the presence of shells or undecomposed vegetables, by its color, being gray to black, by its odor, generally resulting

from, release of gases during excavation of soil. Organic materials should be avoided or considered to be limited in the material due to the possibility of their further decomposition, which leads in leaving voids in the materials, with subsequent reduction of mechanical characteristics of the soil.

1.4.1.2. Mineralogy

The smallest particles known as clays are commonly defined as particles smaller than 0.002mm. The structure of most clay minerals are composed of two basic units, namely silica tetrahedron and alumina octahedron, which do not exist in isolation, but combine to form silica sheet and octahedral sheet, also called a gibbsite sheet. In a tetrahedron unit, a silicon atom, with a positive charge of four, is surrounded by four oxygen atoms, one at each corner of the tetrahedron, with a total negative charge of eight. To form silicate sheet, a single tetrahedron, with a total negative charge of four, is combined with adjacent tetrahedrons by sharing three oxygen atoms at the base of tetrahedron. The silicate sheet has a net negative charge. In a octahedral unit, an aluminum atom is surrounded by six hydroxyls.

When the silica sheet, with a net negative charge, and the electrically neutral octahedral sheet are bonded together, the top oxygen atom of each tetrahedral, with a negative charge of one, replace the hydroxyls to balance their charge. Repeating layers of silica-octahedral sheets, strongly held together by hydrogen bonding, form the layer structure of Kaolinite.

In some layer structures, an octahedral sheet is bonded to one silica sheet at the top and another silica sheet at the bottom, and silicon in the tetrahedral sheets are partially substituted by aluminum, being known as isomorphous substitution, resulting in a negative charge. In illite, which consists of repeated layers of silica-octahedral-silica sheets, this negative charge is balanced by potassium ions, which held the illite layers together.

Montmorillonite consists of silica-octahedral-silica sheets, in which an octahedral sheet is bonded to one silica sheet at the top and another silica sheet at the bottom, with partial substitution of silicon by aluminium in silica sheet and partial substitution of aluminum by magnesium and iron in the octahedral sheets.

1.4.1.3. Compaction and water content

Every natural mass of soil can be characterized by a certain amount of voids. Compaction, a quite vast and complex subject, can be defined as the reduction in the amount of voids present in the soil and subsequent increase of the density of the soil, exerted by mechanical means during the process of construction, which depends upon major components including soil type, moisture content, compactive effort.

The values of optimum water content and maximum density obtained under a given compactive effort may differ widely with different grain size distribution of soil.

The presence of larger grains, smaller grains, clay as well as moisture in the mixture helps in achieving workability as well as a mixture of compaction, good bearing capacity, and stability. Compaction is achieved by smaller grains shifting themselves between the larger ones, reducing the amount of voids, which results in improvement of the maximum density.

Laboratory determination of the compaction optimum water content and corresponding maximum dry density is generally investigated using well specified and widely established tests, either the standard or the modified Proctor tests.

The optimal water content in the soil is evaluated in the field by the lump test, where having enough water content is expected for the soil when it forms a lump in one's hand (DOC (2017)). Another method for evaluation of the moisture content is that if the tossed–up

soil breaks into two pieces in contact with the ground (Khadka and Shakya (2015)), the water content is considered to be close to the OMC and suitable for use.

Several RE guidelines (e.g., Middleton and Schneider 1992; Walker and Standards Australia 2002); recommend "drop test" as a rapid technique for determination of the OWC on site, however this test is an approximate method considerably dependent on the judgment, experience and skills of the operator yielding a wide range of estimates for optimum water content of the material, which may lead to unknown consequences on achieved material characteristic. This is of paramount importance when safety issues of cultural heritage are being dealt with.

1.4.2 Review of geotechnical studies of rammed earth

1.4.2.1 Recommendations of literature for properties of rammed earth material

Some formal documents provide recommendations concerning PSD of soil materials for rammed earth. The review of literature reported by Gomes et al. (2014) has addressed following documents found in the literature with recommended granulometry of soil as follow

Gomes and Folque (1953): 15-31% for clay , 7-17% for silt, 28-51% for sand and 0-33% for gravel.

IETCC (1971): 10-40% clay , 20-40% silt, 10-40% sand and 10-20% gravel.

Doat et al. (1979): 15-25% clay , 20-35% silt, 40-50% for sand and 0-15% for gravel.

Houben and Guillaud (1994): 8-10% for clay , 14-25% for silt, 49-60% for sand and gravel and 0-8% for Pebble.

Keable (1996): 5-15% for clay , 15-30% for silt, 50-70% for sand and gravel.

Walker and Standard Australia (2001): maximum 20% clay , 10-30% silt, 45-75% sand and gravel.

SAZS 724 (2001): 5-15% clay , 15-30% silt, 50-70% sand and gravel.

Keefe (2005): 7-15% for clay , 10-18% for silt, 45% for sand and 30% for gravel.

Walker et al. (2005): 5-20% for clay , 10-30% for silt, 45-80% for sand and gravel.

As reported by Gomes et al. (2014), the maximum particle size of soil has been recommended by IETCC (1971), Keefe (2005), New Mexico Code (2006) as 20, 20, 38.1 mm respectively. Moreover, Gomes and Folque (1953) recommends 20-25 mm for maximum particle size, the soil may contain particles up to 50 mm with a maximum percentage of 20-25% of larger particles. According to Walker et al. (2005) Maximum particle size is often limited to 10-20 mm.

As indicated by Gomes et al. (2014), some recommendation can be found in the literature for liquid limits and plasticity index for unstabilised rammed earth. For LL, the threshold value of 25-50 and 25-46 has been reported by Doat et al. (1979) and Houben and Guillaud (1994), repectively. Doat et al. (1979), Houben and Guillaud (1994), Walker and Standard Australia (2001) and Walker et al. (2005) recommended the value of 30 - 35, 30 - 35, 35 - 45 and <45, respecitively. For PL, the threshold value of 7-29 and 2-30 has been reported by some documents, including Doat et al. (1979) and Houben and Guillaud (1994), repectively. Some documents, Doat et al. (1979), Houben and Guillaud (1994), Walker and Standard Australia (2001) and Walker et al. (2005), recommended the value of 7-18, 12 - 22, 15-30 and 2-30, for PL. Based on a review of literature, for values of the compaction energy and the corresponding moulding moisture content of the soil, Gomes et al. (2014) report that range of values for the OMC of 3.5% to 14% and dry density between 1750 kg/m3 and 2000 kg/m3 was indicated by Houben and Guillaud (2006). (Gomes et al. (2014))

Some references have addressed the requirements for the organic content of soils for rammed earth (Gomes et al. (2014)). As reported by Gomes et al. (2014), Walker et al. (2005) and Houben and Guillaud (2006) indicate quantitative threshold values for the soil's organic content, while some documents recommend the results of smell tests as a criteria for accepting or rejecting a soil for rammed earth, including Walker and Standards Australia (2001); Lehmbau Regeln (2009), and Keable, (1996). Some documents, NZS 4298 (1998); SAZS 724 (2001); and New Mexico Code (2006), advise the rejection of soils that contain organic matter.

1.4.2.2. Geotechnical studies of rammed earth

A review of literature on rammed earth material reveals that investigations on unstabilized RE have been focused on several fundamental factors which are important in determining the geotechnical characteristics, including grain-size distribution, optimum water content and maximum dry density via the Proctor test, Atterberg limits and clay mineralogical composition determined by XRD.

1.4.2.2.1. Grain-size distribution

Characterization of unstabilized RE has been addressed by several studies (Wangmo et al. (2019), Jo et al. (2018), Daoudi et al. (2018), Cavicchioli et al. (2018), Baglioni et al. (2016), Benkmil et al. (2018), Ruiz et al. (2014), Martín-del-Rio et al. (2018), Gomes et al. (2019), Silva et al. (2018), and Gomes et al. (2014)). The granulometry properties of RE material included in these studies has been summarized in Figure 1.2.

The Korean fortress, Ganghwa Jungseong, one of the hundreds of earthen ramparts built in South Korea in the thirteenth century, was analysed by Jo et al. (2018) in order to identify the traditional construction technique for building the rammed earth wall. The analysis included characterisation of different layers of the walls. In this study Jo et al. (2018) investigated and interpreted the mutual homogeneity between the soils of each layer of the rammed earth wall and the surrounding area of the fortress in order to identify the origin of the raw materials. Based on historical records, this site was built in 1250 (Jo et al. (2018)). According to inspection of rampart, the central earth wall was built using rammed earth technique, with height of 1.84 m and width of 4.41 m. The material analysis has shown that the five-layered foundation part has exhibited various colors, from red to brownish yellow, and particle-size distributions from silt loam to sandy loam. The upper layer in the foundation part has featured a pale yellow color, classified as sandy loam with characteristics similar to soft, earthy, typically clay rich saprolite formed via the chemical weathering of igneous, sedimentary, and metamorphic rocks. The body part of the wall, which is composed of silt loam in the lower layers and silt loam and loam in the middle layers, exhibited alternate yellowish red and strong brown color patterns.

Daoudi et al. (2018) investigated particle size of thirty rammed-earth and coating materials collected from the Badii Palace wall (80 cm thick and 6 m high), one of the most prestigious monuments of the Islamic tradition in Marrakech. This study demonstrated wide variation in particle sizes with coarser grain sizes at the base and finer ones at the top. Based on the position in the section of the wall, the rammed-earth materials of Badii Palace are characterized by considerable amount of stone and gravel particles (41–72%), with sand and silt fractions ranging from 7% to 14% and 5% to 32%, respectively. The material has featured a clay fraction not exeeding 18%. Moreover, they reported that the rammed earth material, classified as GA/SL According to the Central Laboratory of Roads and Bridges (LCPC)

(Guillard & Houben, (1989)), is rich in calcareous sand and silt mixed with an extensive addition of lime as stabilizer in order to increase the hardness and strength of the walls (Daoudi et al. (2018)). Based on the comparison of lithological composition of pebbles of the walls and those of the local raw material, they concluded a very likely source for these coarse materials to be the river deposits of Issil from the east of Marrakech, formed from the erosion of the High Atlas. Consequently, they argued the composition of earth material to be coarse earth skeletal material from river alluvium mixed with local fine earth. Supported by observations on the presence of vermiculite and interstratified IS in the fine fraction and its comparison to soils of the region of Haouz ofMarrakech, they argued an origin from the local calcareous soils for fine earth. This study also indicates varied lithological compositions with magmatic (granodiorite, rhyolite, andesite, granite, and gabbros) sedimentary (limestone, sandstone), and metamorphic (schist, quartzite) components for pebbles that form rammed earth material of Badii palace wall.

Cavicchioli et al. (2018) investigated physico-chemical properties of earthen materials that form the 19th century earthen constructions located in the municipalities of Queluz (QZ), Areias (AR), São José do Barreiro (SJB) and Bananal (BA), in the middle valley of the Paraíba do Sul River (South-East Brazil). In this study, 109 specimens of earthen material, including 30 specimens of Wattle-and-daub, 48 of adobe and 31 of rammed earth, and 31 sub-soil samples were collected and investigated. They demonstrated the predominance of silt loam and loam textures in RE materials. One single sample of RE material was characterized by sandy texture. A variety of Brazilian RE exhibit the absence of sand fraction, sometimes compensated by the presence of coarse particles restricted to 5% (Cavicchioli et al. (2018)). However, in the samples with the lowest amount of sand, samples with 15.7% and 15.2% sand, studied by Cavicchioli et al. (2018), coarse particles content does not exceed 2%. The characteristics of RE showed that the manufacture of RE in BA, could have benefited from soils coming from more distant areas, whereas local soils could be used in the construction of RE in the QZ, AR and SJB districts.

An experimental investigation was carried out by Baglioni et al. (2016) on samples from rammed earth walls from different villages of the Drâa valley, namely Amzrou, Tissergat and Zagora. Based on grain size analysis, the sample from Amzrou is a fine grained earth composed of 2.8% gravel, 6.8% coarse sand, 55.4% fine sand, 12.1% silt and 23.2% clay. They also classified the earth as being not active earth, according to activity coefficient (A = 0.17), A-4 class: low compressibility silty earth, according to AASHO, and Lp class (low plasticity silt) according to USCS.

The work performed by Benkmil et al. (2018) aims at contribution to the characterisation of earthen materials in historical architectural heritage in Morocco, by investigating a case study in the center of the city of Marrakech in the center of Morocco. Assessment of construction materials of walls has shown the existence of two construction materials, namely brick and rammed earth. The thickness of the walls has been reported to vary between 30 cm and and 1 m. Benkmil et al. (2018) has reported the material to contain 52.06% of grain size less than 2mm, 14.7% less than 80μm

Historical churches in the central Colombian highlands, dating back to of 16th and 17th centuries, has been addressed by Ruiz et al. (2014). According to records of conducted inspections of these buildings until 1600 by Government officials of the colonial period, these structures were reported to be made of Bahareque. However, based on subsequent inspections in 1635 the existence of churches with rammed earth walls has been revealed. Ruiz et al. (2014) reports the thickness of walls to be 0.84-1.26 m and the heights between 5.04 and 6.72 m. Ruiz et al. (2014) characterized the soil using standard geotechnical tests. Based on standard tests according to ASTM D2216 (ASTM 2010b), the percentage of grains passing No. 200, No. 40 and No.4 were reported to be 22.36%, 39.59% and 69.67%, respectively.

Martín-del-Rio et al. (2018) has addressed the characterization of historical rammed earth walls in the twelfth century ramparts of Seville and Malaga in Spain. According to the analysis of the carbonate content a maximum lime to sand ratio of around 1 to 12 and 1 to 4 was obtained for UE1 and UE2, respectively. Based on the analysis of the two samples, they reported the sample from Seville as being a poorer rammed earth wall with less amount of lime. The particle size distribution analysis indicated the maximum aggregate size was 31.5 mm for UE1 and 63 mm for UE2. In order to determine the granulometry of specimens, the mesh series of the UNE-EN 12620:2003 standard was used, including mesh spacings of 63, 31.5, 16, 8, 4, 2, 1, 0.5, 0.25, 0.125, and 0.063 mm.

In Gomes et al. (2014), the laboratory characterization of the rammed earth materials was performed on samples collected from six old buildings in Portugal, including one from a rural house located in Monte das Covas, Valongo, Avis, being built in 1933, one from a rural house located in Monte Pá Danado, Taliscas, Odemira, dating back to the late nineteenth century, with the soil featuring strong reddish color and a significant amount of gravel, one from a rural house located in Monte Vale Chaim, Taliscas, Odemira, dating back to 1940, featuring browngray colour and large sized aggregates, one from a rural storehouse located in Monte se Deus Quiser, Corte Zorrinha, Almodôvar, originally built in 1930. This house was reported to be one of the few examples of rammed earth in this region, with brown color and large size aggregates. One sample was collected from a rural house, Barranco do Cai Logo, Colos, Ourique, built in 1947/48, featuring brown color and presence of gravel. The last sample was collected from a 200-year-old urban house in Arraiolos, featuring dark brown color with a high percentage of organic matter. Gomes et al. (2014) performed the granulometry analysis of studied rammed earth materials following the methods indicated in LNEC Specifications E239 (1970), wet sieving of the coarse fraction (pebbles, gravel and sand), and E196 (1966), sedimentation of the fine fraction (silt and clay). Based on calcination, according to the method of ASTM D2974-07 (2007), Gomes et al. (2014) investigated the organic content of the six studied earth materials, for which the total content of organic matter were obtained as 0.9%, 4.5%, 3.5%, 1.8%, 3.6% and 5.4%.

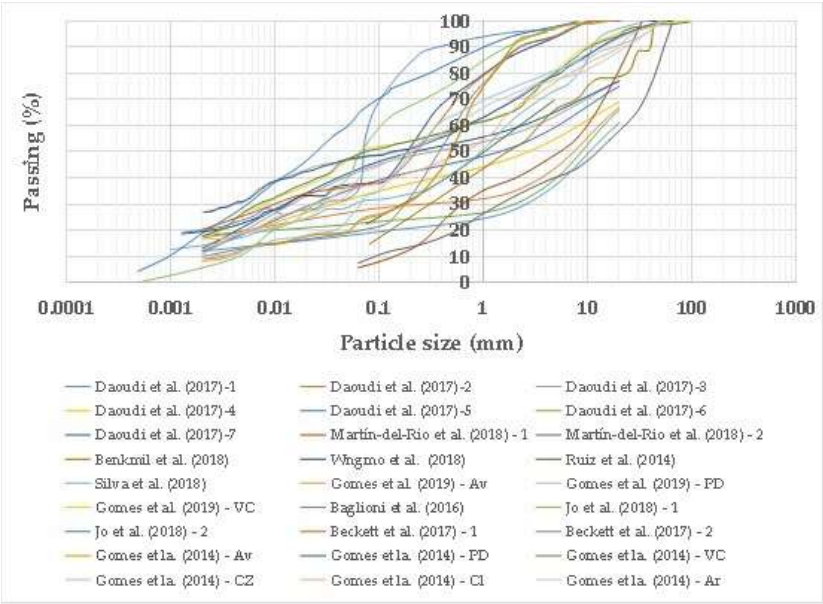

Figure 1.2. Granulometry properties of geotechnical studies of rammed earth in literature

1.4.2.2.2. Mineralogical properties

The mineral composition of the rammed earth wall of Korean fortress, Ganghwa Jungseong, one of the hundreds of earthen ramparts built in South Korea in the thirteenth century, was investigated and reported for each layer by Jo et al. (2018).. For most of the wall samples common minerals were identified, including quartz, K-feldspar, mica, plagioclase, and illite, although some layers did not display kaolinite.

Mineralogical investigation of rammed-earth materials collected from the Badii Palace wall in Marrakech using X-ray diffraction has shown the main composition of rammed-earth materials to be quartz (22–33%), calcite (16–30%), feldspars (plagioclases and K-feldspars) (8–16%), muscovite (8–3%), biotite (0–10%), clays (11–25%), and traces of gypsum (Daoudi et al. (2018)). A detailed examination of clay minerals was performed by Daoudi et al. (2018), based on the XRD patterns of oriented preparations of Ca2+ saturated fine size fractions (< 2 μm), resulting in identification of interstratified illite-smectite (IS) and vermiculite in rammed-earth materials.

The mineral compositions of samples of the 19th century earthen constructions located in the municipalities of Queluz (QZ), Areias (AR), São José do Barreiro (SJB) and Bananal (BA), in the middle valley of the Paraíba do Sul River (South-East Brazil) were investigated by Cavicchioli et al. (2018) using X-ray diffraction (XRD), which was performed on a Bruker D8 Advance Da Vinci diffractometer operated at 40 kV and 40 mA, CuKα radiation, and at a scanning rate of 0.1◦2θ/min. Based on the results of XRD analysis, the mineralogical composition of earthen materials displayed the presence of quartz and kaolinite in all samples and mica in most of them.

An experimental investigation was carried out by Baglioni et al. (2016) on samples from rammed earth walls from different villages of the Drâa valley, namely Amzrou, Tissergat and Zagora. Based on characterization of the principal mineralogical composition of sample from Amzrou using X ray diffraction (XRD), they pointed out that calcite is abundant in the rammed earth sample of Amzrou. According to the mineralogical analysis, they indicated a quite low clay minerals content, composed by higher amount of illite and lower amount of kaolinite, chlorite and smectite, with quartz identified to be the main composition of sandy fraction of material.

In the study investigated by Martín-del-Rio et al. (2018), the mineralogical composition of the samples from historical rammed earth walls in the twelfth century ramparts of Seville and Malaga in Spain was identified by performing X-ray diffraction (XRD) analysis, which had shown that most of the mineral phases in the two case studies are very similar, with Quartz, K-feldspars (orthoclase), plagioclases (anorthite), and phyllosilicates (illite, chlorite, and muscovite) attributed to the aggregate, whereas calcite may be attributed to the earth or the lime used in the manufacturing process.

Gomes et al. (2019) has reported mineralogical characteristics of three different types of earth materials picked up from non-deteriorated parts of old unstabilized rammed earth buildings situated in Alentejo region, in south Portugal, including the earth Av collected from a rural house in Monte das Covas, Valongo, Avis, whose construction dates back to 1993, the earth PD collected from a rural 19th century dwelling in Monte Pa Danado, Taliscas, Odemira, the earth VC collected from a rural house in Monte Vale Chaim, Taliscas, Odemira. Mineralogical characterization of the fine fraction for the earth materials Av, PD, VC were determined by X-ray diffraction (XRD). As reported by Gomes et al. (2019), quartz, mica/illite and feldspars were identified in all earth material. Kaolinite is present in all the earths, with higher proportions identified in earth PD and VC and traces identified in earth Av. The earth VC has displayed the presence of Cholorite, while traces also identified in Av.

The compositional characterization of two historical buildings, the Palacio de los Abencerrajes and Silla del Moro, also known as Castillo de Santa Elena, situated inside the

Alhambra complex, have been investigated by Sebastián et al. (2010). The most significant results obtained by X-ray Diffraction (XRD) have addressed the presence of lime, Portland cement, dolomite, gypsum and phyllosilicates in composition of these materials. Based on comparative analysis of calcite in samples from the walls and the samples from the outcrops of the Alhambra Formation collected nearby, Sebastián et al. (2010) has reported the presence of lime in the construction of the walls, the amount of which vary depending on the period to which the construction of building dates back, the function of the building and the location of sampling on the wall, with higher amount of lime having been identified for the outside of the wall compared to the inside of the wall. The samples taken from the Palacio de los Abencerrajes features higher quantities of lime-binder, around 30%, While in the Silla del Moro, much lower amounts of lime has been characterized in the walls, around 15–20%.

Gomes et al. (2014) has addressed mineralogical characterization of earth material collected from six old buildings in Portugal, including (1) located in Monte das Covas, Valongo, Avis, (2) located in Monte Pá Danado, Taliscas, Odemira, (3) located in Monte Vale Chaim, Taliscas, Odemira, (4) located in Monte se Deus Quiser, Corte Zorrinha, Almodôvar, (5) located in Barranco do Cai Logo, Colos, Ourique, (6) located in Arraiolos. The research performed by Gomes et al. (2014) has reported the result of the XRD analyses performed using a X Philips X´PERT equipment on soil samples oven dried at 40°C. It was observed that Mica was detected in all the materials and kaolinite was detected in case studies 2, 3, 4 and 5.

1.4.2.2.3. Bulk density

The research conducted by Wangmo et al. (2019) has reported bulk density of one of the old walls of Paga Lhakhangand and one newly prepared rammed earth wall specimen, constructed using locally available red clay with small pebbles following the construction procedure practiced in Bhutan. The bulk density of old wall and new wall were reported as 1810 kg/m3 and 2033 kg/m3, respectively.

In the study carried out by Gomes et al. (2019), bulk density of three different types of earth materials (AV, PD and VC), picked up from non-deteriorated parts of old unstabilized rammed earth buildings situated in Alentejo region, in south Portugal, were determined according to EN 1097-3 and reported as 1461 kg/m3, 1105 kg/m3 and 1136.4 kg/m3 for earth Av, PD and VC, respectively.

In an experimental program carried out by Silva et al. (2018), standard proctor maximum dry density of earth material mixture, composed of 50% of soil of Alentejo region, 28% of river sand and 22% of gravel, were reported as 2100 kg/m3.

Maximum dry density of earth material from six case studies, Av, PD, VC, CZ, Cl, Ar, has been measured by Gomes et al. (2014). Gomes et al. (2014) carried out proctor test according to ASTM standard D698-07 (2007). Using a cylindrical steel mould with 101.6 mm diameter and 116.4 mm height, the samples were prepared in 3 layers of equal thickness, each layer being struck 25 times using a standard weight of 2.447 kg that falls from a normalized height of 304.8 mm for compaction. The results of proctor test for five samples were reported as 2018 kg/m3, 1733 kg/m3, 1651 kg/m3, 1600 kg/m3 and 1814 kg/m3 for MDD.

1.4.2.2.4. Water content

The work performed by Benkmil et al. (2018) aims at contribution to the characterization of earthen materials in historical architectural heritage in Morocco, by investigating a case study in the center of the city of Marrakech in the center of Morocco. By studying water

content of rammed earth material, Benkmil et al. (2018) has reported the material to contain 3.3% water.

Ruiz et al. (2014) has characterized historical churches in the central Colombian highlands, dating back to of 16th and 17th centuries, using standard geotechnical tests. Based on standard tests according to ASTM D2216 (ASTM 2010b), the percentage of water content was reported to be 4.2.

In the study carried out by Gomes et al. (2019), optimum water content of three different types of earth materials (AV, PD and VC), picked up from non-deteriorated parts of old unstabilized rammed earth buildings situated in Alentejo region, in south Portugal, was determined by Proctor compaction test and reported to be 8.0%; 17.8% and 21.5% for Av, PD and VC, respectively.

In an experimental program carried out by Silva et al. (2018), standard proctor optimum water content of earth material mixture, composed of 50% of soil of Alentejo region, 28% of river sand and 22% of gravel, was reported as 10.1% .

Optimum water content of earth material from six case studies, Av, PD, VC, CZ, Cl, Ar, has been measured by Gomes et al. (2014). Gomes et al. (2014) carried out proctor test according to ASTM standard D698-07 (2007). Using a cylindrical steel mould with 101.6 mm diameter and 116.4 mm height, the samples were prepared in 3 layers of equal thickness, each layer being struck 25 times using a standard weight of 2.447 kg that falls from a normalized height of 304.8 mm for compaction. The results of proctor test for five samples were reported as 8%, 17.8%, 21.5%, 11.3% and 15.6% for OMC.

1.4.2.2.5. Strength properties

The research conducted by Wangmo et al. (2019) focuses on rammed earth construction in Bhutan, where they investigated one of the walls of Paga Lhakhang. They investigated the characteristics of one of the old walls of Paga Lhakhangand and one newly prepared rammed earth wall specimen, constructed using locally available red clay with small pebbles following the construction procedure practiced in Bhutan. In order to characterize material, mechanical compressive strength and splitting tensile tests were conducted on extracted cylindrical core samples of rammed earth (92 mm diameter and 180 mm height). The compressive strenght and tensile strength of old wall were reported as 0.845 MPa and 0.101 MPa respectively, while compressive strenght and tensile strength of new wall were 0.52 MPa and 0.054 MPa, respectively.

Non-destructive testing of the compressive strength with a Schmidt-hammer was performed by Baglioni et al. (2016) on rammed earth fortifications and houses at Zagora and Tissergat.

An experimental program carried out by Silva et al. (2018) aimed at characterising the in-plane shear behaviour of rammed earth walls. In this study, the behaviour of rammed earth wallets under destructive diagonal compression and non-destructive sonic characteristics were investigated on the wallets. By making corrections on the particle size distribution of the soil collected from Alentejo region, by addition of coarse aggregates, the final earth material mixture was composed of 50% of soil of Alentejo region, 28% of river sand and 22% of gravel. In order to investigate the shear behaviour of the RE material, Silva et al. (2018) documented the progression of cracking during different stages of loading of diagonal compression tests using the digital image correlation (DIC) technique. Compressive strength of unstabilised rammed earth was also reported in the study conducted by Silva et al. (2018). Compression tests were carried out on cylindrical specimens with 100 mm diameter and 200 mm height, manufactured using the earth compacted in three layers with an average dry density of 2065 kg/m3. The behaviour of RE under uniaxial compression loading was

reported to be highly nonlinear with Young's modulus depending considerably on the deformation level.

1.4.2.2.6. Atterberg limits

An experimental investigation was carried out by Baglioni et al. (2016) on samples from rammed earth walls from different villages of the Drâa valley, namely Amzrou, Tissergat and Zagora. They observed the low plasticity and low shrinkage of the material (liquid limit=18.5%, plastic limit=16.7%, plasticity index=1.80%), attributed mainly to the lower amount of smectite with respect to illite, kaolinite and chlorite.

Ruiz et al. (2014) have characterized historical churches in the central Colombian highlands, dating back to of 16th and 17th centuries, using standard geotechnical tests. Liquid Limit, Plastic Limit, and Plasticity Index of soil were determined according to ASTM D4318 and were reported to be 22%, 16% and 6%, respectively.

In an experimental program carried out by Silva et al. (2018), the values of 7%, 23% and 16% were obtained for the liquid limit (LL), plastic limit (PL) and plasticity index (PI) of earth material mixture, composed of 50% of soil of Alentejo region, 28% of river sand and 22% of gravel.

Gomes et al. (2014) have measured Liquid limit and plasticity index of earth material of six case studies, Av, PD, VC, CZ, Cl, Ar, and has reported liquid limit of 14.8, 41.2, 46.1, 17, 35.5 and 26 for case studies Av, PD, VC, CZ, Cl, Ar, respectively. For case studies PD, VC, Cl, Ar, they reported the values of plasticity index as 16.1, 19.4, 13.5 and 6, respectively.

1.4.2.2.7. Suction

Suction is the source of developing strength in rammed earth material (Jaquin et al. (2009) and Bui et al. (2014)). The research performed by Jaquin et al. (2009) confirms that suction is a key factor responsible for strength in rammed earth material. Jaquin et al. (2009) and Bui et al. (2014) have studied and confirmed a link between suction and the strength characteristics of rammed earth material.

Aiming at quantification of suction inside rammed earth, the study performed by Bui et al. (2014) has addressed development and validation of a simplified method to measure the suction within rammed earth samples. Bui et al. (2014) investigated the effect of suction on rammed earth over a wide range of moisture content. They concluded that the simplified method is a reliable approach, yielding well correlated data. This study showed that, in a logarithmic scale, a linear correlation can be drawn for varation of suction with respect to that of the compressive strength and secant modulus of elasticity of unstabilised rammed earth.

It is widely accepted that the capillary force between particles is the source of cohesion in soil material. Being composed of layers of earth, rammed earth is a three-phase mixture, commonly referred to as unsaturated soil, in which the water in soil forms capillary force between particles. This capillary force gives rise to cohesion between soil grains. The importance of the capillary condensation bridge has been addressed by Bui et al. (2014). Indicated by this study, the effect of capillary bridges have been recognized in four phases. At Phase 1, two spherical particles are held together by capillary condensation bridge at their contact point and the cohesion increases nonlinearly with the amount of moisture. At Phase 2, liquid bridge spreads over several particles and the cohesion increases linearly with an increase in moisture content. Phase 3 and Phase 4 correspond to indepency of cohesive force to the amount of water and decrease of cohesion, respectively.

The cohesion of sandy soil material is attributed to the capillary force between particles. In clayey soil the capillary force between particles as well as attractive forces between clay particles due to Van der Waals force gives rise to the cohesion of material (Bui et al. (2014)).

Furthermore, Beckett et al. (2017) has developed an experimental programme to investigate suction-controlled strength characteristics of rammed earth. Two soils were used in this investigation, the first comprised of 19.9% clay, 17.2% silt, 52.7% sand and 10.2% gravel, and the second comprised of 9.9% clay, 9.5% silt, 70.7% sand and 9.9% gravel. The optimum water contents (OWC) and maximum dry densities (MDD) were measured using the Standard Proctor Test (BS 1377), yielding OWC and MMD as 12% and 1940 kg/m3 for the first soil and OWC and MMD as 12% and 1960 kg/m3 for the second soil. The suction was controlled during testing by Vapour Equilibrium method, also called relative humidity technique. They investigated strengths at different suction values.

In this method, an aqueous saturated saline solutions is used to regulate the relative humidity of the surrounding the sample. According to the relative humidity of the air, exchange of water vapor occurs between the specimen and the surrounding. Equilibrating specimens, to set temperatures and relative humidities, imposes a particular value of suction on specimen.

$$s = u_a - u_w = -\frac{R.T(K)}{g.w_v}\ln\left(\frac{p}{p_0}\right) \qquad \textbf{Eq (1.1)}$$

where s is the suction at absolute temperature T (K), ua and uw are pore air pore water pressures, RH is the relative humidity, the ratio of partial vapour pressure P in the considered atmosphere and the saturation vapour pressure Po at absolute temperature T (K), g is acceleration due to gravity, R is universal gas constant, wv is the molecular mass of water vapour.

Beckett et al. (2017) prepared 100mm cube specimens for UCS tests, using soil at the OWC. Specimens were removed from the mould after manufacturing and left to dry under conditions of 45 ±15% RH and 20 ±2◦C. Specimens were then equilibrated to RH=30, 50, 70 or 90% (±3%) and T =15, 20, 30 or 40◦C (±2◦C) using an environmental chamber. Immediately following equilibration, specimens were transferred to a uniaaxial compression testing machine. The moisture content of secimen were measured by oven drying.

1.5. Conclusion

A review of literature on rammed earth material reveals that geotechnical studies on rammed earth have been focused on laboratory or field measurement of several fundamental material parameters, which are important in describing soil material characteristics, including grain-size distribution, optimum water content and maximum dry density via the Proctor test, Atterberg limits and clay mineralogical composition determined by XRD.

Although important efforts have been made by these studies, these contributions into determination of physical and mechanical characteristics do not address all of the controlling properties, inherent to each material structure, on which characterizations of rammed earth material has indicated a dependence and thus, the resultant data can not be comparable. This highlights the need for the establishment of a well-defined experimental program on characterization of rammed earth materials, which has been addressed on Chapter 4 of this dissertation.

References

Alex, D. Recognition of a heritage in danger: rammed-earth architecture in Lyon city, France. In IOP Conference Series: Earth and Environmental Science (Vol. 143, No. 1). IOP Publishing, April 2018; pp. 012054.

ASTM D2974-07. 2007. American Society for Testing and Materials: Test methods for moisture, ash and organic matter of peat and other organic soils. ASTM: United States

ASTM D698-07. 2007. American Society for Testing and Materials: Test methods for laboratory compaction characteristics of soil using standard effort. ASTM: United States.

Baglioni, E.; Fratini, F., and Rovero, L. The characteristics of the earthen materials of the Drâa valley's architecture. *J. Mater. Environ. Sci*. **2016**, *7(10)*, 3538-3547.

Benkmil, R.; Bahi, L.; Aakhssass, A., and Ouadif, L. CONTRIBUTION TO THE CHARACTERIZATION OF CONSTRUCTION MATERIALS OF HISTORICAL MONUMENTS-CASE STUDY. *International Journal of Civil Engineering and Technology*. **2018**, *9*, 1680-1688.

Bui, Q. B.; Morel, J. C.; Hans, S. and Walker, P. Effect of moisture content on the mechanical characteristics of rammed earth. *Construction and Building Materials*. **2014**, *54*, 163–169.

Cavicchioli, A.; Sant'Anna, L. G., and Perroni, M. S. Enlightening the use of materials and techniques in earthen architecture in southeast Brazil during the first coffee cycle (19th century). *Journal of Cultural Heritage*. **2018**, *31*, 208-214.

Cuchí i Burgos, A. La técnica tradicional del tapial. Actas del Primer Congreso Nacional de Historia de la Construcción, 1996, Madrid (Spain), pp. 159–165.

Cui, K.; Wu, G.; Du, Y.; An, X., and Wang, Z. The coupling effects of freeze-thaw cycles and salinization due to snowfall on the rammed earth used in historical freeze-thaw cycles relics in northwest China. *Cold Regions Science and Technology*. **2019**, *160*, 288-299.

Daoudi, L.; Rocha, F.; Costa, C.; Arrebei, N., and Fagel, N. Characterization of rammed-earth materials from the XVIth century Badii Palace in Marrakech, Morocco to ensure authentic and reliable restoration. *Geoarchaeology*. **2018**, *33(5)*, 529-541.

Doat, P., Hays, A., Houben, H., Matuk, S., and Vitoux, F. 1979. Construire en terre. CRATerre - Centre de Recherché et d´Application - Terre. École d'Architecture de Grenoble, France.

DOC. 2017. General Guideline for improved seismic resilient construction techniques for rammed earth structures in Bhutan. Department of Culture, Ministry of Home and Cultural Affairs, Royal Government of Bhutan, Lhazeen Press, Thimpu, Bhutan.

Gomes, M.I.; Gonçalves, T.D., and Faria, P. Unstabilised rammed earth: characterization of the material collected from old constructions in south Portugal and comparison to normative requirements. *International Journal of Architectural heritage*. **2014**, *8(2)*, 185-212.

Gamrani, N. Etude de quelques monuments historiques Saadiens (XVIXVIIème siècle) de la ville de Marrakech (Maroc) : Caractérisation et pathologie (pp. 174). Marrakech: Thèse d'Université Cadi Ayyad, 2014.

Gomes, R., and Folque, J. 1953. Earth use as building material (in Portuguese). Circular de Informação Técnica N.º 9, Série D-4. National Laboratory for Civil Engineering.

Guillard, H., and Houben, H. Traité de construction en terre - encyclopédie de construction e terre (pp.360). Editions Parenthèses, Marseille, 1989.

Houben, H., and Guillaud, H. 2006. Earth construction: a comprehensive guide. London: Intermediate Technology publications, (1st edition 1994).

IETCC. 1971. Obras de Fábrica. Prescripciones del Instituto Eduardo Torroja - PIET - 70. Madrid: Instituto Eduardo Torroja de la Construcción y del Cemento.

Jaquin, P. A., Augarde, C. E., Gallipoli, D., Toll, D. G. and Note, T. The strength of unstabilised rammed earth materials. *Géotechnique.* **2009**, *59(5)*, 487–490.

Jaquin, P. A history of rammed earth in Asia. International workshop on rammed earth materials and sustainable structures & Hakka Tulou Forum. 2011.

Jo, Y. H.; Lee, S. M., and Lee, C. H. Material characteristics and building technique for the rammed earth wall of the 13th Korean fortress in Ganghwa. *Environmental Earth Sciences.* **2018**, *77(17)*, 1-15.
Keable, J. 1996. Rammed earth structure - A code of pratice. Intermediate Technology Publications. London.

Keefe, L. 2005. Earth building - methods and materials, repair and conservation. Taylor & Fancis Group. USA and Canada.

Kourdou, I., and Cherradi, T. Restoration of Built Heritage: Case Study of Earth Constructions-Tiznit. *International Journal of Engineering Research in Africa.* **2016**, *25*, 133-141.

Martín-del-Rio, J.J.; Flores-Alés, V.; Alejandre-Sánchez, F.J.; Blasco-López, F.J. New method for historic rammed-earth wall characterization: The Almohade ramparts of Malaga and Seville. *Stud Conserv*, **2019**, *64(6)*, 363-372.

New México Code. 2006. New México Earthen Building Materials Code 14.7.4. Santa Fé, NM: Construction Industries Division (CID) of the Regulation and Licensing Department.

NZS 4298.1998. New Zealand Standard - Materials and workmanship for earth buildings. Wellington: Standard New
Zealand.

Lehmbau Regeln. 2009. Begriffe, Baustoffe, Bauteile. Dachverband Lehm e.V. (Hrsg.), Germany: Vieweg & Teubner, 3, überarbeitete Auflage. Praxis. Wiesbaden, Germany

Ruiz, D.; López, C.; Unigarro, S., and Domínguez, M. Seismic rehabilitation of sixteenth-and seventeenth-century rammed earth–built churches in the Andean highlands: field and laboratory study. *Journal of Performance of Constructed Facilities.* **2015**, *29(6)*, 04014144.

SAZS 724. 2001. Standards Association Zimbabwe. Standard Code of Practice for Rammed Earth Structures. Harare: Standards Association of Zimbabwe.

Sebastián, E., and Cultrone, G. Technology of rammed-earth Constructions ("Tapial") in Andalusia (Spain): Their restoration and conservation. In Materials, technologies and practice in historic heritage structures (pp. 11-28). Springer, Dordrecht, 2010.

Sebastián Pardo, E.; de la Torre, M.J.; Elert, K., and Rodríguez Navarro, C. The Alhambra and Granada Catedral: study of materials, their decay and conservation. Technical guide. 5th international symposium on the conservation of monuments in the mediterranean Basin, Seville, Spain, 2000.

Specification 196. 1966. National Laboratory for Civil Engineering. Particle size analysis (by dry sieving and sedimentation) (in Portuguese). Lisbon, 1966.

Specification 239. 1970. National Laboratory for Civil Engineering. Particle size analysis by wet sieving (in Portuguese). Lisbon, 1970

Soria, F.J.; Guerrero, L.F., and García, A.B. Traditional rammed earth construction: conservation of built heritage in México. *WIT transactions on the built environment*. **2011**, *118*, 497-506.

Valverde Espinosa, I.; Ontiveros Ortega, E.; and Sebastián Pardo, E. El tapial de las murallas de Granada. *Revista de edificación*, **1997**, *26*, 58–64.

Walker, P., and Standards Australia. 2001. HB 195, The Australian earth building handbook. Sydney (Australia), Standards Australia.

Walker, P., Keable, R., Martin, J., and Maniatidis, V. 2005. Rammed earth: design and construction guidelines. BRE Bookshop. Watford.

Wangmo, P.; Shrestha, K. C.; Miyamoto, M.; Aoki, T. Assessment of out-of-plane behavior of rammed earth walls by pull-down tests. *Int. J. Archit. Heritage*. **2019**, *13(2)*, 273-287.

CHAPTER 2

Automatic identification of cracks and architectural lines in images of rammed earth walls

This chapter reports the research that has been published in Applied sciences Journal (Moghaddam et al. (2020)). The main objective of this section is to investigate the possibility of application of automatic crack detection methodologies on images of rammed earth wall heritage. To gain insight, this section first focuses on investigating fundamental problems in object recognition on rammed earth walls, which reports several specific problems, among them the difficulty in automatic identification of architectural lines and horizontal and vertical cracks. This difficulty highlights the need for the establishment of a simple and flexible automatic object recognition solution that could, in the future, be adopted as useful framework for evaluation of state of rammed earth heritage buildings and subsequently building decision strategies for maintenance activities. Motivated by this difficulty, this research introduces and validates a simple and straightforward machine learning SVM-based bidirectional morphological framework, which, through transforming a surface image of rammed earth wall into an intermediate representation, enables an automatic construction and generation of crack and texture line maps. Rather than applying 8 connectivity rule to combination of horizontal and vertical gradient, this methodology extract edges through development of an edge classifier in the form of a machine learning approach based on important information that often exists in each direction separately.

This automatic algorithmic approach, which couples bidirectional local gradient and geometrical characteristics to a powerful, simple and straightforward framework, comprises of four major elements, including: (1) bidirectional edge maps, (2) bidirectional equivalent connected component maps, (3) machine learning SVM-based classifier and (4) crack and architectural line feature map generation. Alongside, a detailed description of each stage and difficulties that may appear when trying to shape the above-mentioned framework have been reported in each section. Finally, the proposed algorithm are verified through comparative experiments in a set of simulations on surface images of rammed earth with different crack patterns, through which predicted data has been demonstrated to be satisfactorily conforming to labeled data provided manually for images.

2.1. Introduction

Earthen structures, which has been linked throughout history with harvesting and exploiting our planet's natural earth material resources as a construction material in several different ways around the world, represent significant elements of our cultural heritage distributed worldwide. Rammed earth (RE), also known as "taipa", "taipa de pilão" "tapial", "pise de terre", "pisé" or "stampflehm", is one of the most widespread structural types of earthen architectural cultural heritage in the world.

To construct a traditional rammed earth wall, moistened earth mixture is poured into rigid formwork, a temporary wooden support structure, and is then manually compacted to a very high density in layers utilizing a wooden rammer. This building process, constructing the wall a section at a time and moving the form section to section, horizontally and vertically, until building the full wall height, results in a distinctive layered appearance, often regarded as characteristic feature of the rammed earth. The formwork is mainly composed of two panels and several long bolts in the middle, extended through the form holding panels together, which acts as a support to hold the soil in place during ramming and compaction process. On completion of the wall, the panels and bolts, and thus the formwork, are removed, leaving some joint lines in the wall, which are often regarded as characteristic feature of the rammed earth walls (Figure 2.1).

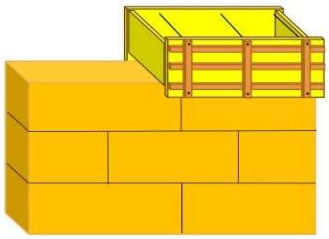

(a)

Figure 2.1. Rammed earth wall (Moghaddam et al. (2020))

Since cracks are one of the most common surface defects of earthen heritage, conservation and restoration of earthen architectural heritage is firmly linked with identification and characterization of existing surface cracks. Identification and characterization of surface cracks is therefore critical to any attempt to conserve earthen heritage. Particularly when monitoring highly vulnerable earthen structures, manually detecting a crack, through traditional human field surveys, is a very intricate and time-consuming procedure. An automatic crack detection approach based on capturing image of surface during heritage surveys provides an adequate procedure for fast and reliable surface defect analysis, and consequently accurate quantitative data on the condition of heritage, upon which conservation strategies is based.

Cracking is a phenomenon frequently present in rammed earth heritage. The presence of cracks, which is a characteristic feature of most earthen building heritage, can act as major pathways for aggressive elements to penetrate into earthen material, enabling further propagation of severe cracks, which may lead to serious deterioration and structural failure. This highlights the need for a precise assessment tool to point out crack regions and to monitor surface cracks at regular intervals from their early stage before they progress to failure, which is fundamental for preservation purposes. Efficient automatic image-based crack detection methodology for rammed earth heritage can aid conservation specialists in identifying efficient conservation strategies. This is the reason why it's important to decide on a robust crack detection methods or algorithms demonstrating good performance on rammed

earth images, which assist in decision making for evaluation and conservation of earthen heritage buildings in a service condition over a period of time.

In the literature, much work has dealt with the problem of crack detection for various purposes, reporting numerous approaches to make use and develop image processing techniques (Broberg, 2013; Sinha and Fieguth, 2006; Merazi-Meksen et al., 2014; Jahanshahi and Masri, 2012; Wang and Huang, 2010; Alam, 2015; Brooks et al., 2015; Iliopoulos et al., 2015; Hamrat et al., 2016; Merazi-Meksen et al., 2010; Vidal et al., 2016; Wolf et al., 2015; Dhital and Lee, 2012; Li et al., 2014; Guo and Vavilov , 2013; Fujita and Hamamoto, 2011; Glud et al., 2016; Talab et al., 2016; Agarwal and Singh, 2015; Gunkel et al., 2012; Xu et al., 2014; Anwar and Abdullah, 2014; Heideklang and Shokouhi, 2015; Rodrı´ guez-Martı´na et al., 2015; Yiyang, 2014; Yamaguchi and Hashimoto, 2010; Nazaryan et al., 2013; Chen et al., 2012; Kabir, 2010; Adhikari, 2014). These techniques, however, are programmed to solve a particular problem, and thus can only be applied to specific types of images and purposes. Although being one of the most ancient construction materials, rammed earth still deals with fundamental questions about structural performance that needs to be solved by researchers and engineers. However, to the author's knowledge, crack detection of rammed earth heritage is a topic not addressed in the literature. This study makes an attempt to address this issue by investigating and developing an automatic crack detection methodology able to extract and analyse crack and non-crack information and patterns from surface images of rammed earth heritage.

An analysis of surface images of rammed earth walls, performed in the framework of this study (Moghaddam et al. (2020)), indicates that architectural line features has a large influence on detection results of existing image processing techniques. An observation that is possible to make thanks to this study regards the fact that horizontal line features may be misidentified as cracks (Figure 2.2). Development of a simple and flexible framework for automatic and accurate detection of cracks in the surface images of rammed earth heritage, able to clearly discriminate between existing cracks and architectural features, is hence a complex task. This chapter ,to address the problem above, concentrates on the creation of an algorithm that transforms surface image of rammed earth into crack map and architectural feature map, avoiding above-mentioned misidentification problem inherent to analysis of surface images of rammed earth walls. Our algorithm consists of exploiting the strong feature learning capabilities of learning-based approaches.

(a)

Figure 2.2. An illustration of misidentification of architectural horizontal lines as cracks in images of rammed earth (Moghaddam et al. (2020))

Machine learning is concerned with the ability of computers to extract and analyse high level information from images, and has seen much success in processing huge amounts of data. However, the task of detection of important regions needs some way to partition image into meaningful segments, requiring extraction of high level information and its subsequent translation into feature representation. Machine learning have been subject of many research works with applications to many fields. Of general interest in all of these areas is crack

detection task. The task of image-based automatic crack detection in itself can be challenging, but in case of surface images of rammed earth, existence of architectural line features with its complex surface texture complicates the problem further (Figure 2.2).
Recognizing different kinds of line objects in surface images of rammed earth is a difficult task, since a surface image of rammed earth wall can be thought of as a skeleton of preexisting architectural line features and cracks. When there are both vertical and horizontal architectural lines, the information and pattern associated with architectural lines are complicated, and it is difficult to distinguish the structure between these architectural line features and cracks. The labeling of surface cracks and architectural lines is a challenging area for rammed earth walls.
The utilization of machine learning methods in raw images of rammed earth may have difficulty in automatic crack detection: they usually detect a set of architectural lines as crack fragments. There is a sense that meaningful relationships between the feature representations needs to be exploited and used in conjunction with learning techniques to make detection decision. In this case, an intermediate image showing geometrical properties in the architectural lines and cracks would be helpful to identify and classify two categories of crack and non-crack objects. In this chapter, characteristics of crack and non-crack object in surface images of rammed earth walls are investigated. Based on mathematical analysis, the variation of important geometrical characteristics is discussed. An attempt is made to investigate and make use of existing learning-based methodologies from different points of views. This research focuses on the development of a novel approach for solving a real-world pattern recognition problem in surface images of rammed earth through exploiting the strong feature learning capabilities of learning-based approaches, whose power lies in extracting a set of geometrical features. By transforming a surface image into a meaningful intermediate feature representation, this algorithm exploits and makes use of a set of mathematical relation to aid in desirable task of crack detection, upon which a successful detection application of machine learning in rammed earth images is firmly bound.

2.2. Developed methodology

The approach developed in this research is based on oriented gradient in horizontal and vertical directions at every location in an image (Figure 2.3). Then, the algorithm makes use of connected component analysis (Haralick and Shapiro (1992)), equivalent to fitting an ellipse, with major axis orientated along direction θ. The second-moments of the equivalent ellipse is equal to that of the connected component (CC) (Figure 2.4). The geometrical properties of elliptical fit estimates the properties of cracks and non-cracks at location (x,y), making a distinction, between crack and non-crack objects, possible. Figure 2.4 presents an example of such equivalent image.
Once CC maps in horizontal and vertical directions were constructed, the algorithm analyses connected components, whose area are more than 30 pixels, from largest to smallest ones. Then the algorithm applies an SVM-based classification scheme for each CC, which classifies it as crack or architectural feature. Then, the algorithm proceeds by adding up corresponding horizontal and vertical derivatives of pixel intensities, followed by binarization using Otsu's method (Otsu, 1979)), as a result of which crack map and architectural feature map are generated. The algorithm repeats this entire procedure until all pixels of horizontal and vertical CCs are analyzed once.

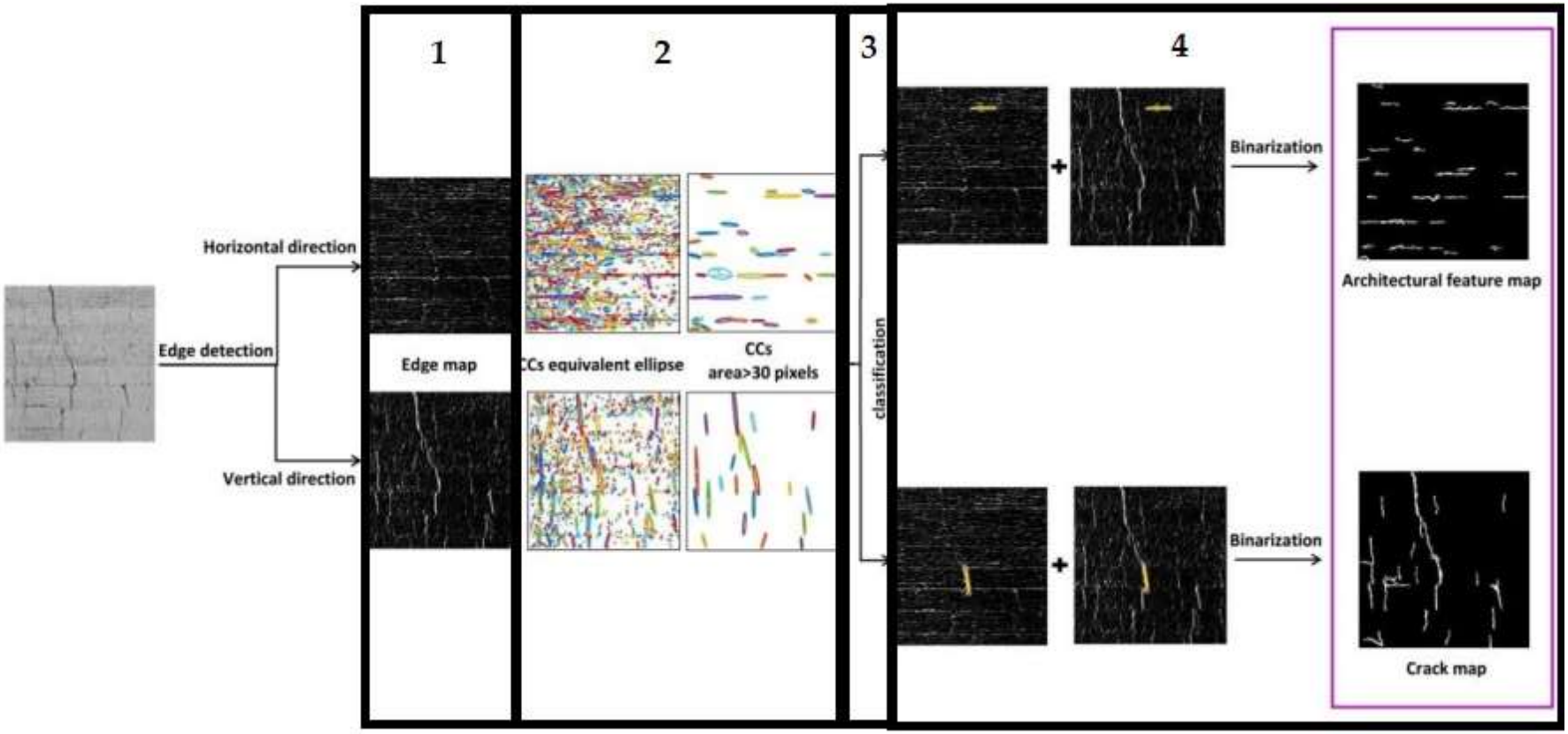

Figure 2.3. Developed Methodology.

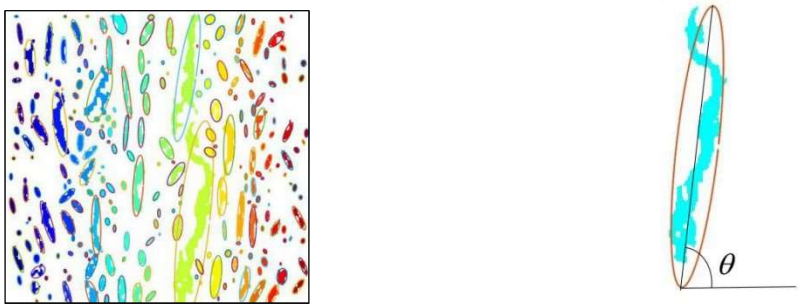

(a) (b)

Figure 2.4. An example of (a) connected component map and (b) equivalent bounding ellipse (Moghaddam et al. (2020))

2.2.1. Constructing edge maps

As the first step in this process, the algorithm converts the input image to grayscale and applies oriented edge detection operator, constructing oriented edge maps in horizontal and vertical directions, independently as shown in Figure 2.3. An analytical investigation is necessary for the selection of an edge detection technique for this task. The main algorithm of this step is inspired by the performance analysis. In order to evaluate the capability of edge detection methods to separate crack objects from the background, a primitive investigation of performance of existing methods in images of rammed earth walls has been performed (Moghaddam et al. (2020)). In follow, performance in crack detection and performance in identification of architectural features, shortcomings of existing edge detection techniques and relevant details have been discussed.

In order to perform performance analysis, the most commonly used edge detection algorithms, Sobel (Parker, 1997), Canny (Canny, 1986), Prewitt (Prewitt, 1970), Laplacian of Gaussian (LoG) (Marr and Hildreth, 1980) and fast Haar transform (FHT) (Bachman and Beckenstein, 2000), are implemented, on selected parts of rammed earth images, to extract crack pixels from background. Full details of this analysis has been reported in (Moghaddam et al. (2020)). It is evident that these algorithms may produce missing or extra edges on complex surface images of rammed earth structures with multiple cracks and architectural lines. The results of this investigation on above-mentioned methods can help in the choice and development of an edge detection algorithm for automatic crack detection of rammed earth heritage.

Motivated by the observed inconsistencies and inaccuracies to distinguish between cracks and architectural features, the problem inherent to crack detection in rammed earth images, main focus is particularly given to find solutions that make a distinction of these two objects possible, having a reasonably good accuracy in automatic identification of the presence of multiple cracks and architectural line objects in images of a rammed wall.

Regarding Sobel, which predicted less missing pixels, although a more noisy output, this experimental study indicates a better performance of Sobel edge operator in identification of crack pixels for rammed earth images (Moghaddam et al. (2020)). Furthermore, this study indicates that the application of crack detection algorithms cannot achieve good accuracy and performance simply by using an edge detection operator on a raw rammed earth image, an observation that may be mainly attributed to the influence of architectural objects on detection results (Figure 2.2). This observation confirms that existing edge detection operators often join horizontal and vertical architectural lines at the corners (Figure 2.5a) or architectural lines and cracks at the intersections (Figure 2.5b), and thus are not appropriate

for complex rammed earth images containing horizontal and vertical architectural line features (Moghaddam et al. (2020)). These above-mentioned observations may inspires an algorithm that constructs edges in horizontal and vertical direction, separately. Therefore, for a given test image, this step of proposed algorithm applies Sobel edge detection operators in horizontal and vertical direction , separately (Figure 2.3), confirming the fact that oriented edge maps themselves carry important feature information, that characterizes specific objects.
Moreover, this study indicates capability of Haar transform method to detect horizontal and vertical line objects. Although this method can extract horizontal and vertical joint lines in a rammed earth image and map them as architectural features, in rammed earth structures containing multiple cracks and architectural line features, this method breaks up directed features of an edge and maps them in different sub-band images, which, in rammed earth images containing multiple cracks and architectural line features, may lead to incorrect detection results (Moghaddam et al. (2020)).
This means that horizontal sub-band obtained by Haar transform method does not only recognizes horizontal lines. Rather, this sub-band image carries information of horizontal features of all line objects in an image. From this, it can be found that a simple directed edge map is not sufficient to benefit from feature classification. In this context, it is useful to associate each feature to an integration of local intensities and connectivity at each direction and then categorize those directed connected components based on learning important geometrical characteristics. Thus, after applying oriented edge operator, the algorithm proceed by treating obtained edge maps as images and applying connected component analysis for each direction separately, as a result of which oriented horizontal CC maps, maps of equivalent ellipses, are generated. This method extracts geometrical characteristic from different horizontal and vertical edge maps, which provides far superior information for the task of crack and non-crack classification, solving the problem of misidentification, the most significant challenge inherent to rammed earth images. Figure 2.6 shows representative horizontal edge map, vertical edge map, horizontal CC map and vertical CC map, which presents the contributions of oriented edge maps in horizontal and vertical directions to the performance of the algorithm, approving the potential capability of proposed approach.

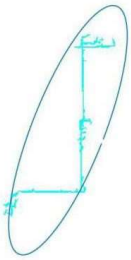

(a)

(b)

Figure 2.5. Misidentification problem of CCs in rammed earth images, implementing existing edge detection methods. (a) The problem of joined horizontal and vertical architectural lines and (b) the problem of joined architectural lines and cracks. (Moghaddam et al. (2020))

2.2.2. Connected component analysis

As previously shown in Figure 2.5, building up CC from detected edges obtained simply by applying an edge detection algorithm, will often mistakenly join architectural lines and cracks, resulting in misidentification problem. Hence, producing oriented gradient maps rather than a single-level edge map provides a high-level solution. This solution is inspired by the intuition that horizontal and vertical architectural line features, on the surface image of the rammed earth walls, carry information of horizontal and vertical discontinuities in intensity and thus geometrical features describe important local information for characterizing the content of such image regions, that proved sufficiently discriminative individually. At this stage, the algorithm builds up CCs by implementing eight connectivity rule (Haralick and Shapiro, 1992) to each group of adjacent pixels in oriented edge maps in horizontal and vertical directions, independently (as shown in Figure 2.6).

An analysis of geometric features of crack and non-crack objects indicates that geometrical characteristics, offering various morphological parameters, provide solution to identify and mathematically classify crack and non-crack objects into different classes. As observed in this study, in rammed earth images, a high value of oriented axis length ratio (Ratio of Major Axis Length to Minor Axis Length) indicates that a CC is more likely to belong to the group of architectural lines.

In this regard, in the proposed algorithm each CC, group of adjacent pixels shaping a roughly linear edge, is represented by an ellipse, whose physical properties are equivalent to the properties of the reference CC. This geometrical-based methodology utilized herein provides a framework that helps subsequent automatic crack analysis. Furthermore, the algorithm expresses the geometrical characteristics in terms of the normalized quantities, offering a scale-invariant feature space. Table 2.1 and Figure 2.7 describes important morphological parameters identified and selected to utilize for the analysis in this study. In this regards, each CC has been defined by the morphological parameters of the equivalent ellipse, assigned to each CC. Figure 2.8 shows the results of CC analysis.

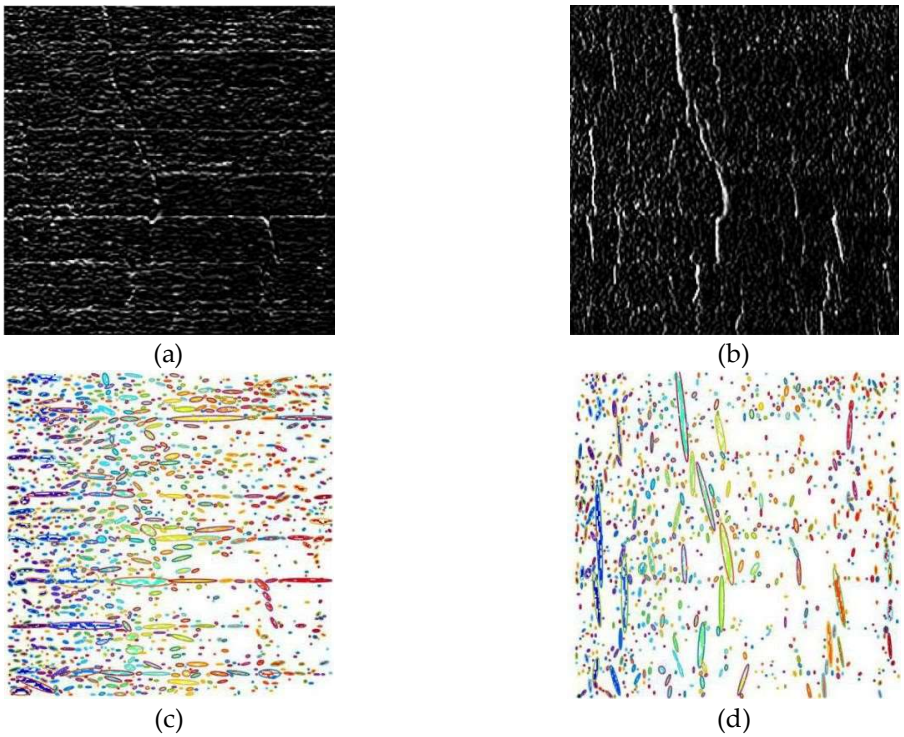

Figure 2.6. Oriented edge maps; (a) Horizontal edge map, (b) vertical edge map, (c) horizontal CC map and (d) vertical CC map. (Moghaddam et al. (2020))

Table 2.1. Morphological parameters for connected component analysis (Moghaddam et al. (2020)).

Area	Number of pixels
Density	Ratio of pixels in the region to pixels in total image
Major axis length	Length (in pixels) of the major axis of the equivalent ellipse
Minor axis length	Length (in pixels) of the minor axis of the equivalent ellipse
Length ratio	Ratio of the major axis length to 256√2
Width ratio	Ratio of the minor axis length to 256√2
Axis length ratio	Ratio of Major Axis Length to Minor axis length
Orientation	Absolute value of the angle between the x-axis and the major axis of the ellipse, ranging from 0 degrees to 90 degrees (Figure 3b).
Orientation ratio	Ratio of orientation to 90 degrees
Convex area	Number of pixels in convex Image (Figure 8c)
Convex area ratio	Ratio of pixels in convex area to pixels in total image
Equivalent diameter	Diameter of an equivalent circle with the same area as the region
Equivalent diameter ratio	Ratio of Equivalent diameter to 256
Extent	Ratio of pixels in the region to pixels in the total bounding box
Solidity	Ratio of area to convex area

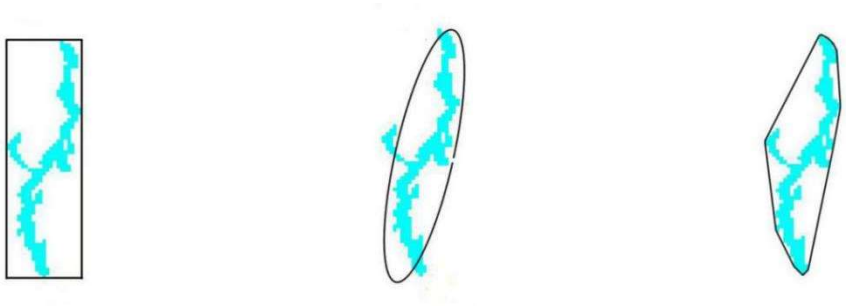

Figure 2.7. An illustration of morphological parameters. (a) Bounding box, (b) bounding ellipse and (c) convex hull. (Moghaddam et al. (2020))

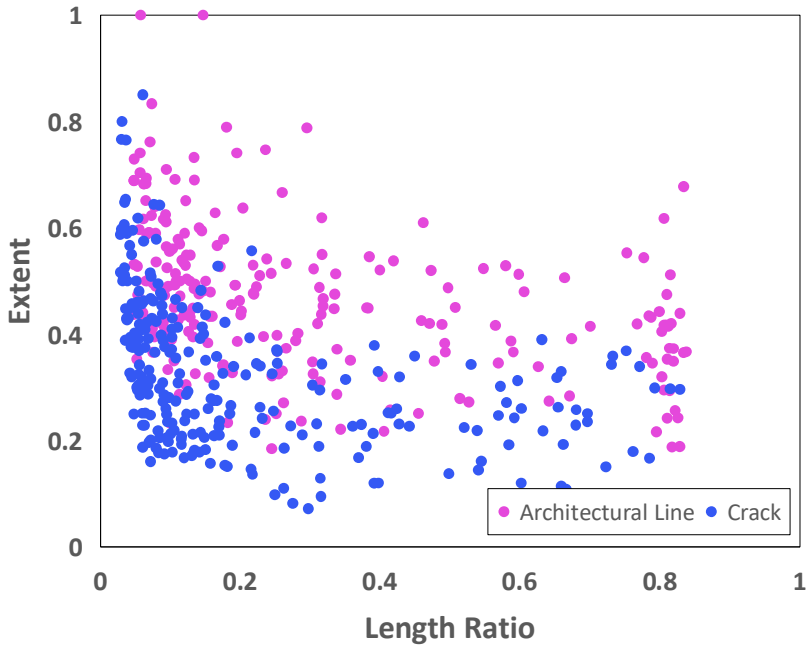
Extent
Length Ratio
Architectural Line
Crack
0
0.2
0.4
0.6
0.8
1

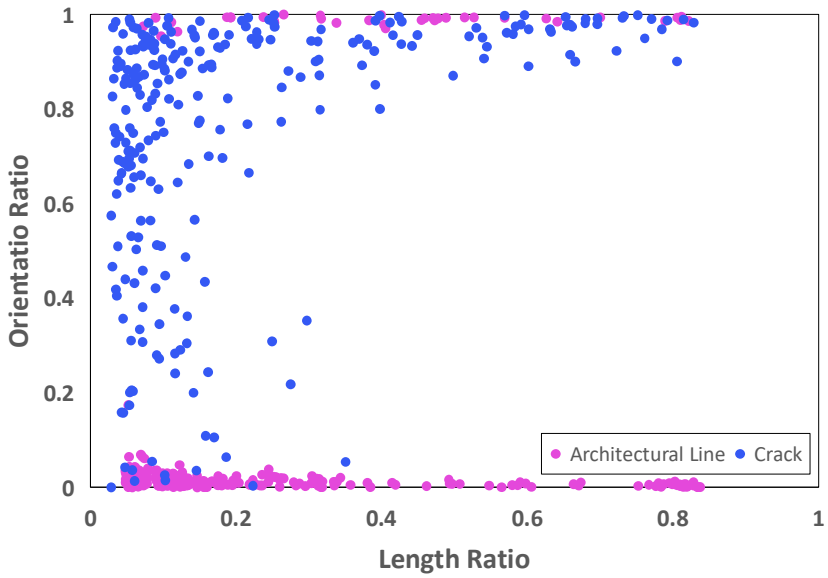
Orientatio Ratio
Length Ratio
Architectural Line
Crack
0
0.2
0.4
0.6
0.8
1

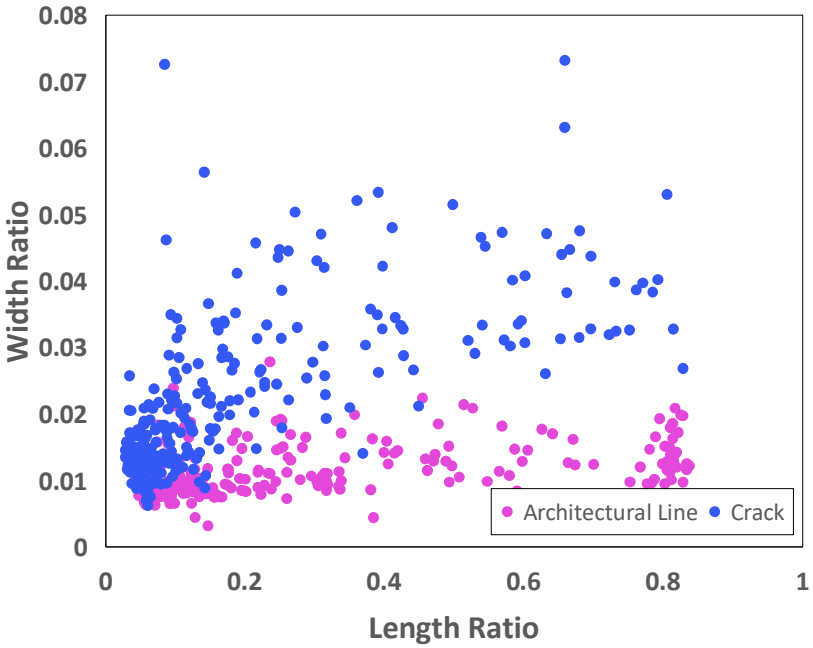
0.08
0.07
0.06
0.05
0.04
0.03
0.02
0.01
0
Width Ratio
0
0.2
0.4
0.6
0.8
1
Length Ratio
Architectural Line
Crack

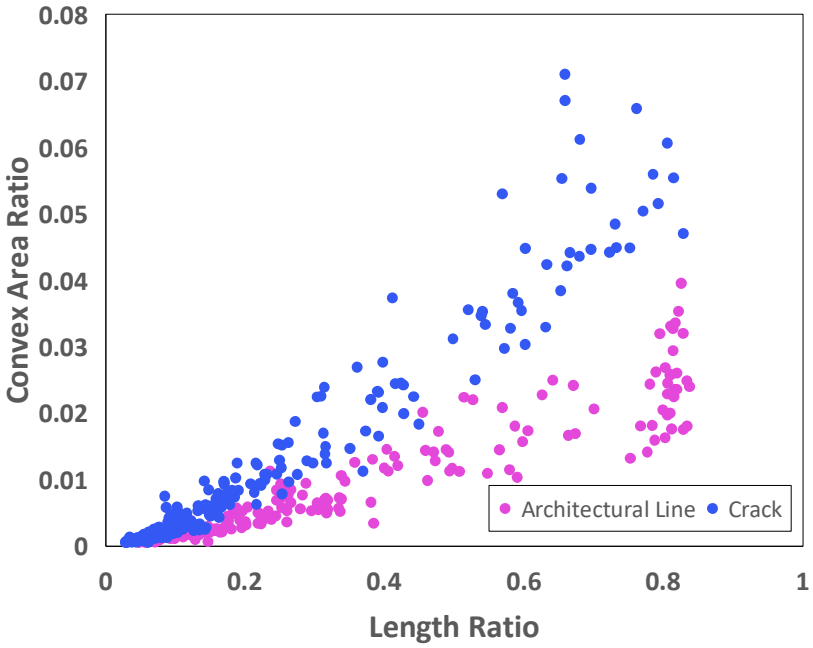
0.08
0.07
0.06
0.05
0.04
0.03
0.02
0.01
0
Convex Area Ratio
0
0.2
0.4
0.6
0.8
1
Length Ratio
Architectural Line
Crack

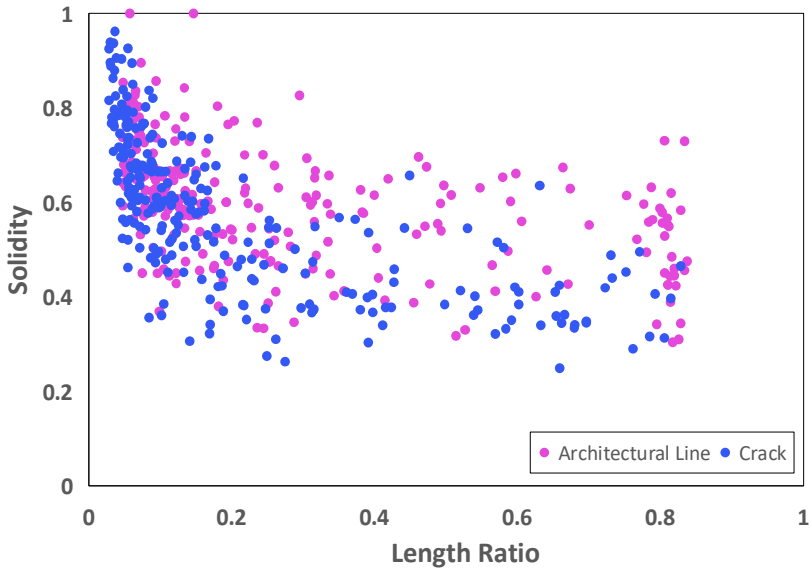
Solidity
Length Ratio
Architectural Line
Crack
0
0.2
0.4
0.6
0.8
1

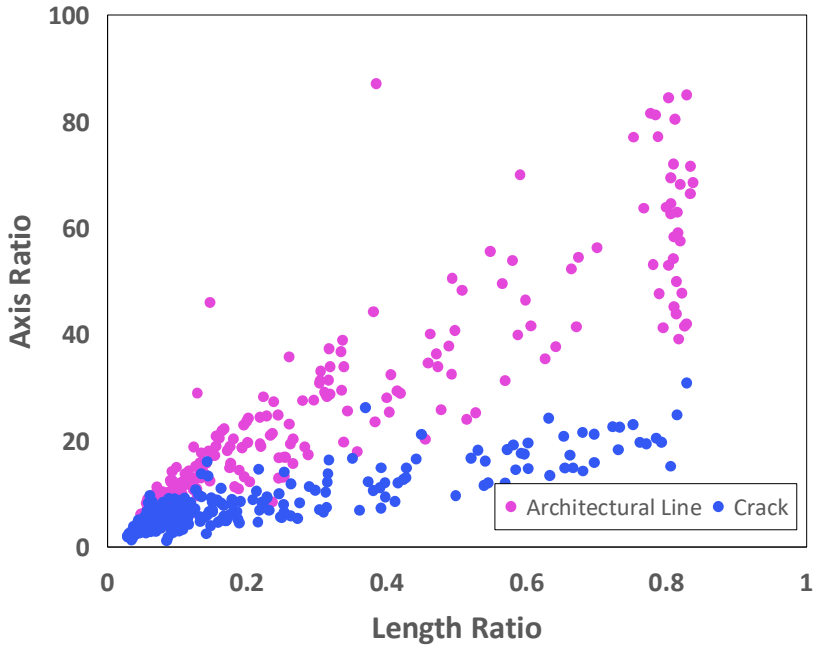
Axis Ratio
Length Ratio
Architectural Line
Crack
0
20
40
60
80
100
0.2
0.4
0.6
0.8
1

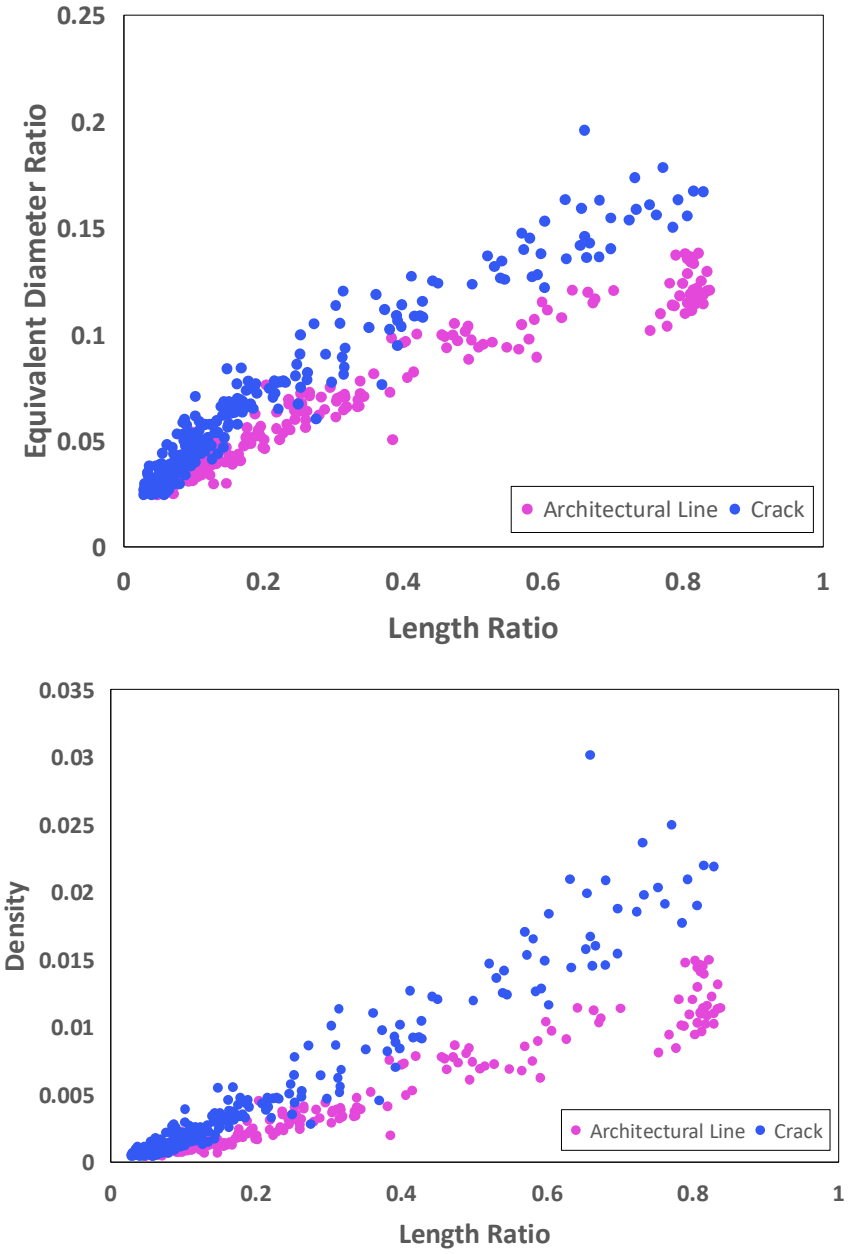

Figure 2.8. The results of connected component analysis. (Moghaddam et al. (2020))

2.2.3. SVM-based classification scheme

Applying the results of CCA, selection of a set of features to reduce the dimensions and computational complexity of data, helps describe data in lower dimensions, while maintaining the meaning of the data. Figure 2.9a visualizes well-separated data in 3D feature space, axis length ratio, orientation and length, three fundamental features used herein as input to train an SVM (Christianini and Shawe-Taylor, 2000). Regarding rammed earth images, reduction in computational complexity, resulted by CCA, as well as high degree of separability for these three parameters, yielding a high degree of variance, make our crack detector methodology a practical tool. Benefiting from these three geometrical parameters is inspired by the fact that two fundamental geometrical information, crack length and width, are often used to describe severity of cracks in monitoring and analytical approaches.

A five-fold cross-validated SVM, which exploits three dimensional feature space (Figure 2.9), is employed herein to ensure proper learning to train a binary model, to classify crack and architectural line features (Figure 2.9). 80% and 20% of data are considered herein as training and test data, yielding the accuracy of 98.10%.

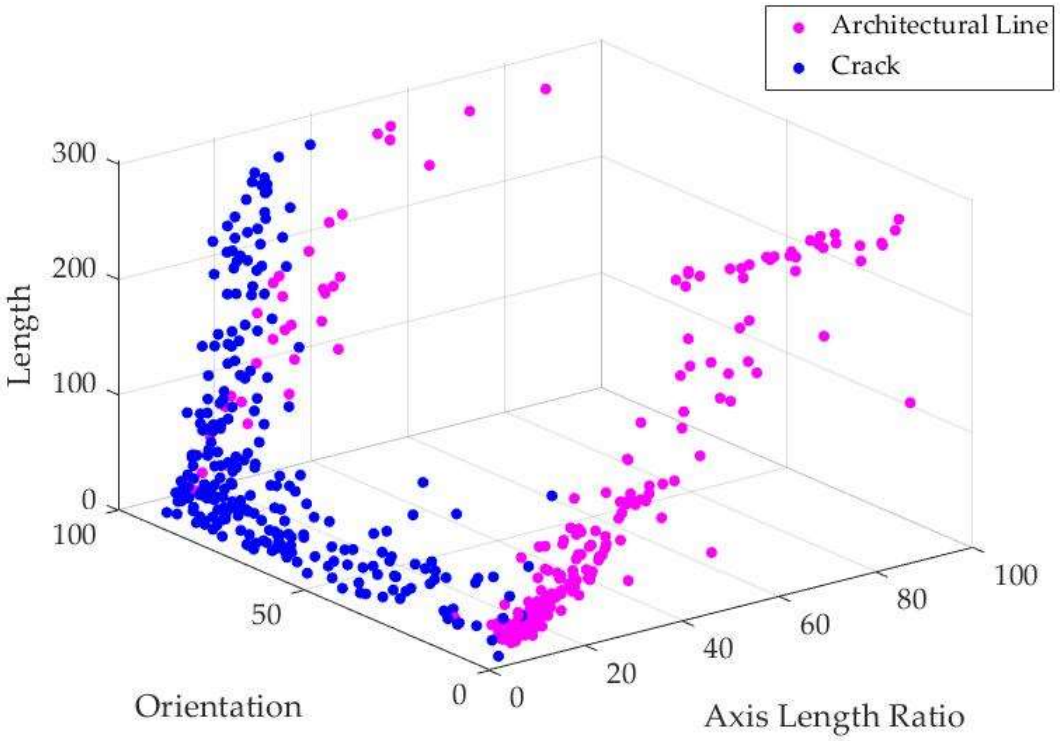

(a)

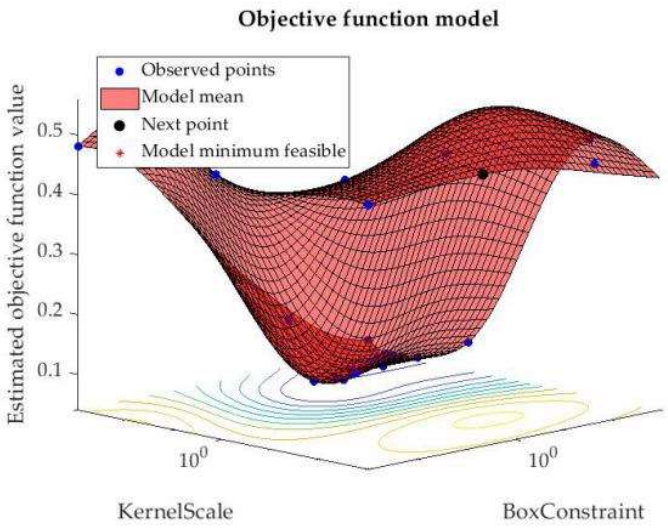

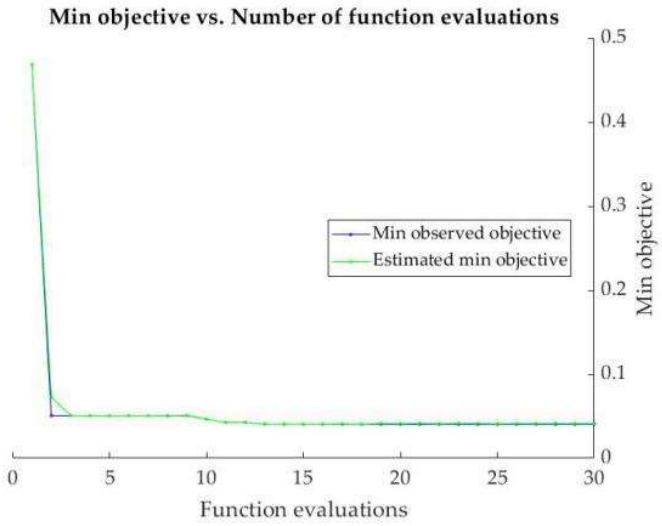

(b)

Figure 2.9. SVM-based classifier. (a) 3D feature space and (b) performance of classification. (Moghaddam et al. (2020))

2.2.4. Map generation

At this stage, to construct crack and architectural feature map, the output of classifier as well as corresponding horizontal and vertical edge pixel intensities for each CC are utilized. Therefore, all CCs with areas more than 30 pixels, in horizontal and vertical CC maps, are taken into account from largest to smallest one. Based on the result of classification obtained at previous stage, which categorizes each CC as crack or architectural feature, the corresponding pixel information from oriented horizontal and vertical edge maps is extracted. In order to generate desirable feature maps, associated pixel intensities in horizontal and vertical edge maps are added up and the procedure is repeated for all CCs, with each pixel of the whole CCs being analyzed once, yielding the output as two feature maps, ultimate crack map and architectural feature map.

2.3. Model evaluation

For evaluation of the classification and performance of proposed technique, different aspects of the methodology are investigated individually, and thus two important results are reported herein. First, some initial experiments was conducted for evaluating classification stage on a new set of data, which has not been used in training and validating the classifier, from rammed earth heritage images. The new data set for this experimentation are shown in Figure 2.10.

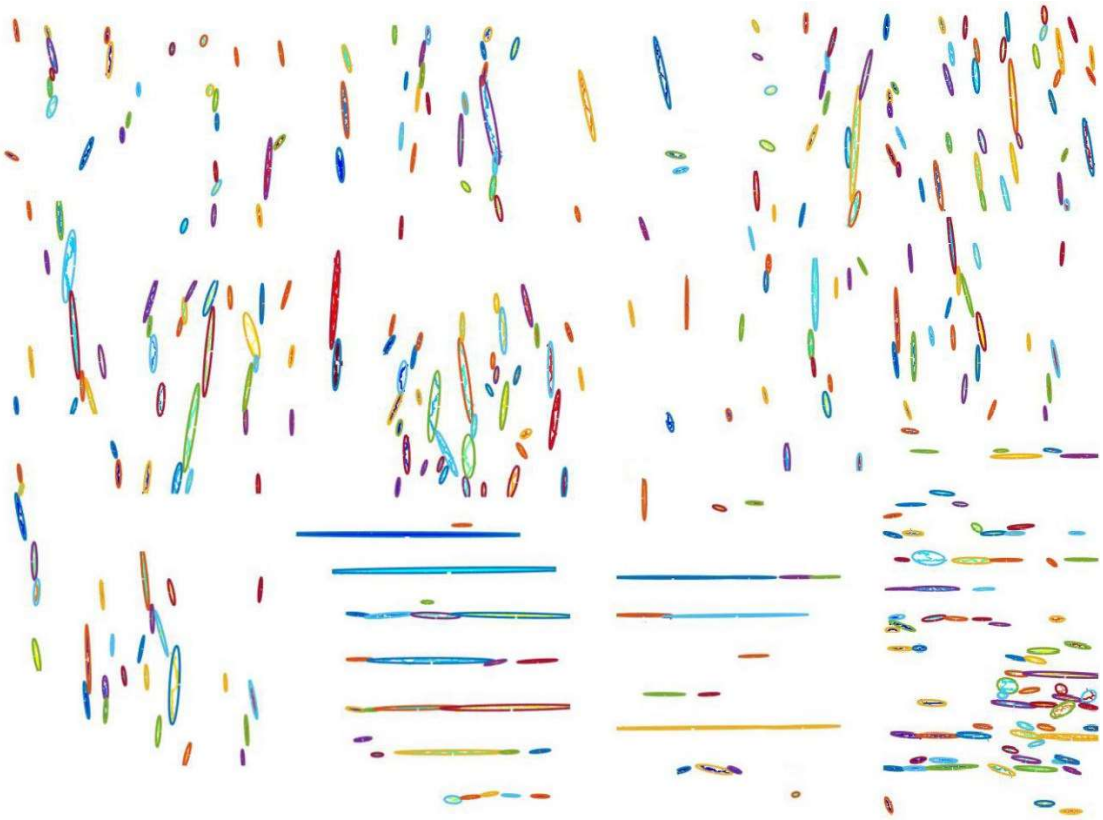

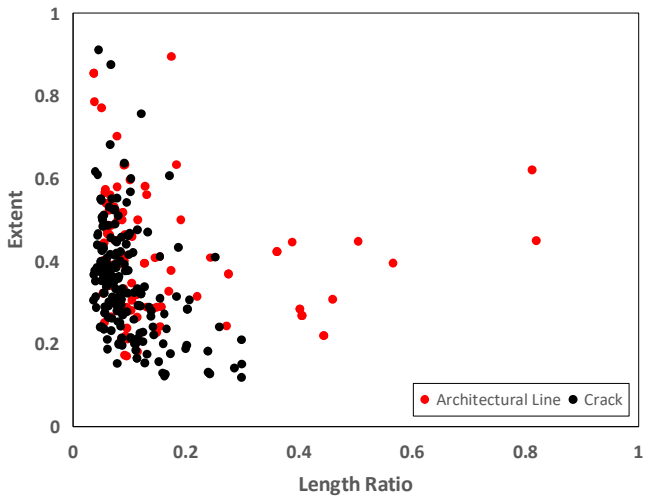
1
0.8
0.6
0.4
0.2
0
Extent
0
0.2
0.4
0.6
0.8
1
Length Ratio
Architectural Line
Crack

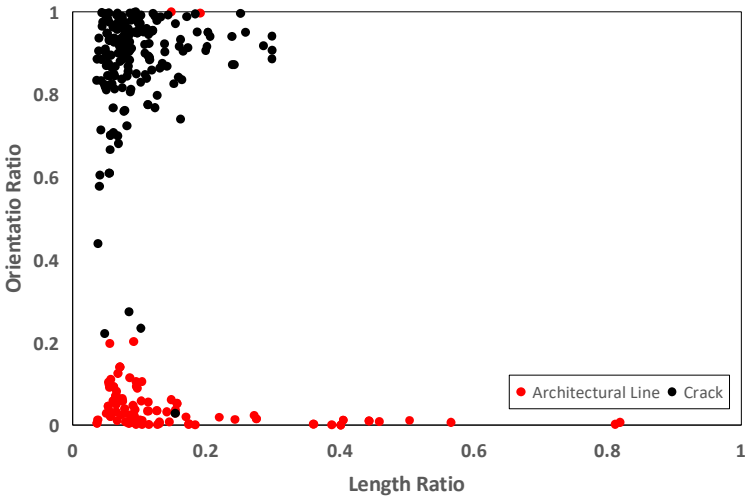
Orientatio Ratio
Length Ratio
Architectural Line
Crack
0
0.2
0.4
0.6
0.8
1

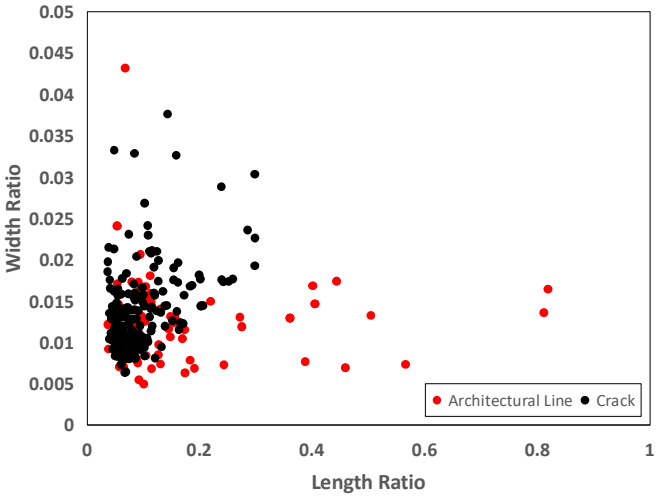
Width Ratio
Length Ratio
Architectural Line
Crack
0
0.005
0.01
0.015
0.02
0.025
0.03
0.035
0.04
0.045
0.05
0.2
0.4
0.6
0.8
1

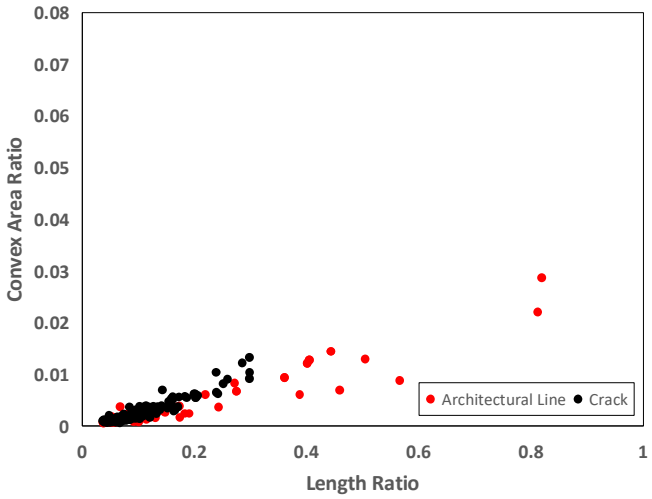
Convex Area Ratio
Length Ratio
Architectural Line
Crack
0
0.01
0.02
0.03
0.04
0.05
0.06
0.07
0.08
0.2
0.4
0.6
0.8
1

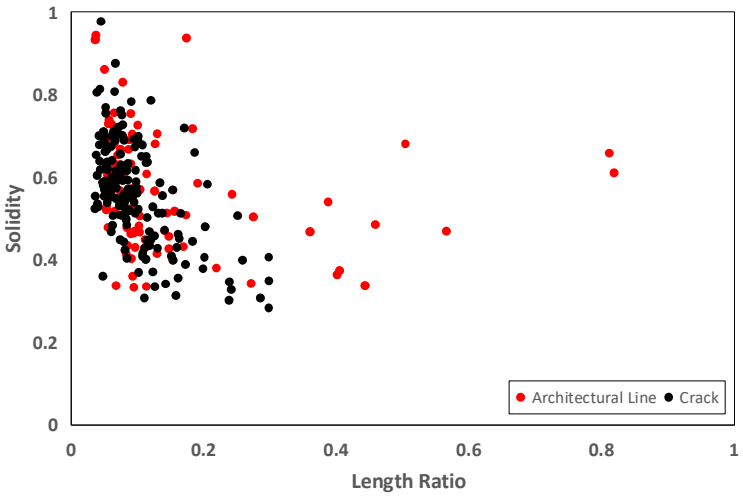
Solidity
Length Ratio
Architectural Line
Crack

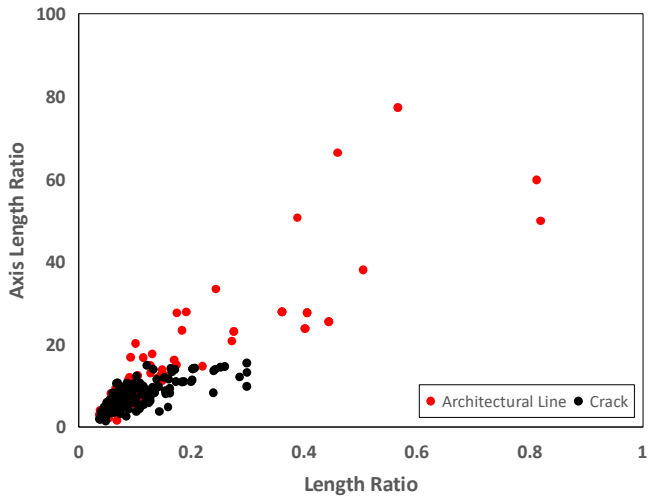
Axis Length Ratio
Length Ratio
Architectural Line
Crack

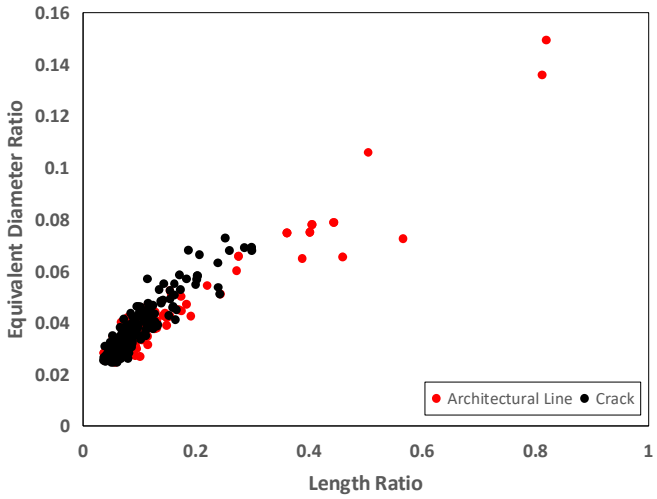
Equivalent Diameter Ratio
Length Ratio
Architectural Line
Crack

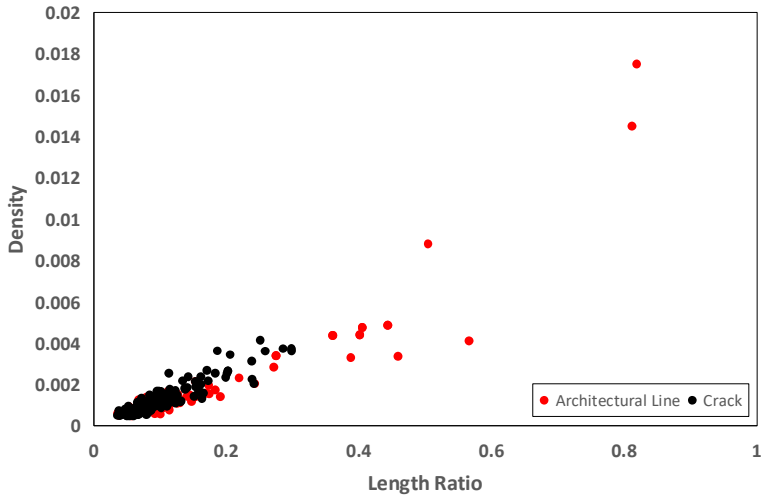

Figure 2.10. New data set for evaluation of classifier (Moghaddam et al. (2020))

As shown in Figure 2.11, this investigation also reports an analysis of the sensitivity of performance of proposed model to any variation in three fundamental features, axis length ratio, orientation and length, based on which following conclusions may be drawn

- For a specific orientation, with an increase in crack length, maximum value of axis length ratio, that model would consider as crack, increases, indicating high performance of the model in extraction of severe and thin cracks for any directions rather than horizontal and vertical ones. Its power lies in prediction of very thin cracks, which may be an indication of structural crack initiation.

- For a specific length of feature, approaching the orientation to horizontal and vertical directions, results in a decrease in boundary value of axis length ratio, highlighting the accuracy of developed algorithm in identifying the presence of very thin architectural lines, inherent to rammed earth walls, as well as severe cracks in horizontal and vertical direction.
-

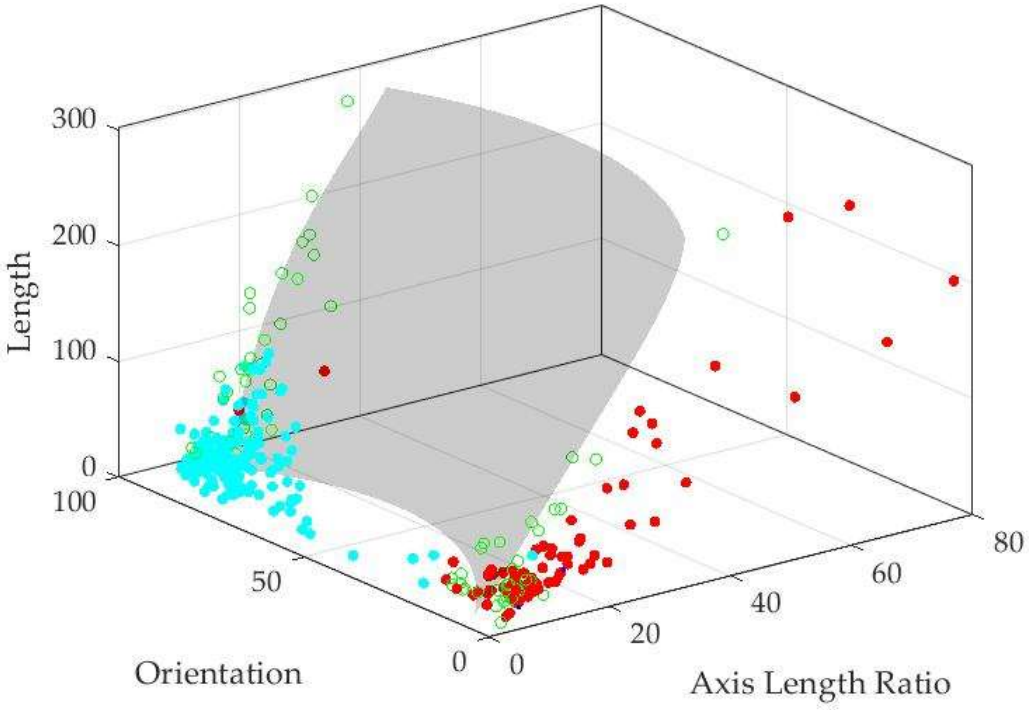

Figure 2.11. Sensitivity to three fundamental parameters in 3D feature space. (Moghaddam et al. (2020))

Figures 2.12, 2.13, 2.14 and 2.15 show results of evaluation of the performance of developed algorithm for producing crack map , with the crack and non-crack experimental labels data provided manually for equivalent ellipses. Of 287 regions examined for performance evaluation of classifier, 98.26% are reported as true positive and false negative, with false positives (0.70%) being concentrated on very thin cracks. Although the model misclassified these cracks as architectural lines, with these cracks usually representing texture cracks rather than structural ones, this misidentification can be still acceptable. Based on the results of this study, for images of rammed earth walls with very specific texture characteristics, true negatives (1.04%) may be reported.

(a)

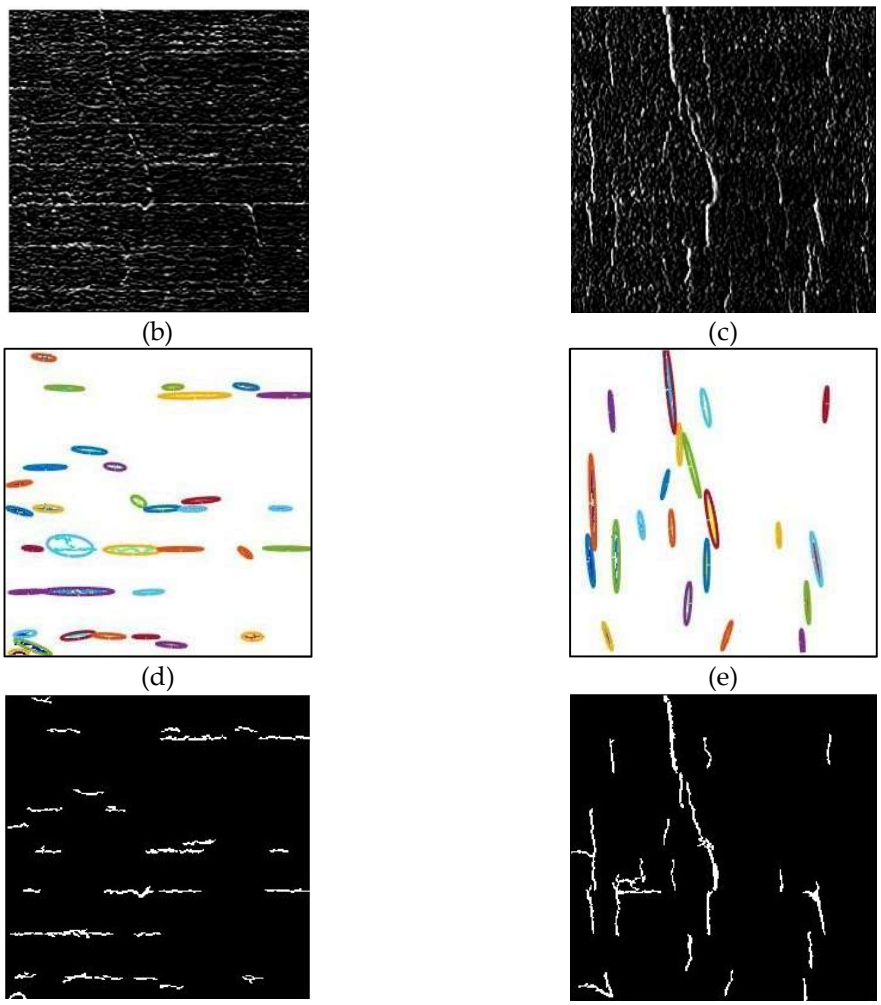

(b) (c) (d) (e) (f) (g)

Figure 2.12. Evaluation of algorithm on surface images of earthen heritage - image1. (a) Original image, (b) horizontal edge map, (c) vertical edge map, (d) horizontal CCs (area>30 pixels), (e) vertical CCs (area>30 pixels), (f) architectural line map and (g) crack map. (Moghaddam et al. (2020))

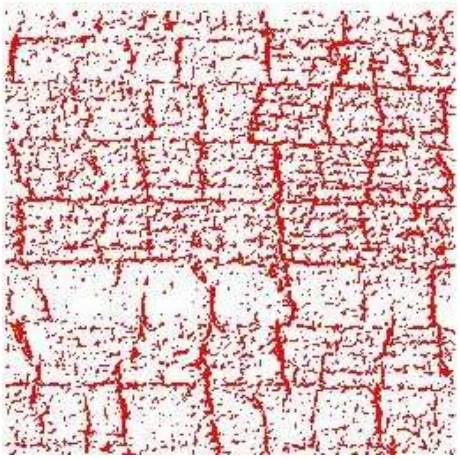

(a)

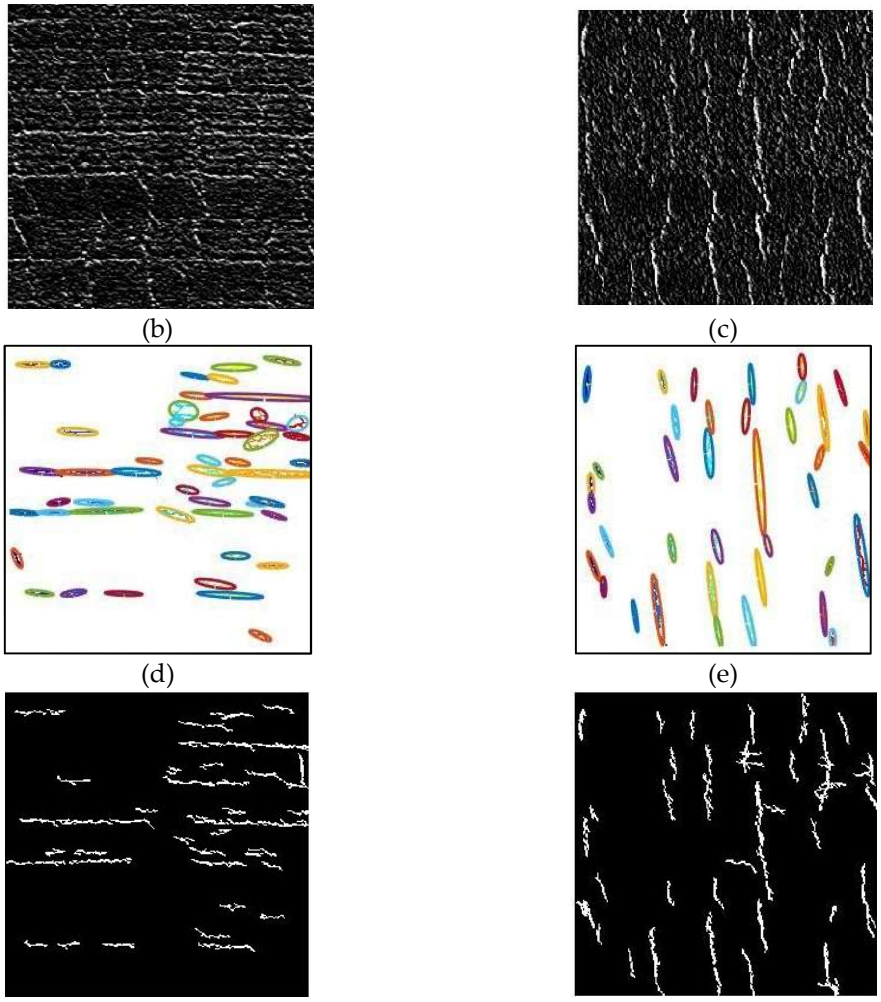

(b) (c)

(d) (e)

(f) (g)

Figure 2.13. Evaluation of algorithm on surface images of earthen heritage-image 2. (a) Original image, (b) horizontal edge map, (c) vertical edge map, (d) horizontal CCs (area>30 pixels), (e) vertical CCs (area>30 pixels), (f) architectural line map and (g) crack map. (Moghaddam et al. (2020))

(a)

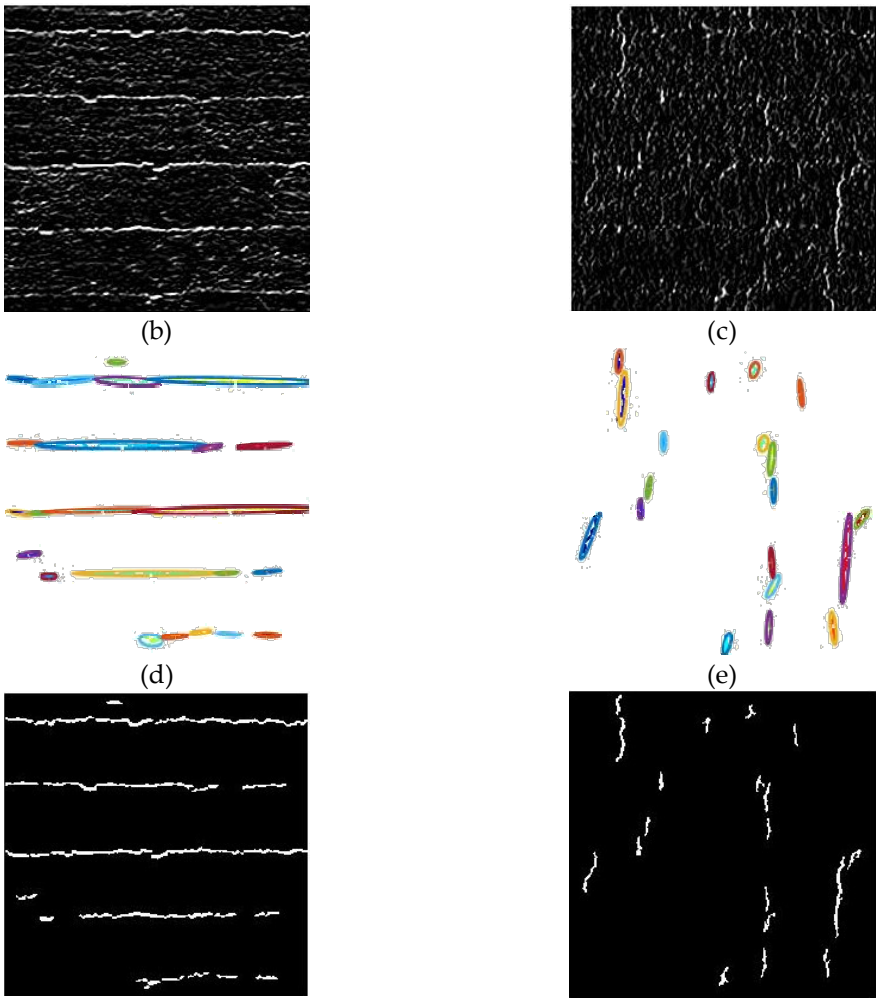

(b) (c) (d) (e) (f) (g)

Figure 2.14. Evaluation of algorithm on surface images of earthen heritage-image 3. (a) Original image, (b) horizontal edge map, (c) vertical edge map, (d) horizontal CCs (area>30 pixels), (e) vertical CCs (area>30 pixels), (f) architectural line map and (g) crack map. (Moghaddam et al. (2020))

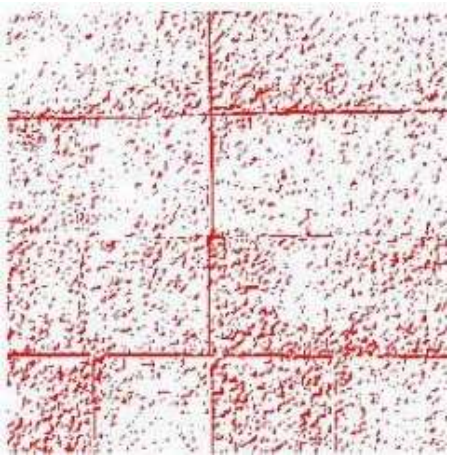

(a)

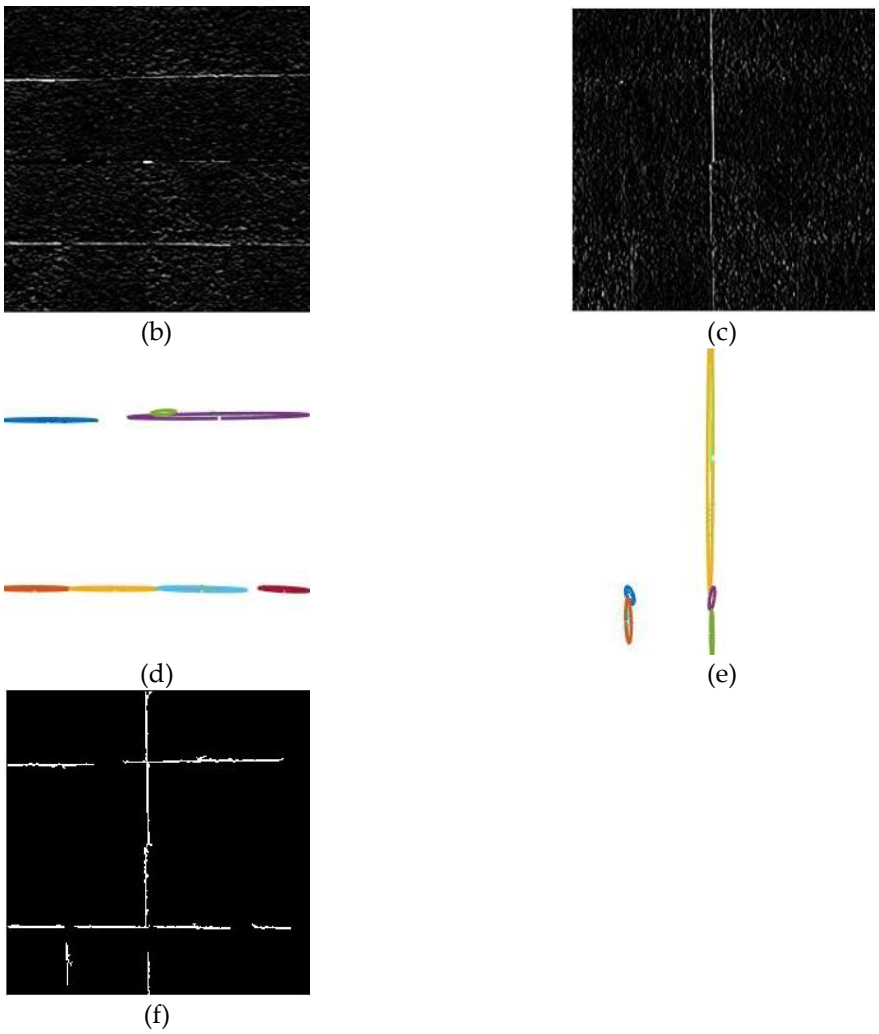

Figure 2.15. Evaluation of algorithm on surface images of earthen heritage-image 4. (a) Original image, (b) horizontal edge map, (c) vertical edge map, (d) horizontal CCs (area>30 pixels), (e) vertical CCs (area>30 pixels) and (f) architectural feature map. (Moghaddam et al. (2020))

2.4. Conclusion

Taking into account geometrical and mathematical characteristics of cracks and surface architectural features in images of rammed earth walls, the current study makes an attempt to develop an scale-invariant framework, which associates with each object morphological characteristics of equivalent ellipses. Based on an investigation in this study, three fundamental features, namely axis length ratio, orientation ratio and length ratio were found to represent objects without compromising the meaning of the data. This model extracts features in horizontal and vertical directions, separately and uses an SVM classifier to generate crack and architectural line feature maps as output. This study indicates that equivalent ellipse provides sufficiently good approximation for our purpose, with three directed morphological characteristics, axis length ratio, orientation ratio and length ratio, contributing positively to detection performance of developed algorithm for rammed earth walls. For complex images containing combination of different cracks and architectural line features and texture characteristics, with the algorithm being quite accurate at classification of horizontal texture lines, good performance of the algorithm was observed. This study highlights the ability of developed model in distinguishing severe vertical cracks and vertical

architectural lines, as well as accuracy of the model in generating crack and architectural feature maps. An still acceptable, although lower, accuracy was obtained for images containing very thin cracks, representing texture cracks rather than structural ones, than images containing the wider ones. It was observed that some true negatives may be reported in rammed earth walls with very specific texture features.

References

Adhikari, R.S.; Moselhi, O.; Bagchi, A. Image-based retrieval of concrete crack properties for bridge inspection. *Autom. Constr.* **2014**, *39*, 180–194.

Agarwal, S.; Singh, D. An adaptive statistical approach for non-destructive underline crack detection of ceramic tiles using millimetre wave imaging radar for industrial application. *IEEE Sens. J.* **2015**, *15*, 7036–7044.

Alam, S.Y.; Loukili, A.; Grondin, F.; Roziere, E. Use of the digital image correlation and acoustic emission technique to study the effect of structural size on cracking of reinforced concrete. *Eng. Fract. Mech.* **2015**, *143*, 17–31.

Anwar, S.A; Abdullah, M.Z. Micro-crack detection of multicrystalline solar cells featuring an improved anisotropic diffusion filter and image segmentation technique. *EURASIP J. Image Video Process.* **2014**, *1*, 15.

Bachman, N.; Beckenstein, F. *Wavelet analysis*; Springer, New York, 2000.

Broberg, P. Surface crack detection in welds using thermography. *NDT E Int.* **2013**, *57*, 69–73.

Brooks, W.S.; Lamb, D.A.; Irvine, S.J. IR reflectance imaging for crystalline Si solar cell crack detection. *IEEE J. Photovolt.* **2015**, *5*, 1271–1275.

Bui, Q.B.; Morel, J.C. Assessing the anisotropy of rammed earth. *Constr Build Mater*. **2009**, 23, 3005-3011.

Canny, J. A computational approach to edge detection. IEEE Trans. *Pattern Anal. Machine Intell.* **1986**, *8*, 679–698.

Chen, X.; Michaels, J.E.; Lee, S.J.; Michaels, T.E. Load-differential imaging for detection and localization of fatigue cracks using Lamb waves. *NDT E Int.* **2012**, *51*, 142–149.

Christianini, N.; Shawe-Taylor J.C. *An Introduction to Support Vector Machines and Other Kernel-Based Learning Methods*; Cambridge University Press: Cambridge, UK, 2000.

Dhital, D.; Lee, J.R. A fully non-contact ultrasonic propagation imaging system for closed surface crack evaluation. *Exp. Mech.* **2012**, *52*, 1111–1122.

Fujita, Y.; Hamamoto, Y. A robust automatic crack detection method from noisy concrete surfaces. *Mach. Vis. Appl.* **2011**, *22*, 245–254.

Glud, J.A.; Dulieu-Barton, J.M.; Thomsen, O.T.; Overgaard, L.C.T. Automated counting of off-axis tunnelling cracksusing digital image processing. *Compos. Sci. Technol.* **2016**, *125*, 80–89.

Guo, X.; Vavilov, V. Crack detection in aluminum parts by using ultrasound-excited infrared thermography. *Infrared Phys. Technol.* **2013**, *61*, 149–156.

Gunkel, C.; Stepper, A.; Müller, A.C; Müller, C.H. Micro crack detection with Dijkstra's shortest path algorithm. *Mach. Vis. Appl.* **2012**, *23*, 589–601.

Hamrat, M.; Boulekbache, B.; Chemrouk, M.; Amziane, S. Flexural cracking behavior of normal strength, high strength and high strength fiber concrete beams, using Digital Image Correlation technique. *Constr. Build. Mater.* **2016**, *106* , 678–692.

Haralick, R.M.; Shapiro, L.G. *Computer and Robot Vision, Volume I*; Addison-Wesley, 1992, pp. 28-48.

Heideklang, R.; Shokouhi, P. Multi-sensor image fusion at signal level for improved near-surface crack detection. *NDT E Int.* **2015**, *71*, 16–22.

Iliopoulos, S.; Aggelis, D.G.; Pyl, L.; Vantomme, J.; Van Marcke, P.; Coppens, E.; Areias, L. Detection and evaluation of cracks in the concrete buffer of the Belgian Nuclear Waste container using combined NDT techniques. *Constr. Build. Mater.* **2015**, *78*, 369–378.

Kabir, S. Imaging-based detection of AAR induced mapcrack damage in concrete structure. *NDT E Int.* **2010**, *43*, 461–469.

Li, X.; Jiang, H.; Yin, G. Detection of surface crack defects on ferrite magnetic tile. *NDT E Int.* **2014**, *62*, 6–13.

Jahanshahi, M.R.; Masri, S.F. Adaptive vision-based crack detection using 3D scene reconstruction for condition assessment of structures. *Autom. Constr.* **2012**, *22*, 567–576.

Marr, D. ; Hildreth, E. Theory of edge detection. In Proceedings of the Royal Society of London. Series B. Biological Sciences. 1980, 207, 187-217.

Merazi-Meksen, T.; Boudraa, M.; Boudraa, B. Mathematical morphology for TOFD image analysis and automatic crack detection. *Ultrasonics.* **2014**, *54*, 1642–1648.

Merazi-Meksen, T; Boudra, B.; Drai, R.; Boudraa, M. Automatic crack detection and characterization during ultrasonic inspection. *J. Nondestr. Eval.* **2010**, *29*, 169–174.

Moghaddam, M.Z.; Umili, G.; Messina, V.; Bonetto, S.; Ferrero, A.M.; Bollini, G.; Gandreau, D. An SVM-Based Scheme for Automatic Identification of Architectural Line Features and Cracks. Appl. Sci. 2020, 10, 5077.

Mohan, A.; Poobal, S. Crack detection using image processing: A critical review and analysis. *Alex. Eng. J.* **2018**, *57*, 787–798.

Nazaryan, N.; Campana, C; Moslehpour, S; Shetty, D. Application of a He–Ne infrared laser source for detection of geometrical dimensions of cracks and scratches on finished surfaces of metals. *Opt. Lasers Eng.* **2013**, *51,* 1360–1367.

Otsu, N. A threshold selection method from gray-level histograms. IEEE Trans. *Syst. Man Cybern.* **1979**, *9*, 62–66.

Parker, J.R. *Algorithms for image processing and computer vision;* Wiley, New York, 1997.

Prewitt, J.M.S. Object enhancement and extraction. In Picture Processing and Psychopictorics; Lipkin, B., Rosenfeld, A., Eds.; Academic Press: New York, NY, USA, 1970.

Rodrı´ guez-Martı´na, M.; Lagu¨ elaa, S.; Gonza´ lez-Aguileraa, D.; Martinezb, J. Prediction of depth model for cracks in steel using infrared thermography. *Infrared Phys Technol.* **2015**, *71*, 592–600.

Sinha, S.K.; Fieguth, P.W. Automated detection of cracks in buried concrete pipe images. *Autom. Constr.* **2006**, *15*, 58–72.

Talab, A.M.A; Huang, Z.; Xi, F.; HaiMing, L. Detection crack in image using Otsu method and multiple filtering in image processing techniques. *Optik – Int. J. Light Electron Opt.* **2016**, *127*, 1030–1033.

Vidal, M.; Ostra, M.; Imaz, N.; Garcı´a-Lecina, E.; Ubide, C. Analysis of SEM digital images to quantify crack network pattern area in chromium electrodeposits. *Surf. Coat. Technol.* **2016**, *285*, 289–297.

Wang, P.; Huang, H. Comparison analysis on present image-based crack detection methods in concrete structures. In Proceedings of the 2010 3rd International Congress on Image and Signal Processing (CISP2010), Yantai, China, 16-18 October 2010; pp. 2530–2533.

Wolf, J.; Pirskawetz, S.; Zang, A. Detection of crack propagation in concrete with embedded ultrasonic sensors. *Eng. Fract. Mech.* **2015**, *146*, 161–171.

Xu, C.; Xie, J.; Chen, G. Weiping Huang, An infrared thermal image processing framework based on superpixel algorithm to detect cracks on metal surface. *Infrared Phys. Technol.* **2014**, *67*, 266–272.

Yamaguchi, T.; Hashimoto, S. Fast crack detection method for large-size concrete surface images using percolationbased image processing. *Mach. Vis. Appl.* **2010**, *21*, 787–809.

Yiyang, Z. The design of glass crack detection system based on image preprocessing technology. In 2014 IEEE 7th Joint International Information Technology and Artificial Intelligence Conference, Chongqing, China, 20-21 Decembre 2014; pp. 39–42.

Zhang, Y.; Wu,L. Classification of fruits using computer vision and a multiclass support vector machine. *Sensors* **2012**, *12*, 12489-12505.

CHAPTER 3

Assessing size effect on strength characteristics of compacted earth for the analysis of earthen buildings

This chapter deals with the quantification of size effect on mechanical strength characteristics of compacted earth material. The role of water content is also discussed. The aim of this work is to provide a simple and useful framework to improve the analysis and interpretation of uniaxial compressive strength for the characterization of earth building materials. Motivated by the difficulty in comparing the uniaxial compressive strength (UCS) of rammed earth specimens in a great variety of geometrical characteristics in literature, this study attempts to extend the current understanding of the size effect on compressive strength of compacted earth. This research focuses on two different areas: 1) the behaviour of soils during the uniaxial compression loading is investigated and experimental data for size effect modelling is obtained from the literature; 2) an analytical approach is developed for the establishment of the compressive strength–size relationship for rammed earth specimens. The present research is the very first analytical approach to size effect in characterization of mechanical strength in rammed earth materials. This data and approach will help in advancing research in the field.

3.1. Introduction

It is well established that earth is one of the most ancient building materials. Depending on the way of implementation, the concept of earthen structures involves several building techniques practiced in different parts of the world, among which rammed earth constitutes one of the most widely used structural type. Based on the materials available at different sites, rammed earth architecture is characterized by many varieties of features that vary from place to place.

A rammed earth wall (Figure 3.1) is composed of compacted layers of moistened earth. To make a rammed earth wall, soil mixture, ideally sandy-clayey gravels, is poured into formwork and compacted in layers. The temporary formwork, which defines the walls thickness and the rammed earth block length, is moved from section to section, horizontally and vertically, until the desired height of the wall is achieved.

Figure 3.1. Rammed earth house (Moghaddam et al. (2020))

To date, several studies on rammed earth (RE) have been conducted by considering several aspects of the material, such as durability, environmental impact, thermal and mechanical properties. Studies on the characterization of RE are of great significance as their importance is twofold.

First, a huge number of existing buildings in the world is composed of raw earth as it is estimated that 30–40% of the world's population currently lives in structures built with raw earth (Hall and Djerbib (2004)). Among these buildings, some of earth-based structures are important elements of the world heritage, with surviving examples discovered in many diverse locations around the world (Miccoli et al. (2014)). Within this frame, conservation and restoration of earthen cultural heritage is firmly bound to the characterization of existing earth materials, which quantitatively helps in solid understanding of structural aspects of the historical buildings, upon which appropriate conservation strategies are based.

Second, rammed earth constructions are acknowledged to present sustainability. The modern interest in earth as a building material throughout the world is largely derived from an increasing awareness in environmental issues and recognized sustainability of earth-based materials (Bui et al. (2014)). Clearly, earth structures can boost excellent sustainability credentials as well as good thermal and acoustic properties (Ciancio et al. (2013)).

The greatest difficulty for application of earth material in modern structures is the variability of resulting properties, which is linked to the variability of soil characteristics. In the case of earth-based structures, the choice of soil type is generally restricted to those available near the site. Mechanical characteristics vary from one site to another and are dependent on available local soil. On the other hand, the earth heritage is well represented throughout the world. Several examples of historical rammed earth structures survive to this day. There are many different historical sites, which can be characterized by different in situ soils. For each of those, the laboratory determination of uniaxial compressive strength (UCS) must be checked for design purposes for new structures and conservative plans for existing structures.

Engineering understanding of rammed earth behavior is firmly bound to the body of laboratory work developed on mechanical characterization, which allows comparative analysis of performance of different soils as building materials and development of recommendations and guidelines for design of modern buildings and conservation and restoration of ancient structures. To ensure safety of existing structures and successful design

and application of modern materials, the required strength of the compacted earth must be adequately evaluated.

Laboratory determination of strength, and the specifications derived from it, are thus adopted as key elements in guiding the design and ensuring that appropriate conservation strategies are achieved. The greatest difficulty for the characterization of earthen material in practice is the variability of specimen geometry such as shape and dimension from one study to another, which makes the comparative and performance analysis of compacted earth challenging. Although some authorities provide limited guidance on specimen size (ASTM D 2166-00 (2002), BSI (1377), Das (2002)), there is no clear consensus in the literature and among the standards. In spite of these obstacles, design methods in routine practice are based on unconfined compressive strength of small-scale specimens. However, they might not be reliable in predicting the strength that might be achieved for larger specimens found in practice. However, different from other building materials such as concrete and masonry, there is a distinct lack of formal technical guidance concerning size effect on strength characteristics of earth materials. The coefficients adopted for size effect in rammed earth are usually those developed for concrete.

Development of constitutive models for analysis of existing and design and construction of modern earth structures is hence a complex task because of the nature of the varying specimen size conditions and range of properties of the materials available in the literature. The link between the mechanical behavior of the RE wall and the specimen size should be considered in successful design and appraisal of earthen structures, through an approach that deduce strength-sample size criterion for different types of earth-based materials.

Due to the intrinsic challenges associated with the characterization of rammed earth materials, a rigorous comparative studies on the physical properties, and mechanical behavior of compacted earth with very different specimen sizes, requires an analytical framework that takes into account influence of geometry on measured strength.

Mechanical characterization of unstabilized and stabilized RE has been addressed by many researches (Hall and Djerbib (2004), Miccoli et al. (2014), Bui et al. (2014), Ciancio et al. (2013) ,Cheah et al. (2012), Ciancio and Gibbings (2012), Jaquin et al. (2009), Olivier and Mesbah (1995), Burroughs (2001), Hall and Djerbib (2004), Hall and Djerbib (2006), Hall and Djerbib (2006), Bui et al. (2008), Bui and Morel (2009), Bui et al. (2013), Jayasinghe and Kamaladasa (2007), Morel and Pkla (2002)). The laboratory determination of the UCS has been carried out by some studies (Miccoli et al. (2017), Silva et al. (2018), Wangmo et al. (2019), Martín-del-Rio et al. (2019), Parracha et al. (2019), Canivell et al. (2018), Silva et al. (2018), El Hajjar et al. (2018), Bruno et al. (2017), Beckett et al. (2018)) on (1) characterization of ancient earthen material in existing architectural heritage and (2) characterization and design of modern rammed earth material. However, a review of literature on rammed earth material reveals that specimens have been produced in a great variety of sizes. Compressive strength of rammed earth material from a later medieval earthen building at Ambel (near Zaragoza, Spain) has been studied by Miccoli et al. (2017) using a cubic specimen 10 cm × 10 cm × 10 cm. Cylindrical specimens (100 mm diameter and 200 mm height) were manufactured by Silva et al. (2018) to assess the compressive strength of the rammed earth material representative of unstabilised rammed earth walls from Alentejo region. Wangmo et al. (2019) determined the strength characteristics of an ancient rammed earth material in Bhutan using cylindrical test samples of sizes about 92 mm diameter and 180 mm height. In the research carried out by Martín-del-Rio et al. (2019), mechanical strength of rammed earth samples from Almohade ramparts of Seville and Malaga under compression was determined with cubic specimens 6–10 cm. The uniaxial compression tests were performed by Parracha et al. (2019) on unstabilized earthen samples with dimensions of 2.00 cm × 0.60 cm × 0.40 cm and 2.00 cm × 0.60 cm × 0.40 cm, collected from the walls of ancient buildings in the Leiria region.

Canivell et al. (2018) studied UCS of cubic specimens 10 cm × 10 cm × 10 cm. Compression tests were performed by Silva et al. (2018) on representative cylindrical specimens, with 150 mm diameter and 300 mm height, manufactured during the construction of modern rammed earth walls. Hajjar et al. (2018) performed a series of unconfined compression tests on cylindrical specimens with a height of 10 cm and a diameter of 5 cm, produced using soil collected from an existing construction site in the vicinity of Vienne in the Auvergne-Rhône-Alpes region in France. Cylindrical samples of 50 mm diameter and 100 mm height have been studied by Bruno et al. (2017) to characterize compressive strength of compacted soil provided by a brickwork factory from the region of Toulouse (France). Beckett et al. (2018) manufactured 100 mm cube specimens for UCS testing of rammed earth material. This is not an exhaustive list of specimen geometries used for laboratory characterization of rammed earth material but it does illustrate the broad range of specimen sizes used.

As specimens are produced in a great variety of sizes, the influence of geometry on measured strength is normally not taken into account. The study of the strength properties of RE currently has gaps in linking properties, such as specimen size and shape, with the mechanical characteristics. An important topic still needing more investigation is the relationship between strength characteristics and geometry of specimens. This highlights the need for the development of strength-size relationship, which acts as a standardized framework for comparison between different specimens, in order to readily achieve the specified requirements. However, to the author's knowledge, the influence of specimen size on characterization of strength of earth-based materials has not been addressed in the literature yet. This may be one of the reasons behind this research on correlation between strength and specimen geometry for rammed earth material. This correlation is of great practical interest due to the fact that, after establishing this relationship, knowing strength properties of earth material for one specimen geometry will make it possible to estimate the strength for another specimen size.

Questions about the assessment or comparison of compacted earth material performance are difficult to answer, given the diversity of specimen shapes, specimen dimensions and material. This difficulty highlights the need for the establishment of an internationally acknowledged analytical framework that could, in the future, be adopted as standards for measuring the engineering properties of compacted earth materials. The purpose of this research is to develop a clear understanding of the compressive strength properties of rammed earth, considering that the relationship between strength properties and geometrical factors in establishing material behaviour is one major reason for the difficulties in conservation of rammed earth. Size effect is also responsible for the difficulties in putting experimental results of UCS into design practice. The difficulty lies in the comparative analysis of the compressive strength of different materials at various dimensions. Therefore, given the results of previous investigations, the effect of specimen size on compressive strength of rammed earth is unclear. This research focuses on two different areas: 1) the behaviour of soils during the uniaxial compression loading is investigated and experimental data for size effect modelling is obtained from the literature; 2) an analytical approach is developed for the establishment of the compressive strength–size relationship for RE specimens.

3.2. Size effect on mechanical strength of compacted earth

3.2.1. An overview of the existing experimental data

Several studies have investigated the strength characteristics of rammed earth materials (Miccoli et al. (2017), Silva et al. (2018), Wangmo et al. (2019), Martín-del-Rio et al. (2019), Parracha et al. (2019), Canivell et al. (2018), Silva et al. (2018), El Hajjar et al. (2018), Bruno et al. (2017), Beckett et al. (2018)). However, very few studies have investigated the effect of the height to width (H/W) ratio on the UCS of compacted earth (Patty and Minium (1945), Walker (1997), Walker (2004), Maniatidis and Walker (2008), Venkatarama Reddy and Prasanna Kumar (2011), Güneyli and Rüşen (2015), Tripura (2015), Merga (2016), Lan et al. (2018), Rengifo-Lópeza et al. (2019)). These studies associated with their experimental data have been summarized in Table 3.1. Figure 3.2 shows granulometry properties of unstabilized earth (UE) and stabilized earth (SE) investigated by these studies.

Patty and Minium (1945) assessed the size effect by performing two sets of uniaxial compression tests on rammed earth materials. In order to investigate ratio of the height of the specimen to its compressive strength, so as to determine the correction coefficient, two series of cylindrical and block specimens was made in three different heights. This study confirms the inverse relationship between the strength and the height of the test piece for rammed earth material.

Walker (1997) carried out an experimental research program to study the influence of geometry on compressive strength of compressed earth unit blocks. They concluded that compressive strength behaviour for the fabricated blocks was influenced by restraint effect reduction at higher aspect ratios (height/thickness). Experimental results revealed that block compressive strengths are closely related to unit aspect ratios and due to reduction in platen restraint effect, blocks with higher aspect ratio obtain lower compressive strength values. Strength reduction was less rapid when specimen aspect ratios were more than 2, with noticeable diagonal shearing mode of failure of the specimen as well as the material spalling associated with crushing.

Walker (2004) assessed the influence of specimen geometry on strength characteristics. This study also considers the effect of water content on the strength of compressed earth blocks associated with specimen size and reports dry and wet compressive strength for soil specimens. They confirmed that platen restraint results in significant influence of block geometry on recorded compressive strength of prismatic specimens.

Maniatidis and walker (2008) experimentally investigated load bearing capacity of rammed earth material, including small-scale 100 mm × 200 mm cylinders, large-scale 300 mm × 600 mm prisms, and nine full-scale columns of three different series, each 300 mm wide by 300 mm thick, comprising of three specimens from each series with approximate heights of 1.8 m, 2.4 m, and 3.0 m.

Venkatarama Reddy and Prasanna Kumar (2011) investigated the strength and structural behavior of rammed-earth specimens and discussed results of the compressive strength of prisms, wallettes, and story-high walls. They studied the effect of geometry and slenderness on strength of earthen material by carrying out compression test on specimens with dimensions of 150 mm × 150 mm × 300 mm, 600 mm × 155 mm × 720 mm and 750 mm × 152 mm × 3000 mm. They observed a nearly 30% reduction in strength as the height-to-thickness ratio increases from about 4.65 to 19.74. The shear failures developed in the story-high walls resembled the shear failures of short-height prism and wallette specimens.

Güneyli and Rüşen (2015) examined the effect of specimen size on the UCS values and failure pattern of the specimens of four clay soils, including Handere clay, Samtekin clay, Almanpinari clay, and Kaolin clay. They performed unconfined compressive strength tests on eleven different sizes of cylindrical specimens with diameter of 48 mm and

length-to-diameter (H/D) ratios ranging from 0.5 to 3. They concluded that increasing H/D ratios up to 3 decreases the UCS values in the cylindrical samples of four types of soil.

Another observation confirms that the standard deviation of the unconfined compressive strength value for specimens of four types of soil increases considerably with increasing H/D ratio and the variation of the standard deviation is more profound for higher H/D ratios. On the other hand, they concluded that higher H/D ratio causes brittle deformation, characterized by a distinct failure plane, to predominate. The failure mechanism of soil specimens is mostly complex and chaotic at larger H/D ratios. The failure pattern changes from brittle to ductile with decreasing H/D ratio. They highlighted the importance of development of correction equations for converting the UCS values of non-standard-sized clay soil samples to ''standard'' UCS values, for application in engineering practice. Based on an analysis of the results, correction formulas were determined for the four types of soil tested. In this sudy "standard'' UCS values were considered to correspond to the UCS values for H/D ratios of 2, 2.5 and 3.

Tripura (2015) experimentally investigated the behaviour of rammed earth cylinders and prisms, and large-scale specimens, of square, rectangular and circular sections, under axial compression. Uniaxial compression tests were performed on 45 full-scale rammed earth specimens of three different cross sections, 150 mm × 150 mm, 190 mm × 150 mm and 230 mm × 150 mm, each with approximate heights of 0.9 m, 1.2 m, and 1.5 m, constructed using the soil collected from Agartala, Northeast India. Tripura (2015) observed that the lateral and vertical displacement increases with increasing the value of height to width ratio. Specimens with the least height to width ratio were found to possess the highest value of peak strength and the least standard deviation. Vertical cracks were initially formed at the platen-column interface. The specimens failed with the development of shear failure zones, at top and bottom, and tension failure zone in the middle of the specimen leading to splitting at the later stages of loading.

Merga (2016) carried out unconfined compression tests on compacted red clay soil samples in Addis Ababa with four various H/D ratios ranged from 1 to 2.5. The diameter of specimens was 38 mm. They investigated the effect of the specimen size on the stress-strain behavior of compacted cylindrical specimens at different moisture contents. The study demonstrated that the specimens with H/D=1 attains its peak strength at large axial strains and peak strain value tends to decrease considerably as specimen H/D increases. They concluded that the values of uniaxial peak strength were found to be much higher in samples with an H/D ratio of 1. The strength of the soil specimen significantly decreases with increasing the H/D ratio from 1 to 2.5. In addition, the failure mechanism of soil is highly influenced by sample height. The failure pattern generally changes from uniform to non-uniform as H/D ratio of the specimen increases. For the H/D=1, the failure plane and deformation are uniformly distributed within the entire of specimen height and as the specimen H/D ratio increases, the deformation and failure distribution becomes quite complex and are localized to some portions of the specimens.

Lan et al. (2018) performed unconfined compression tests on cubic and cylindrical compressed earth to evaluate the influence of specimen geometry on the compressive strength and strain properties of compressed earth blocks. They concluded that the combined influence of platen constraint effect and distribution and inhomogeneity of earth materials defects causes the unconfined compressive strength to decrease for higher specimen sizes. Moreover, they noticed that the failure pattern of cylindrical specimens shows columnar distribution with lateral sides tending to spall, while cubic specimens mainly fail due to the cracks in the corners and the exfoliation of the lateral sides.

Lopez et al. (Rengifo-Lópeza et al. (2019)) investigated the effect of specimen geometry and shape, i.e., aspect ratio and height-to-width ratio on the compressive strength and stress-strain response of compressed earth blocks through uniaxial compression tests.

Experimental results show a significant increase in compressive strength at decreasing aspect ratios, which can be attributed to the confinement effect exerted by the loading platens on prismatic specimens. In addition, strain distribution along the height of a prismatic specimen is highly influenced by the aspect ratio. Approximately uniform strain distribution is observed only in the middle-third portion of specimens with an aspect ratio of 2.0. Instead, the combined effect of boundary conditions and propagation of cracks throughout the specimens results in a non-uniform strain profile in specimens with an aspect ratio of 0.7 and 1.2.

Table 3.1. Experimental data on size effect

Reference study	Specimen type	Number of specimens	Granulometry	D50 (mm)	D60 (mm)	Compaction characteristics	Length (mm)	Width (mm)	Height (mm)	Compressive strength (MPa)	Water Content (%)	Dry density (D) or Weight (W) at test
Patty and Minium (1945)	Prismatic	4	Clay&Silt (<0.075 mm) = 25.18% Sand (0.075-6.35 mm) = 55.95% Gravel (>6.35 mm) = 18.87%	0.65	1.4	-	228.6	228.6	56.896	8.5	0.33	W = 6.804 kg
		4				-	228.6	228.6	111.76	4.6	0.45	W = 43.608 kg
		4				-	228.6	228.6	169.418	2.3	0.85	W = 110.412 kg
		4				-	228.6	228.6	226.06	1.3	1.32	W = 214.123 kg
	Cylindrical	4	Clay&Silt (<0.075 mm) = 89.641% Sand (0.075-6.35 mm) = 10.359%	-	-	Compaction with a 18-pound steel hand rammer		228.6	101.6	6.2	The specimens were stored in the temperature of 65 to 70F for six months	W = 5.153 kg
		4						228.6	152.4	4.7		W = 24.493 kg
		4						228.6	228.6	2.5		W = 61.732 kg
	Cylindrical	4	Clay&Silt (<0.075 mm) = 62.44% Sand (0.075-6.35 mm) = 36.071% Gravel(>6.35 mm) = 2.488%	-	-			228.6	101.6	7.0		W = 6.672 kg
		4						228.6	152.4	6.5		W = 31.528 kg
		4						228.6	228.6	4.3		W = 78.662 kg
	Cylindrical	4	Clay&Silt (<0.075 mm) = 25.18% Sand (0.075-6.35 mm) = 55.95% Gravel(>6.35 mm) = 18.87%	0.65	1.4			228.6	101.6	7.0		W = 6.740 kg
		4						228.6	152.4	5.2		W = 33.040 kg
		4						228.6	228.6	3.4		W = 84.502 kg
Walker (1997)	Prismatic	5	Fine gravel (2-6 mm) = 8.2% Coarse sand (0.6-2 mm) = 32.8% Medium sand (0.2-0.6 mm) = 25.4% Fine sand (0.06-0.2 mm) = 18.4% Silt (0.002-0.06 mm) = 4% Clay (<0.002 mm) = 11.2% Cement = 10%	0.42	0.6	Standard proctor for optimum moisture Content Compaction pressure = 2 MN/m2	40	20	12	5.7	Prior to testing, blocks were immersed in a curing tank for 24 hours.	-
		5					40	20	22	4.7		-
		5					40	20	41	4.0		-
		5					40	20	64	3.0		-
		5					40	20	86	2.1		-
		5					40	20	107	2.6		-
		-					295	140	120	6.4		-
	Prismatic	5					40	20	12	7.8	Prior to testing, blocks were oven-dried.	-
		5					40	20	22	6.4		-
		5					40	20	41	3.0		-
		5					40	20	64	5.0		-
		5					40	20	86	3.4		-
		5					40	20	107	2.3		-
		-					295	140	120	12.5		-
	Prismatic	5	Fine gravel (2-6 mm) = 12.4% Coarse sand (0.6-2 mm) = 29.6% Medium sand (0.2-0.6 mm) = 19.8% Fine sand (0.06-0.2 mm) = 14.8% Silt (0.002-0.06 mm) = 4% Clay (<0.002 mm) = 19.4% Cement = 5%	0.4	0.65		140	70	23	3.4	Prior to testing, blocks were immersed in a curing tank for 24 hours.	-
		5					140	70	47	1.1		-
		5					140	70	77	1.0		-
		5					140	70	113	0.5		-
		-					295	140	120	2.2		-
	Prismatic	5					140	70	23	7.5	Prior to testing, blocks were oven-dried.	-
		5					140	70	47	3.0		-
		5					140	70	77	2.2		-
		5					140	70	113	1.0		-
		-					295	140	120	5.5		-
Walker (2004)	Prismatic	5	Sand (0.06-2 mm) = 78%	0.27	0.38	Compaction pressure = 1.1 MPa	295	140	45	5.8	Prior to testing, blocks were	D = 1775 kg/m^3
		5					295	140	96	4.4		D = 1851 kg/m^3

		5	Silt (0.002-0.06 mm) = 11% Clay (<0.002 mm) = 11% Cement = 5%				294	140	125	3.9	immersed in a curing tank for 24 hours.	D = 1829 kg/m^3
		5					225	110	81	3.8		D = 1851 kg/m^3
	Prismatic	5					295	140	45	16.0	Prior to testing, blocks were oven-dried.	D = 1775 kg/m^3
		5					295	140	96	10.2		D = 1851 kg/m^3
		5					294	140	125	8.5		D = 1829 kg/m^3
		5					225	110	81	12.8		D = 1851 kg/m^3
	Prismatic	5	Fine gravel (2-6 mm) = 8% Sand (0.06-2 mm) = 77% Silt (0.002-0.06 mm) = 4% Clay (<0.002 mm) = 11% Cement = 10%	0.37	0.52	Compaction pressure = 1.8 MPa	40	20	12	10.3	Prior to testing, blocks were immersed in a curing tank for 24 hours.	D = 1775 kg/m^3
		5					40	20	22	6.9		D = 1775 kg/m^3
		5					40	20	41	5.4		D = 1775 kg/m^3
		5					40	20	64	5.2		D = 1775 kg/m^3
		5					40	20	86	3.5		D = 1775 kg/m^3
		5					40	20	107	4.2		D = 1775 kg/m^3
	Prismatic	5					40	20	12	11	Prior to testing, blocks were oven-dried.	D = 1775 kg/m^3
		5					40	20	22	11.2		D = 1775 kg/m^3
		5					40	20	41	6.1		D = 1775 kg/m^3
		5					40	20	64	8.3		D = 1775 kg/m^3
		5					40	20	86	6.4		D = 1775 kg/m^3
		5					40	20	107	4.5		D = 1775 kg/m^3
	Prismatic	5	Fine gravel (2-6 mm) = 13% Sand (0.06-2 mm) = 63% Silt (0.002-0.06 mm) = 4% Clay (<0.002 mm) = 20% Cement = 5%	0.32	0.51	Compaction pressure = 1.8 MPa	140	70	23	5.4	Prior to testing, blocks were Immersed in a curing tank for 24 hours.	D = 1644 kg/m^3
		5					140	70	47	1.8		D = 1620 kg/m^3
		5					140	70	77	1.2		D = 1616 kg/m^3
		5					140	70	113	0.6		D = 1567 kg/m^3
	Prismatic	5					140	70	23	8.8	Prior to testing, blocks were oven-dried.	D = 1644 kg/m^3
		5					140	70	47	4		D = 1620 kg/m^3
		5					140	70	77	3		D = 1616 kg/m^3
		5					140	70	113	1.4		D = 1567 kg/m^3
Maniatidis and walker (2008)	Prismatic	3	Gravel (>2 mm) = 30% Sand (0.06-2 mm) = 45% Silt (0.002-0.06 mm) = 13% Clay (<0.002 mm) = 12%	0.47	0.91	Modified Proctor effort OMC=12.5% MDD = 1850 kg/m^3	300	300	600	0.6	5.1	-
		3					300	300	1800	0.5	5.73	-
	Prismatic	3					300	300	600	0.8	7.5	-
		3					300	300	2400	0.7	6.6	-
	Prismatic	3					300	300	600	1.0	7	-
		3					300	300	3000	0.6	6.5	-
Reddy and Kumar (2011)	Prismatic	3	Sand (0.075-4.75 mm) = 72.6% Silt (0.002-0.075 mm) = 11.6% Clay (<0.002 mm) = 15.8% Cement = 8%	0.37	0.63	Standard proctor OMC = 10.7% MDD = 2030 kg/m^3	150	150	300	6.5	6.2	-
		3					600	155	720	5.5	6.61	-
		3					750	152	3000	3.9	6.47	-
Güneyli and Rüşen (2015)	Cylindrical	-	**Sam-Tekin clay** Sand (0.075-4.75 mm) = 5% Silt (0.002-0.075 mm) = 40% Clay (<0.002 mm) = 55%	0.0017	0.0035	Standard proctor energy=600 KN m/m^3 OMC = 26% MDD = 16.8 KN/m^3		48	24	3.5	-	-
		-						48	36	3.3	-	-
		-						48	48	3.0	-	-
		-						48	60	2.6	-	-
		-						48	72	2.5	-	-
		-						48	84	2.3	-	-
		-						48	96	2.2	-	-

		-						48	108	2.2	-	-	
		-						48	120	2.1	-	-	
		-						48	132	2.0	-	-	
		-						48	144	1.9	-	-	
	Cylindrical	-	**Kaolinite** Sand (0.075-4.75 mm) =49% Silt (0.002-0.075 mm) = 33% Clay (<0.002 mm) = 16%	0.07	0.11	Standard proctor energy=600 KN m/m^3 OMC = 21.4% MDD = 17.2 KN/m^3		48	24	2.3	-	-	
		-						48	36	1.9	-	-	
		-						48	48	1.7	-	-	
		-						48	60	1.7	-	-	
		-						48	72	1.5	-	-	
		-						48	84	1.4	-	-	
		-						48	96	1.3	-	-	
		-						48	108	1.2	-	-	
		-						48	120	1.1	-	-	
		-						48	132	0.7	-	-	
		-						48	144	0.6	-	-	
	Cylindrical	-	**Handere clay** Sand (0.075-4.75 mm) = 1% Silt (0.002-0.075 mm) = 62% Clay (<0.002 mm) = 37%	0.0004	0.00065	Standard proctor energy=600 KN m/m^3 OMC = 19.3% MDD = 16.2 KN/m^3		48	24	2.0	-	-	
		-						48	36	1.8	-	-	
		-						48	48	1.2	-	-	
		-						48	60	1.1	-	-	
		-						48	72	1.0	-	-	
		-						48	84	1.0	-	-	
		-						48	96	0.9	-	-	
		-						48	108	0.9	-	-	
		-						48	120	0.9	-	-	
		-						48	132	0.8	-	-	
		-						48	144	0.7	-	-	
	Cylindrical	-	**Almanpınarı clay** Sand (0.075-4.75 mm) = 12% Silt (0.002-0.075 mm) = 33% Clay (<0.002 mm) = 55%	0.0016	0.0029	Standard proctor energy=600 KN m/m^3 OMC = 19.1% MDD = 16.8 KN/m^3		48	24	4.3	-	-	
		-						48	36	4.0	-	-	
		-						48	48	3.8	-	-	
		-						48	60	3.3	-	-	
		-						48	72	3.1	-	-	
		-						48	84	2.9	-	-	
		-						48	96	2.6	-	-	
		-						48	108	2.5	-	-	
		-						48	120	2.4	-	-	
		-						48	132	1.9	-	-	
		-						48	144	1.9	-	-	
Tripura (2015)	Cylindrical	5	Sand (0.03-4.75 mm) = 79% Silt (0.002-0.03 mm) = 13% Clay (<0.002 mm) = 8% Cement = 10%	0.075	0.12	Standard proctor OMC = 19% MDD = 1710 kg/m^3		150	300	4.6	4.87	D=1820 kg/m^3	
		5						150	900	3.8	5.40	D=1810 kg/m^3	
		5						150	1200	3.4	5.26	D=1800 kg/m^3	
		5						150	1500	3.1	4.82	D=1810 kg/m^3	
	Prismatic	5					150	150	300	5.3	5.01	D=1820 kg/m^3	
		5					150	150	900	4.3	5.03	D=1810 kg/m^3	
		5					150	150	1200	3.9	4.93	D=1810 kg/m^3	
		5					150	150	1500	3.6	6.09	D=1800 kg/m^3	
	Prismatic	5					190	150	900	4.1	5.05	D=1810 kg/m^3	
		5					190	150	1200	3.8	5.36	D=1790 kg/m^3	

		5					190	150	1500	3.4	4.68	D=1810 kg/m^3
	Prismatic	5					230	150	900	3.9	4.99	D=1750 kg/m^3
		5					230	150	1200	3.6	6.06	D=1780 kg/m^3
		5					230	150	1500	3.3	5.62	D=1800 kg/m^3
Merga (2016)	Cylindrical	1	Sand (0.075-4.75 mm) = 3.86% Silt (0.002-0.075 mm) = 34.77% Clay (<0.002 mm) = 61.37%	-	0.002	Standard proctor energy = 600 KN m/m^3 OMC = 26% MDD = 1.47 KN/m^3		38	38	0.5	26	-
		1						38	57	0.4		-
		1						38	76	0.4		-
		1						38	95	0.4		-
	Cylindrical	1						38	38	0.6		-
		1						38	57	0.5		-
		1						38	76	0.4		-
		1						38	95	0.4		-
	Cylindrical	1						38	38	0.6		-
		1						38	57	0.5		-
		1						38	76	0.4		-
		1						38	95	0.3		-
	Cylindrical	1	Sand (0.075-4.75 mm) = 5.76% Silt (0.002-0.075 mm) = 35.24% Clay (<0.002 mm) = 59%	-	0.003	Standard proctor energy=600 KN m/m^3 OMC = 25% MDD = 1.53 KN/m^3		38	38	0.6	25	-
		1						38	57	0.5		-
		1						38	76	0.5		-
		1						38	95	0.4		-
	Cylindrical	1						38	38	0.7		-
		1						38	57	0.5		-
		1						38	76	0.5		-
		1						38	95	0.4		-
	Cylindrical	1						38	38	0.6		-
		1						38	57	0.6		-
		1						38	76	0.5		-
		1						38	95	0.4		-
	Cylindrical	1	Sand (0.075-4.75 mm) = 3.86% Silt (0.002-0.075 mm) = 34.77% Clay (<0.002 mm) = 61.37%	-	0.002	Standard proctor energy = 600 KN m/m3 OMC = 26% MDD = 1.47 KN/m^3		38	38	0.9	21.95	-
		1						38	57	0.8		-
		1						38	76	0.7		-
		1						38	95	0.6		-
	Cylindrical	1						38	38	0.8		-
		1						38	57	0.7		-
		1						38	76	0.6		-
		1						38	95	0.6		-
	Cylindrical	1	Sand (0.075-4.75 mm) = 5.76% Silt (0.002-0.075 mm) = 35.24% Clay (<0.002 mm) = 59%	-	0.003	Standard proctor energy=600 KN m/m3 OMC = 25% MDD = 1.53 KN/m^3		38	38	1.3	20.41	-
		1						38	57	1.1		-
		1						38	76	1.0		-
		1						38	95	0.7		-
	Cylindrical	1						38	38	1.2		-
		1						38	57	1.2		-
		1						38	76	1.1		-
		1						38	95	0.7		-
	Cylindrical	1	Sand (0.075-4.75 mm) = 3.86% Silt (0.002-0.075 mm) = 34.77% Clay (<0.002 mm) = 61.37%	-	0.002	Standard proctor energy = 600 KN m/m3 OMC = 26%		38	38	0.3	27.5	-
		1						38	57	0.2		-
		1						38	76	0.2		-

		1				MDD = 1.47 KN/m^3		38	95	0.2		-
	Cylindrical	1	Sand (0.075-4.75 mm) = 5.76% Silt (0.002-0.075 mm) = 35.24% Clay (<0.002 mm) = 59%	-	0.003	Standard proctor energy=600 KN m/m3 OMC = 25% MDD = 1.53 KN/m^3		38	38	0.3	28	-
		1						38	57	0.3		-
		1						38	76	0.2		-
		1						38	95	0.2		-
Lan et al. (2018)	Prismatic	10	Gravel (>2 mm) = 7.8% Sand (0.075-2 mm) = 36.1% Silt (0.005-0.075 mm) = 38.5% Clay (<0.005 mm) = 17.6%	0.06	0.1	Compaction by a hydraulic Jack OMC = 18.2% MDD = 1.9 g/cm^3	100	100	100	3.2	5.62	Average dry density 1.88 g/cm^3
		10					150	150	150	2.5		
		10					200	200	200	1.5		
	Cylindrical	10						100	100	2.7		
	Prismatic	10					100	100	100	3.6		
		10					150	150	150	2.3		
		10					200	200	200	1.4		
	Cylindrical	10						100	100	2.7		
	Prismatic	10					100	100	100	2.9		
		10					150	150	150	1.8		
		10					200	200	200	1.3		
	Cylindrical	10						100	100	3.1		
	Prismatic	10					100	100	100	2.8		
		10					150	150	150	2.0		
		10					200	200	200	1.1		
	Cylindrical	10						100	100	3.0		
Rengifo-Lopez et al. (2019)	Prismatic	12	Sand (0.06-2 mm) = 22% Silt (0.002-0.06 mm) = 52% Clay (<0.002 mm) = 26% Cement = 6%	0.02	0.03	Compaction pressure 10.3 MPa	178	127	89	5.5	-	A 30-day specific weight of 1670 kg/m^3
		8					76	76	89	4.3	-	
		10					89	84	178	3.3	-	

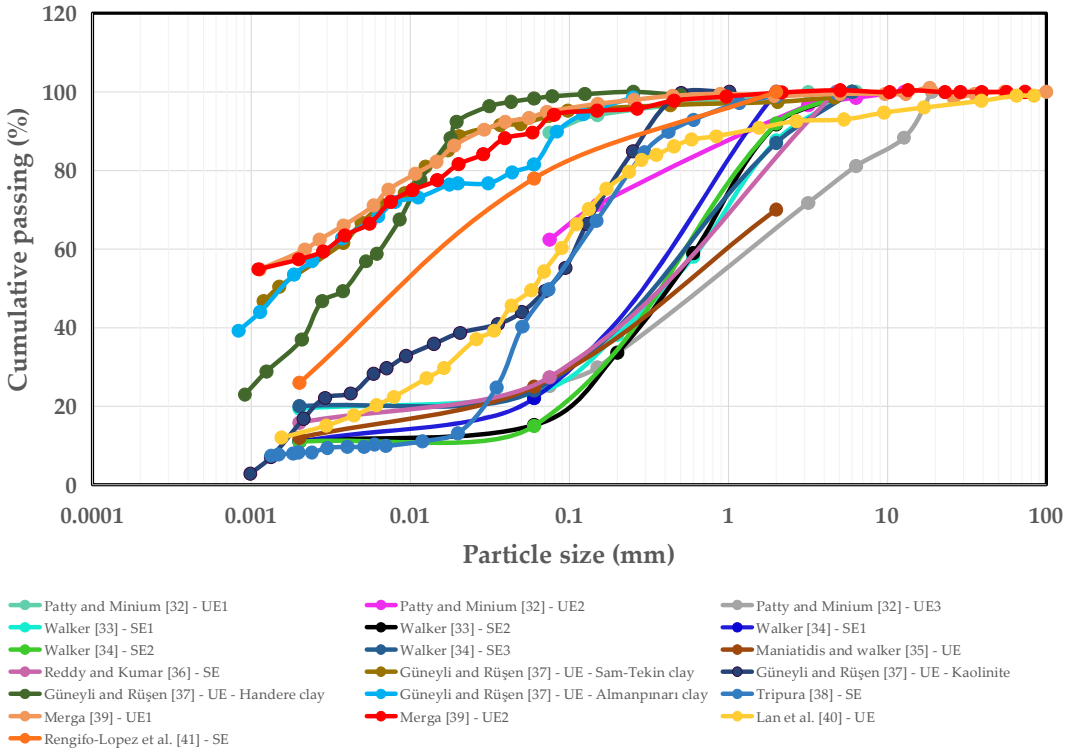

Figure 3.2. Granulometry properties of the earth in existing experimental studies

3.2.2 Cracks in rammed earth

Fracture propagation mechanism can provide significant insight into design and analysis of rammed earth structures. It will be particularly helpful in the evaluation of size effect in analysis of mechanical characteristics. For this purpose, it is necessary to investigate progressive fracture properties of earth material. Before proceeding to the analysis of experimental data, it is worth describing the theories linking the influence of specimen size and the source of fracture. The knowledge about the underlying fundamental phenomena will be useful to understand and be able to handle the effects of sample geometry on compressive strength and to formulate material's behaviour.

Compacted earth is not a continuous solid material and it contains microscale heterogeneities and discontinuities such as cracks, pores, etc. The mechanical characteristics of an earthen structure is generally affected by the presence of such defects. Discontinuities develop in rammed earth as a result of a range of processes that determines their nature, physical and mechanical properties. Discontinuities form in rammed earth during construction for the following reasons

- Differential settlement caused by volume change or compaction form and develop cracks in earth material
- Insufficient compaction of individual layers or a weak bond between them can cause discontinuities inside a layer or at the interface (Figure 3.3)
- Horizontal shear stress caused by compacting hammers will cause cracks during construction
- Deformation of the earth materials due to weight
- Differences in material properties in adjacent layers

- As rammed earth dries, due to shrinkage

Very little is known about the role discontinuities play in the failure process of earth materials when subjected to compressive loads. Vallejo (1989) reports laboratory investigations that were designed to understand the influence that orientation, length, number and arrangement of preexisting cracks have on the uniaxial compressive strength of a stiff fissured clay. According to this study, the state of stress is an important factor in developing secondary cracks from the tip of preexisting cracks in specimens (Vallejo (1989)). It was observed that, under uniaxial compression, the samples with one inclined preexisting crack failed when secondary cracks developed at the tips of the preexisting cracks (Figure 3.4) and propagated very rapidly in a direction parallel to the direction of the uniaxial compressive load.

In summary, discontinuities can be one cause of progressive failure in compacted earth material under compression, which promote tensile stresses in areas close to them (Figure 3.4a). With respect to the influence of cracks' number on compressive strength, Vallejo concluded that, due to overstressing effect, a higher value of strength is obtained for samples with one crack than those with more than one crack (Figure 3.4a,b). Vollejo (1989) pointed out, depending upon the arrangement of the preexisting cracks in a specimen under uniaxial compression, the difference in compressive strength can be explained by the way the intensified zones of tensile and compressive stresses overlap (Figure 3.4b,c,d). This study indicated that failure in tension prevails over compressive or shear failure in regions close to the discontinuities (Figure 3.4c and 3.4d).

In terms of strength, the existence of discontinuities produces size effect on compressive strength induced by discontinuities parameters such as number and arrangement of cracks. The compressive strength measured in the laboratory depends on the extent of discontinuities, and their arrangement. Size of the specimen controls the crack distribution which, in turn, affects the mechanical response of the structure. For specimens with an uniform arrangement of cracks, laboratory tests of a reasonable size can give reliable measures of large-scale strength.

The link between the mechanical behavior of compacted earth (in terms of strength and deformation) and the size of the specimen should be considered in the design and appraisal of such a structure through an approach that considers the mechanical strength-specimen size relationship.

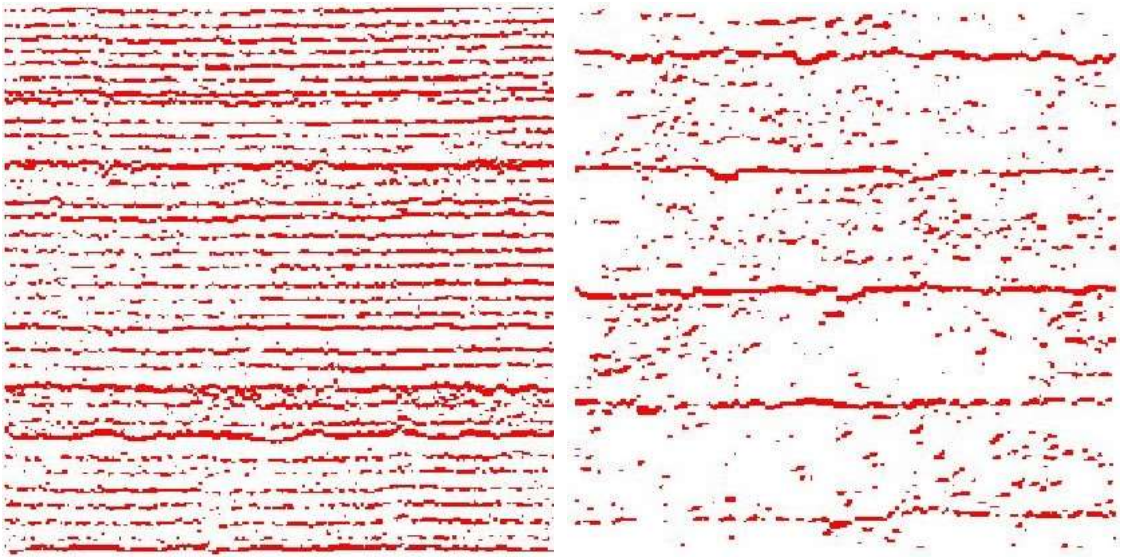

Figure 3.3. Discontinuities left on rammed earth wall due to construction technology

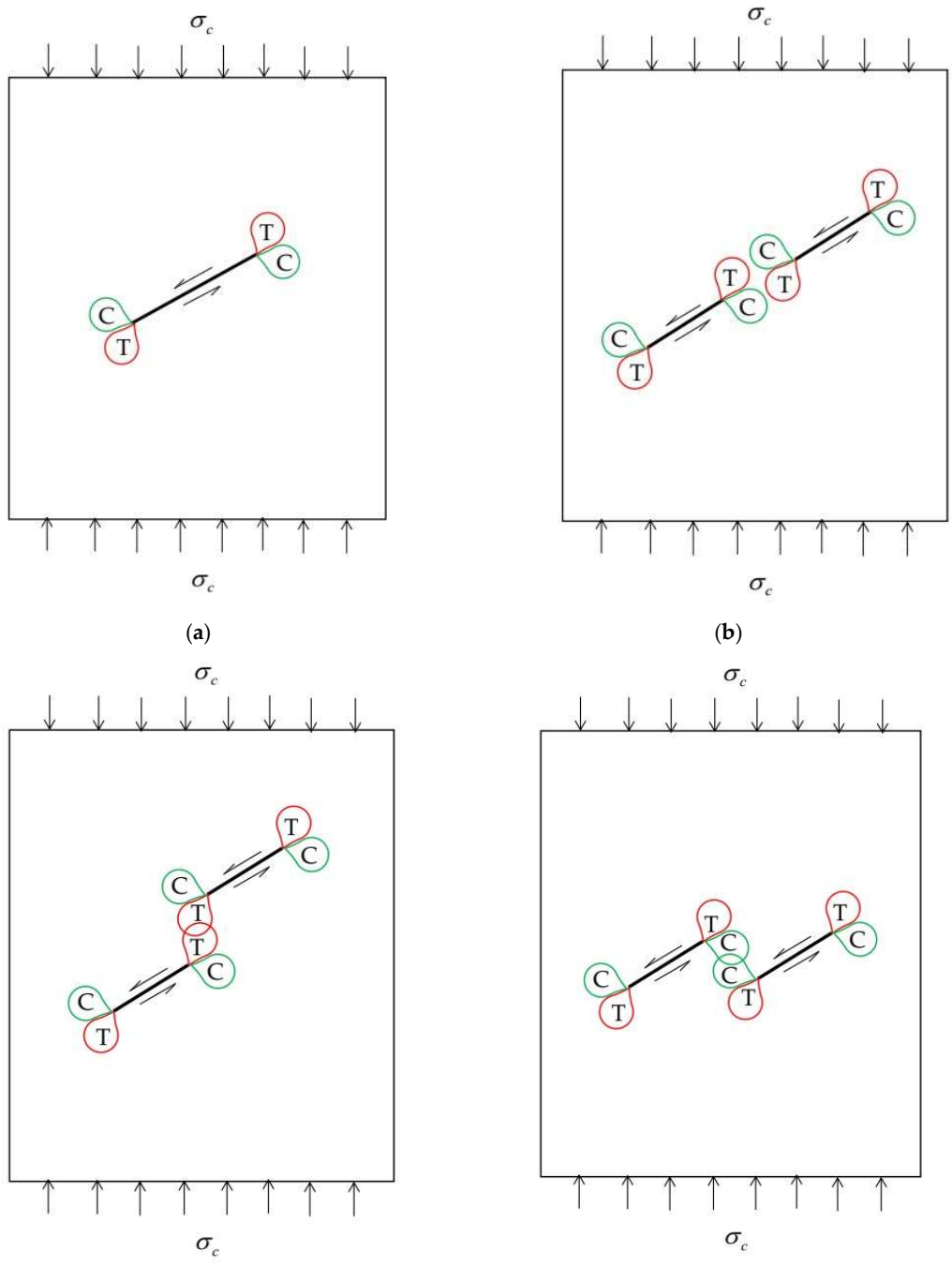

Figure 3.4. Tensile and compressive stresses in clay under uniaxial compression loading, as investigated by Vollejo (1989); (a) one preexisting crack, (b) two aligned preexisting cracks, (c) two left-stepping preexisting cracks, (d) two right-stepping preexisting cracks

3.2.3. Quantification of size effect

A database containing the results of uniaxal compression tests on rammed earth is employed herein to assess the relationship between mechanical strength and specimen size. It contains 39 series of test results gathered from the literature, which include 20 and 19 series of cylindrical and prismatic specimens, respectively. Figure 3.5 shows the database of UCS versus specimen height to width ratio (H/W). It can be inferred from Figure 3.5 that each

group of experimental data shows the statistically significant trend associated with relationship between the UCS and the H/W. With a decrease in the height to width ratio, the end constraint of specimens increases and inside the compacted earth specimens triaxial stress field is induced and hence an increase in unconfined compressive strength and ratio of ductile to brittle zones by a decrease in height to width ratio is observed. Therefore, it can be helpful to establish an empirical relationship relating the UCS of a specimen having a height to width ratio H/W to the UCS of the specimen having the reference H/W. Due to the natural variation of material characteristics, moisture content and difference of time to failure between different series of tests, the reference strength level (strength at the reference H/W) enables the results of laboratory tests, on different types of earth materials with a wide variety of characteristics, to be analyzed on a common basis (Figure 3.6). As no reference H/W does exist, the specimen height to width ratio of 1 is used as a reference H/W herein. It worth mentioning that any H/W ratio can be used as a reference, depending on the situation. Giving the uniaxial compressive strength of RE at a specified specimen H/W, one can easily estimate the UCS for any specimen H/W using the formulas suggested.

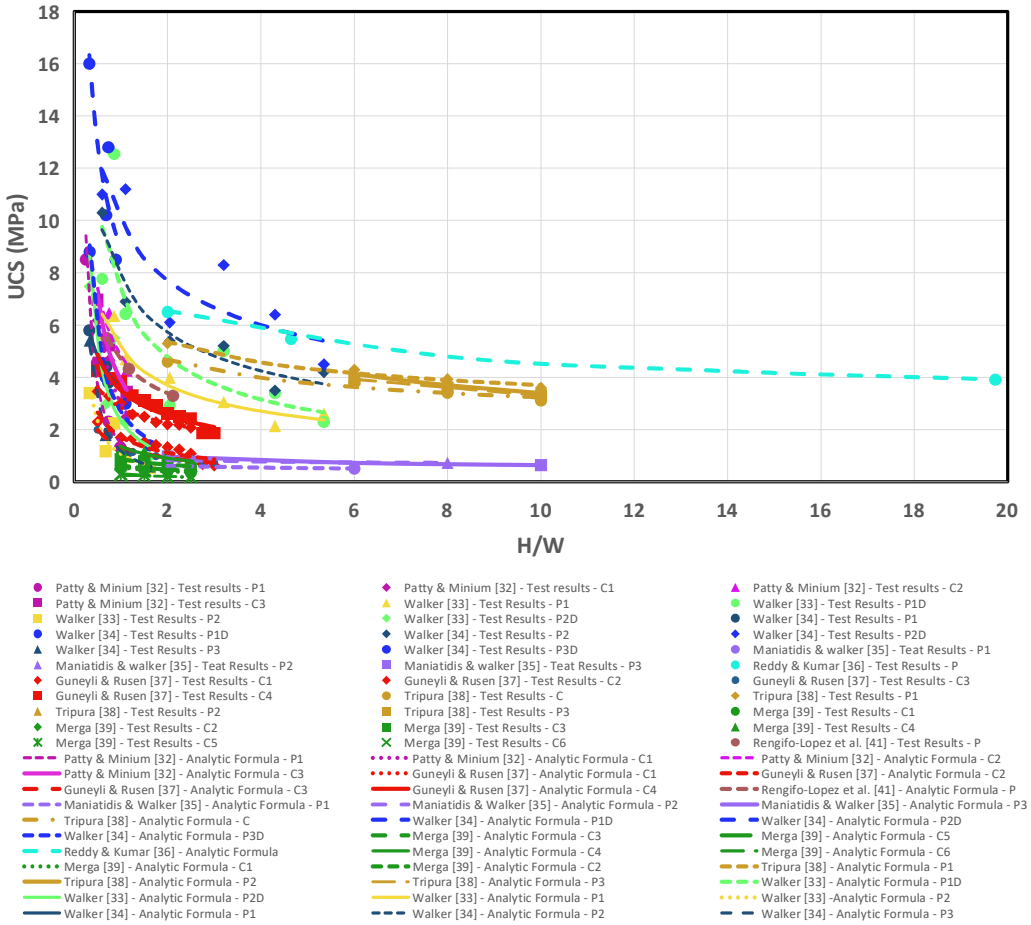

Figure 3.5. Experimental data and power law trend for size effect on compressive strength of compacted earth

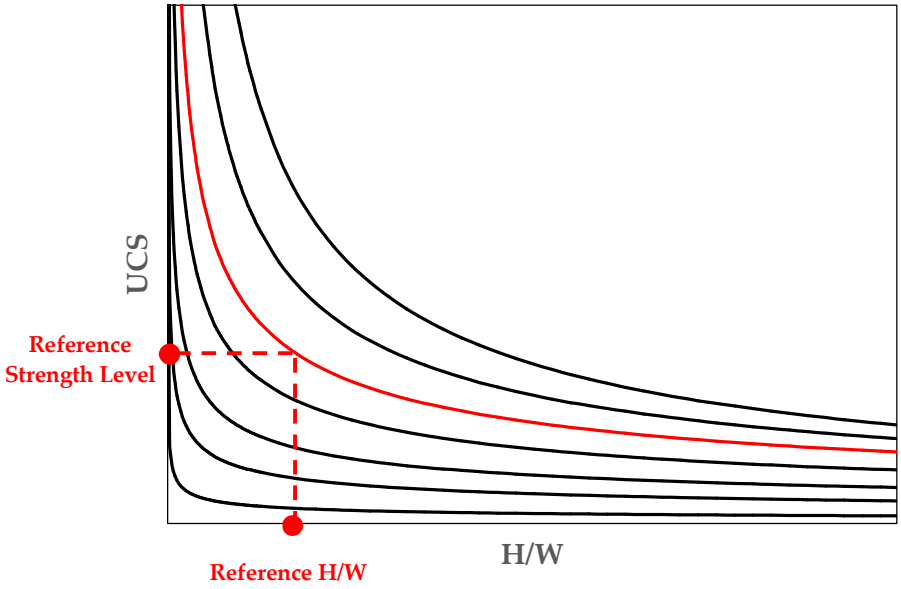

Figure 3.6. Size effect modelling for compressive strength of compacted earth

Figure 3.5 presents the correlation between uniaxial compressive strength and the specimen height to width ratio. The correlation is based on a general power law which is formulated as below

$$UCS_{\frac{H}{W}} = USC_1\left(\frac{H}{W}\right)^m \qquad \text{Eq (3.1)}$$

where UCS_1 and $UCS_{H/W}$ are the compressive strength at height to width ratio of 1 and H/W, respectively. m is a model parameter. The values of UCS_1 and m are calculated for all the experimental data-sets and presented in Table 3.2 and Figure 3.7.

Table 3.2. Variables, USC_1 and m, calculated for all the experimental data-sets.

Reference study	Specimen type	m	UCS_1	R^2
Patty and Minium (1945)	Prismatic	-1.333	1.4729	0.97
	Cylindrical	-1.121	3.0088	0.954
	Cylindrical	-0.614	4.8364	0.8683
	Cylindrical	-0.869	3.8941	0.9891
Walker (1997)	Prismatic	-0.456	5.0878	0.9013
	Prismatic	-0.594	7.1988	0.7024
	Prismatic	-1.068	1.0752	0.7762
	Prismatic	-1.168	2.36	0.7508
Walker (2004)	Prismatic	-0.415	3.6094	0.9256
	Prismatic	-0.531	8.9329	0.7528
	Prismatic	-0.432	7.7343	0.9136
	Prismatic	-0.361	9.9107	0.7172
	Prismatic	-1.329	1.1913	0.9862
	Prismatic	-1.085	2.7044	0.9627
Maniatidis and walker (2008)	Prismatic	-0.162	0.6937	1
	Prismatic	-0.1	0.9004	1

	Prismatic	-0.18	1	0.9817
Reddy and Kumar (2011)	Prismatic	-0.223	7.6327	0.999
Güneyli and Rüşen (2015)	Cylindrical	-0.355	2.8523	0.9765
	Cylindrical	-0.623	1.728	0.7926
	Cylindrical	-0.547	1.3528	0.9707
	Cylindrical	-0.469	3.5103	0.8945
Tripura (2015)	Cylindrical	-0.229	5.4714	0.9576
	Prismatic	-0.23	6.2816	0.9773
	Prismatic	-0.379	8.1549	0.9759
	Prismatic	-0.334	7.1765	0.9938
Merga (2016)	Cylindrical	-0.471	0.5683	0.9955
	Cylindrical	-0.403	0.6343	0.97
	Cylindrical	-0.401	0.8814	0.9478
	Cylindrical	-0.566	1.3525	0.7416
	Cylindrical	-0.543	0.304	0.9698
	Cylindrical	-0.325	0.2679	0.8617
Rengifo-Lopez et al. (2019)	Prismatic	-0.461	4.66	0.9999

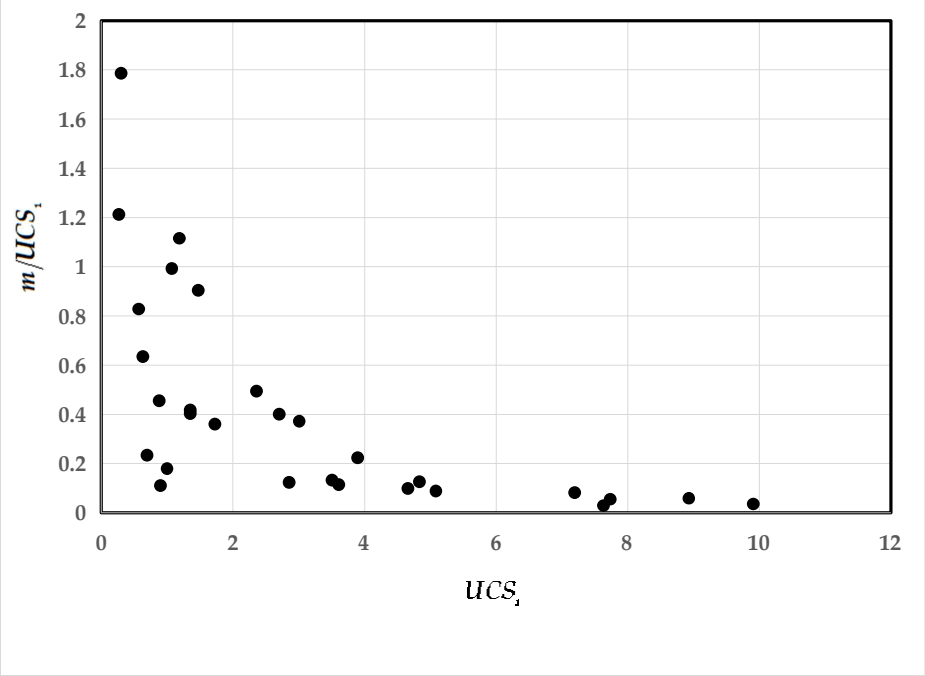

Figure 3.7. Variation of m/UCS_1 versus UCS_1, calculated from experimental data

The next step is to introduce an appropriate function of UCS_1 for the prediction of the parameter m. Before proceeding further, let's examine the influence of moisture content on the form of UCS-H/W curves for compacted earth material. One of the factors which has a direct influence on the mechanical strength of RE walls is water content. Moisture content variations thus lead to a variation of mechanical capacity of the rammed earth structure. Experimental investigation of size effect on UCS for earth specimens with different water contents are quite limited in the literature (see e.g., Walker (1997), Walker (2004), and Merga (2016)). Experimental results of these studies for UCS-H/W curves are shown in Figures

3.8-3.10. To shed more light on the efficiency of proposed mathematical form for specimens with different water contents, the prediction of the formula are shown for these sets of test data in Figures 3.8-3.10. The overall observation is that the form of UCS-H/W curve for a specimen with lower water content is similar to that of a specimen with higher strength. This suggests that, regardless of the level of water content, size effect may be efficiently related to the level of strength at H/W=1. However, in light of future research, it may be possible to examine the efficiency of the proposed formula for prediction of size effect at different water contents.

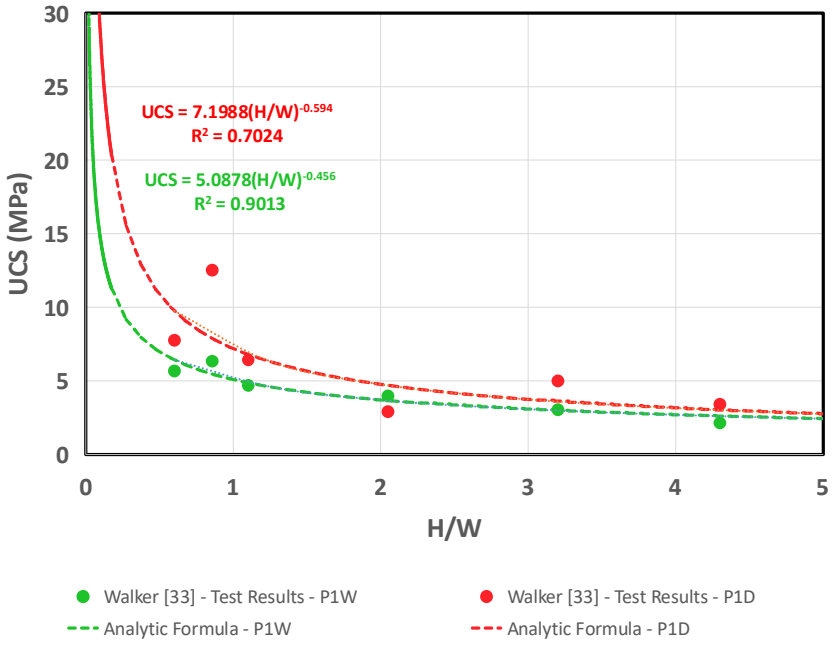

(a)

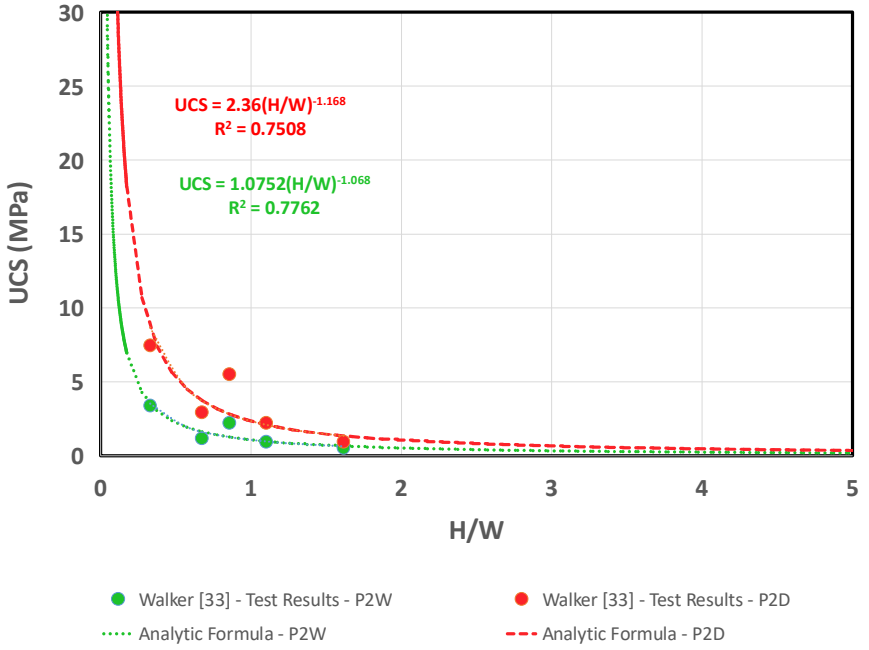

(b)

Figure 3.8. Influence of moisture content on the parameters of proposed formula for experimental data of Walker (1997); (a) Prismatic specimen 1, (b) prismatic specimen 2

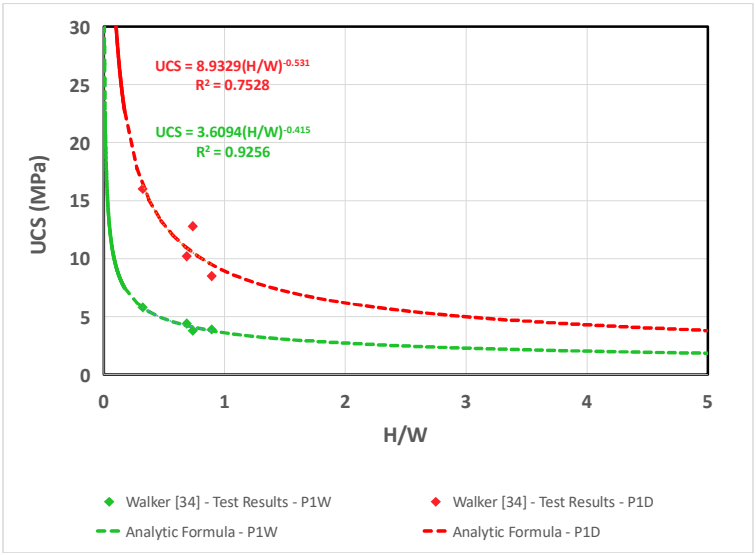

(a)

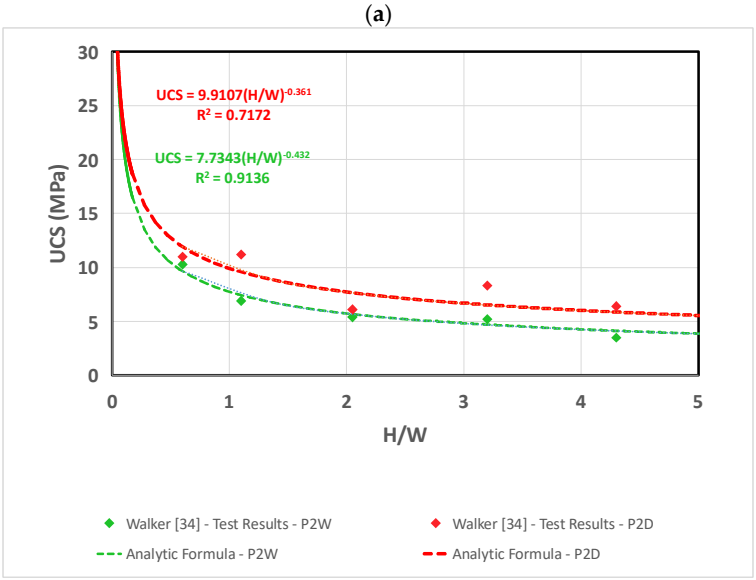

(b)

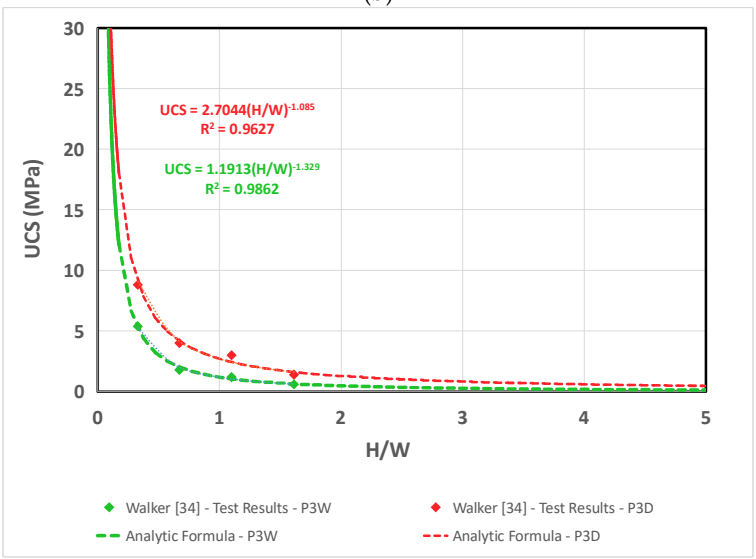

(c)

Figure 3.9. Influence of moisture content on the parameters of proposed formula for experimental data of Walker (2004); (a) Prismatic specimen 1, (b) prismatic specimen 2, (c) prismatic specimen 3

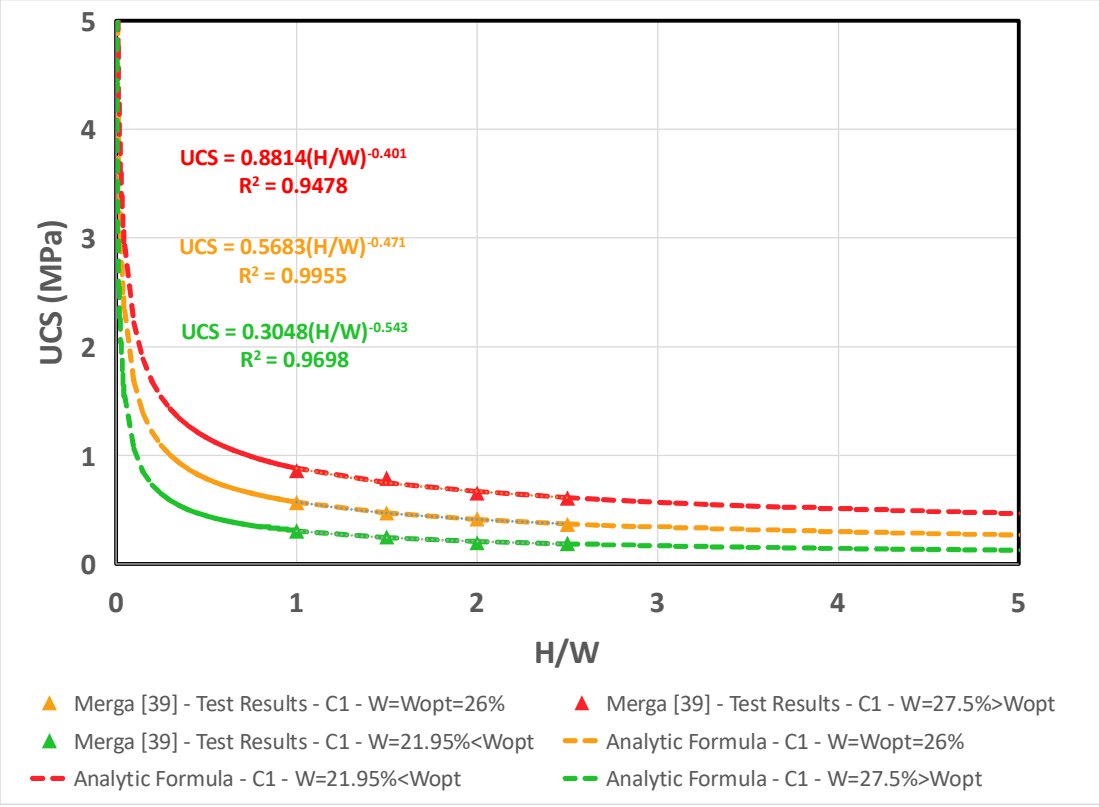

(a)

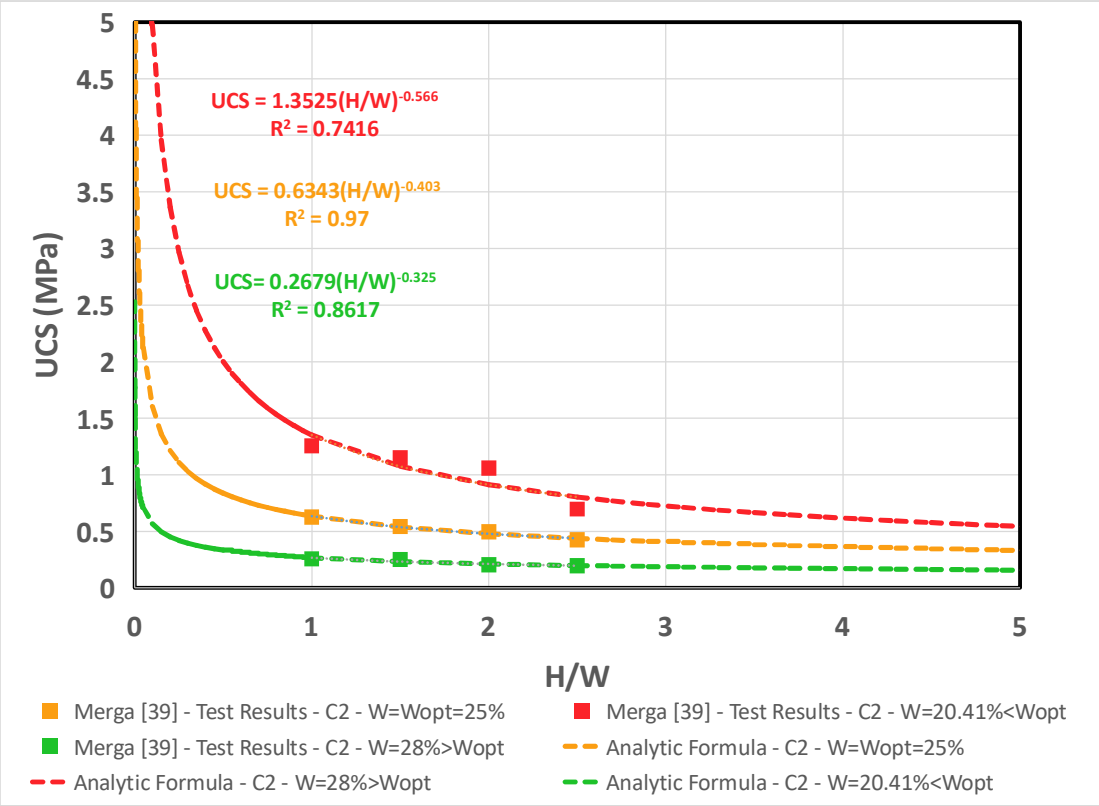

(b)

Figure 3.10. Influence of moisture content on the parameters of proposed formula for experimental data of Merga (2016); (a) Cylindrical specimen 1, (b) cylindrical specimen 2

As can be seen in Figure 3.11, as UCS_1 increases, lower values of m/UCS_1 are obtained. Hence, a formula in the form of Eq. 3.1 with a constant m would be an inefficient solution for the accurate estimation of $UCS_{H/W}$ within the whole range of UCS_1. Figure 3.11 confirms that, for the proposed formula (Eq. 3.1) to be accurate enough for both low and high values of strength at H/W=1, the m/UCS_1-UCS_1 curve should be separately formulated for USC_1 <1 and USC_1 >1 (Eq. 3.2). Motivated by this observation, Eq. 3.2 is calibrated against the experimental results and thus, assuming that m in Eq. 3.1 is an independent variable, the following form is finally suggested

$$\frac{m}{UCS_1} = k(UCS_1)^{-c} \qquad \text{Eq (3.2)}$$

$k = 0.1982$
$c = 1.679$, $UCS_1 < 1$

$k = 1.0743$
$c = 1.517$, $UCS_1 > 1$

For low values of strength at H/W=1, the computed values of two constants k and c are 0.1982 and 1.679, respectively. However, as UCS_1 increases, higher value of k and lower value of c is obtained. However, the following equation is found flexible enough for the prediction of measured $UCS_{H/w}$ in the whole range of UCS_1.

$$UCS_{\frac{H}{W}} = USG_1\left(\frac{H}{W}\right)^m$$

$$\frac{m}{UCS_1} = k(UCS_1)^{-c} \qquad \text{Eq (3.3)}$$

$k = 0.5483$
$c = 1.11$

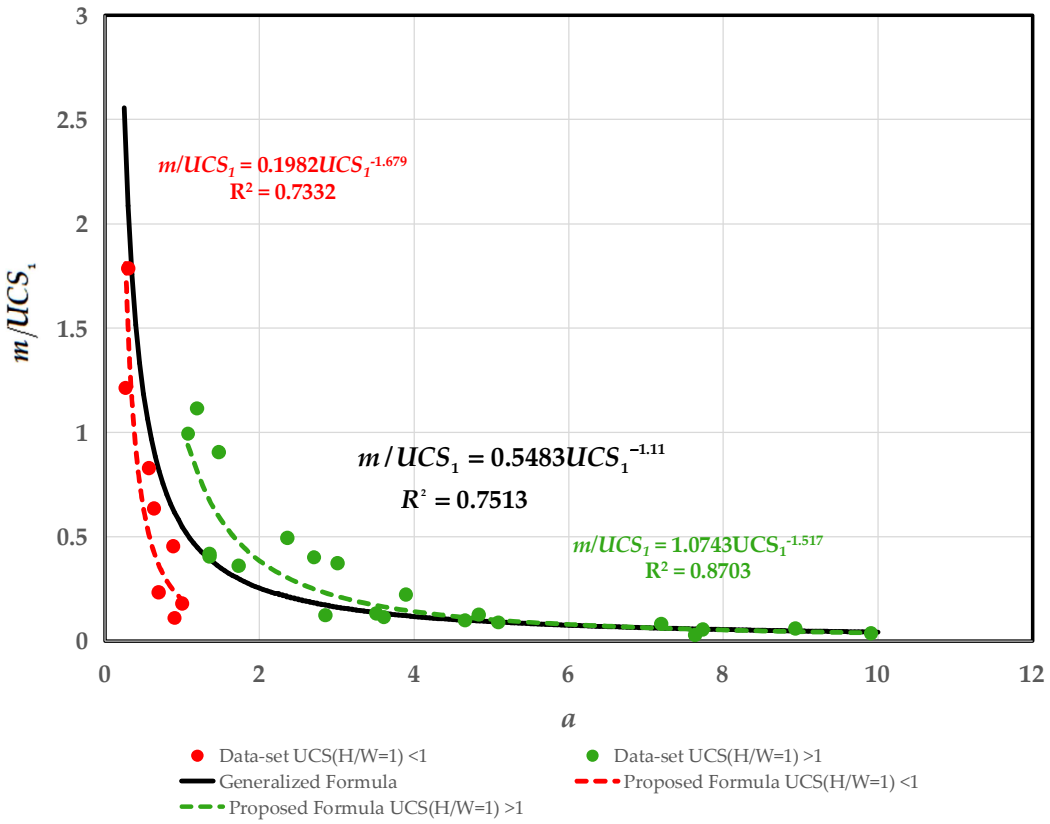

Figure 3.11. Proposed formulas for estimating the parameters of the power law trend

It needs to note that the analytical framework presented in this research is the very first analytical approach to size effect in characterization of mechanical strength in rammed earth materials and therefore, in view of the very limited published experimental data available, further laboratory investigation is necessary to examine the validity of the proposed formulas for other soils with very different specimen and material properties.

3.3. Conclusions

The first part of the paper reviews the existing experimental investigations on the influence of specimen geometry on strength characteristics of earth material. It is clarified that each group of experimental data shows the statistically significant trend associated with relationship between the uniaxial compressive strength (UCS) and the height to width ratio (H/W) of specimens. Next, using a database containing 39 series of test results gathered from the literature, which includes 20 and 19 series of cylindrical and prismatic specimens with a broad range of H/W, an analytical UCS-H/W model is introduced for compacted earth material. The present research is the very first analytical approach to size effect in characterization of mechanical strength in rammed earth materials and therefore it is, to a certain extent, bound to further investigation. In view of the very limited published experimental data available on this subject, there is a clear need for further laboratory work on the estimation of size effect in uniaxial compressive strength of rammed earth. However, in light of future research, it may be possible to examine the efficiency of the proposed formula for prediction of size effect at different water contents.

References

[1] Moghaddam, M.Z.; Umili, G.; Messina, V.; Bonetto, S.; Ferrero, A.M.; Bollini, G.; Gandreau, D. An SVM-Based Scheme for Automatic Identification of Architectural Line Features and Cracks. *Appl. Sci.* **2020**, *10*, 5077.

[2] Hall, M.; Djerbib, Y. Rammed earth sample production: context, recommendations and consistency. *Constr Build Mater*. **2004** , *18(4)*, 281-286.

[3] Miccoli, L.; Müller, U.; Fontana, P. Mechanical behaviour of earthen materials: A comparison between earth block masonry, rammed earth and cob. *Constr Build Mater*. **2014**, *61*, 327-339.

[4] Bui, Q.B.; Morel, J.C.; Hans, S.; Walker, P. Effect of moisture content on the mechanical characteristics of rammed earth. *Constr Build Mater*. **2014**, *54*, 163-169.

[5] Ciancio, D.; Jaquin, P.; Walker, P. Advances on the assessment of soil suitability for rammed earth. *Constr Build Mater*. **2013**, *42*, 40-47.

[6] ASTM *D 2166-00: Standard test method for unconfined compressive strength of cohesive soil. In: Annual book of ASTM standards*; American Society for Testing and Materials, West Conshohocken, 2002; pp. 1–6.

[7] BSI. *British Standard Methods of Test for Soils for Civil Engineering Purposes. Part 7: Shear strength tests (total stress) tests*; British Standards Institution, London, 1377.

[8] Das, B.M. *Soil mechanics laboratory manual, 6th edn*; Oxford University Press, Oxford, 2002; pp. 216.

[9] Cheah, J.S.J.; Walker, P.; Heath, A.; Morgan, T.K.K.B. Evaluating shear test methods for stabilised rammed earth. Proceedings of the Institution of Civil Engineers-Construction Materials, 2012, 165(6); pp. 325-334.

[10] Ciancio, D.; Gibbings, J. Experimental investigation on the compressive strength of cored and molded cement-stabilized rammed earth specimens. *Constr Build Mater.* **2012**, *28(1)*, 294–304.

[11] Jaquin, P.A.; Augarde, C.E.; Gallipoli, D.; Toll, D.G. The strength of unstabilised rammed earth materials. *Géotechnique.* **2009**, *59(5)*, 487–490.

[12] Olivier, M.; Mesbah, A. Constitutive equations for compacted soils. In: Proceedings of the first international conference on unsaturated soils, Paris, 1995; pp. 765-573.

[13] Burroughs, V.S. Quantitative criteria for the selection and stabilisation of soils for rammed earth wall construction. PhD Thesis, University of New South Wales, Australia, 2001.

[14] Hall, M.; Djerbib, Y. Moisture ingress in rammed earth: part 1 – the effect of soil particle-size distribution on the rate of capillary suction. *Constr Build Mater.* **2004**, *18,* 269–280.

[15] Hall, M.; Djerbib, Y. Moisture ingress in rammed earth: part 2 – the effect of soil particle-size distribution on the absorption of static pressure-driven water. *Constr Build Mater.* **2006**, *20*, 374–383.

[16] Hall, M.; Djerbib, Y. Moisture ingress in rammed earth: part 3 – sorptivity, surface receptiveness and surface inflow velocity. *Constr Build Mater.* **2006**, *20*, 384–395.

[17] Bui, QB.; Morel, JC.; Reddy, BVV.; Ghayad, W. Durability of rammed earth walls exposed to 20 years of natural weathering. *Build Environ.* **2008**, *44*, 912–919.

[18] Bui, QB.; Morel, JC. Assessing the anisotropy of rammed earth. *Constr Build Mater.* **2009**, *23*, 3005–3011.

[19] Bui Q.B.; Morel J.C.; Hans, S.; Walker, P. Water effects on the mechanical characteristics of rammed earth buildings: a double-edged sword. Constr Build Mater. **2013**.

[20] Jayasinghe, C.; Kamaladasa, N. Compressive strength characteristics of cement stabilized rammed earth walls. *Constr Build Mater.* **2007**, *21(11)*, 1971–1976.

[21] Morel, J.C.; Pkla, A. A model to measure compressive strength of compressed earth blocks with the '3 points bending test'. *Constr Build Mater.* **2002**, *16(5)*, 303–310.

[22] Miccoli, L.; Gerrard, C.; Perrone, C.; Gardei, A.; Ziegert, C. A collaborative engineering and archaeology project to investigate decay in historic rammed earth structures: The case of the Medieval preceptory in Ambel. *Int. J. Archit. Heritage.* **2017**, *11(5)*, 636-655.

[23] Silva, R.A.; Domínguez-Martínez, O.; Oliveira, D.V.; Pereira, E.B. Comparison of the performance of hydraulic lime-and clay-based grouts in the repair of rammed earth. *Constr Build Mater*. **2018**, *193*, 384-394.

[24] Wangmo, P.; Shrestha, K. C.; Miyamoto, M.; Aoki, T. Assessment of out-of-plane behavior of rammed earth walls by pull-down tests. *Int. J. Archit. Heritage.* **2019**, *13(2)*, 273-287.

[25] Martín-del-Rio, J.J.; Flores-Alés, V.; Alejandre-Sánchez, F.J.; Blasco-López, F.J. New method for historic rammed-earth wall characterization: The Almohade ramparts of Malaga and Seville. *Stud Conserv*, **2019**, *64(6)*, 363-372.

[26] Parracha, J.L.; Lima, J.; Freire, M.T.; Ferreira, M.; Faria, P. Vernacular earthen buildings from Leiria, Portugal–material characterization. *Int. J. Archit. Heritage.* **2019**, 1-16.
[27] Canivell, J.; Martin-del-Rio, J.J.; Alejandre, F.J.; García-Heras, J.; Jimenez-Aguilar, A. Considerations on the physical and mechanical properties of lime-stabilized rammed earth walls and their evaluation by ultrasonic pulse velocity testing. *Constr Build Mater.* **2018**, *191*, 826-836.
[28] Silva, R.A.; Mendes, N.; Oliveira, D.V.; Romanazzi, A.; Domínguez-Martínez, O.; Miranda, T. Evaluating the seismic behaviour of rammed earth buildings from Portugal: From simple tools to advanced approaches. *Eng. Struct.* **2018**, *157*, 144-156.
[29] El Hajjar, A.; Chauhan, P.; Prime, N.; Olivier, P. Effect of suction on the mechanical characteristics of uniformly compacted rammed earth. In IOP Conference Series: Earth and Environmental Science (Vol. 143, No. 1, p. 012045), April 2018.
[30] Bruno, A.W.; Gallipoli, D.; Perlot, C.; Mendes, J. Mechanical behaviour of hypercompacted earth for building construction. *Mater Struct*. **2017**, *50(2)*, 160.
[31] Beckett, C.T.S.; Augarde, C.E.; Easton, D.; Easton, T. Strength characterisation of soil-based construction materials. *Géotechnique*, **2018**, *68(5)*, 400-409.
[32] Patty, R.L.; Minium, L.W. *Rammed earth walls for farm buildings*, 1945.
[33] Walker, P. Characteristics of pressed earth blocks in compression. In Proceedings of the 11th international brick/block masonry conference, Shanghai, China, October 1997; pp. 14-16.
[34] Walker, P.J. Strength and erosion characteristics of earth blocks and earth block masonry. *J. Mater. Civ.* **2004**, *16(5)*, 497-506.
[35] Maniatidis, V.; Walker, P. Structural capacity of rammed earth in compression. *J. Mater. Civ.* **2008**, *20(3)*, 230-238.
[36] Venkatarama Reddy, B.V.; Prasanna Kumar, P. Structural behavior of story-high cement-stabilized rammed-earth walls under compression. *J. Mater. Civ.* **2011**, 23(3), 240-247.
[37] Güneyli, H.; Rüşen, T. Effect of length-to-diameter ratio on the unconfined compressive strength of cohesive soil specimens. *Bull. Eng. Geol. Environ.*, **2015**, *75(2)*, 793-806.
[38] Tripura, D.D. Structural Behaviour of Unreinforced and Reinforced Cement Stabilized Rammed Earth Columns Under Axial Compression. Doctor of philosophy thesis, indian institute of technology Guwahati, Guwahati, India, 2015.
[39] Merga, S. Effect of sample height on stress-strain behaviour of undrained shear strength of Addis Ababa red clay soil using UCS test. Master of Science thesis, Addis Ababa University, Addis Ababa, 2016.
[40] Lan, G.Q.; Wang, Y.H.; Chao, S.S. Influences of specimen geometry and loading rate on compressive strength of unstabilized compacted earth block. *Adv. Mater. Sci. Eng.*, 2018.
[41] Rengifo-Lópeza, E.L.; Kumarb, N.; Mattaa, F.; Barbatob, M. Experimental characterization and numerical simulation of compressive behavior of compressed and stabilized earth block specimens. Conference Earth USA, Santa Fe, New Mexico, USA, October 2019.
[42] Vallejo, L.E. Fissure parameters in stiff clays under compression. *J. Geotech. Eng.*, **1989**, *115(9)*, 1303-1317.

CHAPTER 4

Reconstruction of rammed earth material in laboratory and physico-mechanical characterization of material

This section reports the work aiming at contributing to the development of the limited knowledge and clear understanding on properties of rammed earth. The aim of the experimental work is to reproduce rammed earth in a controlled way in the lab and to analyse the influence of different constitutive components. The soil material, which is the constituent of rammed earth buildings, is the main subject of geotechnical studies. Therefore, in the framework of Tech4Culture program, an experimental program has been defined by the department of earth science of UNITO based on geotechnical and geophysical tests. Rammed earth specimens have been reconstructed in laboratory and an investigation was performed on characteristics of rammed earth material, involving characterization of compaction curves and uniaxial compression test and digital image correlation (DIC) analysis. This section addresses the work performed on characterization of rammed earth specimens and uniaxial compression test. It is obvious that such a narrow range of mixture characteristics cannot cover the wide variation of material property, which might be encountered in the numerous types of rammed earth structures found in cultural heritage. However, they do provide an enhanced understanding of the behaviour of rammed earth material for advancement of research in this field. Another important fact is that numerous influencing factors lead to the uncertainties and the variabilities of parameters considering only one type of granulometric property and experimental data which do not include all of the controlling parameters, involved in structural characterizations of material, can not be necessarily comparable. Therefore, due to the inherent variability of controlling parameters for different types of rammed earth material, the results of such experiments can not be extrapolated over a wider range outside of the range investigated.

4.1. Introduction

Mechanical behaviour of rammed earth has been addressed by many studies (Hall and Djerbib (2004), Miccoli et al. (2014), Bui et al. (2014), Ciancio et al. (2013) ,Cheah et al. (2012), Ciancio and Gibbings (2012), Jaquin et al. (2009), Olivier and Mesbah (1995), Burroughs (2001), Hall and Djerbib (2004), Hall and Djerbib (2006), Hall and Djerbib (2006), Bui et al. (2008), Bui and Morel (2009), Bui et al. (2013), Jayasinghe and Kamaladasa (2007), Morel and Pkla (2002), Miccoli et al. (2017), Silva et al. (2018), Wangmo et al. (2019), Martín-del-Rio et al. (2019), Parracha et al. (2019), Canivell et al. (2018), Silva et al. (2018), El Hajjar et al. (2018), Bruno et al.

(2017), Beckett et al. (2018), Canivell et al. (2018), Silva (2013) and Bernat-Maso et al. (2017)). A review of above-mentioned literature indicates that mechanical behaviour of compacted earth material is strongly affected by their numerous intrinsic physical and geotechnical parameters. Determining a finite set of interinsic geotechnical properties able to characterize main mechanical and structural behaviour is challenged by the complexity of earthen specimens, where many major intrinsic physical and geotechnical factors, in particular: particle size distribution, mineralogy of the particles, water content, density, void ratio and porosity, and several other factors affect the engineering properties significantly, which can sometimes lead to not always consistent testing results.

Another important fact is that various indexes involved in geotechnical characterization are not independent, but are interrelated in a very complex manner, which leads to difficulty in selecting the characteristic indexes describing behavioural properties.

In order to determine the engineering properties of the test materials, a series of specimens has been produced and tested. Under the study reported here, four soil mixtures of clay and sand in varying fractions of coarse and fine components were employed as test materials. It is obvious that such a narrow range of mixture characteristics cannot cover the wide variation of material property which might be encountered in the numerous types of rammed earth structures found in cultural heritage. However, they do provide an enhanced understanding of the behaviour of rammed earth material for advancement of research in this field.

The goal of this chapter is to have a better understanding of the influence of physical and geotechnical parameters on the mechanical behaviour of rammed earth material, to know how these parameters affects and controls the engineering behaviour of compacted sand-clay-water mixtures. For this purpose, this chapter reports the obtained test results, interrelating basic knowledge and a series of controlling parameters which characterizes the behaviour of mixtures.

4.2. Physical and mineralogical characterization of the utilized materials

Based on the granulometry of rammed earth heritage material around the world, four different mixtures with granulometric properties composed of clay with different percentage of sand (0, 5, 15 and 40), as shown in Figure 4.1a, has been considered for specimen preparation in order to reproduce rammed earth in a controlled way in the lab. Figure 4.1 shows the Mineralogical characteristics of clay. As reported by the department of earth science of University of Turin, the sample (Figure 4.1b) contains a couple of straightforward phases, like quartz, calcite and orthoclase. Regarding the clay minerals, their unambigous identification by X-ray diffraction can be very challenging, because of important peak superposition, due to high structure similarities between different families. Therefore, a sequential treatment was applied in order to selectively verify the presence of each type of clay minerals (Figure 4.1c):

1- Glicole substitution, for expandable minerals (i.e. smectites like montmorillonite)
2- Thermal treatment at 350 °C, for hydrate phases (i.e. vermiculite)
3- Thermal treatment at 500 °C, for more stable phases (i.e. chlorites, serpentines, kaolinite).

The peak at d_{HKL} around 14Å is partially affected by the first treatment, meaning that expandable minerals are present, although in very low quantity. Moreover, the absence of a distinguishable peak at lower 2-Theta points to mixed minerals, typical of young soil, where the stacking of the octahedral and tetrahedral sheets is not fully ordered. The residual intensity of the peak is removed during the first thermal treatment, allowing the assignment to an hydrate phase like vermiculite.

The peak at around 9.8Å is not affected by the treatment and can be safely attributed to illite.

The peak at around 7Å is removed by heating to 500 °C, pointing to kaolinite rather than chlorite or serpentine.

It should be mentioned that the chemical formulae are just an example, since these types of minerals can have different degree of substitution and composition, which are impossible to determine solely by powder X-ray diffraction.

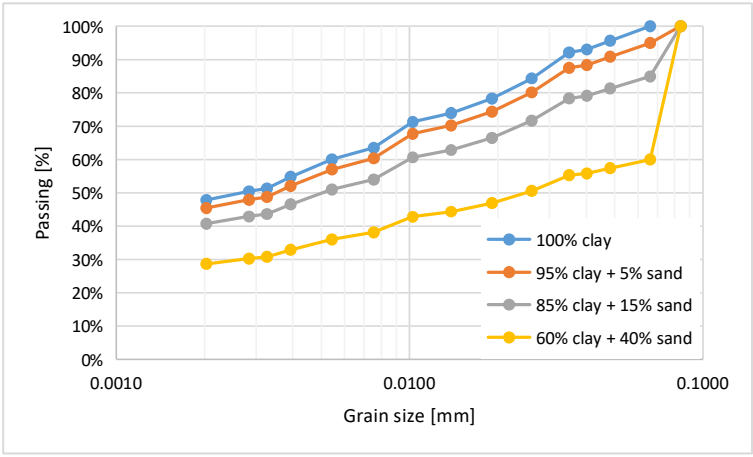

(a)

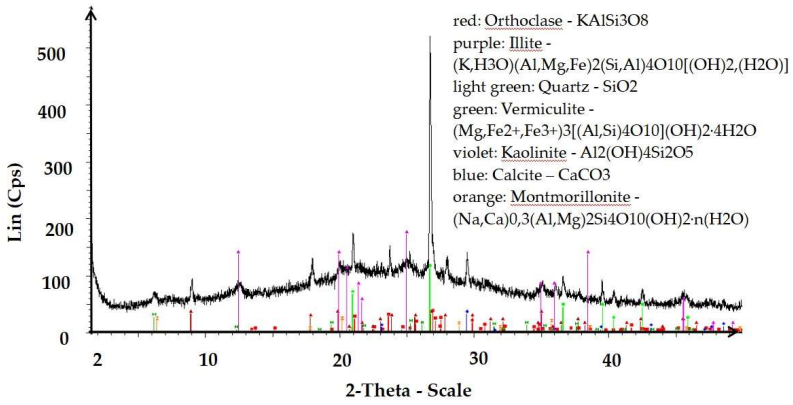

(b)

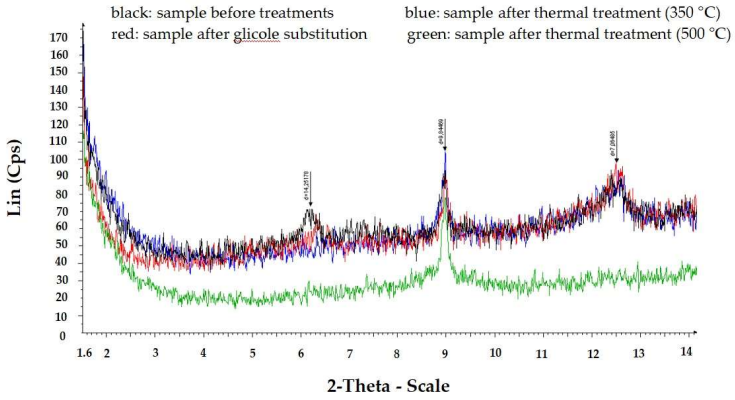

(c)

Figure 4.1. Characteristics of material used for production of specimens, (a) granulometry, (b) mineralogical composition

4.3. Specimen preparation

As previously mentioned, based on the granulometry of rammed earth heritage, four different mixtures with granulometric properties shown in Figure 4.1a, has been considered for specimen preparation in order to reproduce rammed earth in a controlled way in the lab. Therefore, for each granulometric curve, the three-layer samples were prepared by varying the water content and the number of blows needed for reaching the compactive efforts. The soil is compacted in a cylindrical mold of volume 206.23 cm^3 attached to an extension of volume 102.089 cm^3 at the top and to a baseplate at the bottom (Figure 4.2). The diameter of the mold is 51 mm. The height of the mold and the extension is 102 and 50 mm, respectively.
The specimen preparation procedure is made of four steps:

- weight 500 g of earth material with granulometry properties as shown in Figure 4.1a, which are composed of mixture of specific percentage (in weight) of sand (0%, 5%, 15% and 40%) and clay;
- add the needed amount of pure water for reaching the target water content (from 8% to 20%);
- prepare the three-layer specimen in the Proctor apparatus by compacting each layer with the same number of blows (8, 11 and 16.5)
- extract the specimen from the Proctor mold and cut it in 2 parts with average height of 100 and 50 mm respectively. Figure 4.2 shows the laboratory equipment. The first cylinder is used for performing ultrasonic pulse measurements and UCS tests. The compacted earth in the extension mold is used to determine the moisture content and the density of the compacted soil in the laboratory.

The first series of laboratory tests was performed to deliver different amount of compactive effort to determine the optimum moisture content of the soil. In the first series of the laboratory test, 500 g clay is mixed with varying amount of water and is compacted in three equal layers by a hammer. The number of blows in each layer according to E1, E2 and E3 has been considered in this study (Table 4.1).
In the second series of the laboratory test, 500 g earth material containing clay and sand is mixed with varying amount of water and is compacted in three equal layers by the hammer.
In the third series of the laboratory test, 500 g earth material containing optimum water content is compacted in three equal layers by the hammer.
The prepared specimens can be summarized as follow
(1)
-Specimens containing clay=100% compacted by number of blows corresponding to E2
-Specimens containing clay=100% compacted by number of blows corresponding to E3
(2)
-Specimens containing clay=95%, Sand=5%, compacted by number of blows corresponding to E2
-Specimens containing clay=85%, Sand=15%, compacted by number of blows corresponding to E2
-Specimens containing clay=60%, Sand=40%, compacted by number of blows corresponding to E2
(3)
-Specimens with optimum water content
-Specimens containing clay=100% compacted by number of blows corresponding to E2
-Specimens containing clay=85%, Sand=15%, Silt=0%, compacted by number of blows corresponding to E2

-Specimens containing clay=60%, Sand=40%, Silt=0%, compacted by number of blows corresponding to E2

Table 4.1. Number of blows per layer corresponding to each compactive efforts

	Number of blows Layer 1	Number of blows Layer 2	Number of blows Layer 3
E1	8	8.5	8
E2	11	11	11
E3	16.5	16.5	16.5
E4	25	25	25

(a)

(b)

(c)

(d)

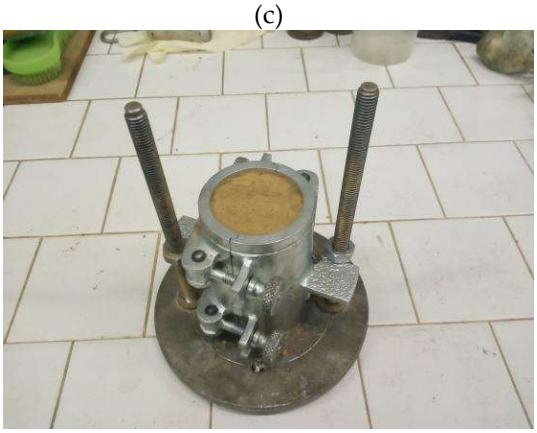

(e)

(f)

(g)

(h)

(i)

(j)

(k)

(l)

Figure 4.2. Equipment and the procedure for production of specimens; (a) cylindrical mold and extension mold, (b) preparation of the mixture, (c) the first layer of the mixture poured into the mold, (d) the compacted first layer, (e) the second layer of the mixture poured into the mold, (f) the compacted second layer, (g) the third layer of the mixture poured into the mold, (h) the cap placed on the mixture in the mold , (i) removal of the extension after compaction, (j) removal of the cap, (k) the specimen in the mold after cutting the compacted earth in the extension part, (l) the specimen, after removal of the mold

4.4. Characterization of density-moisture content curve

This section reports the assessment of the compaction effort and the moisture content during compaction on wet and dry density of earth material. The list of specimens and their

characteristics have been summarized in Table 1.1 in Appendix 1. Moreover, Table 1.2 in Appendix 1 reports some specific measurement of weight and geometry (Figure 1.1 in Appendix 1). The specimens produced in the current study have been shown in Figure 4.3.

The moisture content (w), often expressed as a percentage, is the ratio of the weight of water to the weight of solids in a volume of soil. The "moisture content added" refers to the percentage of water added to the grains to make the mixture. For each test, the density, unit weight, is defined as the ratio of the weight of soil to the total volume.

The values of dry density is plotted against the corresponding water contents to obtain dry density-moisture content curve, and thus the optimum moisture content, for the soil. Figures 4.4 and 4.5 show such plots for the clay and mixtures of sand and clay, respectively. Figures 4.6 and 4.7 show the results of density-moisture content curves for varying compacting effort and varying amount of sand for compaction effort of E2, respectively.

As demonstrated in Figure 4.4, which shows three compaction curves obtained for clay, when compaction effort changes, the dry density-moisture content curve also changes. The number of layers of clay was three for all cases, while the number of compacting blows was changed and thus compacting effort was varied from E1 to E3 (Table 4.1). An increase in compacting effort from E1 to E3 results in a higher value of maximum dry density accompanied by a decrease in the optimum moisture content. Moreover, Figure 4.5 shows the obtained dry density-moisture content curves for soils containing clay and 0%, 5%, 15% and 40% sand. The compacting effort was the same for all cases, E2. The curve for soil with higher sand content is situated above and to the left of the curve for soils with lower sand content. Thus, a higher sand content results in an increase in the value of maximum dry density and, thus decrease of optimum water content.

For a given moisture content, the theoretical maximum dry density, zero air voids dry density, occurs when the degree of saturation equals 100%. The theoretically calculated curve for zero air voids dry density-water content (Gs of clay 2.7 and Gs of sand 2.65), referred to the saturation line, is shown in Figures 4.4 and 4.5. It worth mentioning that the calculated curve representing the dry density–water content at a particular compactive effort must lie completely to the left of the saturation line.

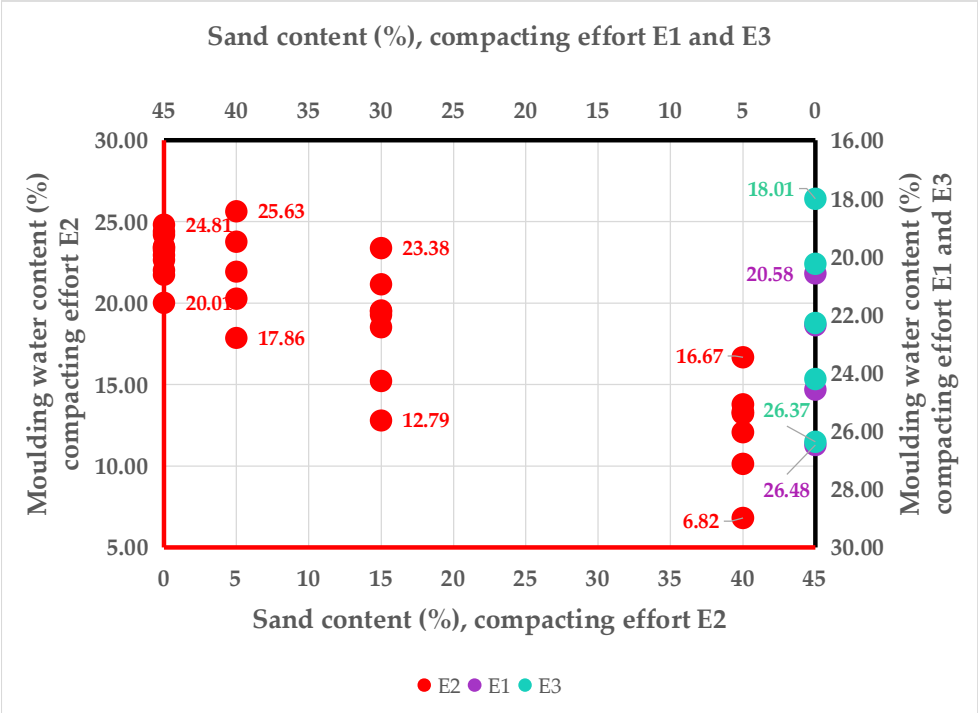

Figure 4.3. The specimens produced in current study

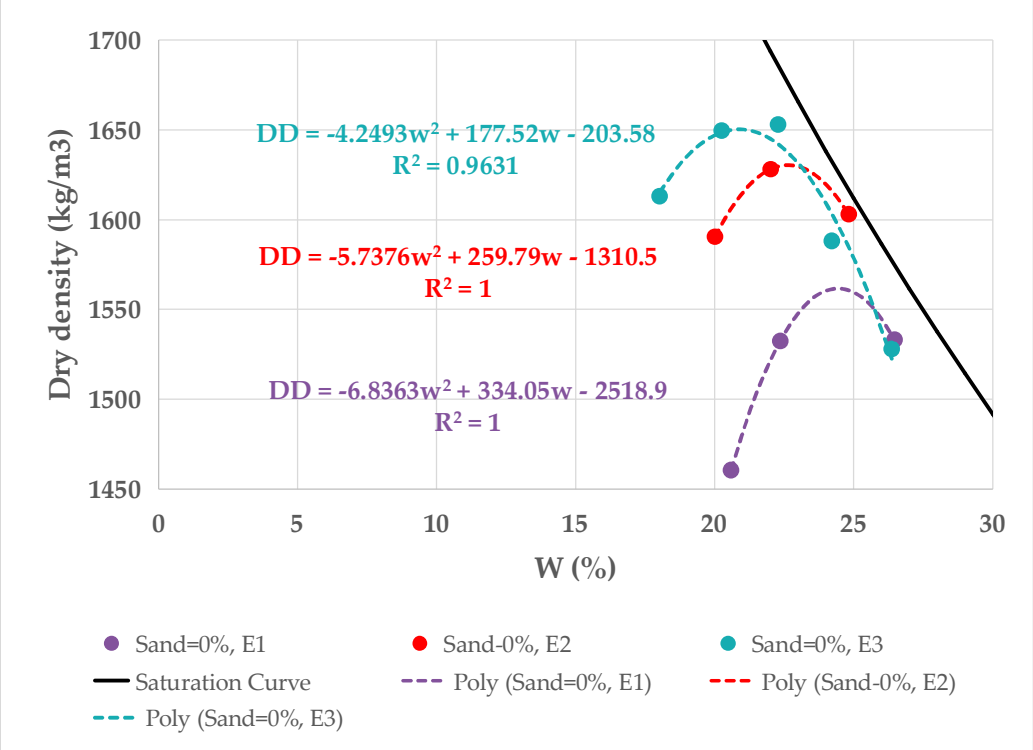

Figure 4.4. Dry density-moisture content curve for specimens with different compactive effort

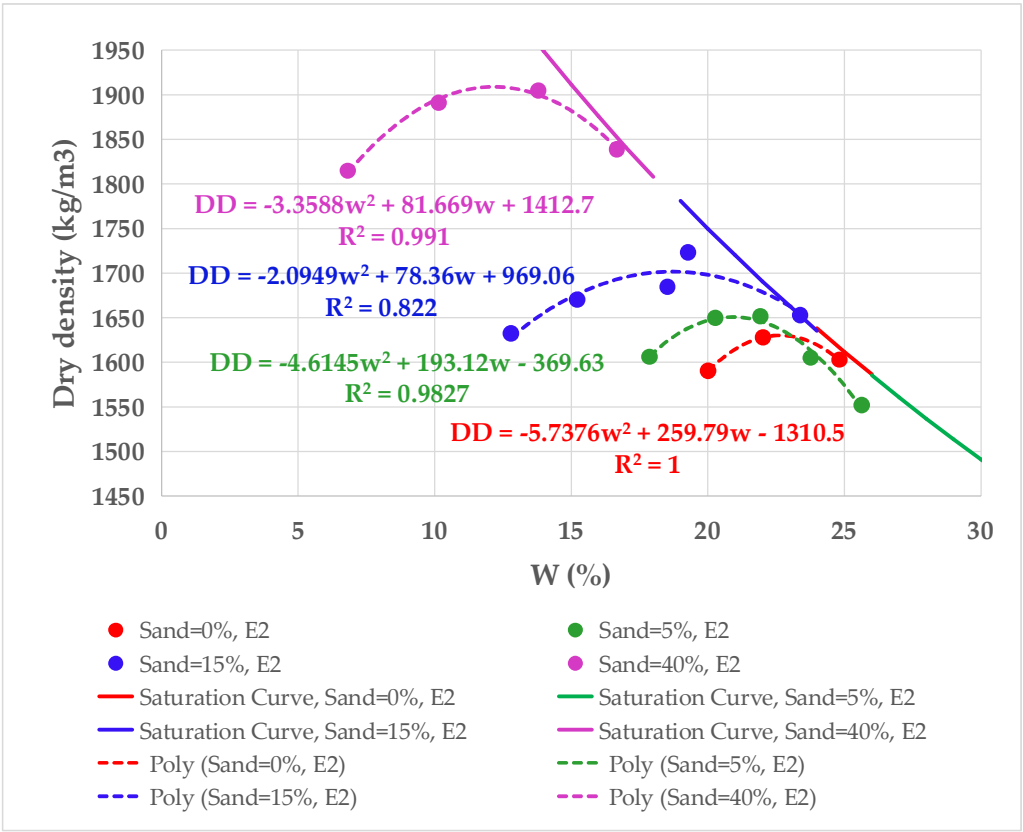

Figure 4.5. Dry dnsity-moisture content curve for specimens with different sand content

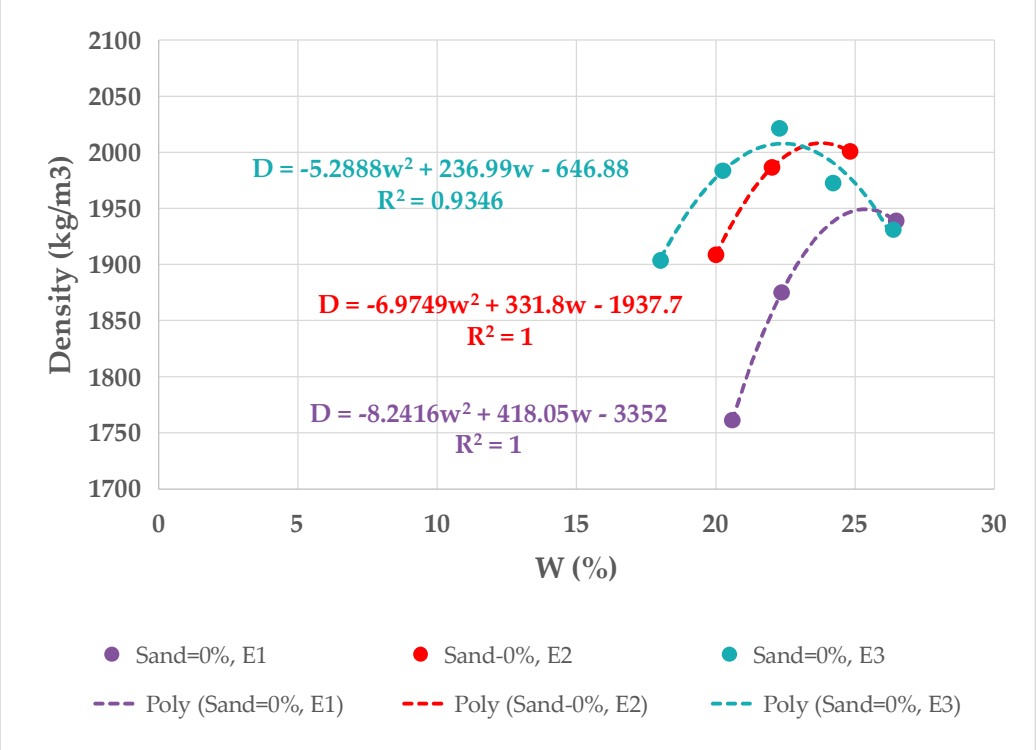

Figure 4.6. Density-moisture content curve for specimens with different compactive efforts

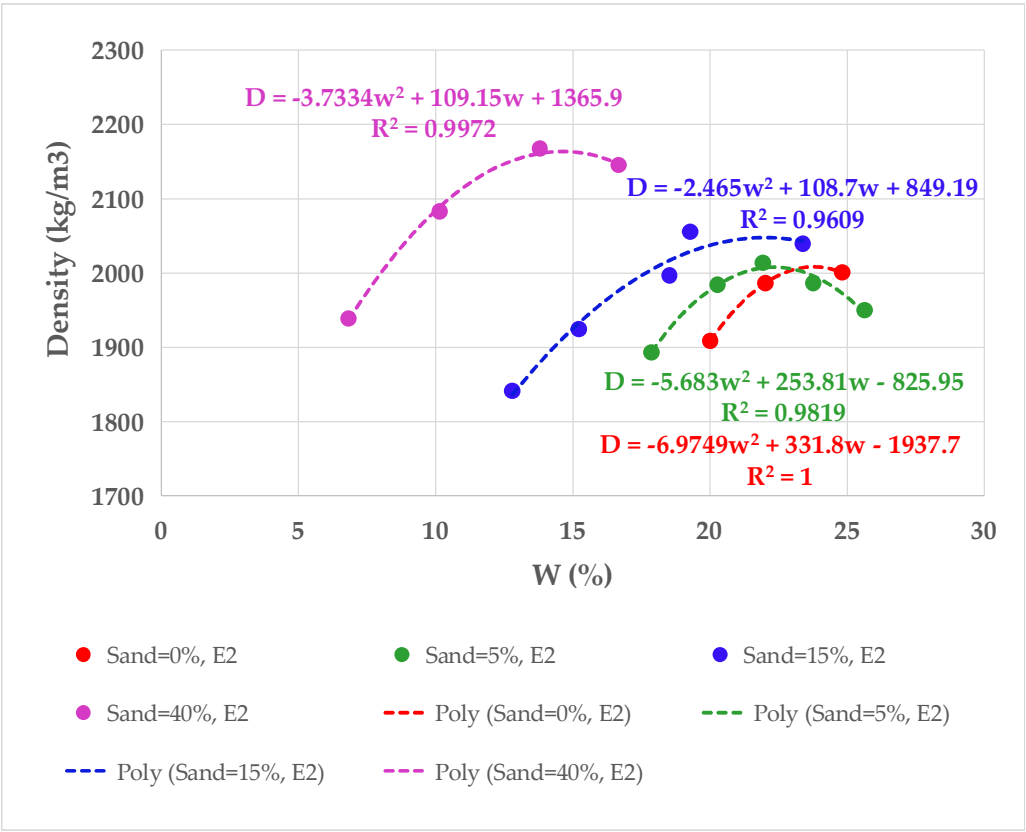

Figure 4.7. Density-moisture content curve for specimens with different sand content

As data demonstrate, a general order 2 polynomial trendline can be considered for variation of dry density or density versus water content for rammed earth specimens (Eq. 4.1).

$$D = aw^2 + bw + c \qquad \textbf{Eq. (4.1)}$$
$$DD = aw^2 + bw + c$$

Based on regression analysis, the constants of Eq. 4.1 have been obtained for materials included in this study, which has been demonstrated in Figures 4.4-4.7 and summarized in Table 4.2.

Table 4.2. Results of regression analysis for density-water content and dry density-water content curves of specimens

Specimens	Parameters for Density-Water content					Parameters for Dry density-Water content				
	a	b	c	W_{opt} (%)	D_{opt} (Kg/m^3)	a	b	c	W_{opt} (%)	D_{opt} (Kg/m^3)
S01Sa0Si0W20E1	-8.2416	418.05	-3352	25.36	1949	-6.8363	334.05	-2518.9	24.43	1562
S02Sa0Si0W18E1										
S03Sa0Si0W16E1										
S04Sa0Si0W14E1										
S01Sa0Si0W20E2	-6.9749	331.8	-1937.7	23.79	2008	-5.7376	259.79	-1310.5	22.64	1630
S02Sa0Si0W18E2										
S03Sa0Si0W16E2										
S04Sa0Si0W14E2										
S01Sa0Si0W20E3	-5.2888	236.99	-646.88	22.40	2008	-4.2493	177.52	-203.58	20.89	1650
S02Sa0Si0W18E3										
S03Sa0Si0W16E3										
S04Sa0Si0W14E3										
S05Sa0Si0W12E3										
S01Sa5Si0W20E2	-5.683	253.81	-825.95	22.33	2008	-4.6145	193.12	-369.63	20.93	1651
S02Sa5Si0W18E2										
S03Sa5Si0W16E2										
S04Sa5Si0W14E2										
S05Sa5Si0W12E2										
S01Sa15Si0W16E2	-2.465	108.7	849.19	22.05	2048	-2.0949	78.36	969.06	18.70	1702
S02Sa15Si0W14E2										
S03Sa15Si0W12E2										
S04Sa15Si0W10E2										
S05Sa15Si0W08E2										
S01Sa40Si0W12E2	-3.7334	109.15	1365.9	14.62	2164	-3.3588	81.669	1412.7	12.16	1909
S02Sa40Si0W10E2										
S03Sa40Si0W8E2										
S04Sa40Si0W6E2										

4.5. Characterization of soil-water-air system

Unsaturated soil is a three phase soil-water-air system with certain intrinsic properties of each phase. Clarification of relationships between the volume and mass of each phase is prerequisite for better understanding the roles that they play on the properties of rammed earth. The relationship between these phases is important in understanding and estimating unsaturated soil response.

In an element of unsaturated soil, common indexes include void ratio (e), porosity (P), and specific volume (V_{sp}) described as below

$$e = \frac{V_V}{V_s} \qquad \textbf{Eq. (4.2)}$$

$$P = \frac{V_V}{V}$$

$$V_{sp} = \frac{V}{V_s}$$

where

V_V volume of void space, water and air spaces
V_S volume of solids
V volume of soil
V_{sp} specific volume

Water content can be described in terms of degree of saturation (Sr), gravimetric water content (w), and volumetric water content (vwc), which are defined and related to each other as follow

$$Sr = \frac{V_W}{V_V} \qquad \textbf{Eq. (4.3)}$$

$$w = \frac{M_W}{M_S}$$

$$vwc = \frac{V_W}{V}$$

where

V_W volume of pore water
M_S mass of solids
M_W mass of pore water

One specific parameter that is essential to describe physical properties and that affects the mechanical property is the void ratio of the soil. Void ratio is described as a measure of the relationship between distribution of voids, containing air and water, and solid phase, and thus water storage capacity of soil. As the amount of water in the soil is changed, the variation of stress state contributes to the variation of the distribution of the solid, water and air phases, and thus void spaces change. As the water content is increased, more voids are filled with water, forcing out or entrapping and compressing air, the soil moves from a drier condition to saturated state. In an unsaturated soil component, air voids exists in the form of continuous or discontinuous channels.

The void ratio of one soil can change considerably. It is important to mention that specimens with the same particle size distribution but different compaction characteristics such as moulding water content and compactive effort, and thus void ratio and porosity, should be

treated as different soils, presenting different engineering properties. In this regard, this section focuses on the soil structure and its contributions to the mechanical properties of compacted soil.

Soil structure, the arrangement of particles and pore spaces within soil, has great influence on the properties of compacted soils. Orientation of the particles in a soil mass is the result of many factors and exhibits two extreme soil structures, namely dispersed, parallel arrangement, and flocculated, random arrangement, with an infinite number of intermediate arrangements.

One important factor that controls the soil fabric is the compaction process. The soil structure is mainly influenced by the compaction characteristics such as moulding water content or compactive effort. The initial soil structure is controlled by the molding water content. Depending on whether the soil is compacted on the wet or dry side of optimum, soil particles may have a random arrangement, flocculated structure, or parallel arrangement, dispersed structure. It is well known that compaction on the wet side of optimum generally gives rise to a more dispersed structure, while compaction at a water content on the dry side of optimum value is considered to produce a more flocculated structure.

Figure 4.8 shows the variation of void ratio and porosity with granulometry property of soil mixture. As data illustrate, rammed earth specimens with higher sand content are characterized by lower void ratio and porosity. Generally, in the mixture of sand and clay, clay particles occupies a proportion of the sand void space. In the mixture with more sand content, more clay particles occupy the void between sand grains, leading to the development of a condition with lower void ratio and thus porosity.

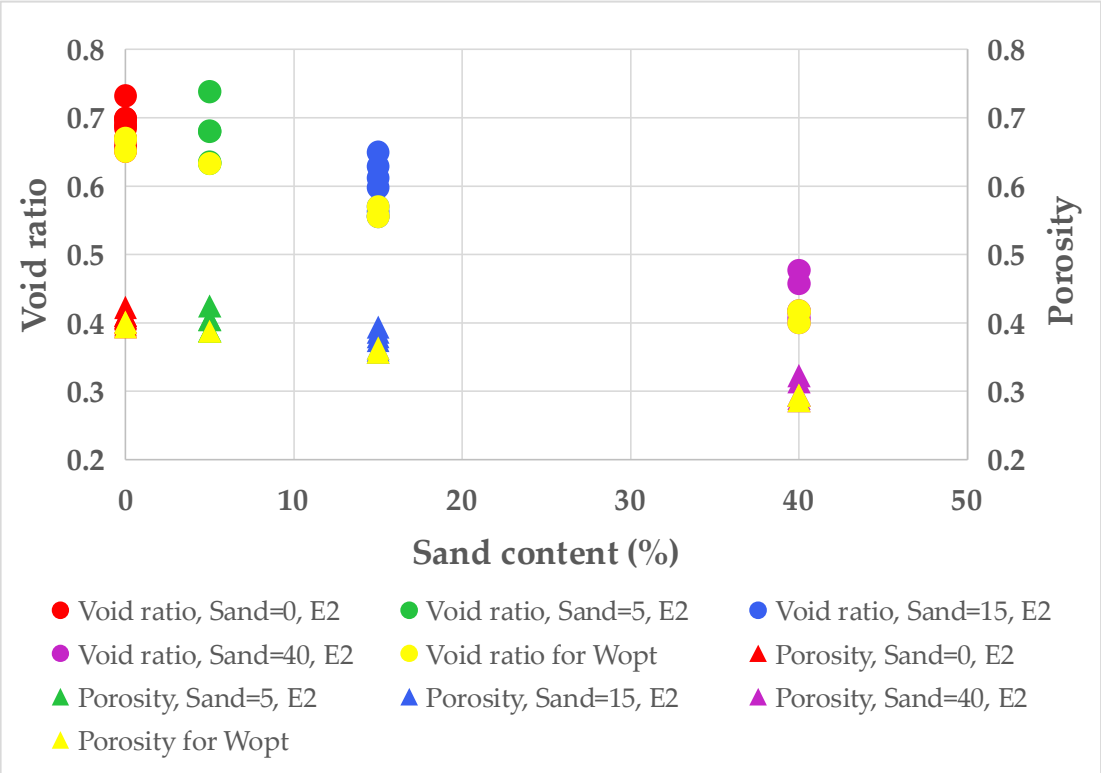

Figure 4.8. Variation of void ratio and porosity with sand content of specimens

4.6. Uniaxial compression test

In order to determine the compressive strength of rammed earth materials, specimens were loaded uniaxially up to the failure with a constant strain rate of 0.25 mm/min in the Uniaxial Apparatus. Axial displacements were measured throughout the test with a LVDT sensor. Figure 4.9 shows the uniaxial testing apparatus.

Figure 4.9. Uniaxial compression tests

Table 1.3 in Appendix 1 summarizes uniaxial compressive strength of specimens. Furthermore, void ratio (e), the ratio of the volume of void space to the volume of solids, and Degree of saturation (Sr), the ratio of the volume of water to the volume of voids, have been calculated for each specimen in this investigation, which have been reported in Table 1.3 in

Appendix 1. It should be mentioned that Gs of clay and sand was assumed to be 2.7 and 2.65, respectively.

Figure 4.10 shows the stress-strain curves for specimens under uniaxial compression loading. Strain-Stress curve for different compacting effort and different quantities of sand have been demonstrated in Figures 4.11a & 4.11b. Strain-Stress curve for specimens constructed with optimum water content has been shown in Figure 4.11c. It worth mentioning that in order to calibrate uniaxial testing machine, two preliminary tests of specimens S02Sa0Si0W16E2 with loading rate of 0.08 mm/min and S02Sa0Si0W20E2 with loading rate of 0.25 mm/min was performed. Figure 4.12 shows stress-strain curve for specimens constructed using 100% clay and 14% water added to the mixture, tested uniaxially with different loading speed of 0.125, 0.25, 0.5 and 1 mm/min.

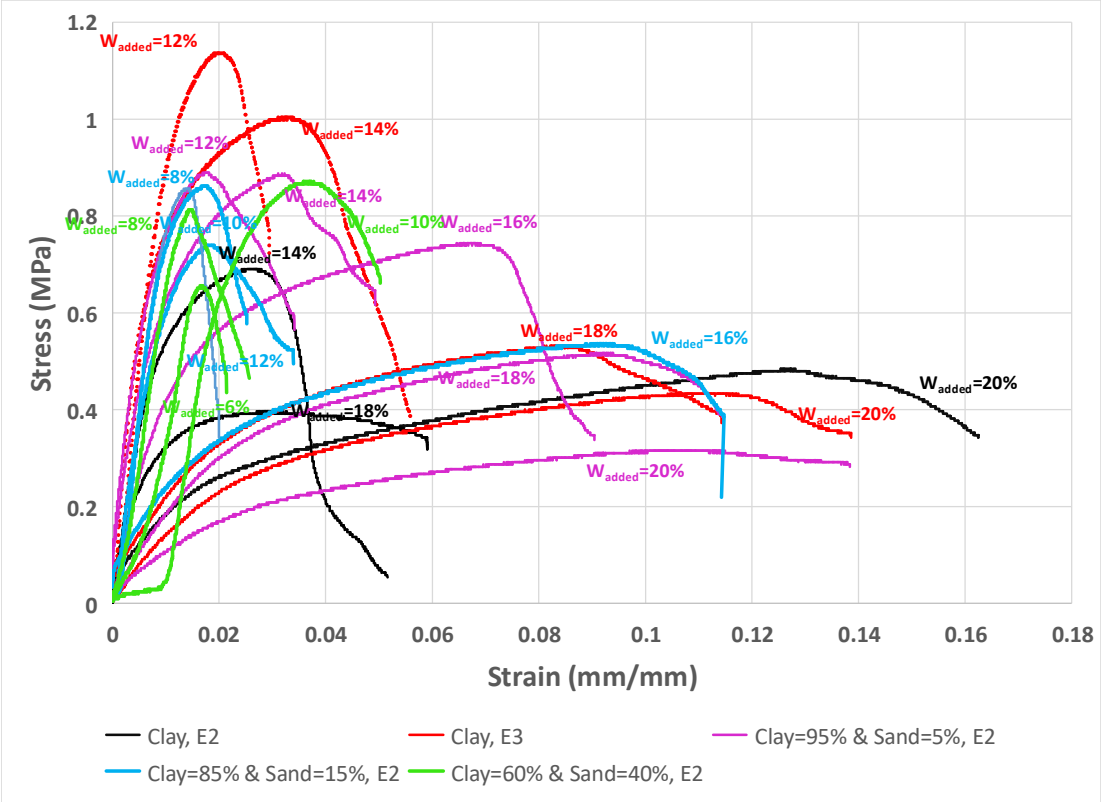

Figure 4.10. Uniaxial stress-strain curves

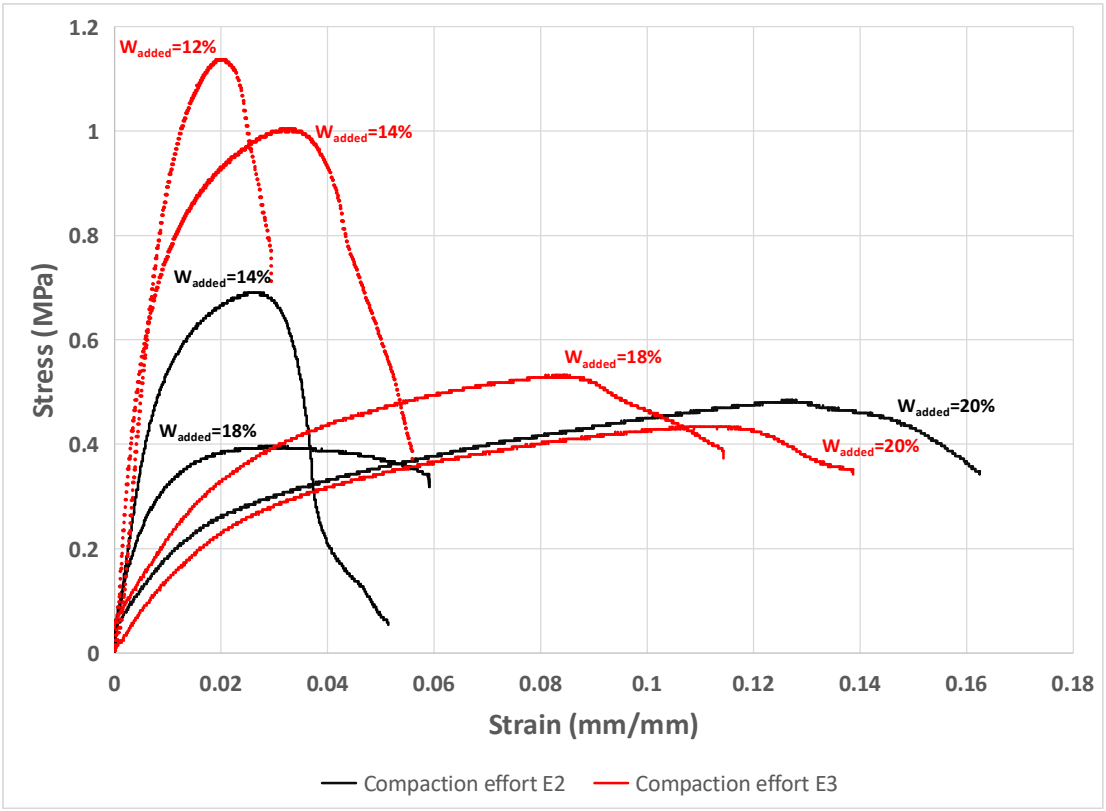
Stress (MPa)
Strain (mm/mm)
W_added=12%
W_added=14%
W_added=14%
W_added=18%
W_added=18%
W_added=20%
W_added=20%
Compaction effort E2
Compaction effort E3

(a)

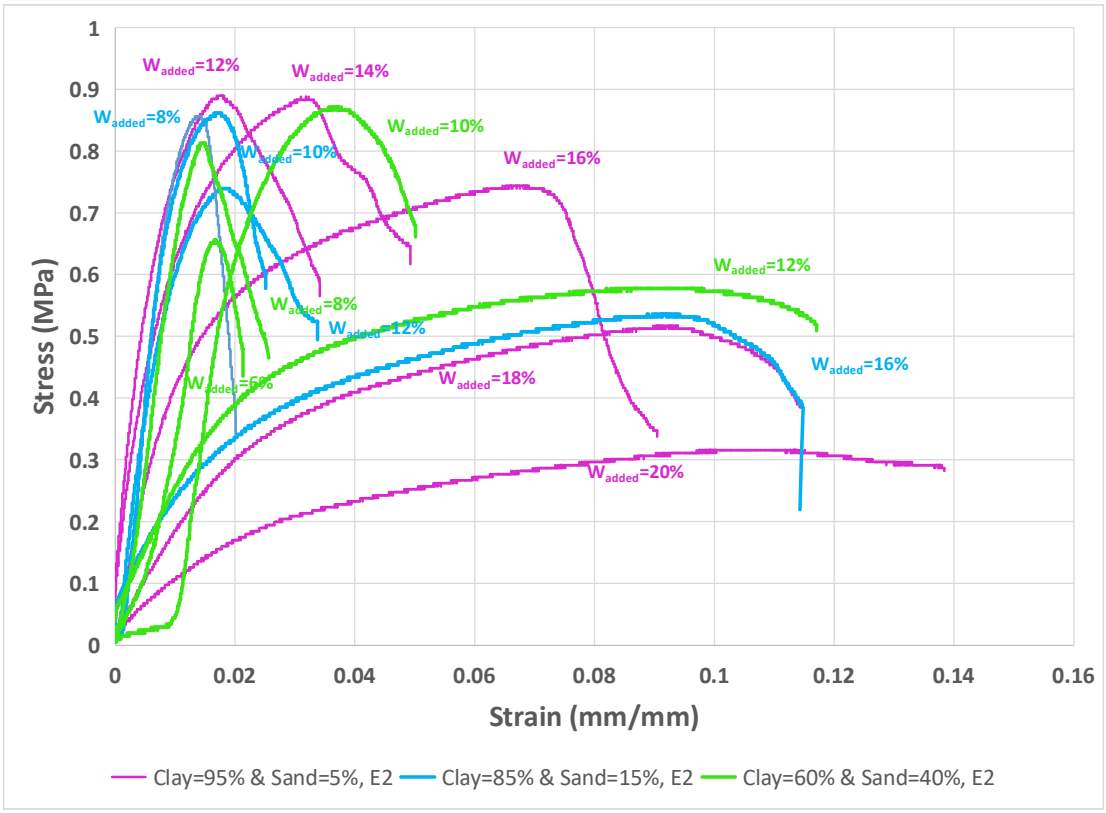
Stress (MPa)
Strain (mm/mm)
W_added=12%
W_added=14%
W_added=8%
W_added=10%
W_added=10%
W_added=16%
W_added=12%
W_added=8%
W_added=12%
W_added=6%
W_added=18%
W_added=16%
W_added=20%
Clay=95% & Sand=5%, E2
Clay=85% & Sand=15%, E2
Clay=60% & Sand=40%, E2

(b)

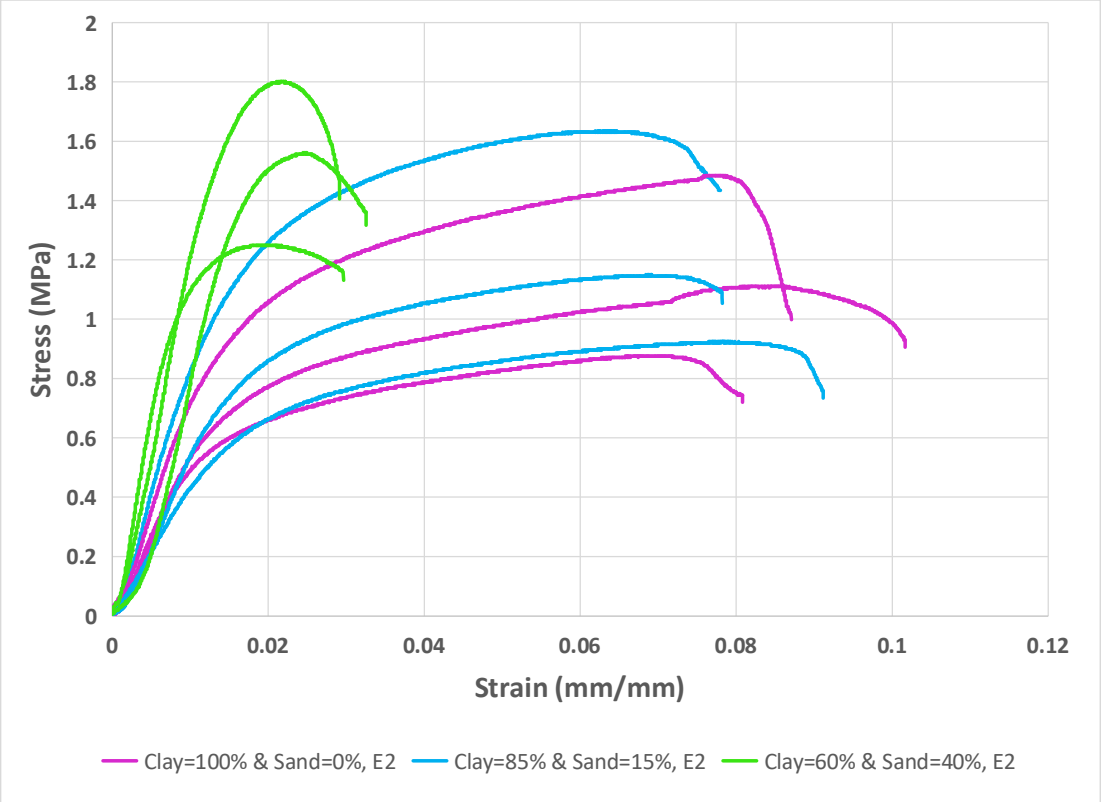

(c)

Figure 4.11. Uniaxial stress-strain curves; (a) different compactive efforts, (b) different quantities of sand, (c) specimens with optimum value of water content

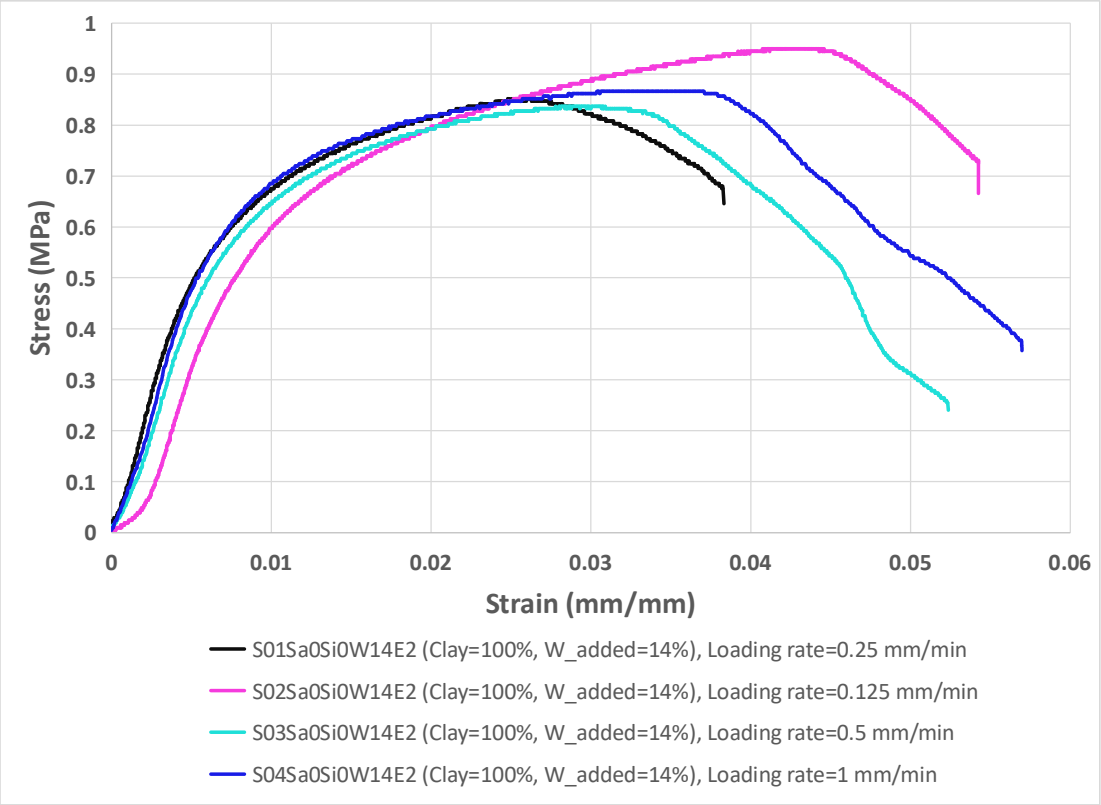

Figure 4.12. Uniaxial stress-strain curves for four different speeds of loading

4.7. Analysis of UCS results

4.7.1. Some factors affecting mechanical behaviour of rammed earth

Uniaxial compressive behaviour in rammed earth materials is a complex phenomenon involving physical, chemical, and mechanical parameters of material. Considering this coupling of different parameters, it would be ideal to explore the results of set of uniaxial compression testings performed on specimens with different material properties, so that the effects of some of the fundamental factors, that would seem to affect the mechanical behaviour of rammed earth, could be investigated.

4.7.1.1. Effect of grain size distribution

The results of the set of uniaxial compression testing performed on specimens with four different amount of sand content, 0%, 5%, 15%, and 40%, presented in Figures 4.10 and 4.11b, suggest that sand content plays a significant role in mechanical behaviour and the strength level of rammed earth material.

As demonstrated in Figure 4.10, addition of sand content generally increases the magnitude of compressive strength of material. This observed mechanical behaviour would seem to indicate that higher sand content makes it more difficult for cracks to form and propagate. Under uniaxial loading conditions, the rammed earth material with higher amount of sand requires higher stresses to initiate cracking and higher stresses to maintain crack propagation, relative to specimens with lower amount of sand. Addition of sand content shows that as the moulding water content is varied the influence of sand content on mechanical behaviour changes. These effects are found to be dependent on the interaction between water content and sand content associated with composition and structure of material.

It would also appear that, the rate of strength achievement for lower sand content may be smaller. Analysis of stress-strain plots for the test specimens (Figure 4.10) shows that the brittleness of the material significantly increases with increasing sand content, whereas lower sand content provides a longer stress-strain paths for development of the maximum stress level obtained.

Moreover, the stress-strain results suggest that with the addition of sand content the level of deformation, and thus the level of stain, required to achieve maximum stress should be lower than that required for specimens with lower amount of sand content.

Furthermore, observations reveal that the strength enhancement attributable to increase of sand content in the specimens with higher amount of sand content is significantly lower than that seen in the specimens with lower amount of sand content (Figure 4.10).

4.7.1.2. Effect of compactive effort

Compacting effort would seem to have a great influence on mechanical behaviour of rammed earth. Uniaxial compression testing of specimens constructed with different compacting effort (Figure 4.11a) reveals that, although the composition of these specimens are similar, the variation in compactive effort results in differing mechanical behaviour.

Uniaxial compressive strength for specimens constructed with lower compacting effort were found to be smaller than that for the specimens constructed with higher compacting effort (Figure 4.11a). This would be expected since strength properties generally increase with increasing density.

It should also be noted that, unlike the results obtained for the specimens S02Sa0Si0W18E2 and S04Sa0Si0W14E2, an increase in strength due to increase of compactive effort did not occur for the specimen S01Sa0Si0W20E2. Surprisingly, the strength of the specimen constructed with 20% water content, and with compacting effort E2, seems to be slightly higher than that of specimen constructed with 20% water content and compacting effort E3. This might be explained by the observation that there exists an upper limit for water content, characteristic to each rammed earth material, within which an increase in water content contributes in an increase in dry density. Once this upper limit water content was reached, with an increase in water content, the magnitude of dry density begins to decline (Figure 4.14). Lower strength of specimen S01Sa0Si0W20E3, compared to the specimen S01Sa0Si0W20E2, seems to suggest that the stress-strain behaviour is linked to a complex interaction of water content and compactive effort. This would also seem to suggest that the strength properties of specimens with an amount of water content close to saturation state are partly independent of compacting effort, and thus it can be noted that in such extreme cases, other material properties might control or partly control the overall mechanical behaviour of the specimen.

The compacting effort, which is shown to be relatively unimportant in specimens with higher water content, plays a decisive role in engineering behavior of those with lower water content (Figure 4.11a). This suggests that the strength properties of more plastic type rammed earth materials may slightly increase with increasing compacting effort.

4.7.1.3. Effect of water content

On other hand, water content influences the engineering behavior of rammed earth specimens. The plot in Figure 4.11b shows that for specimens constructed with 60% of clay and 40% of sand, an increase in water content from 6% to 8% and then 10% has resulted in an increase in strength, whereas an increase in water content from 10% to 12% has contributed to a decrease in strength of material. This might be explained by the observation that there exists an upper limit for water content, characteristic to each rammed earth material, whereby the much larger water content seem to induce lower dry density. A similar pattern can be seen for specimens with 95% of clay and 5% of sand, and specimens with 85% of clay and 15% of sand, however the upper limits for water content are different.

4.7.2. Deformation behaviour of rammed earth specimens

From the stress-strain and the deformation behaviour of different rammed earth material compositions the following may be suggested.

Both ductile and brittle types of deformation behavior are observed in rammed earth specimens under different conditions subjected to uniaxial compression loading. From the Figures 4.10 and 4.11, it can be seen that the stress-strain behavior of the specimens at relatively lower water contents is such that the slope of the curves in the post-peak region are closer to being horizontal, indicating a more ductile type of deformation behavior. The results also indicate that the strain values at peak strength for these specimens seem to be greater. The strain at peak strength tend to increase with increasing water content, suggesting a more ductile behaviour. At higher water contents of these specimens the strain at peak strength tends to be higher at lower sand contents.

At low water contents a prominent peak is observed in the stress strain curves of the specimens, indicating a more brittle type of deformation. This is very clearly noticeable in the specimens at high sand contents (Figures 4.10 and 4.11), where at peak strength a rapid loss

in strength with a slight increase in axial strain occurs. The above results therefore suggest that the deformation behavior tends to be more of a brittle type when the water content is decreased and more of a ductile type at higher water content, closer to their saturation state.

4.7.3. Strength characteristics

The variation of compressive strength (CS) with sand content has been shown in Figure 4.13. As data illustrate (Figure 4.14 and 4.15), specimens with water content close to optimum value displays higher compressive strength. Since specimens with optimum water content are shown to have the lowest void ratio and porosity (as shown in Figure 4.8), higher strength of specimens with optimum value of water content can be interpreted to indicate that as the void ratio decreases, the uniaxial compression strength increases. Strength in soil is well acknowledged as the result of the development of high density and low void ratio.

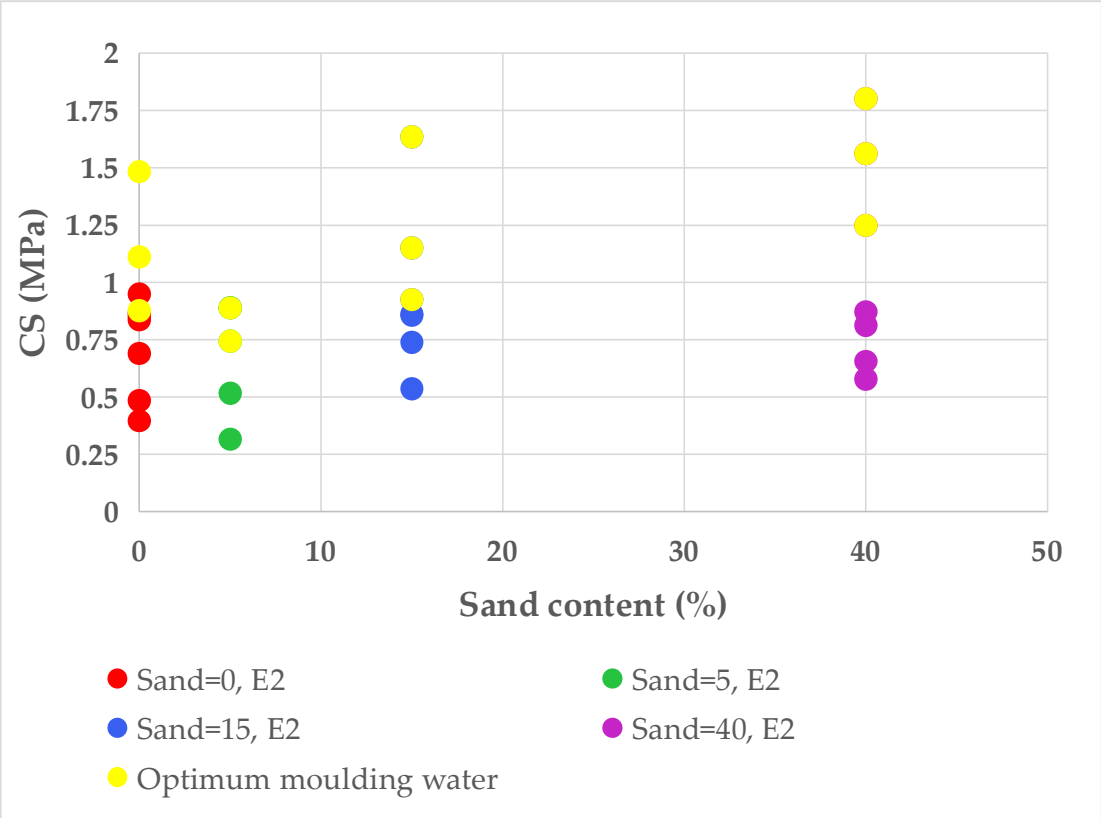

Figure 4.13. Variation of compressive strength (CS) with sand content

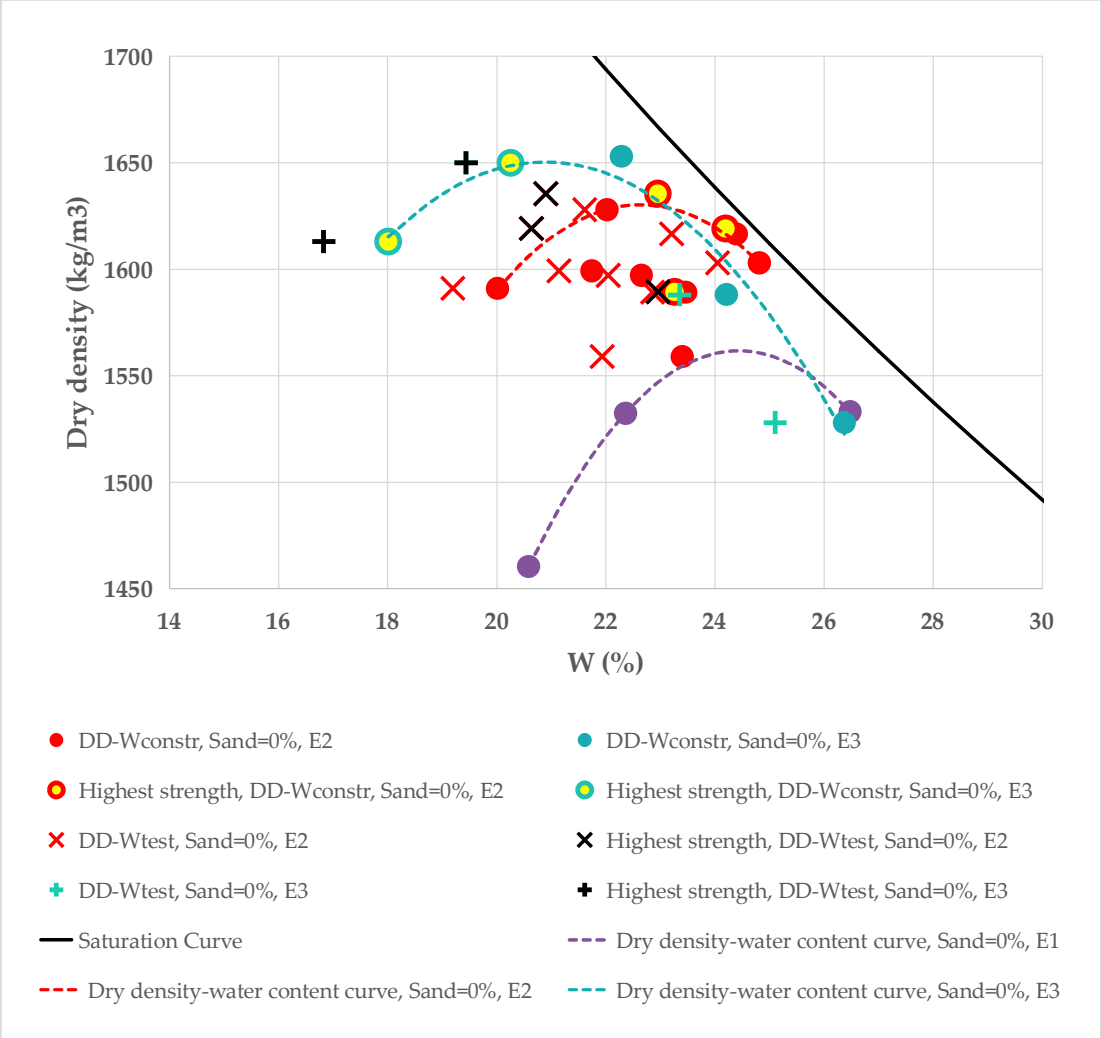

Figure 4.14. Association of highest strength specimens with dry density and water content at construction (Wconst) and water content at test (Wtest) for different compactive effort

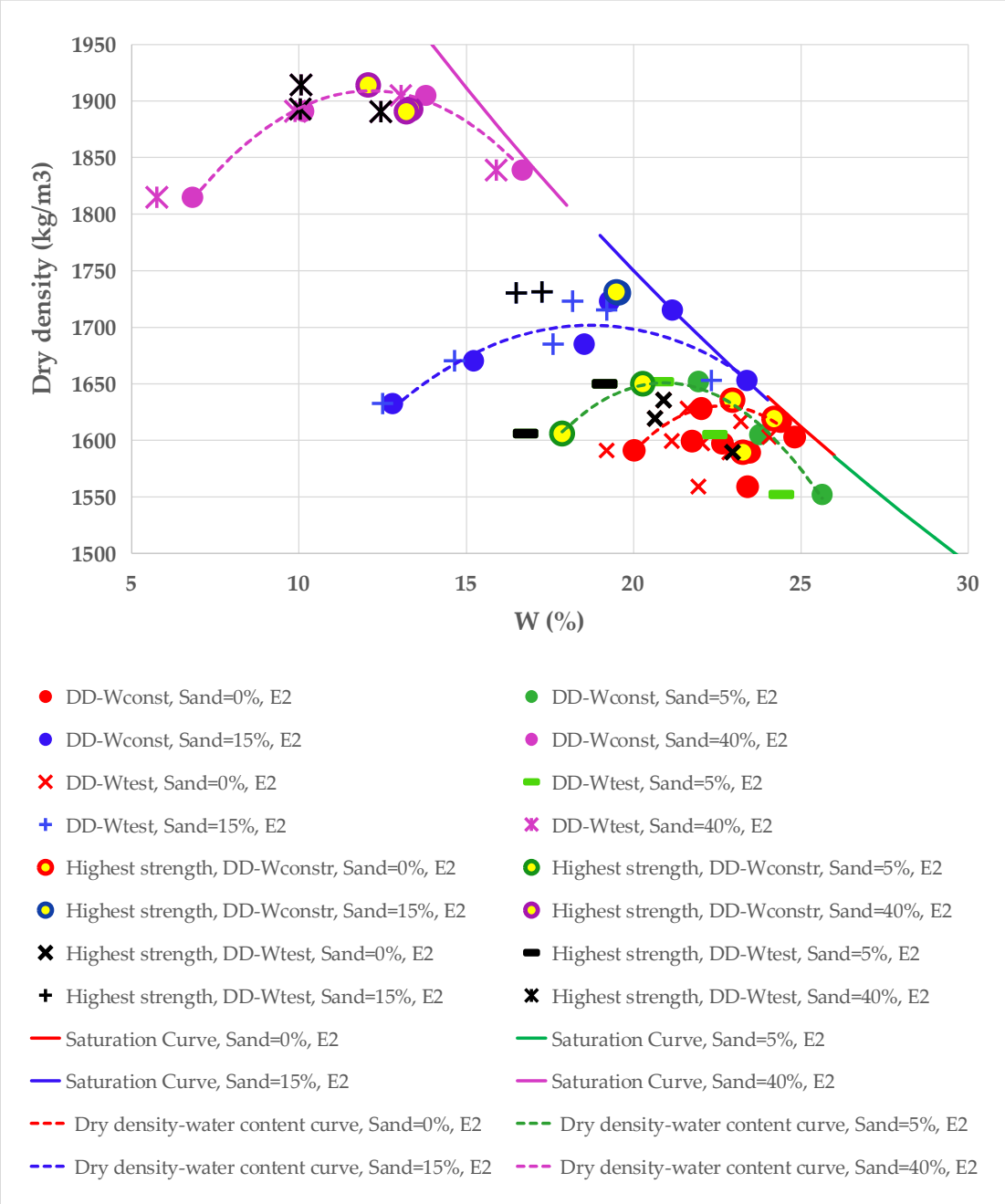

Figure 4.15. Association of highest strength specimens with dry density and water content at construction (Wconst) and water content at test (Wtest) for different sand content

4.7.4. Suction

As previously mentioned, rammed earth heritage are constructed using compacted soils. The engineering properties of compacted earth are influenced by soil fabric, controlled by the type of soil and compaction characteristics, such as compactive effort and design water content. Exposure of rammed earth heritage to different conditions at post construction alters the initial design water content, and thus degree of saturation during their lifetime. Due to the lack of data in this regards, little is known on how this can affect the mechanical properties and engineering behaviour.

The water content that is known to have a profound influence on mechanical behaviour, and thus strength, includes not only the level of moisture content at which the soil is compacted, i.e. the molding water content, but also any variations in moisture content during lifetime after construction. Under these conditions, changes in strength upon drying, the relationship between the strength and saturation, and hence, soil suction, are particularly important in understanding and estimating contribution of this complex phenomena in engineering behaviour of rammed earth over time.

The three categories of specimens, SU1, SU2 and SU3 (Table 4.3), each constructed with the same mixture of material at optimum water content (as detailed in Table 1.1 Appendix 1), has been considered herein for observation of compacted earth behaviour during drying. The observed relationships between the water content and corresponding compressive strength characteristics of these three soil fabrics has been shown in Figure 4.16. The observed changes in properties of rammed earth during drying can provide practical insights on the contributions of suction to strength gain of material, when dealing with this problem.

Table 4.3. Group of specimens for investigation of the influence of drying on CS

SU1	S01Sa0Si0W17E2
	S02Sa0Si0W17E2
	S03Sa0Si0W17E2
SU2	S01Sa15Si0W14.7E2
	S02Sa15Si0W14.7E2
	S03Sa15Si0W14.7E2
SU3	S01Sa40Si0W9.2E2
	S02Sa40Si0W9.2E2
	S03Sa40Si0W9.2E2

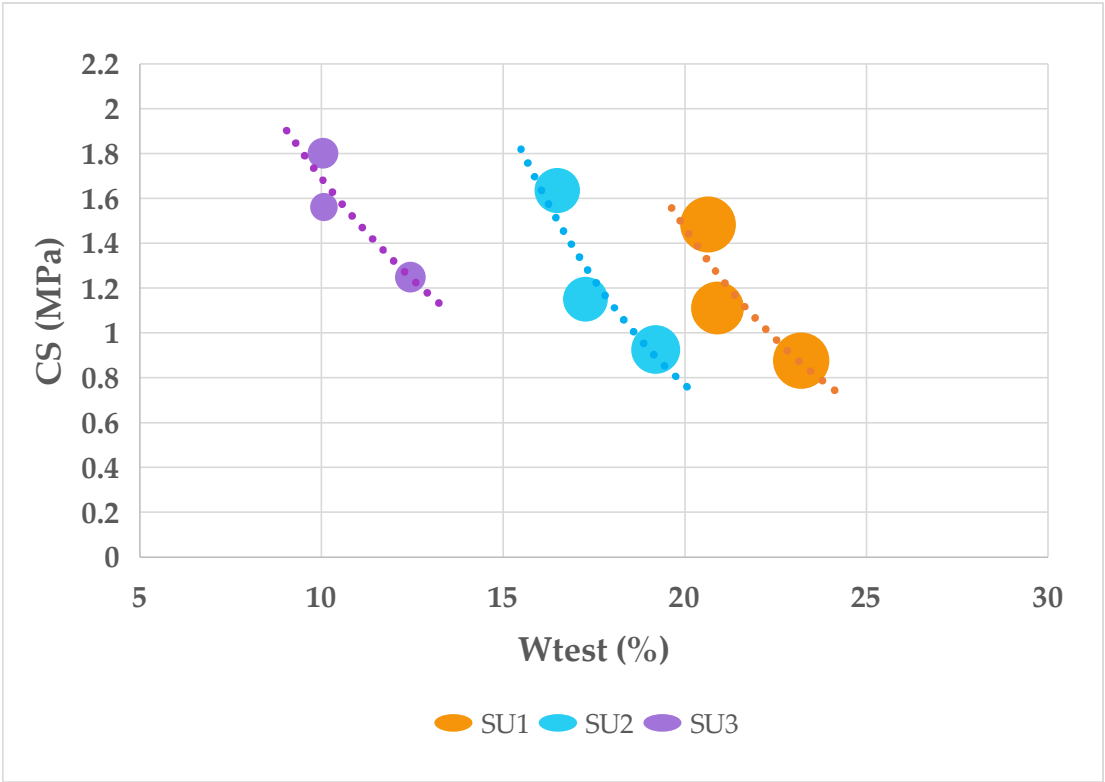

Figure 4.16. Influence of drying on CS

4.7.5. Assessment of stress-strain curves

The observed stress-strain behaviour of compacted earth can be related more to the soil structure, attributed to the complex effect of many soil factors, than to any single soil variable. Therefore, it can be concluded that, of the numerous factors affecting stress-strain response of rammed earth specimens, soil structure is one of those playing a controlling role. It can be observed in Figures 4.10 and 4.11 that varying the molding water content considerably varies stress-strain behaviour, which is primarily affected by the soil structure.

As observed in Figure 4.11a, by increasing the compactive effort at a given moisture content, corresponding to the same weigh of water added to the mixture, a pronounced variation in stress-strain behaviour is produced. As the data illustrate, stress-strain property of rammed earth is strongly affected by compactive effort. Since the effect of compactive effort plays a vital role in the establishment of soil structure, it can be inferred that soil structure makes a major contribution in controlling strain-stress behaviour of rammed earth material. This indicates that mechanical properties of compacted earth vary with soil structure.

The shape of stress-strain curve can be considered to be dependent on the soil structure. Different shapes of Stress-strain curves of specimens, as presented in Figure 4.10 and 4.11, can be associated to different soil structures. The stress-strain curves of specimens with different compactive effort of E2 and E3 are shown in Figure 4.11a, demonstrating that higher compactive effort resulted in higher compressive strength and an increase in the corresponding strain at peak stress.

In some specimens, such as S01Sa0Si0W20E2, loading the specimens resulted in compaction and thus rearrangement of soil particles and reduction of pore sizes, leading to resistance of the soil to external load. In these specimens, the failure can be attributed to the dilatancy, when dilatancy resulted in gradual loss of bearing capacity. This exhibited plastic failure behaviour can be due to the structure of the soil.

In another group of specimens, such as S03Sa40Si0W8E2, as the axial strain increases, the axial stress initially increases, followed by a decreasing trend after reaching peak stress, strain-softening.

It is commonly accepted to associate higher levels of dispersion in the microfabric of soil to flatter stress-strain curves, presenting more plastic failure, where resistance of the soil to external stress may continue to increase at high uniaxial deformations.

The pattern of behaviour during compression of compacted soil attributed to higher level of flocculation in the structure of the soil is different from the typical behaviour observed for a more dispersed fabric. Consequently, higher level of flocculation in the structure of the soil is linked to the development of peak stress at low strains, characterised by a steeper stress-strain curves.

This indicates that a flocculated arrangement of soil particles can be characterised by higher strength and lower compressibility, and hence, resulting in a brittle mode of deformation. On the contrary, higher level of dispersion in the arrangement of particles can be characterized by lower strength, higher compressibility, leading to a ductile mode of deformation.

Since the variation in the specimens are either results of sand content or compactive effort introduced, the variation in characteristics of stress-strain curves, can be attributed, either directly or indirectly, to the structural solid-air-water system established in the soil during construction. Therefore, the strength of specimens is related to the load required to overcome resistance of the soil structure.

Therefore, brittle stress-strain behaviour observed in specimens such as S03Sa40Si0W8E2, can be attributed to the establishment of a more flocculated structure. In these specimens with a predominant flocculated fabric, a high energy open structural configuration due to

interparticle attraction, results in greater difficulty of displacing and reorientating particles. Therefore, it is evident that a sufficient external load is required to overcome structural strength, its resistance to reorientation, and cause movement and rearrangement of particles and subsequently collapse of structure.

For specimens such as S01Sa0Si0W20E2, a more ductile behaviour can be observed, which can be attributed to a more dispersed fabric of these specimens. In these specimens, uniaxial compressive loading gives rise to movement and some reorientation of particles to a more parallel oriented soil structure.

Moreover, for a given weigh of water added to the mixture on the wet side of optimum, specimens with higher compactive effort tend to show a stress-strain curve of a more disperesed structure. This may be interpreted to indicate that the fabric of the specimens compacted at the higher compactive effort on the wet of optimum tend to be more dispersed.

4.8. Conclusion

The results of this study reveals that soil structure appears to influence the mechanical behaviour of specimens. Stress-strain behaviour and uniaxial compression properties indicated a dependence on the structure of the soil and compaction characteristics. The sand content and compaction properties, such as moulding water content, has shown a significant influence on compressive strength. Increasing compactive effort on dry side of optimum has resulted in an increase in compressive strength. It should be mentioned that higher level of compaction on wet side of optimum may contribute to a lower strength value accompanied by a small decrease in strain at failure.

References

Beckett, C.T.S.; Augarde, C.E.; Easton, D.; Easton, T. Strength characterisation of soil-based construction materials. Géotechnique, 2018, 68(5), 400-409.

Bruno, A.W.; Gallipoli, D.; Perlot, C.; Mendes, J. Mechanical behaviour of hypercompacted earth for building construction. Mater Struct. 2017, 50(2), 160.

Bui, Q.B.; Morel, J.C.; Hans, S.; Walker, P. Effect of moisture content on the mechanical characteristics of rammed earth. Constr Build Mater. 2014, 54, 163-169.

Bui, QB.; Morel, JC.; Reddy, BVV.; Ghayad, W. Durability of rammed earth walls exposed to 20 years of natural weathering. Build Environ. 2008, 44, 912–919.

Bui, QB.; Morel, JC. Assessing the anisotropy of rammed earth. Constr Build Mater. 2009, 23, 3005–3011.

Bui Q.B.; Morel J.C.; Hans, S.; Walker, P. Water effects on the mechanical characteristics of rammed earth buildings: a double-edged sword. Constr Build Mater. 2013.

Burroughs, V.S. Quantitative criteria for the selection and stabilisation of soils for rammed earth wall construction. PhD Thesis, University of New South Wales, Australia, 2001.

Canivell, J.; Martin-del-Rio, J.J.; Alejandre, F.J.; García-Heras, J.; Jimenez-Aguilar, A. Considerations on the physical and mechanical properties of lime-stabilized rammed earth walls and their evaluation by ultrasonic pulse velocity testing. Constr Build Mater. 2018, 191, 826-836.

Cheah, J.S.J.; Walker, P.; Heath, A.; Morgan, T.K.K.B. Evaluating shear test methods for stabilised rammed earth. Proceedings of the Institution of Civil Engineers-Construction Materials, 2012, 165(6); pp. 325-334.

Ciancio, D.; Gibbings, J. Experimental investigation on the compressive strength of cored and molded cement-stabilized rammed earth specimens. Constr Build Mater. 2012, 28(1), 294–304.

Ciancio, D.; Jaquin, P.; Walker, P. Advances on the assessment of soil suitability for rammed earth. Constr Build Mater. 2013, 42, 40-47.

El Hajjar, A.; Chauhan, P.; Prime, N.; Olivier, P. Effect of suction on the mechanical characteristics of uniformly compacted rammed earth. In IOP Conference Series: Earth and Environmental Science (Vol. 143, No. 1, p. 012045), April 2018.

Hall, M.; Djerbib, Y. Rammed earth sample production: context, recommendations and consistency. Constr Build Mater. 2004 , 18(4), 281-286.

Hall, M.; Djerbib, Y. Moisture ingress in rammed earth: part 1 – the effect of soil particle-size distribution on the rate of capillary suction. Constr Build Mater. 2004, 18, 269–280.

Hall, M.; Djerbib, Y. Moisture ingress in rammed earth: part 2 – the effect of soil particle-size distribution on the absorption of static pressure-driven water. Constr Build Mater. 2006, 20, 374–383.

Hall, M.; Djerbib, Y. Moisture ingress in rammed earth: part 3 – sorptivity, surface receptiveness and surface inflow velocity. Constr Build Mater. 2006, 20, 384–395.

Jaquin, P.A.; Augarde, C.E.; Gallipoli, D.; Toll, D.G. The strength of unstabilised rammed earth materials. Géotechnique. 2009, 59(5), 487–490.

Jayasinghe, C.; Kamaladasa, N. Compressive strength characteristics of cement stabilized rammed earth walls. Constr Build Mater. 2007, 21(11), 1971–1976.

Miccoli, L.; Müller, U.; Fontana, P. Mechanical behaviour of earthen materials: A comparison between earth block masonry, rammed earth and cob. Constr Build Mater. 2014, 61, 327-339.

Miccoli, L.; Gerrard, C.; Perrone, C.; Gardei, A.; Ziegert, C. A collaborative engineering and archaeology project to investigate decay in historic rammed earth structures: The case of the Medieval preceptory in Ambel. Int. J. Archit. Heritage. 2017, 11(5), 636-655.

Martín-del-Rio, J.J.; Flores-Alés, V.; Alejandre-Sánchez, F.J.; Blasco-López, F.J. New method for historic rammed-earth wall characterization: The Almohade ramparts of Malaga and Seville. Stud Conserv, 2019, 64(6), 363-372.

Morel, J.C.; Pkla, A. A model to measure compressive strength of compressed earth blocks with the '3 points bending test'. Constr Build Mater. 2002, 16(5), 303–310.

Olivier, M.; Mesbah, A. Constitutive equations for compacted soils. In: Proceedings of the first international conference on unsaturated soils, Paris, 1995; pp. 765-573.

Parracha, J.L.; Lima, J.; Freire, M.T.; Ferreira, M.; Faria, P. Vernacular earthen buildings from Leiria, Portugal–material characterization. Int. J. Archit. Heritage. 2019, 1-16.

Silva, R.A.; Domínguez-Martínez, O.; Oliveira, D.V.; Pereira, E.B. Comparison of the performance of hydraulic lime-and clay-based grouts in the repair of rammed earth. Constr Build Mater. 2018, 193, 384-394.

Silva, R.A.; Mendes, N.; Oliveira, D.V.; Romanazzi, A.; Domínguez-Martínez, O.; Miranda, T. Evaluating the seismic behaviour of rammed earth buildings from Portugal: From simple tools to advanced approaches. Eng. Struct. 2018, 157, 144-156.

Wangmo, P.; Shrestha, K. C.; Miyamoto, M.; Aoki, T. Assessment of out-of-plane behavior of rammed earth walls by pull-down tests. Int. J. Archit. Heritage. 2019, 13(2), 273-287.

CHAPTER 5

Interrelating non-destructive ultrasonic pulse velocity (UPV) and destructive uniaxial compression measurements for rammed earth specimens

The conservation of rammed earth heritage needs understanding of the state of material to adequately evaluate state of conservation of buildings. Therefore, the main objective of this research is to evaluate and develop the application of ultrasonic pulse velocity test in investigating the rammed earth physical and mechanical-related properties. To that aim, we have combined non-destructive UPV and destructive uniaxial compression testing measurements for rammed earth specimens, which are described in detail in this chapter. This experimental investigation has provided data whose analysis produces evidence on the material behaviour under varying conditions. Cylindrical specimens (51 mm diameter and 102 mm height) of rammed earth were produced to perform a series of uniaxial compression test and ultrasonic pulse velocity measurements.

The main objective of this chapter is to investigate the ultrasonic pulse velocity, compression and shear wave velocities of rammed earth specimens for four different granulometric distributions, to attempt evaluating the relationship between the UPV and mechanical properties - also evaluated through destructive uniaxial compression testing - and the effects of different parameters of rammed earth material on measured ultrasonic pulse velocity. This chapter discusses the behaviour of UPV through rammed earth with respect to compactive effort, grain-size distribution, water content, density, void ratio and saturation degree, and resulting modulus of elasticity. It was observed that variation in ultrasonic velocities is a comprehensive result of variation in physical and mechanical characteristics of material, will all the above-mentioned material characteristics.

5.1. Introduction

Common approaches for evaluation of structural performance and state of conservation of buildings are based on visual inspections or the assessment of their actual mechanical properties through destructive testing of a sample drilled or cut of the structure to perform standard tests . The information provided by visual inspection approach is very limited. While destructive testing of extracted core samples from structures could provide accurate information, it causes further damage to the structure, which substantially limits its use in conservation practices of cultural heritage structures.

Non destructive methods have the advantage of providing information for assessment of architectural heritage without damaging the existing structure. Ultrasonic Pulse Velocity (UPV) as one of the most commonly used non-destructive testing technique can significantly contribute to many advantages in diagnostic activities on architectural heritage and the low invasive in situ characterization of architectural heritage, strong necessity related to the conservation when dealing with the historical architectures.

The propagation velocities of ultrasonic waves in a material interrelates with the quality and strength of the material, varying as a function of many material characteristics, including the density, elastic constants of the specimen and its homogeneity. Therefore, the method of ultrasonic testing can be used to investigate the properties and structure of rammed earth material which influence the propagation velocity of ultrasonic waves. However, rammed earth is an inhomogeneous material, which contains voids and a wide variety of aggregate sizes, and thus nonuniform density distribution. Even though, the application of UPV for non-destructive characterization of materials have been subject of studies for decades , its behaviours through rammed earth is a topic little addressed in literature. Therefore, as the propagation properties of ultrasonic waves in rammed earth material is not clarified, application of the ultrasonic testing method for inspection of rammed earth heritage remains unclear. As any testing method is of value if and only if the results of it's measurements are indicative of the actual properties and state of the target material being tested, there are problems to be solved for improving the usefulness of ultrasonic test for the quality evaluation of rammed earth based on the ultrasonic velocities. Therefore, the general objective of this research is to investigate the relationship of the physical and mechanical properties obtained through destructive laboratory testings and the non-destructive ultrasonic pulse velocity measurements of rammed earth.

This study investigates the results of the ultrasonic test method for rammed earth material and the feasibility of correlating it's behavioural patterns with results obtained by destructive testing methods of investigations, herein uniaxial compression testing. The influence of compactive effort, water content and granulometry of material are of primary concern in this study.

The soil material, which is the constituent of rammed earth buildings, is the main subject of geotechnical studies. Therefore, in the framework of Tech4Culture program, an experimental program has been defined and carried out based on geotechnical and geophysical tests. Rammed earth specimens have been reconstructed in laboratory and an investigation was performed on the effectiveness of UPV in the evaluation of some characteristics of rammed earth material. Variations induced in pulse velocities by physical and mechanical characteristics, including density, water content and uniaxial compression strength have been addressed in this study.

Little has been reported in the literature discussing the behaviour of ultrasonic pulse waves through rammed earth material. Important contributions advancing our knowledge in this area include those of Silva (2013), Bernat-Maso et al. (2017), Liang et la. (2013) and Canivell et al. (2018).

In this line, it is worth highlighting the research presented by Liang et la. (2013), reporting several case studies oriented to analyse the state of existing buildings. The study performed by Liang et la. (2013) reports UPV measurements of several field-studied representative Hakka earth buildings, including 100 years old Zhencheng Tulou, 320 years old Huanji Tulou, 500 years old Wuyun Tulou and 1240 years old Fuxing Tulou. It should be mentioned that Fuxing Tulou data has been measured on wet walls due to rain.

A review of literature highlights experimental researches in which attempts have been made to correlate the UPV results with certain physical and mechanical properties of rammed earth, including porosity, dry density and uniaxial compressive strength (Canivell et al. (2018)), flexural strength (Silva (2013)), or water content (Bernat-Maso et al. (2017)). Figures

5.1 and 5.2 show the data provided by these experimentations, which has been indeed reported in Appendix 2.

An experimental campaign on rammed earth specimens carried out by Silva (2013) by means of UPV technique has addressed the repair effectiveness of mud grouts. The rammed earth specimens consisted on twelve medium-scale beams with dimensions 150x150x600 mm^3, manufactured using granulometry of 14% clay, 16% silt, 32% sand, 37% gravel, 1% pebbles. Beam specimens were manufactured in three layers of 10.42 kg weight and 50 mm thickness. Tests were performed after drying for 6 weeks at a room temperature of about 22±2ºC. The UPV measurements were performed by a testing equipment provided by MATEST and piezoelectric probes of a natural resonance frequency of about 55 kHz. The ultrasonic pulse velocities were measured immediately before the three-point bending test using the indirect method, in which the transmission and receiver probes were placed on the same surface at a given distance of 100, 200, 300, 400 and 500 mm between them. Ultrasound gel was used between the probes and the specimens.

Another remarkable work is the research conducted by Canivell et al. (2018), who used a statistics-based approach to analyse the relationships between physical and mechanical properties and ultrasonic pulse velocity in RE specimens with different moulding moisture content (MMC). In this study 40 specimens were manufactured in 5 batches of 8 cubic samples 01×0.1×0.1 m, consisted of a mixture of sand, calcareous soil known locally as ''albero'', sub-soil from the surrounding area and hydraulic lime, with the dosage in volume of 5 soil: 2 sand: 2 ''albero'': 2 lime, corresponded approximately to a ratio of sand, gravel and silty clay of 5:4:1. OM and corresponding DD of the mixture was 18.25% and 1.63 gr/cm^3, respectively. Moulding water content of batches of 1 to 5 were designed to be 18.5, 17.5, 16.5, 15.5 and 14.5. The specimens were cured for 28 days in the same environmental conditions (20 C ± 2 C and 65 ± 5% relative humidity). Following UNE-EN 12504-4 standard, ultrasonic pulse velocities were measured with an Ultrasonic-Tester BP-7 Series (UltraTestGmbH), in three directions, namely X-UPV, Y-UPV, and Z-UPV, with orientation Z corresponding to the direction of compaction.

Bernat-Maso et al. (2017) has addressed the relationship between the moisture content and the ultrasound pulse velocities of the earthen material during the drying process. In this experimental campaign, Clayey-sand soil, composed of 10% clay and silt, 65% of sand with particles up to 2mm diameter and 25% of sand with particles up to 5 mm diameter, at 12.6% of moisture content was used to produce twenty rectangular samples (100mm width × 100mm thick × 90mm height) and to study the drying process using UPV method. The methodology consisted in the desirable moisture content of 12.6%. Ultrasound pulse velocities were measured after five different curing procedures, consisted in subjecting the five groups of specimens to the curing environment (Temperature 20±2°C, RH>95%) for five different times: 0days, 3days, 7 days, 14 days and 21 days. Following the specifications of ASTM standard D 2845–05, probes of a natural resonance frequency of about 55 kHz were used to transmit and receive ultrasonic pulse in this study. Ultrasound pulse velocities were measured daily while specimens were drying at indoor environmental conditions.

An important fact is that physical and mechanical parameters which have been reported in one study has not been addressed in another, and have sometimes been ignored completely. Therefore, despite important efforts made by these contributions, the experimental data do not include all of the controlling parameters involved in characterizations of rammed earth material and thus, can not be comparable.

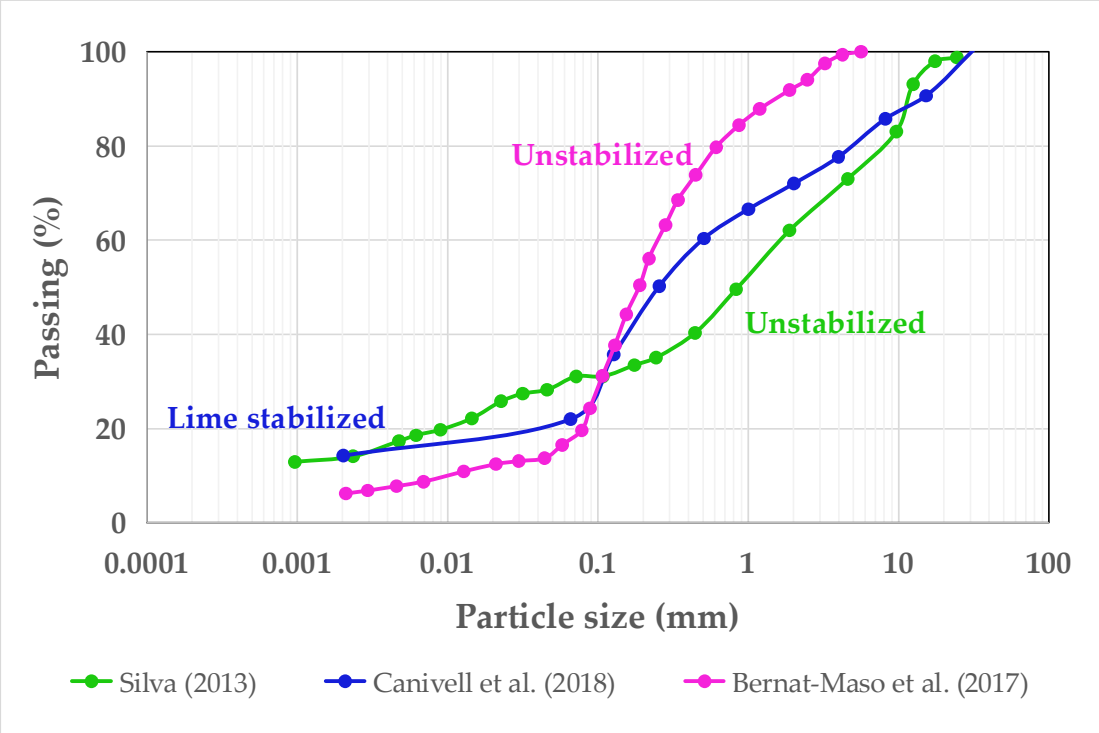

Figure 5.1. Granulometry of rammed earth in investigation of UPV in literature

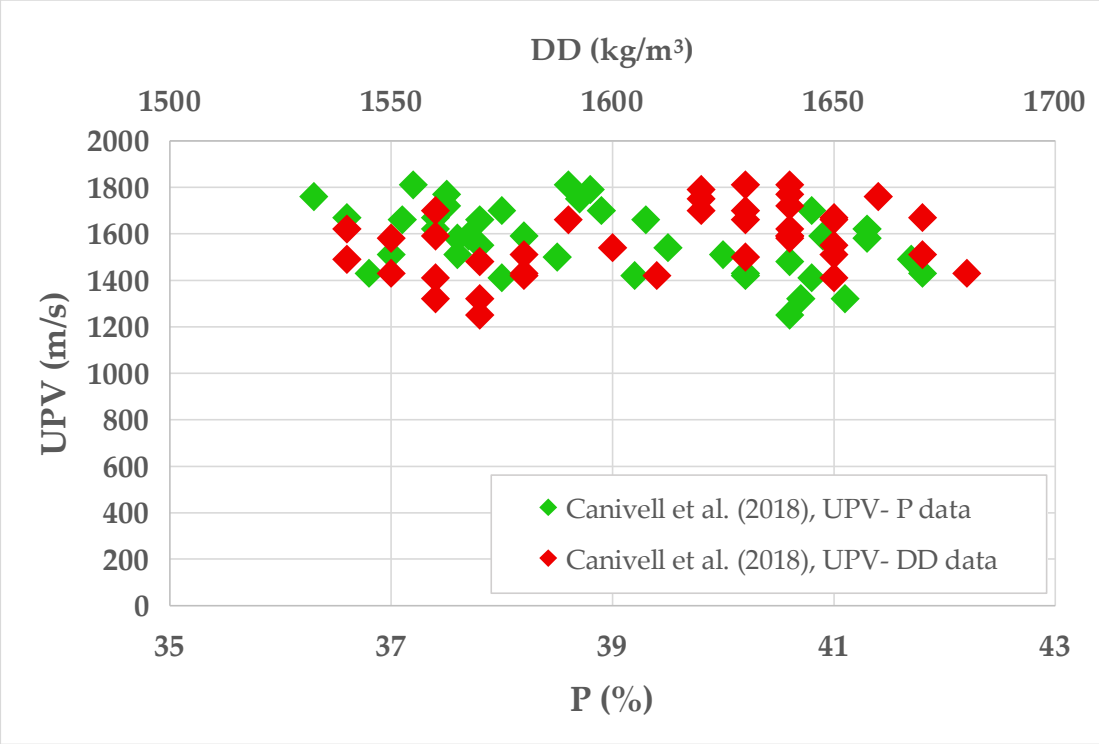

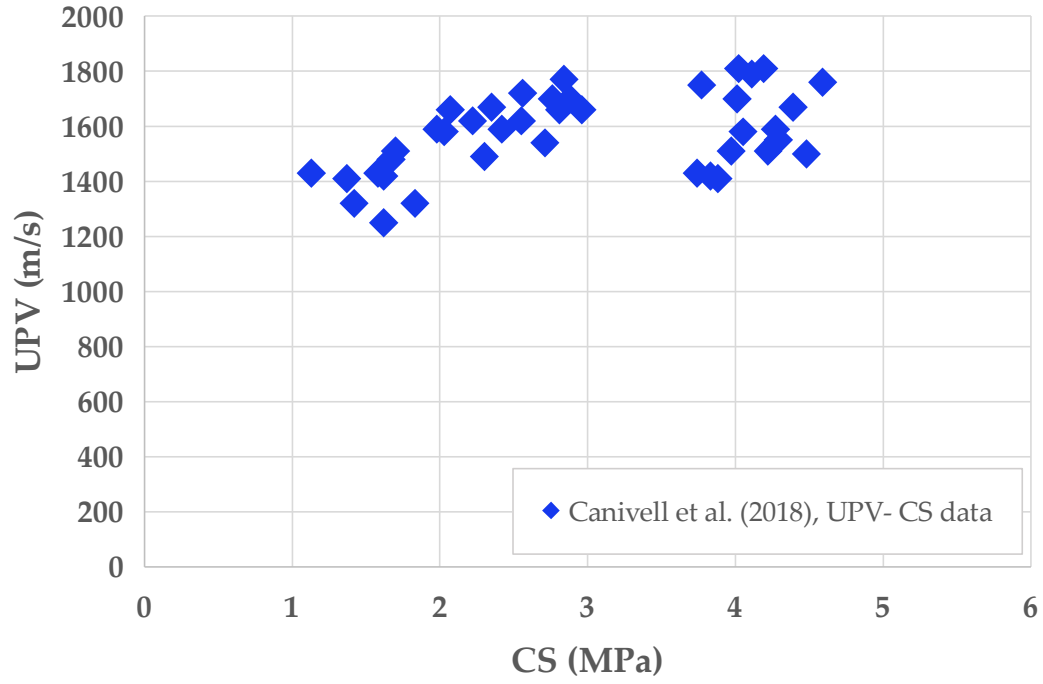
2000
1800
1600
1400
1200
1000
800
600
400
200
0
UPV (m/s)
0
1
2
3
4
5
6
CS (MPa)
Canivell et al. (2018), UPV- CS data

(a)

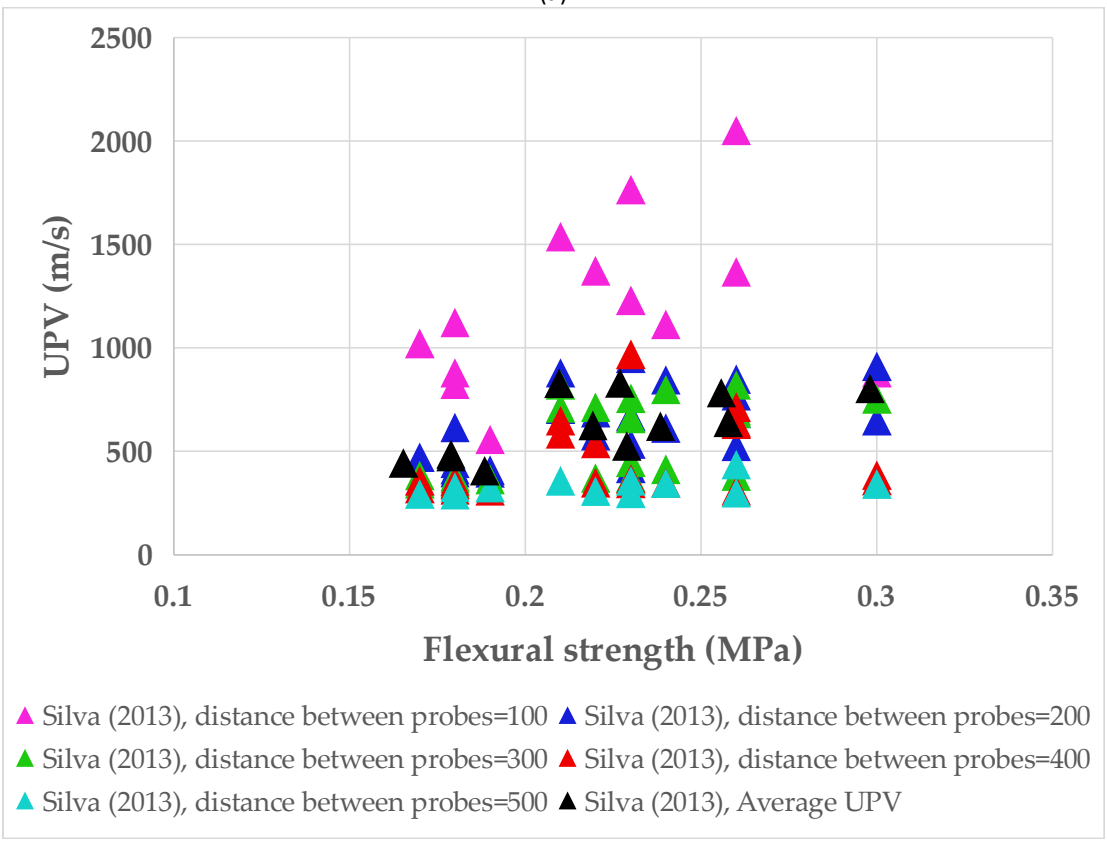
2500
2000
1500
1000
500
0
UPV (m/s)
0.1
0.15
0.2
0.25
0.3
0.35
Flexural strength (MPa)
Silva (2013), distance between probes=100
Silva (2013), distance between probes=200
Silva (2013), distance between probes=300
Silva (2013), distance between probes=400
Silva (2013), distance between probes=500
Silva (2013), Average UPV

(b)

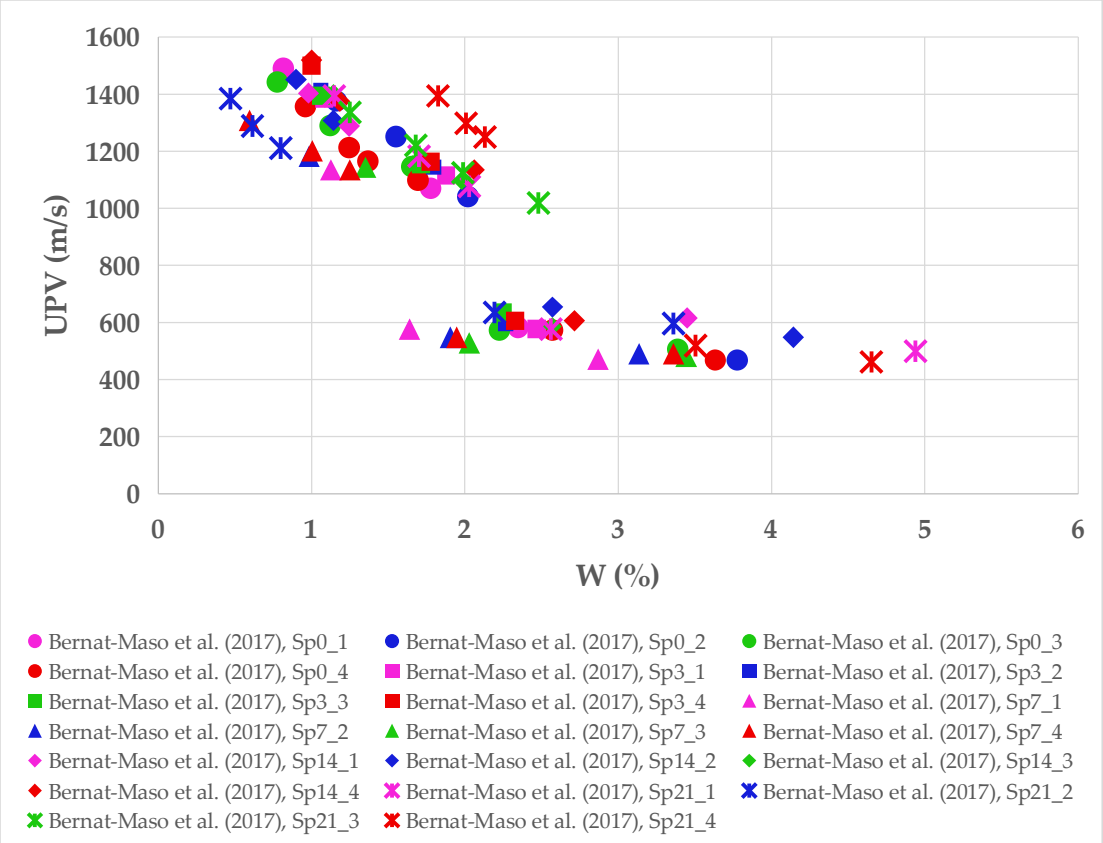

(c)

Figure 5.2. Variation of UPV versus physical and mechanical parameters of rammed earth material in literature; (a) Canivell et al. (2018), (b) Silva (2013) and (c) Bernat-Maso et al. (2017)

5.2. UPV measurements

Ultrasonic testing is considered to be an efficient nondestructive method for evaluation of materials and structures. Ultrasonic waves are stress waves with frequencies higher than 20 kHz, above the frequency range of human hearing, that transmits through the medium in solids, liquids, and gases. In UPV measurements, ultrasonic waves are introduced into a material by means of an appropriate pulse transmitter, and are received from an appropriate pulse receiver. The stress waves are transmitted and received using ultrasonic sensors, piezoelectric transducers, the function of which are to convert electric energy into mechanical energy. In the typical arrangement of transducers, direct transmission technique, waves are introduced into the media using a transmitting transducer positioned on one end surface of the specimen. The propagated wave through the material are received by the receiver transducer positioned on the opposite end surfaces of the specimens. Figure 5.3 shows such configuration for transducers, which has been used to introduce and receive ultrasonic waves in rammed earth specimens for ultrasonic measurements in the current study.

Depending upon displacement of particle relative to the direction of propagation of wave, ultrasonic waves transmit through material, with particle displacement of compression wave, P-wave, and shear wave, S-wave, being parallel and transverse to the direction of wave propagation (Figure 5.4). Figure 5.4 shows a simple illustration of the ultrasonic P-wave and S-wave produced in a medium. The velocity of transmission of various waves is a function of physical and mechanical characteristics of medium. When performing a UPV, P and S-waves are identified. The arrival of the P-waves are faster than S-waves but P-waves have a lower amplitude. The arrival of the S-waves corresponds to the time at which it is possible to see an

increase in the amplitude of the signal. S-waves are transmitted slower but are characterized by a higher amplitude, thus can be identified with the first peak.

As mentioned above, the transmission of these waves is related to the characteristics of the material, and therefore it is possible to calculate the ultrasonic elastic constants, i.e. Young's modulus of elasticity (ASTM D2845-08 standard).

The velocities of the compression and shear waves and Young's modulus of elasticity are calculated according to Standard Test Method for Laboratory Determination of Pulse Velocities and Ultrasonic Elastic Constants of Rock as follows (ASTM D2845-08 standard):

$$V = \frac{L}{T} \qquad \textbf{Eq (5.1)}$$

where
V= pulse velocity (m/s)
L= pulse travel distance (m)
T= effective pulse travel time (s)

$$Edyn = \frac{\left[\rho V_s \left(3V_p^2 - 4V_s^2\right)\right]}{V_p^2 - V_s^2} \qquad \textbf{Eq (5.2)}$$

where
= density (kg/m3)
Edyn = Young's modulus of elasticity (Pa)

Figure 5.3. Configuration for transducers in the current study, direct transmission technique

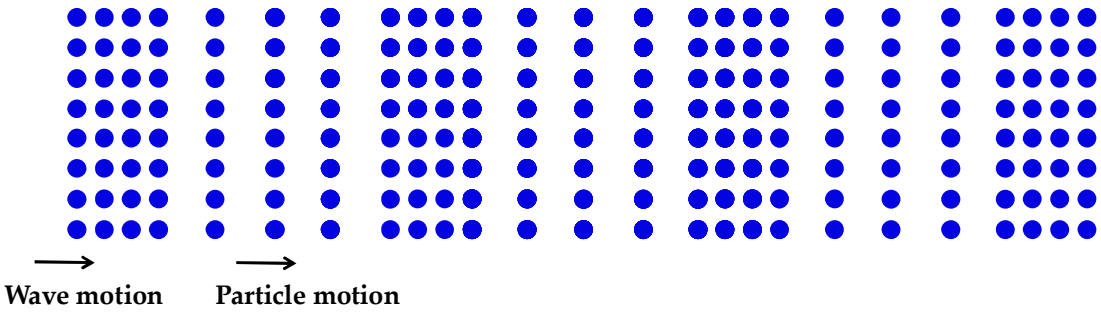

(a)

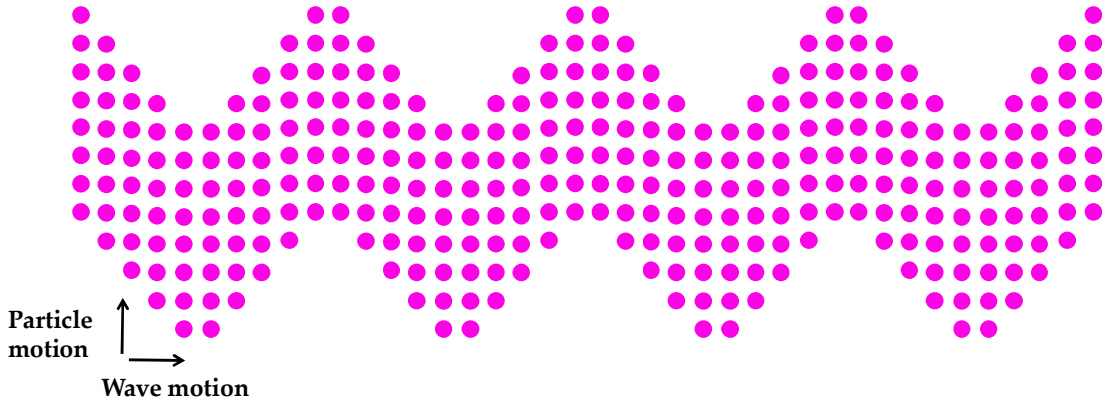

(b)

Figure 5.4. A simple illustration of the ultrasonic P-wave and S-wave produced in a medium; (a) P-wave, (b) S-wave

In the present study, a total of 23 specimens were cast and tested for UPV investigations (Figure 5.5). The details of their production and characteristics have been described in Chapter 4. UPV measurements were performed on above-mentioned specimens using an ultrasonic pulse generation and acquisition system (Pundit Lab, Proceq). Cylindrical 250-kHz transmitter-receiver (tx-rx) probes were employed for P-wave (Vp) and S-wave (Vs) measurements, along the same core direction. Measurements were conducted following ASTM D2845-08 standard requirements. For each sample, 20 ultrasonic traces were recorded, using a sampling frequency of 2 MHz. The arrival time of the P- and S-wave was picked on the traces and correspondent ultrasonic velocities were calculated and averaged over the 20 measurements. Young's, Edyn, at low-strain conditions were calculated for each specimen following the equations provided in ASTM D2845-08 standard. Appendix 2 summarizes the results of ultrasonic pulse measurements. An example of A-scan is reported in Figure 5.6. Standard deviation of 20 ultrasonic traces of each measurement has been reported in Appendix 2.

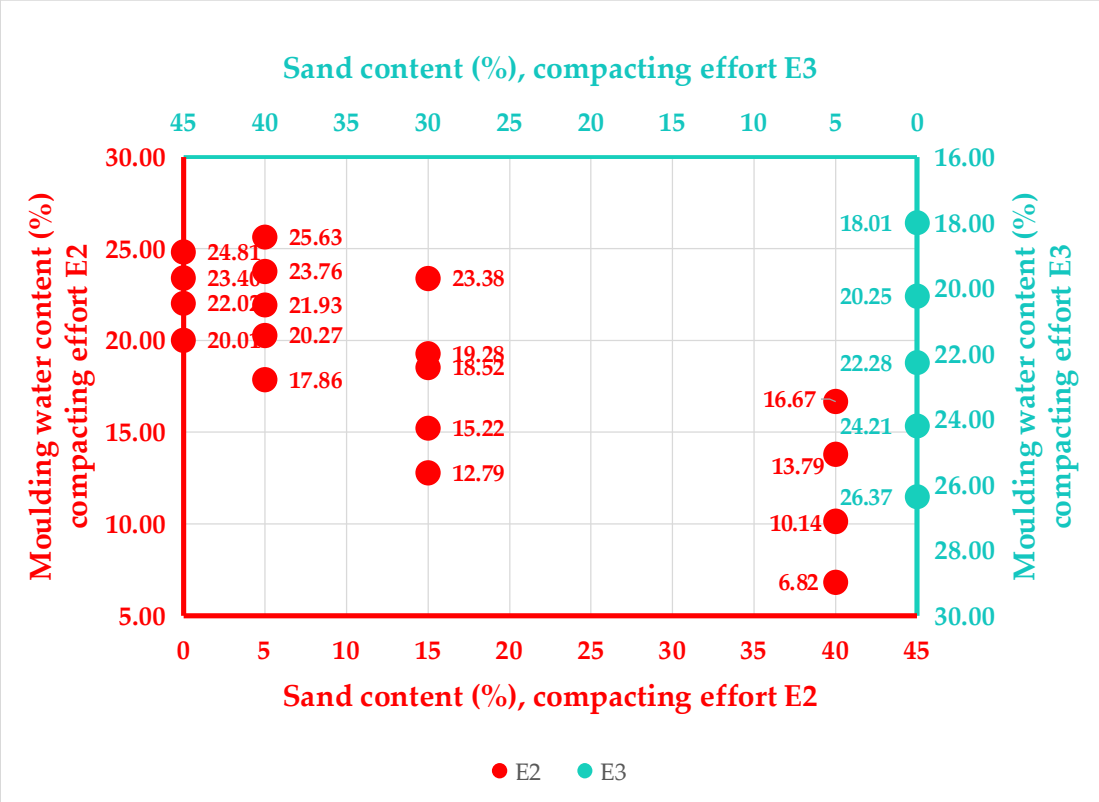

Figure 5.5. Specimens for investigation UPV

According to ASTM, in order to measure the true dilational wave velocity in UPV measurements, the minimum lateral dimension of 5 times the wavelength of the compression wave for the specimen is required, with the minimum wavelength being 3 times the average grain size. This interconnection between lateral dimension of specimen, average grain size, pulse propagation velocity (compression) and natural resonance frequency of transducers has been defined as follow (ASTM D2845)

$$D \geq 5\left(Vp/f\right) \geq 15d \qquad \textbf{Eq (5.3)}$$

where D is the minimum lateral dimension of the specimen,Vp is the pulse velocity, f is the natural resonance frequency of transducers, and d is the average grain size of the specimen. In the current study, dimension of the specimen meet the above-mentioned relationship.

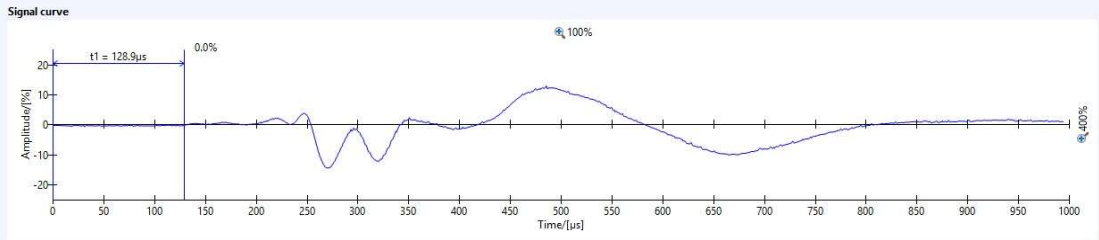

Figure 5.6. An example of A-scan for UPV measurements

5.3. Discussion of UPV results

Understanding the behaviour of ultrasonic pulse velocities through rammed earth specimens is important because mechanical properties of rammed earth material have a dependency on variation of material characteristics. In order to assist and guide in developing a better understanding of the correlations between non-destructive and destructive tests' parameters, this section reports an evaluation of ultrasonic velocities of rammed earth specimens as a function of physical and mechanical properties. Crucial mechanical properties and parameters have been related to the pulse velocities via empirical formulas.

The resultant data of the above-mentioned experimental program, designed and conducted at the department of earth science of University of Turin, was used to investigate the ultrasonic pulse velocity and mechanical properties of rammed earth material.

It worth mentioning that, although the UPV method is an efficient method for non-destructive characterization of material properties, the results are affected by a number of factors, arising from skill of operator or incorrect interpretations and the ability of the operator to interpret the result. Application of UPV method involves uncertainties. A satisfactory interpretation of the first arrival of the waves highly rely on the application of experience and good judgement. Difficulties in clearly identifying the first arrival of the transverse wave, pose difficulties in the interpretation of the results of UPV measurements, and thus evaluating mechanical properties of material. Furthermore, the scatter of data can also be attributed to the type of material and non-homogeneity in the structure of the material, which, apart from operator and operation errors, are probably the most obvious attributing factors, influencing the results.

5.3.1. Assessment of compactive effort

In this section. ultrasonic pulse velocity measurements have been performed to investigate compaction characteristics. Measured P-wave velocities for pure clay specimens prepared at compactive effort of E2 and E3 varies between 436.31 m/s and 686.08 m/s for compactive effort of E2 and between 349.34 and 766.52 for compactive effort of E3.

As shown in Figures 5.7 and 5.8, it can be found that the variation of wave velocity with water content follows a trend for each compactive effort. The results show that for the specimens with compactive effort of E2, specimens with lower water content have higher values of UPV. On the other hand, for compactive effort of E3, with increasing water content, P-wave and S-wave velocities increase to a maximum value. Thereafter, an increase in water content results in decrease of pulse velocities. Furthermore, as can be seen in Figures 5.7 and 5.8, there is not considerable variation between the velocities measured in specimens constructed using compactive effort of E2 and those compacted with compactive effort of E3.

However, based on these observations, a general order 2 polynomial trendline can be considered for variation of pulse velocities versus water content for rammed earth material (Eq. 5.4). These trendlines have been shown in Figures 5.7 and 5.8 and reported in Table 5.1.

$$V = aw^2 + bw + c \qquad \textbf{Eq (5.4)}$$

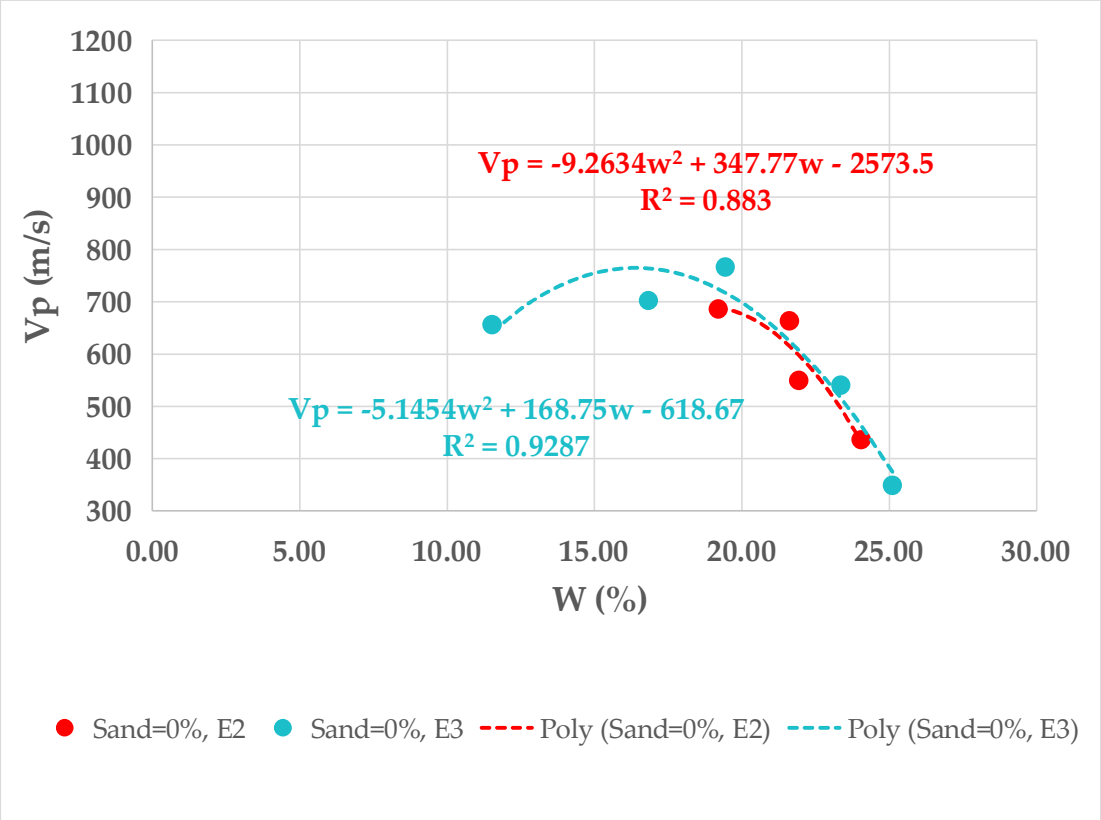

Figure 5.7. Variation of P-wave velocity versus water content for two different compactive effort

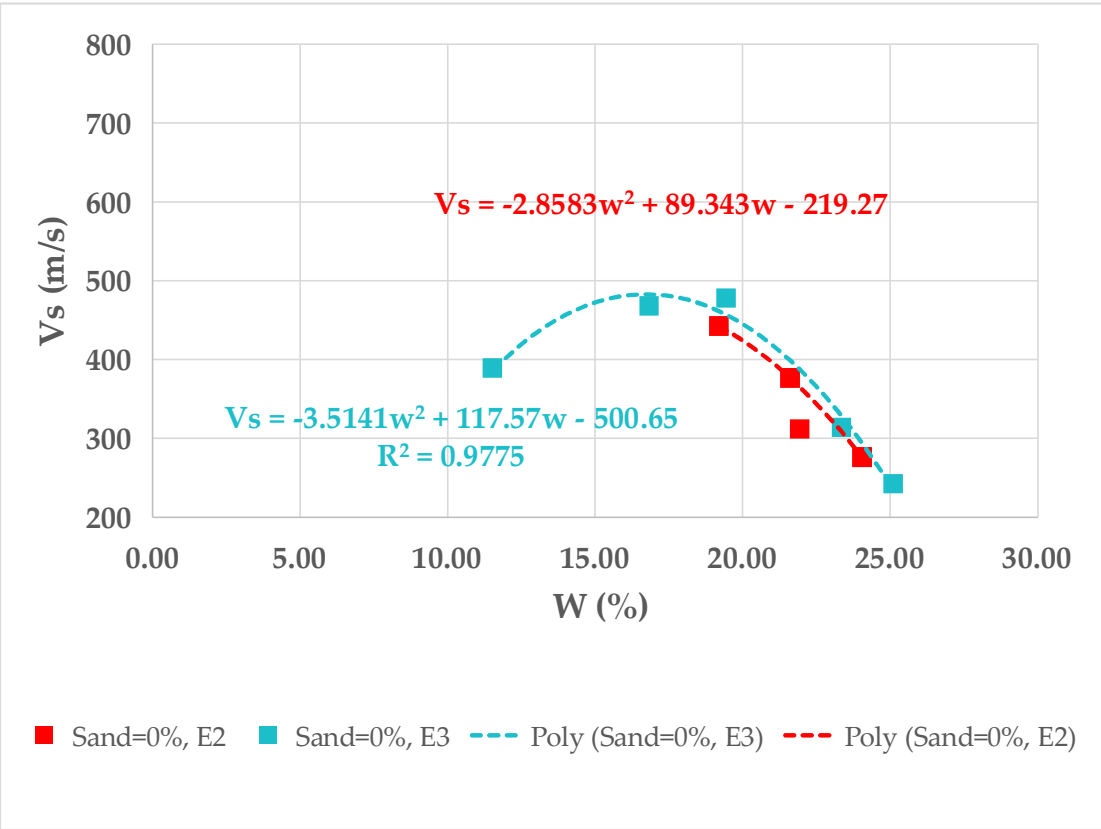

Figure 5.8. Variation of S-wave velocity versus water content for two different compactive effort

5.3.2. Influence of water content

Figures 5.9 and 5.10 show the effects of the water content on the pulse velocities for different mixtures of material. It can be observed that the variation of water content in rammed earth specimens greatly influences the velocity of the P-wave (Figure 5.9). The variation of amount of water does not, however, significantly influence the measured S-wave velocity (Figure 5.10).

It can be observed that for materials with 0% sand and 15% sand content and compactive effort of E2 , lower water content, and thus more aggregate content, has increased the pulse velocity, while specimens with 5% and 40% sand content, P-wave and S-wave velocities increases to a maximum value. Thereafter, an increase in water content results in decrease of pulse velocities. The general order 2 polynomial trendline can be considered for variation of pulse velocities versus water content for rammed earth material for different sand content (Eq. 5.4), which have been shown in Figures 5.9 and 5.10 and Table 5.1.

Table 5.1. Parameters of trendlines for Vp-W and Vs-W

	Vp-W			Vs-W		
	a	**b**	**c**	**a**	**b**	**c**
Sand=0%, E2	-9.263	347.77	-2573.5	-2.8583	89.343	-219.27
Sand=0%, E3	-5.1454	168.75	-618.67	-3.5141	117.57	-500.65
Sand=5%, E2	-11.114	409.72	-3074.6	-4.6177	157.02	-891.64
Sand=15%, E2	-3.4735	98.299	78.718	-1.2999	25.981	362.68
Sand=40%, E2	-11.604	226.38	-11.422	-5.4156	108.93	125.1

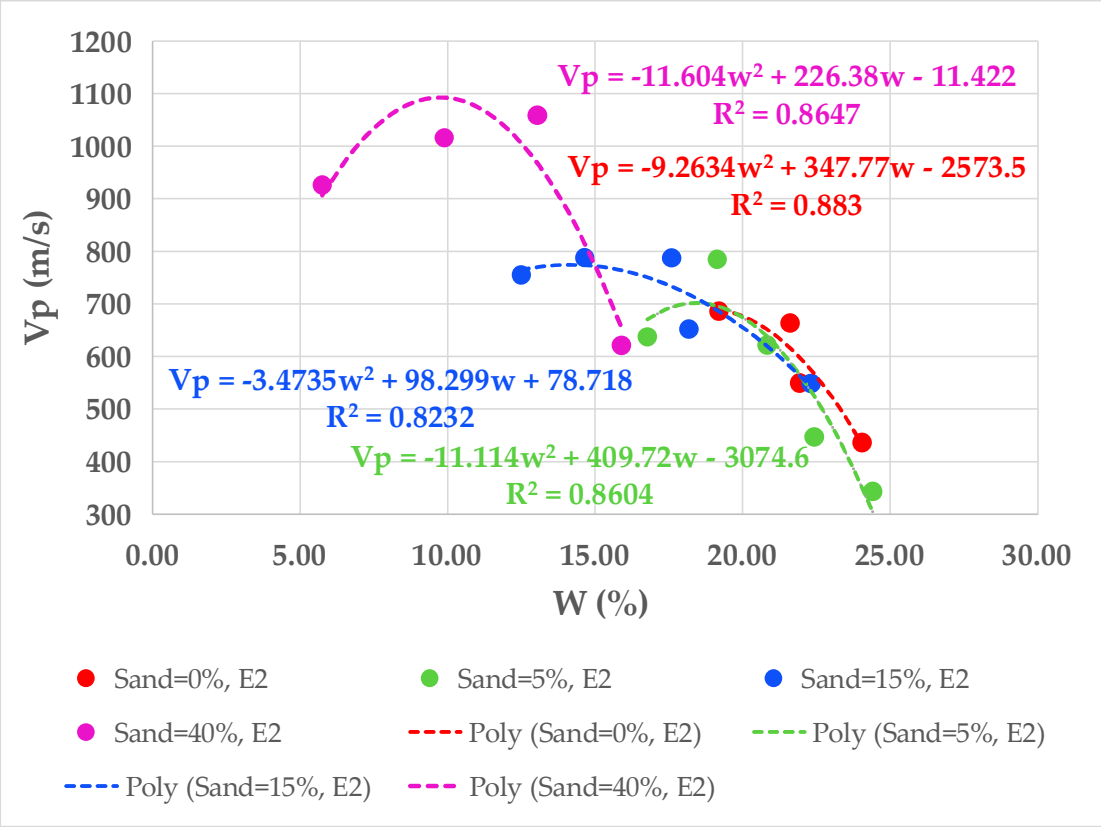

Figure 5.9. Variation of P-wave velocity versus water content for four different mixture of

rammed earth material

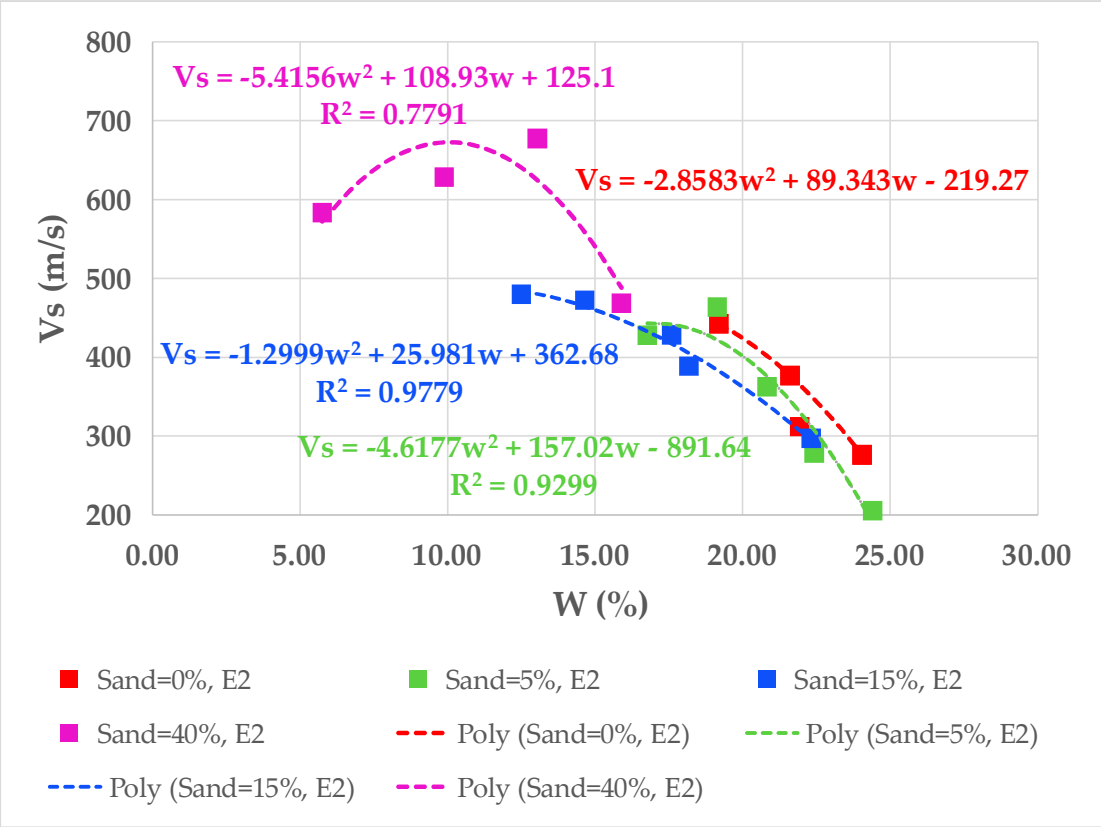

Figure 5.10. Variation of S-wave velocity versus water content for four different mixture of rammed earth material

5.3.3. Assessment of granulometry of rammed earth

As previously mentioned, experiments on rammed earth specimens with various grain-size distribution were carried out to achieve the intended objective. This study shows that the grain-size distribution significantly affects the UPV of rammed earth. Therefore, the role of granulometry of rammed earth should be considered for accurate prediction of properties using UPV. Based on Figures 5.11 and 5.12, a strong relation between sand content and ultrasonic velocities can be observed.

Specimens with sand possess a density much higher than clay specimens. Consequently, addition of sand increases the unit weight of rammed earth specimens, indicating that for the same water content, rammed earth having higher sand content resulted in higher pulse velocity value. In the mixture of sand and clay, the finer grain clay particles have a capacity to fill void spaces, creating a good bondage between fine and large particles, which contributes to higher density of these rammed earth specimens, as well as reducing void ratio.

Therefore, it can be found that the UPV values decreases with increasing clay replacement of sand in the mixture (Figures 5.13 and 5.14). Rammed earth material containing 60% clay and 40% sand had the highest UPV values as shown in Figures 5.13 and 5.14.

However, this study showed that the UPV is much less enhanced for higher sand contents (Figure 5.13 and 5.14). The reason behind this may be the development of non-homogeneity in rammed earth material, which highly contributes to retardation of the UPV.

Based on wave propagation theory, the lower the material density, the lower the wave velocity through material. For rammed earth specimens of lower density, the value of UPV is also expected to be lower. The addition of sand content to clay material is normally considered to increase its density. It is clear that the rammed earth material gets denser with increasing sand content. Higher amounts of sand results in decrease in void spaces and thus the increase in density. The lower the volume of pores and thus higher the density with addition of sand, the greater the velocity of pulse propagated through the rammed earth due to the lower pulse velocity values through voids compared to solids and liquids. Moreover, this study shows that dry density does not affect the P-wave and S-wave velocity the same degree. That is, compared to S-Wave, the P-wave is more sensitive for variations of sand content and thus, dry density (Figure 5.15).

Variation of UPV versus dry density as well as the trendline fitted using regression analysis is shown in Figure 5.15. It can be observed that the trends observed in the Vp-DD data are more pronounced than the trend observed in Vs-DD data. It can be observed that velocities of the rammed earth specimens increase with increasing dry density with generally higher velocities obtained for the specimens with higher sand content, with clearly less enhanced UPV values for higher dry densities.

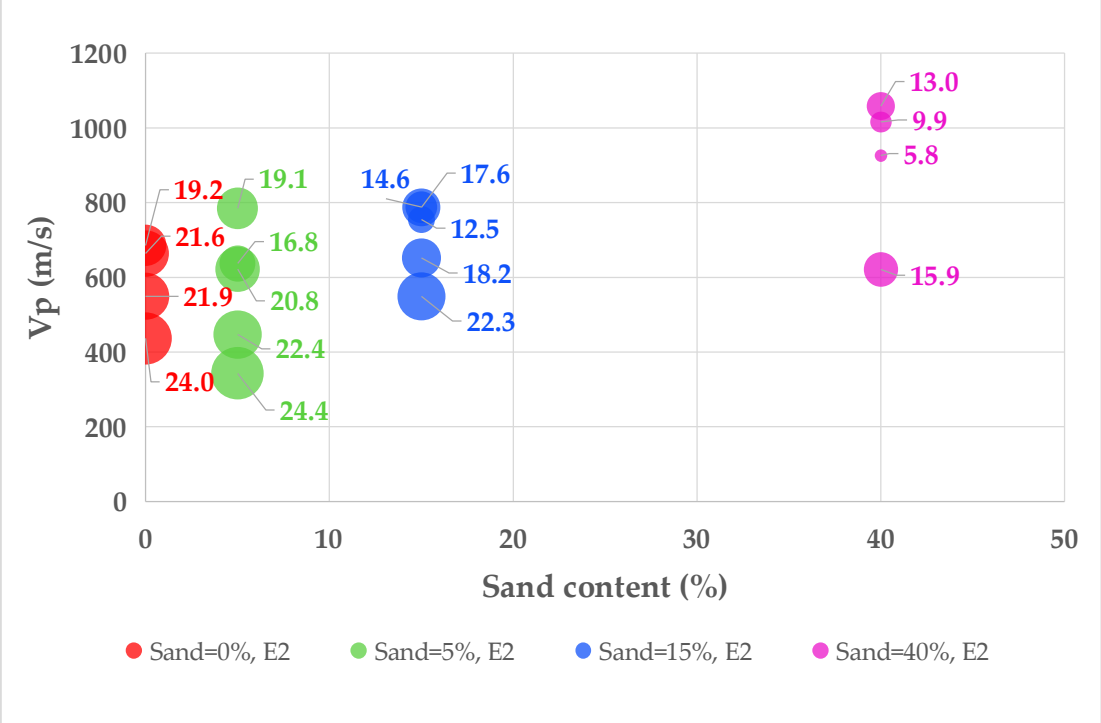

Figure 5.11. Variation of P-wave velocity versus sand content for four different mixture of rammed earth material (data labels present water content)

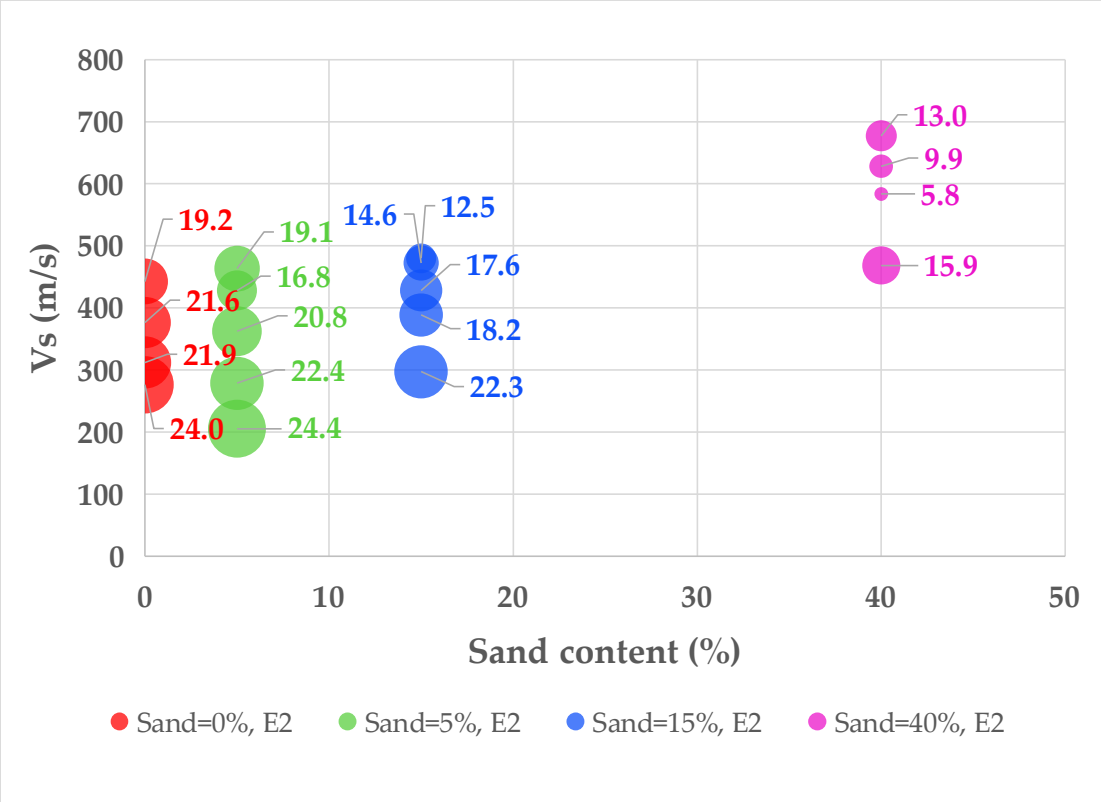

Figure 5.12. Variation of S-wave velocity versus sand content for four different mixture of rammed earth material (data labels present water content)

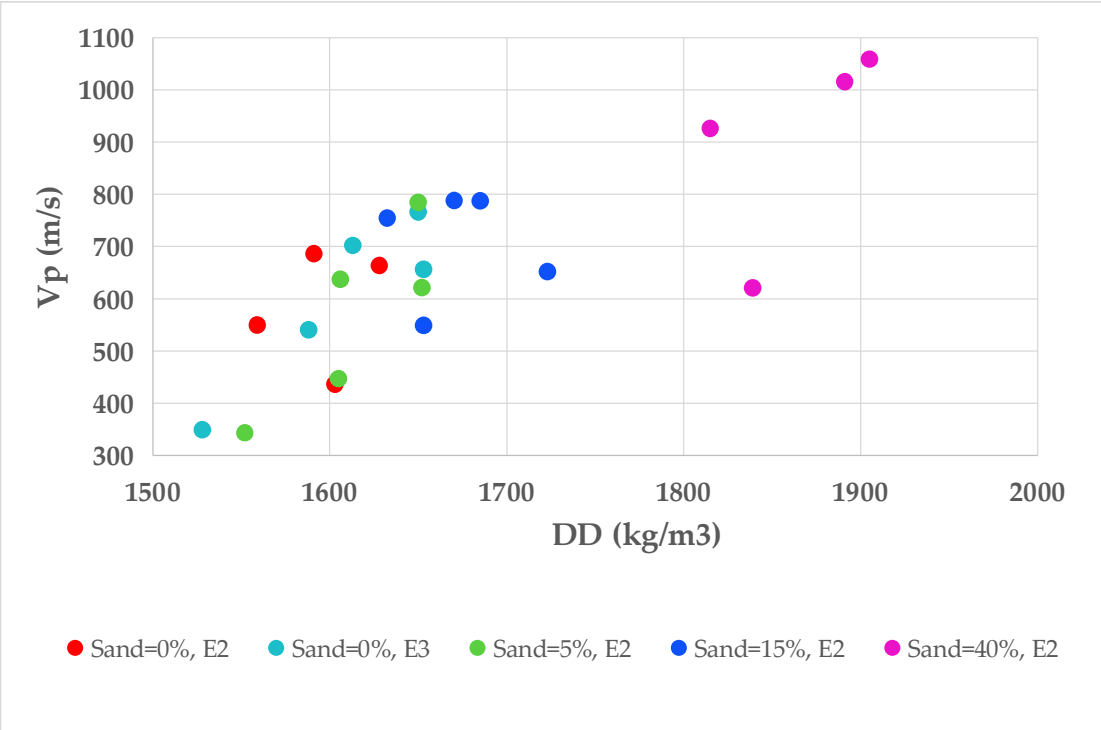

Figure 5.13. Variation of P-wave velocity versus dry density for four different mixture of rammed earth material

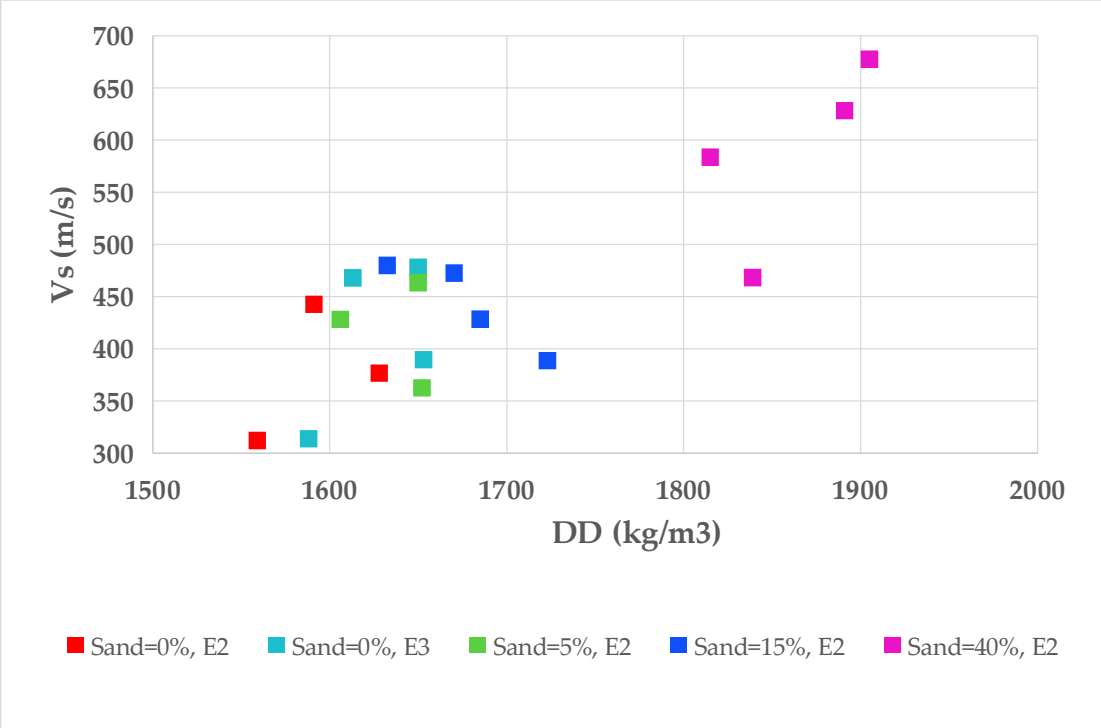

Figure 5.14. Variation of S-wave velocity versus sand content for four different mixture of rammed earth material

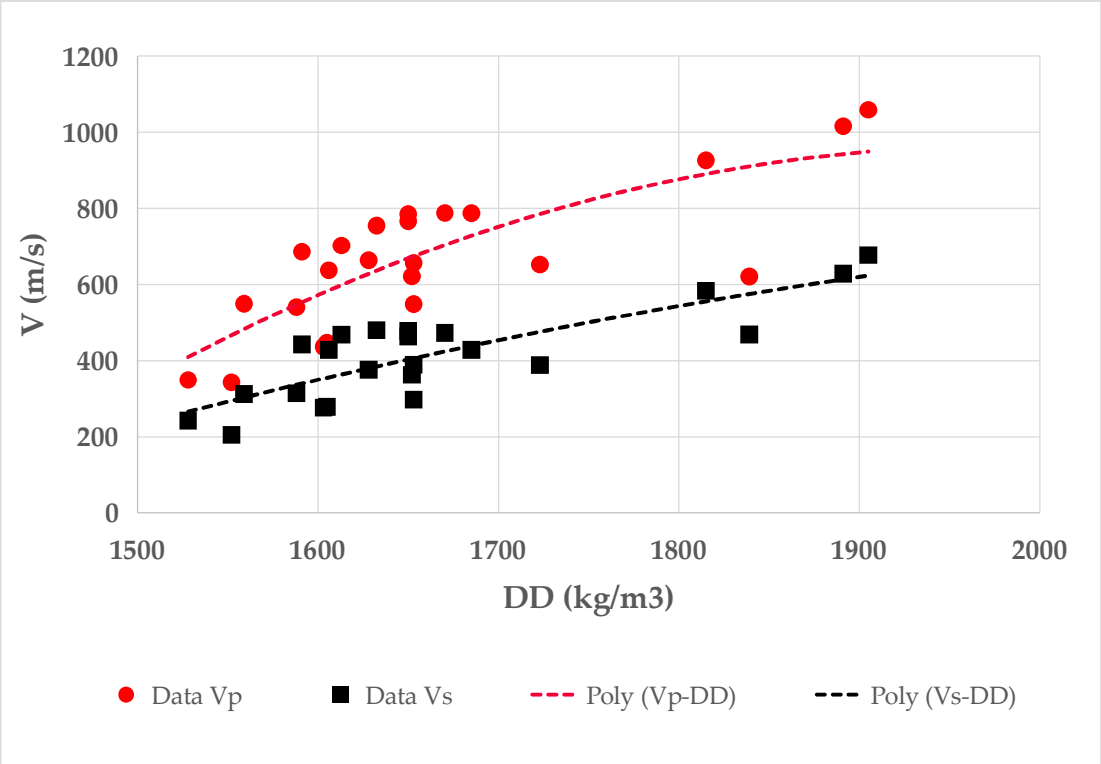

Figure 5.15. Variation of UPV versus dry density

Moreover, an investigate on the ratio of compressional to shear wave velocity (Vp/Vs) for rammed earth mixtures of the current study has been presented in Figure 5.16. Figure 5.16 shows compressional and shear wave velocities for mixtures reported in this study, indicating almost uniform distribution of these data for the highly variable

composition of rammed earth materials. According to Figure 6.16, Vp/Vs for rammed earth mixtures of the current study tends to lie mostly within a narrow band between 1.5 and 2.

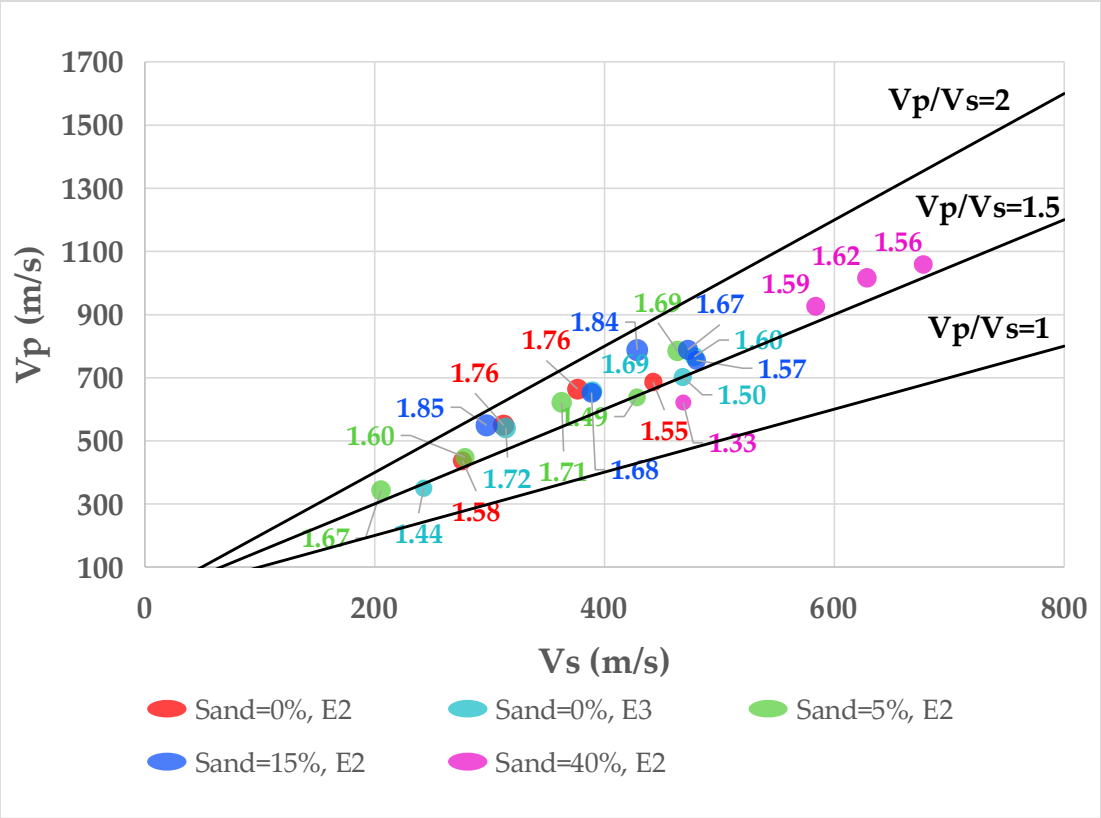

Figure 5.16. Variation of P-wave velocity versus S-wave velocity for rammed earth specimens (data labels present Vp/Vs values)

A plot of P-wave velocity-void ratio and S-wave velocity-void ratio curve for two ranges of degree of saturation, Sr>0.86 and Sr< 0.87 are shown in Figures 5.17 and 5.18, respectively. The lines in Figures 5.17 and 5.18 represent linear regression analysis of variation of wave velocity versus void ratio for two given degree of saturation of Sr>0.86 and Sr< 0.87.

From the measurements on specimens with varying amount of sand, it can be observed that the void ratio is one of the attributing factors influencing the wave velocities, whereas, the influence of level of degree of saturation were found to be less pronounced. It can be readily seen from Figures 5.17 and 5.18 that all data lies within a relatively narrow band. It can be observed that an increase of void ratio in any given range of degree of saturation contributes to decrease of the P-wave and S-wave velocities. It can be noted that the slope of the regression lines for two different ranges of degree of saturation are approximately equal. Based on observations in Figures 5.17 and 5.18, a general trend of lower P-wave and S-wave velocities with increasing degree of saturation at a constant void ratio and decrease of wave velocities with an increase in void ratios at a given range of saturation degree is evident.

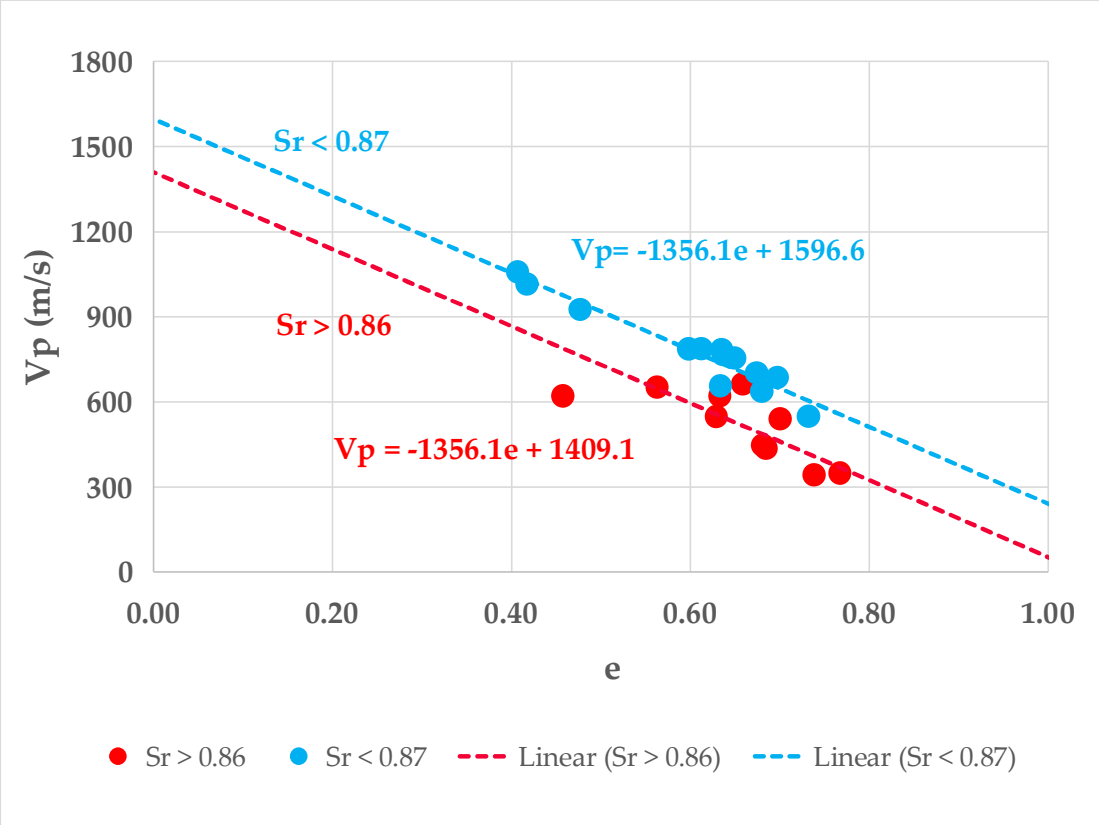

Figure 5.17. Variation of P-wave velocity versus void ratio for two ranges of degree of saturation, Sr>0.86 and Sr< 0.87, for rammed earth specimens

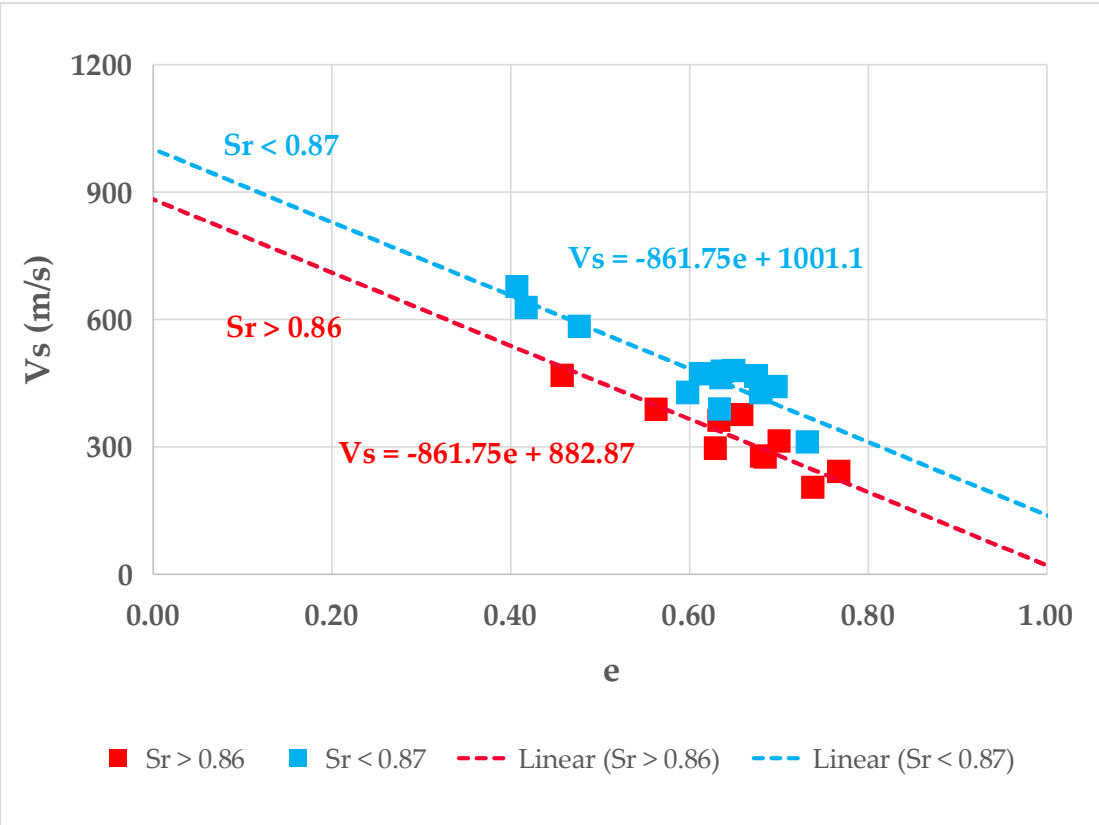

Figure 5.18. Variation of S-wave velocity versus void ratio for two ranges of degree of saturation, Sr>0.86 and Sr< 0.87, for rammed earth specimens

5.3.4. Assessment of Modulus of elasticity of rammed earth

Measurements of longitudinal and transverse wave velocities allows the calculation of several important material elastic parameters, also known as dynamic constants, such as dynamic modulus of elasticity, Edyn. Ultrasonic longitudinal and shear wave velocities are key parameters in ultrasonic sensing applications, as each medium can be characterised by its own value of the ultrasonic velocities that are usually representative of the elastic properties of the medium. Elastic properties of solid can be evaluated by these wave velocities, which means that the variation of elastic parameters are commonly established as a function of ultrasonic wave velocities.

The objective of this section is to provide some relevant data on dynamic modulus of elasticity, in which the physical and mechanical characteristics of rammed earth are the main subject of investigation. In order to analyse dynamic modulus of elasticity of rammed earth specimens, UPV of specimens were experimentally obtained and the dynamic values of modulus of elasticity were calculated. In this section, the results are presented with the correlation of dynamic and static values of modulus of elasticity of rammed earth specimens.

It can be observed that for each rammed earth composition of material, increasing water content generally contributes to the increase of P-wave and S-wave velocities to a maximum value. Thereafter, an increase in water content results in decrease of Edyn (Figure 5.19). Therefore, based on these observations, variation of Edyn versus water content for rammed earth materials can be defined as a general order 2 polynomial trendline (Eq. 5.4). Based on regression analysis, the constants of Eq. 5.4 have been obtained for materials included in this study, which has been demonstrated in Figure 5.17 and summarized in Table 5.2.

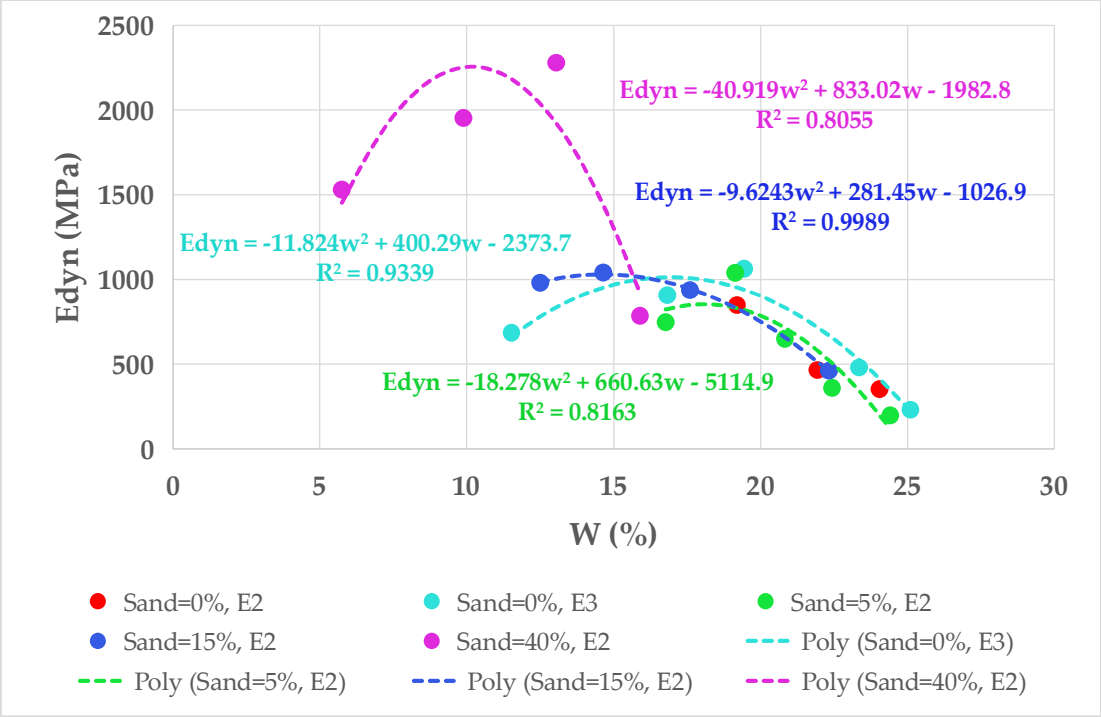

Figure 5.19. Variation of Edyn versus water content for two ranges of degree of saturation, Sr>0.86 and Sr< 0.87, for rammed earth specimens included in this study

Table 5.2. Results of regression analysis for characterization of Edyn

	Edyn-W			Edyn/Esec$_{0.5US}$	Edyn/E$_{US}$
	a	**b**	**c**		
Sand=0%, E2	-	-	-	11.138	32.951
Sand=0%, E3	-11.824	400.29	-2373.7	6.3413	10.378
Sand=5%, E2	-18.278	660.63	-5114.9	8.8133	21.481
Sand=15%, E2	-9.6243	281.45	-1026.9	13.014	18.61
Sand=40%, E2	-40.919	833.02	-1982.8	40.599	42.74

Generally, modulus of elasticity has been a key component in prediction and the judgement of durability of existing structures. The modulus of elasticity used for safety diagnosis and analysis of structures is the static modulus of elasticity, generally secant modulus, usually measured experimentally using uniaxial compression testing. The tangent modulus (Etan) determined from slope of stress-strain curve under the uniaxial compression loading, is also considered to be a static modulus representative of the dynamic modulus, which refers to almost purely elastic low strain effects.

During an uniaxial compression testing of material, as the stress increases, the slope of stress-strain curve and thus the secant and tangent modulus changes significantly. This variable value of the secant modulus requires the statement of the level of stress or strain at which the modulus of elasticity has been defined.

It can be noted that the data of variation of velocities with respect to variation of Esec at a stress level of 50% of US, presented in Figures 5.20 and 5.21, shows a reasonably linear trend, which means that for each rammed earth composition of material, compressional and shear wave velocities increase almost linearly with increasing elastic modulus. Furthermore, Figure 5.22 presents a plot of Vp/Vs, versus Esec$_{0.5Us}$. According to Figure 5.22, Vp/Vs ratio is almost constant for most rammed earth specimens, and it is independent of Esec$_{0.5US}$.

Figures 5.23 and 5.24 show the variation of Edyn with variation of ratio of stress to strain (Esec) at stress level of half of US and at US level, respectively. Moreover, Figure 5.25 show variation of the ratio of Edyn versus Etan for specimens in the current study. It can be observed that dynamic modulus is significantly higher than the static, secant or tangent, modulus. Based on Figure 5.25, it can be observed that higher amount of sand content generally contributes to increase of the ratio of Edyn to Etan.

Because the behaviour of the rammed earth material under uniaxial compression varies with variation of compactive effort and granulometry, and modulus of elasticity is a function of the uniaxial compression behaviour, the relationship between dynamic modulus and static modulus also varies as a function of these properties, which means that there is no simple conversion of the value of the dynamic modulus to the static modulus. However, various empirical relations, as shown in Figures 5.23, 5.24, and 5.25 and summarized in Table 5.2, can be drawn for various composition of rammed earth material.

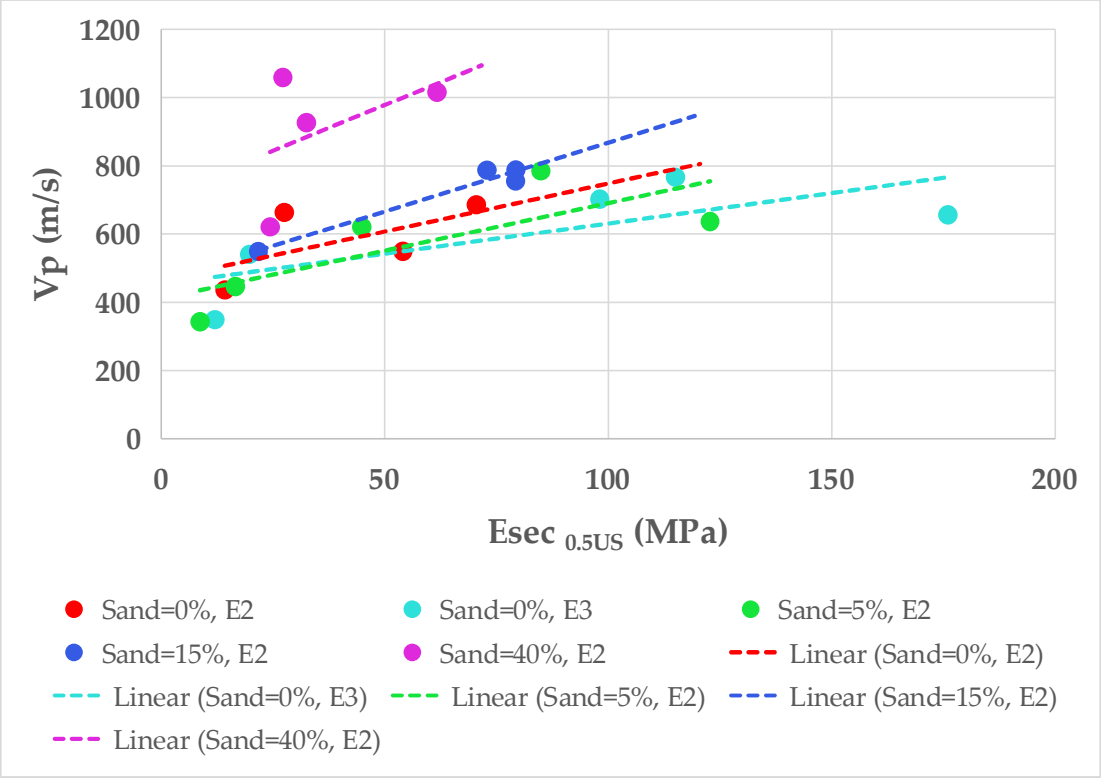

Figure 5.20. Variation of P-wave velocity versus $Esec_{0.5US}$

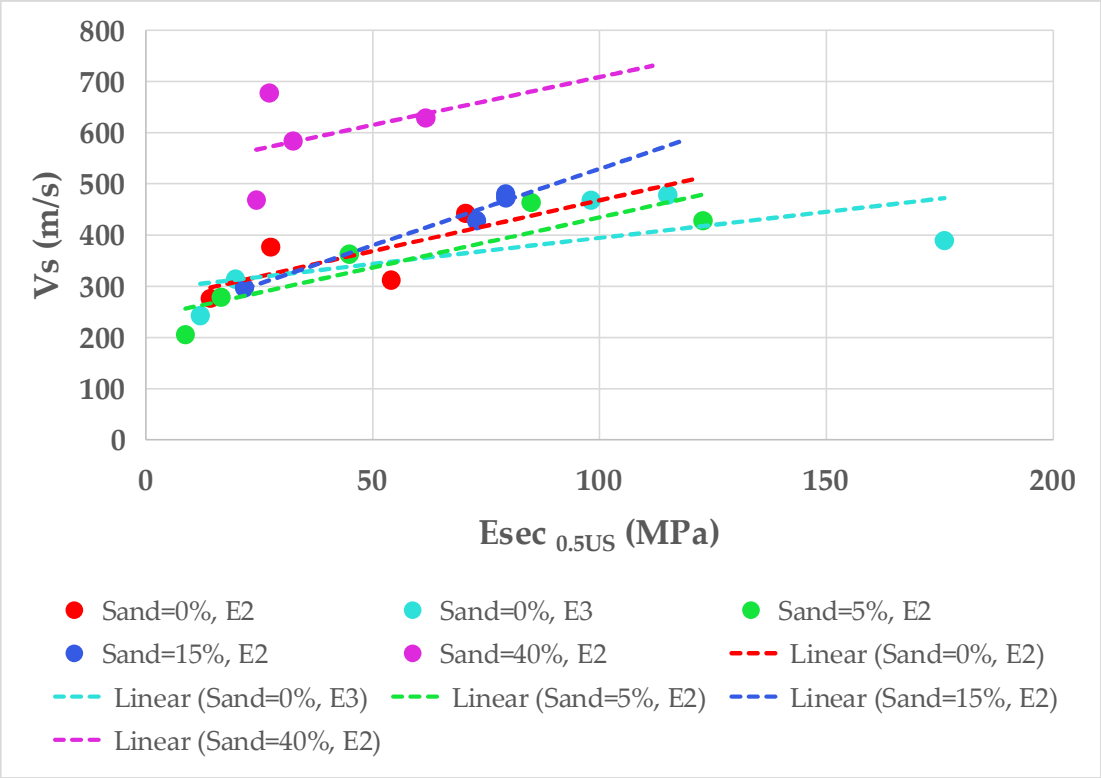

Figure 5.21. Variation of S-wave velocity versus $Esec_{0.5US}$

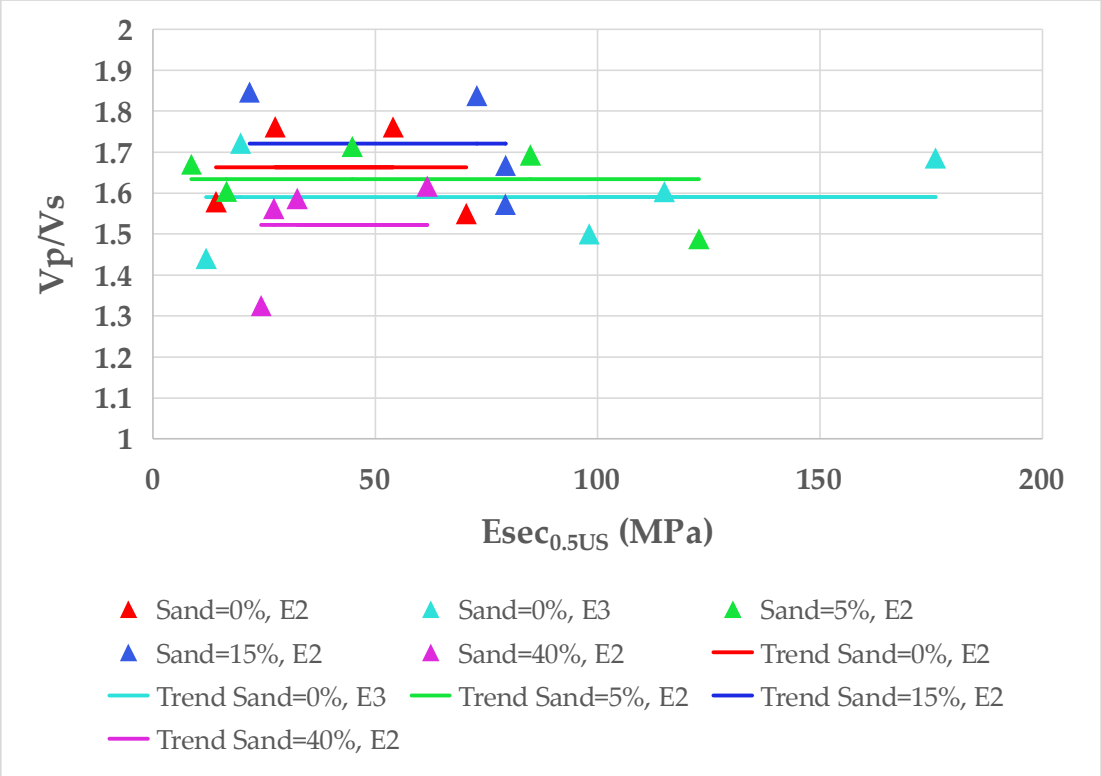

Figure 5.22. Variation of Vp/Vs versus $Esec_{0.5US}$

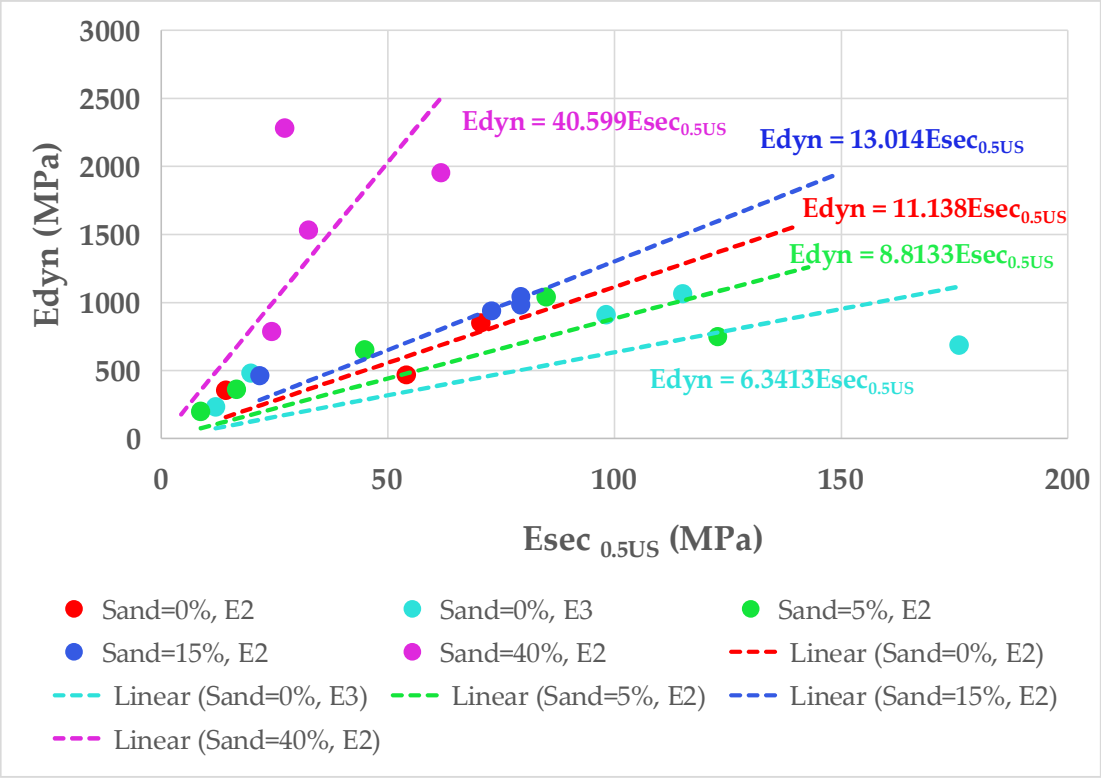

Figure 5.23. Variation of Edyn versus $Esec_{0.5US}$

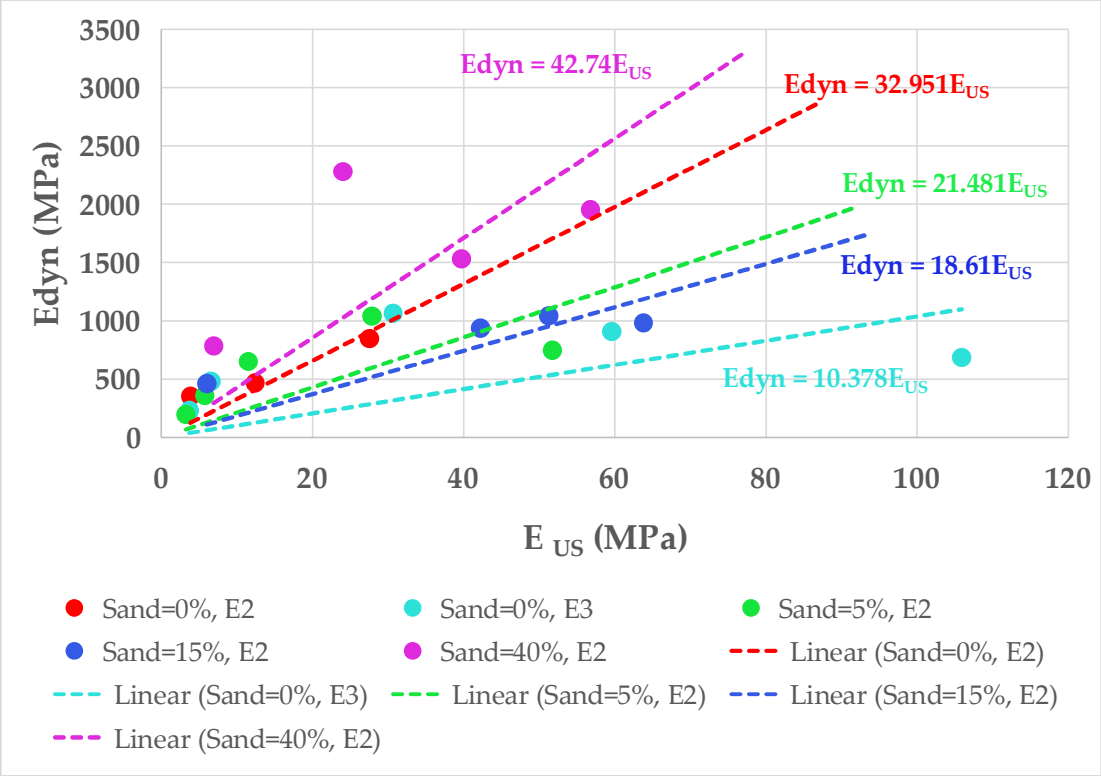

Figure 5.24. Variation of Edyn versus Esec$_{US}$

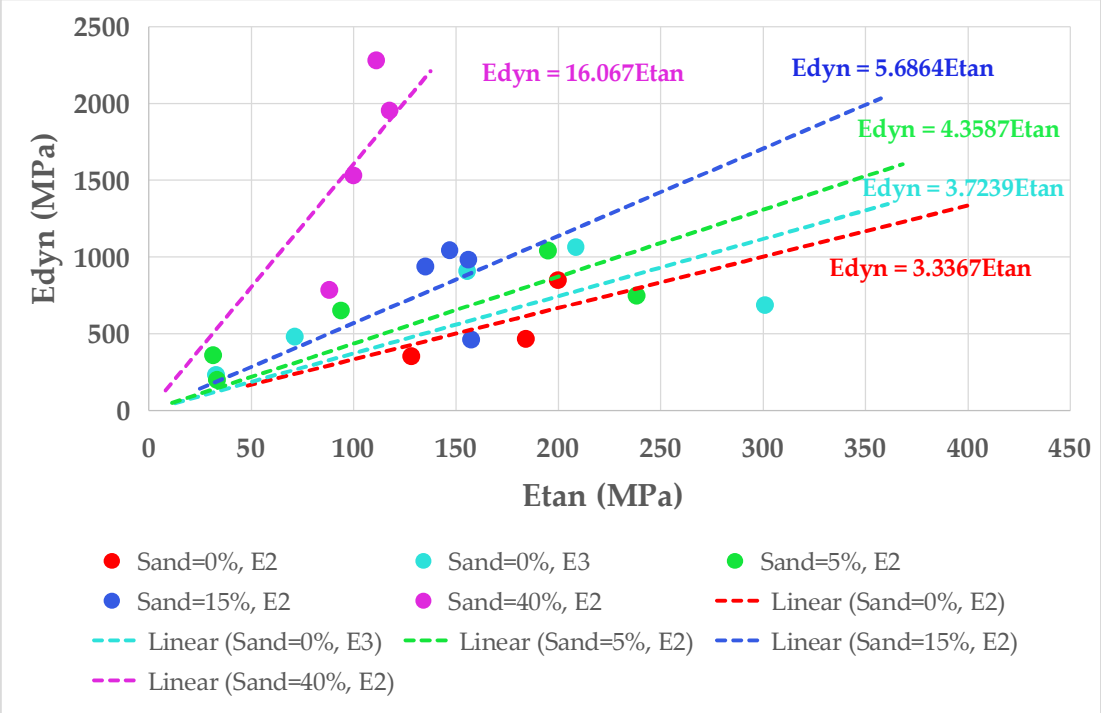

Figure 5.25. Variation of Edyn versus Etan

5.4. Conclusion

The feasibility of using non-destructive ultrasonic pulse velocity properties to characterize rammed earth material was investigated in this study. This study has been mainly consisted of determination of P-wave and S-wave velocities in relation with physico-mechanical characteristics of rammed earth specimens, including compactive effort, grain-size distribution, water content, density, void ratio and saturation degree, and resulting modulus of elasticity. A strong relation between sand content and ultrasonic velocities has been observed in the current study, showing that the grain-size distribution is one of important parameters controlling the UPV of rammed earth. It was observed that the UPV values decreases with increasing clay replacement of sand in the mixture, with rammed earth material containing 60% clay and 40% sand having the highest UPV values. Another observation confirms that dry density does not affect the P-wave and S-wave velocity the same degree. That is, compared to S-Wave, the P-wave is more sensitive for variations of sand content and thus, dry density. Moreover, variation of UPV versus dry density as well as the trendline fitted using regression analysis was investigated in this study, showing that the trends observed in the Vp-DD data are more pronounced than the trend observed in Vs-DD data. According to obtained results, Vp/Vs for rammed earth mixtures of the current study tended to lie mostly within a narrow band between 1.5 and 2.

Furthermore, an analysis of dynamic modulus of elasticity of rammed earth specimens with respect to UPV of specimens were addressed in this study. It can be observed that for each rammed earth composition of material, increasing water content generally contributes to the increase of P-wave and S-wave velocities to a maximum value. Thereafter, an increase in water content results in decrease of Edyn.

The present research is the very first analytical study in interrelating non-destructive ultrasonic pulse velocities and destructive uniaxial compression measurements for rammed earth specimens and therefore it is, to a certain extent, bound to further investigation. In view of the very limited experimental work in this study, there is a clear need for further laboratory work on UPV properties of rammed earth specimens. However, in light of future research, it may be possible to examine and improve the efficiency of the proposed formulas for non-destructive characterization of rammed earth heritage.

References

Silva, R. A. M. (2013). Repair of earth constructions by means of grout injection (Doctoral dissertation, Universidade do Minho (Portugal)).

Canivell, J., Martin-del-Rio, J. J., Alejandre, F. J., García-Heras, J., & Jimenez-Aguilar, A. (2018). Considerations on the physical and mechanical properties of lime-stabilized rammed earth walls and their evaluation by ultrasonic pulse velocity testing. Construction and Building Materials, 191, 826-836.

Bernat-Maso, E., Teneva, E., Escrig, C., & Gil, L. (2017). Ultrasound transmission method to assess raw earthen materials. Construction and Building Materials, 156, 555-564.

Liang, R., Hota, G., Lei, Y., Li, Y., Stanislawski, D., & Jiang, Y. (2013). Nondestructive evaluation of historic Hakka rammed earth structures. Sustainability, 5(1), 298-315.

ASTM D2845-08 standard (2000). Standard Test Method for Laboratory Determination of Pulse Velocities and Ultrasonic Elastic Constants of Rock.

CHAPTER 6

Discussion of failure pattern development and underlying mechanisms

This section focuses on the mechanics of crack development and failure of rammed earth material under uniaxial compression stress condition. Therefore, aiming at contributing to advance the understanding of crack propagation in rammed earth specimens, by using uniaxial compression testing and digital image correlation technique, an experimental campaign was conducted on cylindrical specimens of clay-sand, as described in chapter 4. Beginning with this experimental investigation, a more theoretical analysis of different pattern of cracking and possible driver of crack propagation for different material texture is now further investigated.

6.1. Introduction

The fracture pattern of compacted earth under uniaxial compression is a complex phenomenon, which carries with it clues to the state of soil structure, and strains and stresses imposed, important information useful to describe earlier events in the structure of material and to provide an idea about possible subsequent mechanisms of behaviour of material.

It is known that the soil structure and fabric, varies with compaction characteristics, in particular: moulding water content and compactive effort. Fracture propagation seems to be a fabric driven process wherein soil structure can be of extreme importance in development of crack during stages of loading.

Very little is known about the influence of the soil structure on the stress-strain behaviour of rammed earth materials and on the way the cracks propagate in these materials. A review of literature reveals the absence of fully monitored laboratory tests focusing on crack development in rammed earth specimens.

The need for a quantitative estimation of the stress-strain curve of loaded rock specimen has made Digital Image Correlation (DIC), commonly used in mechanical engineering, quite popular recently (Ferrero & Migliazza, 2009; Nguyen et al. 2011; Zhang et al. 2012; Stirling et al. 2013; Yang et al. 2015; Guy et al. 2018; Caselle et al., 2019). DIC is a robust non-contact technique for measuring the relative displacements of points between a reference image and a subsequent one, shot from the same position during a test on a sample of a certain material (Vendroux & Knauss, 1998; Blaber et al., 2015). The open-source, freely available 2D subset-based DIC software package called Ncorr (Blaber et al., 2015) is a complete, updated, efficient and flexible code. The authors chose to use it for processing images of uniaxially loaded specimens, to obtain maps of stress and displacement.

The section focuses on an experimental campaign aiming at contributing to advance the understanding of crack propagation in rammed earth specimens. This study reports the results of a laboratory investigation designed to understand mechanics of failure in rammed earth, cylindrical specimens of clay-sand measuring 103 mm in height and 51 mm in diametre, subjected to uniaxial compression stress conditions. The results and conclusions were drawn from a multidisciplinary approach incorporating characterization by uniaxial compression testing and digital image correlation technique, to monitor crack propagation and explain the theoretical aspects of the observed processes involved in cracking rammed earth specimens.

6.2. Theoretical analysis

Through the combined use of laboratory uniaxial compression testing and digital image correlation methodology, aiding in the monitoring and characterization of fracture processes and conceptualization of the mechanisms that may act at micro-scale during fracturing processes, this section attempts to provide contributions into understanding how physico-mechanical characteristics results in the processes responsible for different stages of crack development, and thus the gradual strength loss of material mass leading up to failure. Results from this interdisciplinary laboratory incremental loading tests are used to qualify the state of soil structure and fracturing and to investigate and clarify its effects on the accumulation of damage with respect to stress-strain characteristics.

6.3. Uniaxial Stress-strain curves and drived stages of failure pattern in rammed earth specimens

In this section, a review of the mechanical and fracturing behaviour of rammed earth under uniaxial compression loading will be presented. After a brief discussion of stress-strain behaviour and crack processes, different mechanisms that were observed to play an important role in failure process of different materials will be debated.

6.3.1. Failure characteristics of rammed earth masses

Rammed earth contains a number of discontinuities or micro-cracks in their structure, developed during their construction process or induced by settlement, which contribute to division of small sections of an material, otherwise being continuous. As stress concentrators, discontinuities, causing the stress to increase in localized regions, plays a governing role in the formation and propagation of cracks. As a result of an induced combination of external and internal stresses, further propagation of discontinuities and interaction of propagated cracks leads to failure of these materials.

The crack development process at different stages with respect to corresponding deformation and stress state of laboratory tested rammed earth specimens are investigated in this section. Figures 3.1-3.7 in Appendix 3 shows the way the cracks propagated in the specimens under uniaxial compression loadings. The results of digital image correlation analysis have been reported in Figures 4.1-4.19 in Appendix 4.

Ncorr v.1.2.2 software (Blaber et al., 2015), implementing Digital Image Correlation (DIC) algorithms, was used to process frames. The software is able to estimate displacement and strain of a sample under deformation through the use of image processing techniques. The method consists in comparing each progressive image with the reference one.

We chose to extract from each video the frames corresponding to 50%, 75%, 90% and 100% of the maximum load. Figures 4.1-4.19 in Appendix 4 presents the results obtained from this laboratory campaign and subsequent analysis designed to isolate different stages of fracture development and to explore its relationship to the state of stress and deformation. As observed in Figures 4.1-4.19 in Appendix 4, rammed earth specimens pass from an unbroken to a broken condition through a process involving initiation and extension of micro and macrocracks, due to an additional load.

The results and conclusion drawn from this study highlights that the observed failure process displayed during uniaxial compression loading can be broken down into several stages, that may include, (1) closure of pre-existing cracks, due to axial compaction imposed by loading demonstrated through settling down the specimen; (2) nearly linear elastic behaviour; (3) crack initiation and propagation leading to failure.

The first stage, closure of pre-existing cracks, is characterized by the mechanism in which material deforms as a result of vertical loading. In a broad sense, this stage involves settling down process driven by vertical deformation behaviour of the material and the corresponding changes of its characteristics, contributing to reaching the state of extreme compaction of material.

As observed, the following stage of stress-strain behaviour, the elastic stress-strain behaviour, can be characterized by a maximum tangent Young's modulus of material, beyond which with a general increase in curvature and decrease in the tangent, the material reaches the maximum compressive stress, displaying strength of the material. As indicated by data, another identified stage of behaviour corresponds to the stable growth of crack, through which the effect of initiation and growth of the number or size of isolated microcracks and cracks gradually leads to decrease of tangent Young's modulus of material until the peak is reached.

6.3.2. Mechanisms

The cracking in rammed earth under uniaxial compression condition is a complicated three dimensional fracture growth process, with many different events involved at different scales of micro, meso and macro, which depending on the constituting elements of the material may include plasticity events, frictional effects, interaction of machine platens and specimen and soil material structural effects, leading to a resultant macroscale nonlinear stress-strain behaviour and crack pattern. Obviously, for such cases where many different physico-mechanical mechanisms is expected to play an important role on the failure process and cracking behaviour of the material, complications arise.

Based on Figures 3.1-3.7 in Appendix 3 and 4.1-4.19 in Appendix 4, it can be observed that there are major differences in the way different rammed earth materials crack, and possibly the driver of progress of crack and pattern of crack propagation, when subjected to uniaxial compression incremental loading. In specimens with a more brittle stress-strain behaviour, an almost single crack, parallel to the axial load and perpendicular to the tension, propagates, leading to specimen failure, whereas in some specimens such as S04Sa0Si0W14E2, failure can be attributed to coalescence of multiple cracks developed parallel to the compressive loads.

A number of mechanisms can be highlighted in fracture of specimens in compression. As this data illustrate, when a specimens is subjected to compressive external loads, the zones of compression and tension develop around a discontinuity (Appendix 4). Further uniaxial compressive loading has resulted in progress and inclination of the these original discontinuities in the specimens and development of secondary cracks, whose development at the tips or intermediate corners of primary cracks resulted in crack propagation and

interactions in a direction parallel to that of the uniaxial compressive stress, leading to failure of specimens. It can be observed in Appendix 4 that vertical cracks in specimens subjected to a compressive stress field propagates only when the global compressive stress is reached a higher value.

Figures 6.1-6.5 highlight the way crack initiated and propagated for the specimens. As depicted in Figures 3.1-3.7 in Appendix 3, Figures 4.1-4.19 in Appendix 4 and Figures 6.1-6.5, a number of various mechanisms may serve as crack initiation and growth processes. These observations seem to indicate that rammed earth can fail as a direct result from the three-dimensional nature of the cracking development, along inclined shear crack driven by the development of shear zones or through tensile splitting mechanism, or through the combination of both mechanisms (Appendix 3). The prevailing mechanism will clearly depend on a number of physico-mechanical structural parameters. Another observation confirms that, with further increase of the global compressive stress, initially inclined shear crack did not necessarily propagate through the growth of cracks in the presumably shear direction along the sides of the shear zones, but rather oriented in the vertical direction parallel to the compression loads, causing tensile fracture propagation.

Different constituting materials and structure of rammed earth give different stress-strain characteristic behaviour, which can be mainly characterized by a number of parameters, such as tangent Young's modulus, peak stress and corresponding peak strain. As data indicate, rammed earth materials with brittle and ductile stress-srain behaviour have distinctive crack pattern properties, however, some similarities can still be identified in these two categories of materials with some entirely contrasting characteristics.

As data illustrate, many factors control crack pattern, with the common factor being the development of tensile stress within a narrow region of the specimens at each stage of loading. Based on these observations, it seems that the soil structure gives a clear picture of soil cracking behaviour under different states. Soil structure plays an important role in cracking behaviour, as it can be considered an indication of many physical and mechanical soil parameters. As shown in Figures 4.1-4.19 in Appendix 4, in one type of failure, large zones of plastic deformation develop before crack initiation and growth. Another group of specimen is characterised by a failure in which inelastic deformation is small before crack initiation and growth. This may indicate that under uniaxial compressive stress condition, the vertical and lateral pressure induced by vertical and lateral displacements results in failure in rammed earth material.

It could be noticed from the results that the failure characteristics of studied rammed earth specimens are dependent on the soil structure and characteristic stress-strain behaviour, which undoubtedly plays an important role on the resistance of soil to initiate and propagate cracks. As data indicate, in specimens with brittle stress-strain behaviour deformations tend to localize in a narrow zone.

One of the processes substantially noticed in the specimens with higher sand content, is interfacial crack, cracking around the boundaries of aggregate, driven by the bonding between sand aggregates and clay contributing to lateral tension. Uniformly loading the specimens from the top, at particle level, leads to concentrations of compressive or tensile stress at aggregates level, which depending on the bonding between sand particles and clay, may contribute to development of tension and subsequently cracks at the interface between sand and clay. Another important mechanism occurring at the scale of particles is the development of well-known shear zones on top and below the aggregates, driven by the triaxial stress state at this scale, which might be attributed to the existing difference between stiffness, and consequently lateral deformation, of stiffer aggregates and softer clay.

Another observation confirms the local compaction occurring in the porous zones in the material, through which large deformations observed during pre-peak stages in some specimens (Appendix 4) could be explained.

It can be noticed that in rammed earth specimens with more uniform soil structure, specimens constituting only clay particles, the more identical ratio between the strength of constituting elements of material leads to diminish non-linear behaviour during pre-peak stages. This is more evident in the specimen S01Sa0Si0W20E2.

The interaction of specimen and loading platens of machine, the boundary restraint of the loading platens, was revealed to play an important role specificly when the size of cracks and lateral deformation reaches a large value with respect to size of specimen. In some specimens boundary shear regions can be observed, which can be attributed to the boundary restraint, which contributes to the development of triaxially confined parts in the regions in contact with the loading platens.

Another important observation is that highly non-uniform lateral deformation occur near the peak and post peak. In fact, such observation can be inferred to indicate that in these specimens failure occurs from the outside to the inside (Appendix 3 and 4). In these specimens, post peak load bearing capacity can be attributed to an remaining intact core part of the specimens.

It can also be observed that increasing dry density or decreasing moisture content, contributes to increase the capability of resisting crack propagation, and thus compressive strength. As observed, decrease of moisture content from the wet side of optimum to the dry side of optimum, contributes to higher level of roughness of material, and thus to higher level of frictional resistance to further progress of cracking.

Figures 3.1-3.7 in Appendix 3 and 4.1-4.19 in Appendix 4 indicates that the horizontally directed pre-existing discontinuities and cracks tended to close under the uniaxial compressive stress. The reason for this can be attributed to the higher water content, causing the material to become more plastic and ductile. This observation also indicates that in specimens with higher water content the uniaxial compressive stress is more effective in closing the discontinuities and cracks.

An analysis of data from laboratory investigation indicates that the roughness of material and, thus roughness of the cracks, had a large influence on the uniaxial compressive strength of material. It can be observed that the greater was the roughness of the material, the greater was the value of the compressive strength of the specimens.

As Figures 3.1-3.7 in Appendix 3 depicts, the specimens with a planar crack and the sample with a rough crack whose sides are inclined at a few degrees tend to have similar strengths (specimens S03Sa40Si0W8E2 and S04Sa5Si0W14E2). However, the specimens with rough texture of material tended to develop rougher cracks. The specimens that developed rough cracks with more inclined sides was shown to be stronger, with specimen S03Sa40Si0W8E2 being stronger than S04Sa40Si0W6E2. The reason for this may include the higher shear strength of more inclined rougher cracks. Due to rough texture of these materials, the cracks takes the form of a stepped configuration, introducing a frictional resistance to further progress of cracking, which in turn may affect the way cracks propagate. This is more evident in the specimen S03Sa0Si0W16E3, displaying very stepped inclined crack pattern with the highest obtained uniaxial strength.

From the detailed results of DIC analysis as well as stress-strain behaviour for the specimen S02Sa0Si0W17E2, constructed with 0% sand and 17% water content compacted with compactive effort E2, shown in Figure 6.6, the following may be suggested.

The specimen passes from an unbroken to a broken condition through a process involving initiation and extension of cracks, due to an additional load in the direction of its long axis. The results would seem to indicate to a more plastic type of behaviour of the specimen associated with relatively large deformation occurred before reaching a relatively constant but significantly low level.of stress. Further examination of the resultant plots reveals exposition of the specimen to low level of stress before reaching a steep stress increasing trend at initial stages of loading, as can be observed in Figure 6.6. This results indicate that

uniaxial compressive loading induces a degree of non-linearity in stress-strain behaviour during initial stages of loading, which would seem to be attributable to the crack closure achieved during the first increments of loading, demonstrated through axial compaction imposed by loading contributing to settling down the specimen. The non-linear stress-strain behaviour exhibits an increase in axial stiffness, before the axial stiffness begins to behave in a more linear fashion. As shown in Figure 6.6, large zones of lateral deformation develop before crack initiation and growth. Whereas visible cracks were difficult to find during initial stages of uniaxial loading, crack growth parallel to the direction of loading contributes to enlarging the crack continuously until the vertical splitting crack was visible in relatively high axial deformation, which might be attributed to excessive transverse tensile stresses developed under higher axial compressive stresses causing the failure. Tensile vertical cracking was found to be caused mainly by overburden pressures, formed from a zone in which most of the transverse deformation is localized. This may seem to indicate that under uniaxial compressive stress condition, the vertical and lateral pressure induced by vertical and highly non-uniform lateral displacements results in failure of the specimen. This observation would seem to reveal that in this specimen failure occurs from the outside to the inside. The illustration shown in Figure 6.6 would also seem to indicate crack formation and propagation at respectively low stress levels, which could be attesting to the ease at which cracks are formed.

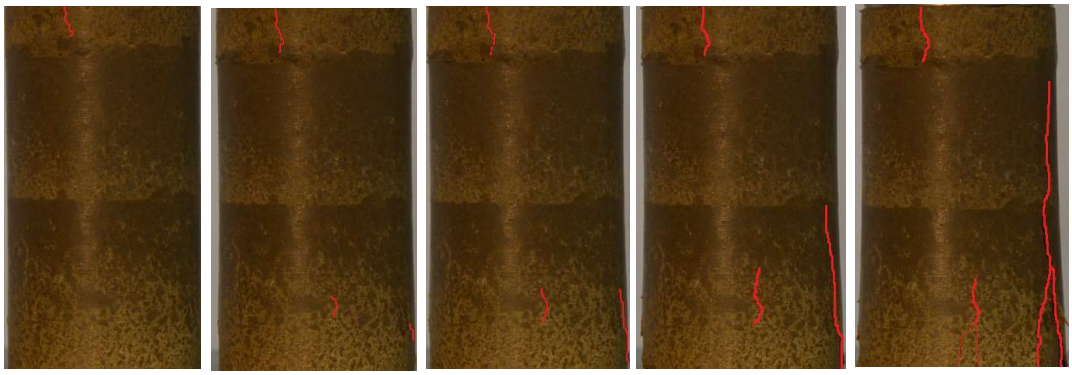

S04Sa0Si0W14E2

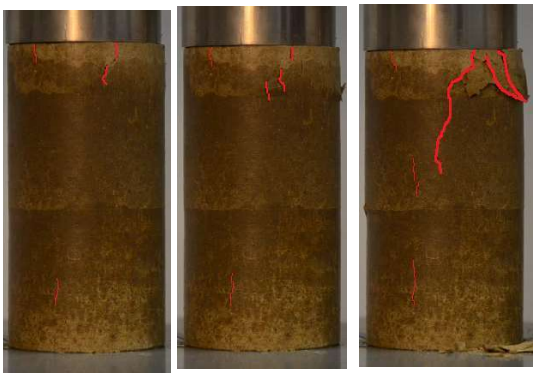

S03Sa0Si0W16E2

S02Sa0Si0W18E2

Figure 6.1. Crack development in clay specimens with compactive effort E2

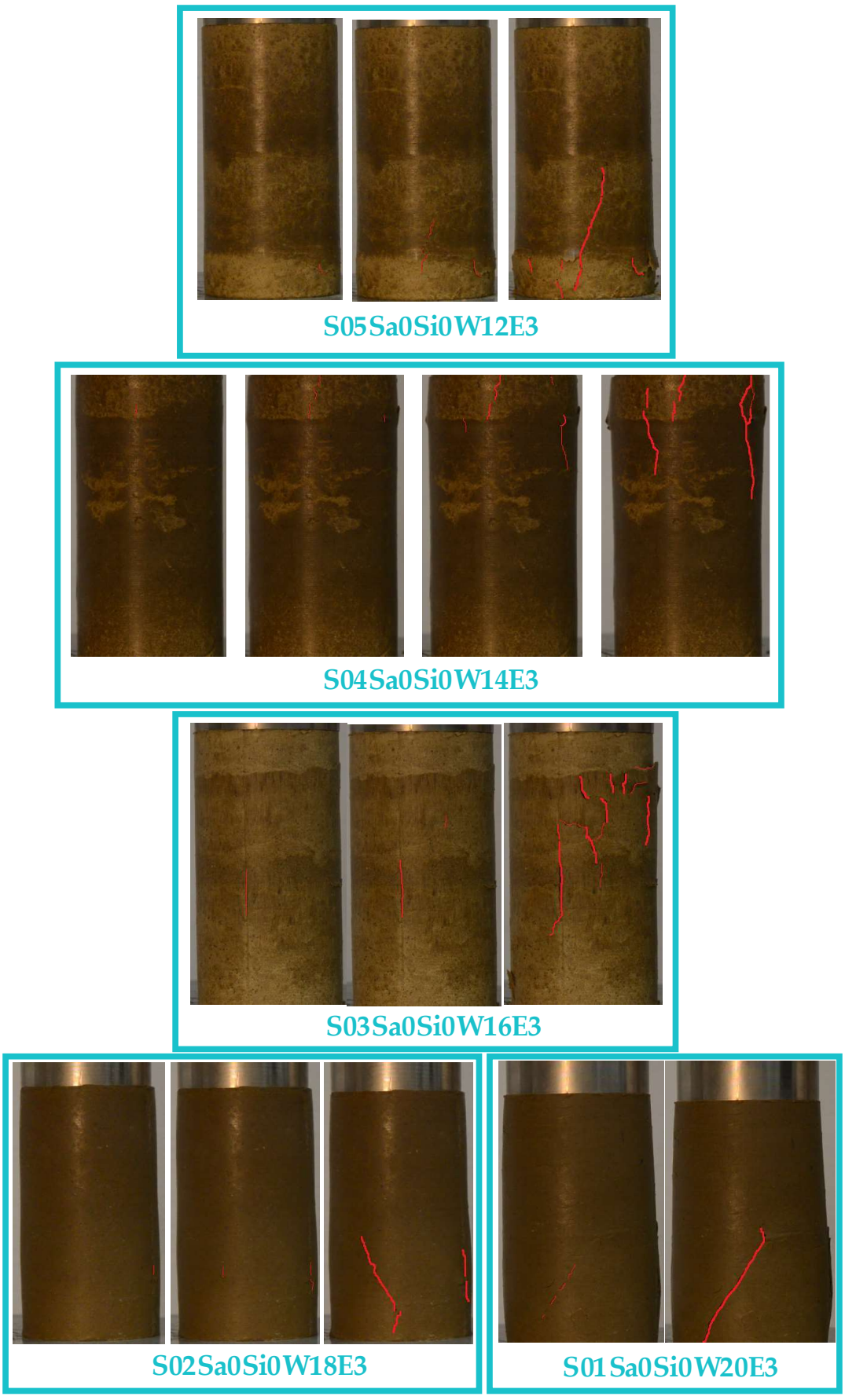

Figure 6.2. Crack development in clay specimens with compactive effort E3

Figure 6.3. Crack development in clay-sand specimens with sand content 5% and compactive effort E2

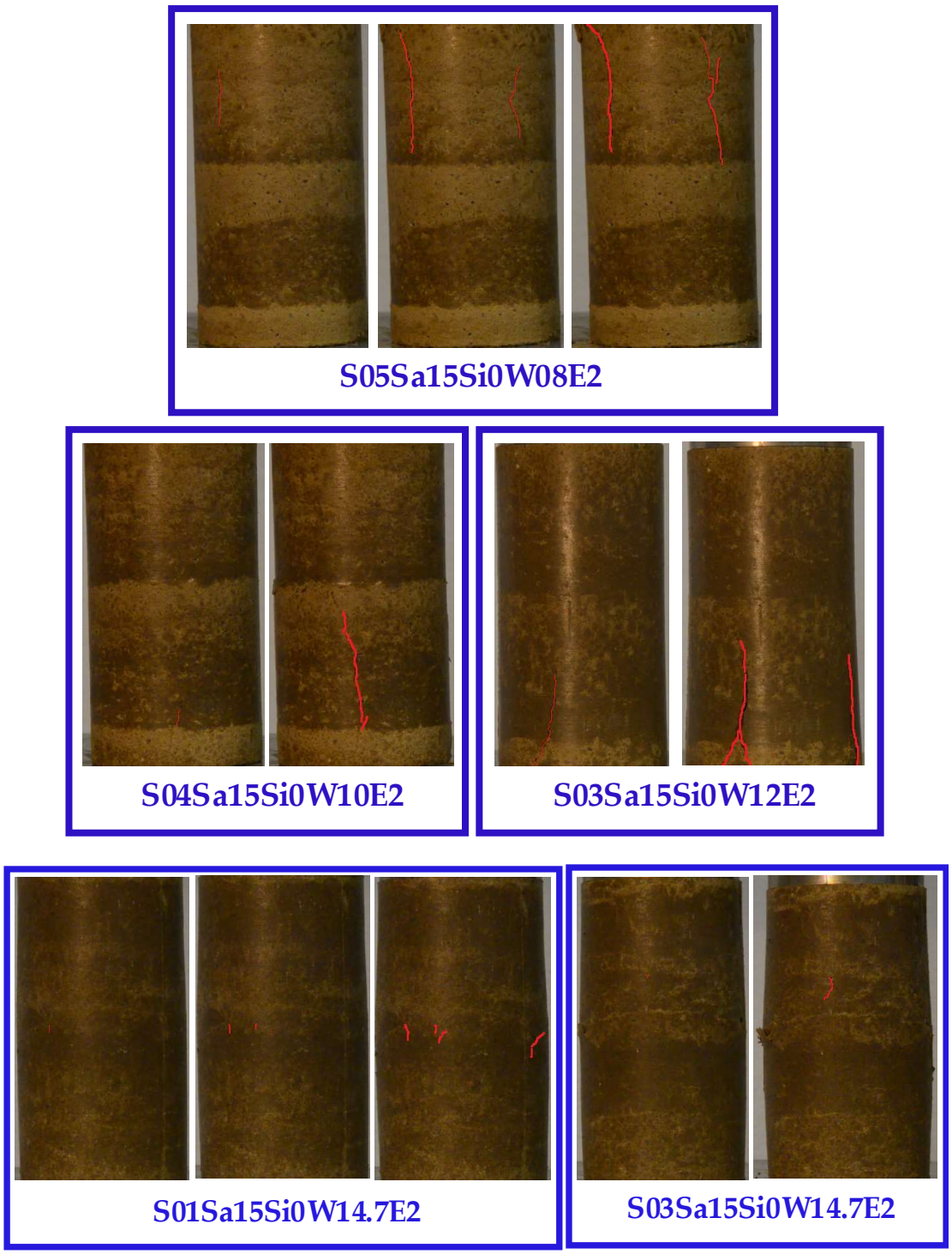

Figure 6.4. Crack development in clay-sand specimens with sand content 15% and compactive effort E2

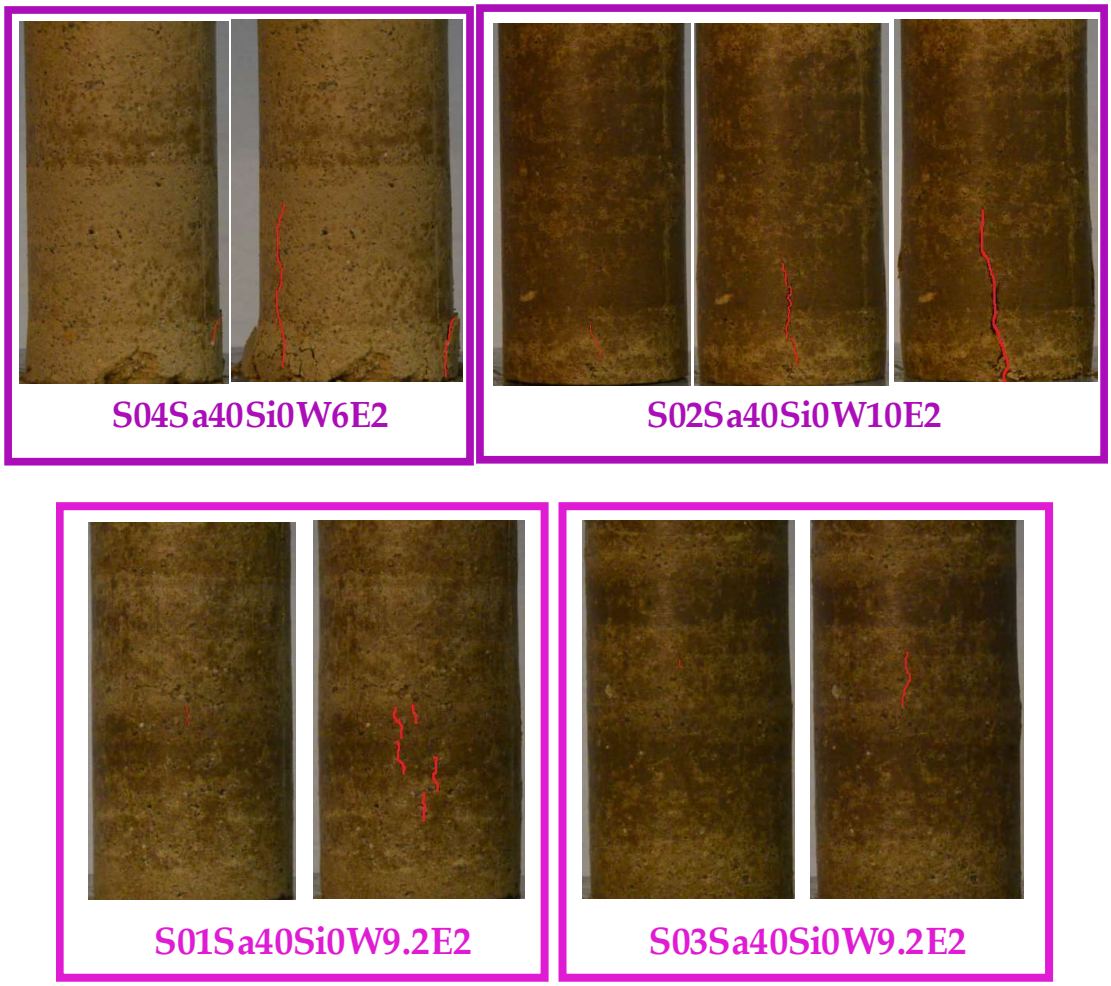

Figure 6.5. Crack development in clay-sand specimens with sand content 40% and compactive effort E2

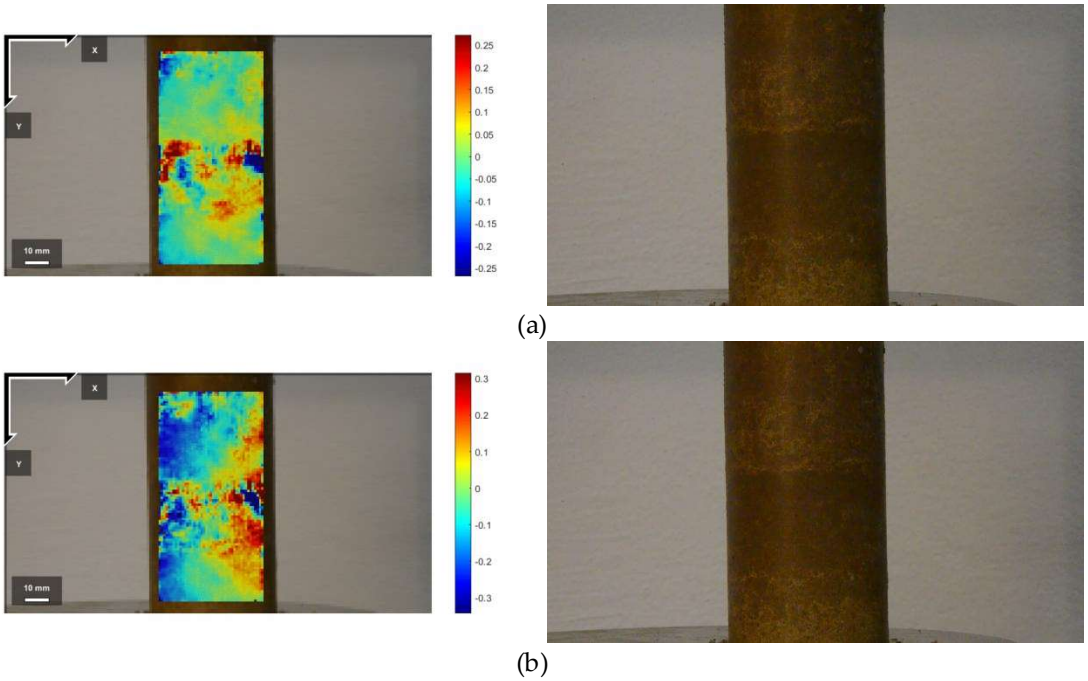

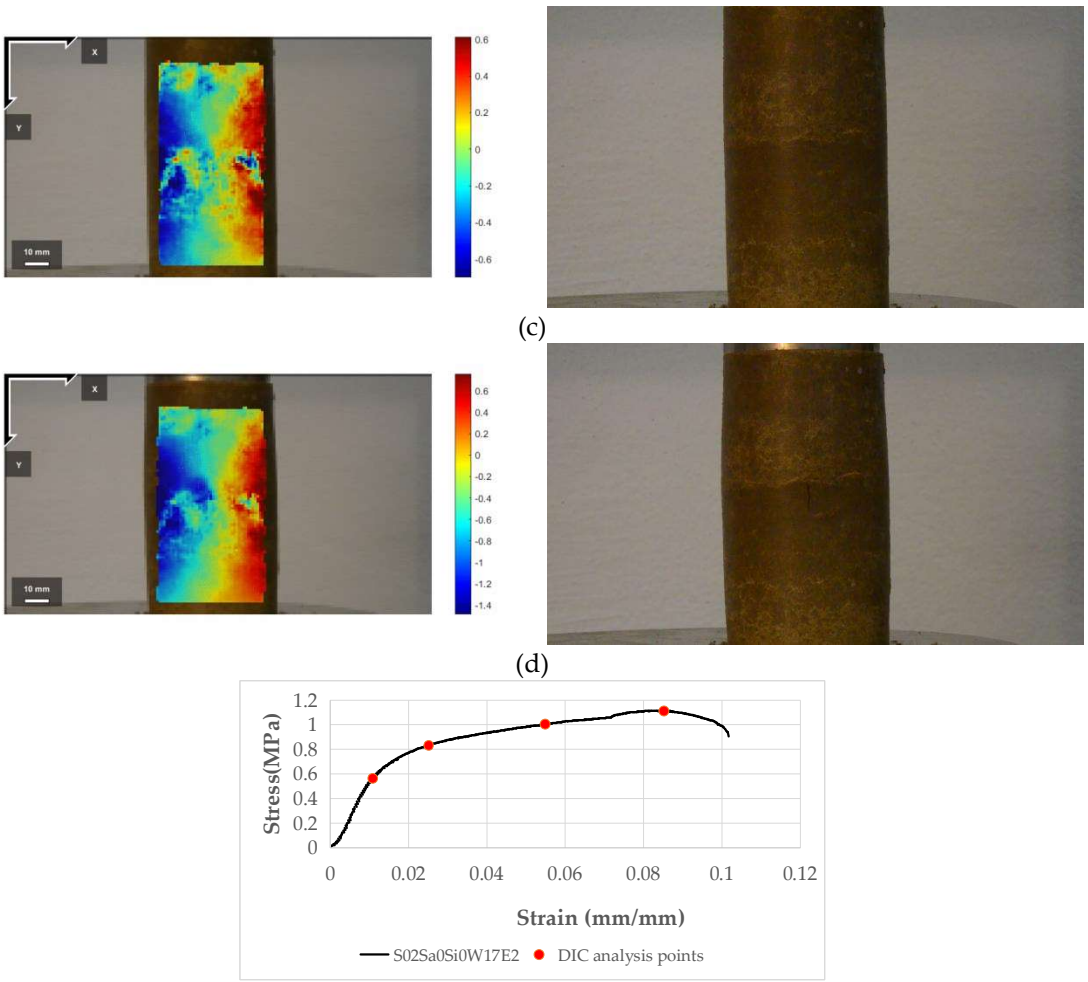

Figure 6.6. DIC Displacement in horizontal direction S02Sa0Si0W17E2, (a) 0.5*Strength, (b) 0.75*Strength, (c) 0.9*Strength, (d) Strength, (e) analysis points

6.4. Conclusion

In this research, which focused on the effects of soil structure on mechanical behaviour of a compacted soil incorporating cracking process, a series of uniaxial compression tests were conducted on different soil fabric, different mixture of compacted soil at different water contents and at different compactive effort. The progressive cracks induced by compression were monitored and analysed by image processing technique. Based on the obtained data, the coupling effects of physical and mechanical properties of soil on observed cracking and failure behaviour are herein analysed and discussed. Particularly, the relationship between stress-strain state of material and development of crack pattern of the soil is qualitatively characterized. The observed failure patterns indicate that rammed earth specimens can fail along inclined shear crack driven by the development of shear zones or through tensile splitting mechanism, or through the combination of both mechanisms. The prevailing mechanism clearly depends on soil structure, which is indicative of a number of physico-mechanical structural parameters.

References

Ferrero AM, Migliazza MR (2009). Theoretical and numerical study on uniaxial compressive behaviour of marl. Mechanics of Materials 41:561–572. doi.org/10.1016/j.mechmat.2009.01.011

Nguyen TL, Hall SA, Vacher P, Viggiani G (2011). Fracture mechanisms in soft rock: Identification and quantification of evolving displacement discontinuities by extended digital image correlation. Tectonophysics 503:117–128. doi.org/10.1016/j.tecto.2010.09.024

Zhang H, Huang G, Song H, Kang Y (2012). Experimental investigation of deformation and failure mechanisms in rock under indentation by digital image correlation. Engineering Fracture Mechanics 96: 667–675. doi.org/10.1016/j.engfracmech.2012.09.012

Stirling RA, Simpson DJ, Davie CT (2013). The application of digital image correlation to Brazilian testing of sandstone. International Journal of Rock Mechanics & Mining Sciences 60:1–11. doi.org/10.1016/j.ijrmms.2012.12.026

Yang G, Cai Z, Zhang X, Fu D (2015). An experimental investigation on the damage of granite under uniaxial tension by using a digital image correlation method. Optics and Lasers in Engineering 73: 46–52. doi.org/10.1016/j.optlaseng.2015.04.004

Guy N, Seyedi DM, Hild F (2018). Characterizing Fracturing of Clay-Rich Lower Watrous Rock: From Laboratory Experiments to Nonlocal Damage-Based Simulations. Rock Mech Rock Eng 51, 1777–1787. doi.org/10.1007/s00603-018-1432-2

Caselle C, Umili G, Bonetto S and Ferrero A M 2019 Application of DIC analysis method to the study of failure initiation in gypsum rocks Géotechnique Lett. 9 35–45

Blaber J, Adair B, Antoniou A (2015). Ncorr: Open-Source 2D Digital Image Correlation Matlab Software. Experimental Mechanics 55(6):1105-1122. doi.org/10.1007/s11340-015-0009-1

Vendroux G, Knauss W (1998). Submicron deformation field measurements: Part 2. Improved digital image correlation. Exp Mech 38(2):86–92. doi.org/10.1007/BF02321649

CHAPTER 7

Identification of material parameters for rammed earth specimens

This study evaluates the effectiveness of back analysis in parameter identification of rammed earth material using finite element analysis and laboratory examination results. Motivated by the complexity of the shape of stress-strain curve, which is inherent to each soil structure, and the consequent difficulty in the selection of appropriate Young's modulus of rammed earth specimens, a general equalization is applied which describes the behaviour of a wide range of rammed earth material by a single framework. Based on this semi-inverse analytical approach, in order to simplifying the curve into a uniform form, a generalized equivalent stress-strain curve is defined, upon which the inverse analysis is mainly employed. This equivalent stress-strain curve provides useful equivalent parameters by which to interpret the behaviour of various rammed earth composition observed in laboratory testing.
Whether the analytical procedure examined in this study can be extended to include more comprehensively important aspects associated with the behaviour of rammed earth material will be an issue requiring further examination. The present research is the very first analytical approach to back analysis of rammed earth specimens and therefore it is, to a certain extent, bound to further investigation. In view of the very limited experimental data, in which important material characteristics have not been investigated, there is a clear need for further laboratory work on characterization of rammed earth material. However, in light of future research, it may be possible to develop a more efficient approach for prediction of parameters.

7.1. Introduction

Besides laboratory experiments and analyses, numerical simulation is an important method of study of architectural heritage. Therefore, after conducting series of laboratory experimentation and analysis on rammed earth materials, as described in previous chapters, this section focuses on finite element simulations of uniaxial compression loading and discussion of important parameters essential for the task at hand. A better understanding of how material parameters change as a result of soil composition and structure is believed to be critical for many applications of simulation of rammed earth structures in conservation of cultural heritage rammed earth buildings.

Improving the tools and methods based on analytical solution are critically important for the numerical simulation of rammed earth heritage. Mathematical and finite element analysis methods are widely used for estimation of state of material and structure, and strains and

stresses imposed, providing an idea about possible subsequent behavioural mechanics, and thus aiding in prediction of future possible behaviour and safety.

In the present study, a total of 16 rammed earth specimens were investigated for finite element analysis under uniaxial compression loading (Figure 7.1). The details of their production and characteristics have been described in Chapter 4, which have been summarized in Appendix 1. Finite element analysis were performed on above-mentioned specimens using COMSOL software.

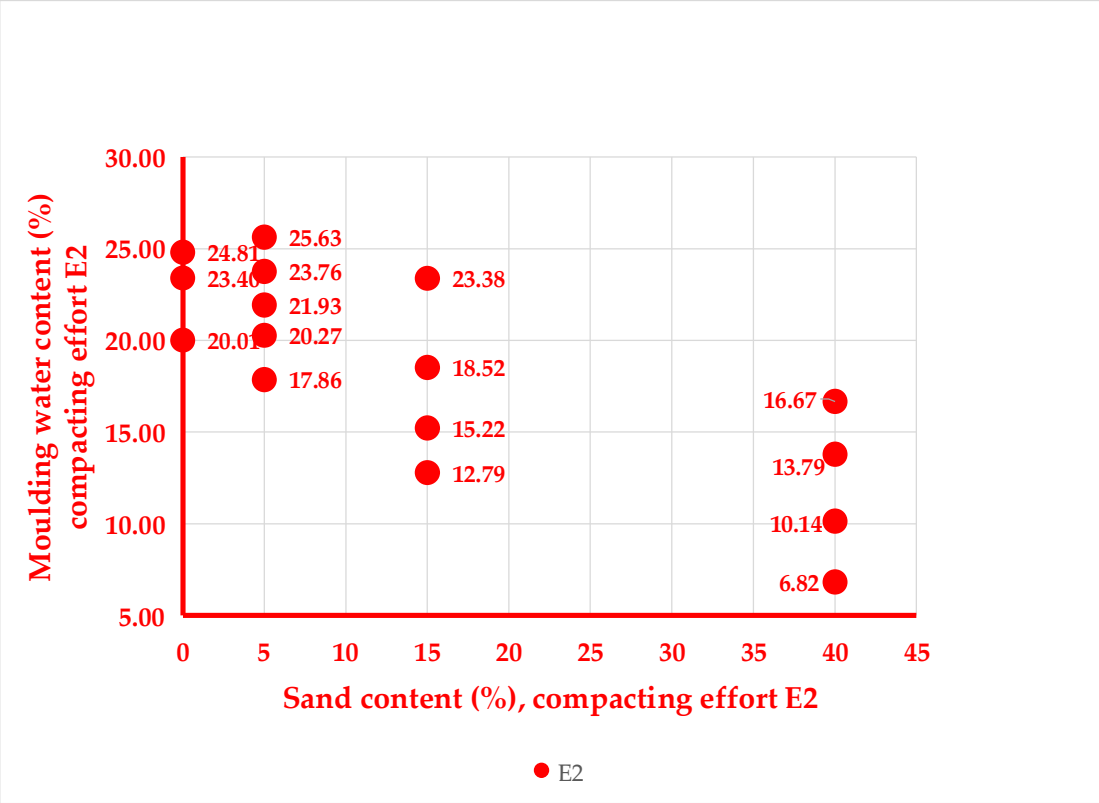

Figure 7.1. Specimens in this study

There are several principal material parameters of major interest to describe the mechanical response of a compacted earth material to applied loading (Chapter1). For characterizing soil properties, a common requirement is to obtain values of parameters based on laboratory or field measurements or judgement and experience (Wangmo et al. (2019), Jo et al. (2018), Daoudi et al. (2018), Cavicchioli et al. (2018), Baglioni et al. (2016), Benkmil et al. (2018), Ruiz et al. (2014), Martín-del-Rio et al. (2018), Silva et al. (2018), and Gomes et al. (2014)). Thus, in development of the models to capture important features of soil behaviour, parameter identification pose significant challenges.

The simulation of above-mentioned rammed earth specimens seems to be challenging. A potential difficulty in modeling is the complexity of the shape of stress-strain curve, which is inherent to each soil structure. On one side, it requires constitutive model that can describe a very different mechanical behaviour and characteristic load-deformation curves of each rammed earth specimens, which is characterized by different stages; Secondly, each stage of load-deformation is associated to soil structure, represented by soil composition and capturing different stages is challenging.

Considerable variability of obtained stress-strain results was also noted between clay and clay-sand specimens (Figure 7.2). Interpretation can be found in dissimilar nature and structure of the materials in these specimens. The stress-strain behaviour developed along initial stages of loading impose difficulty in the selection of appropriate Young's modulus.

For specimens with more sand content, longer exposition of the specimen to low level of stress before a steep stress increasing trend can be observed. In other group of specimens uniaxial load-deformation behaviour begins with a steep stress increasing trend followed by a curvature change before reaching very linear section of load-deformation (Figure 7.2).

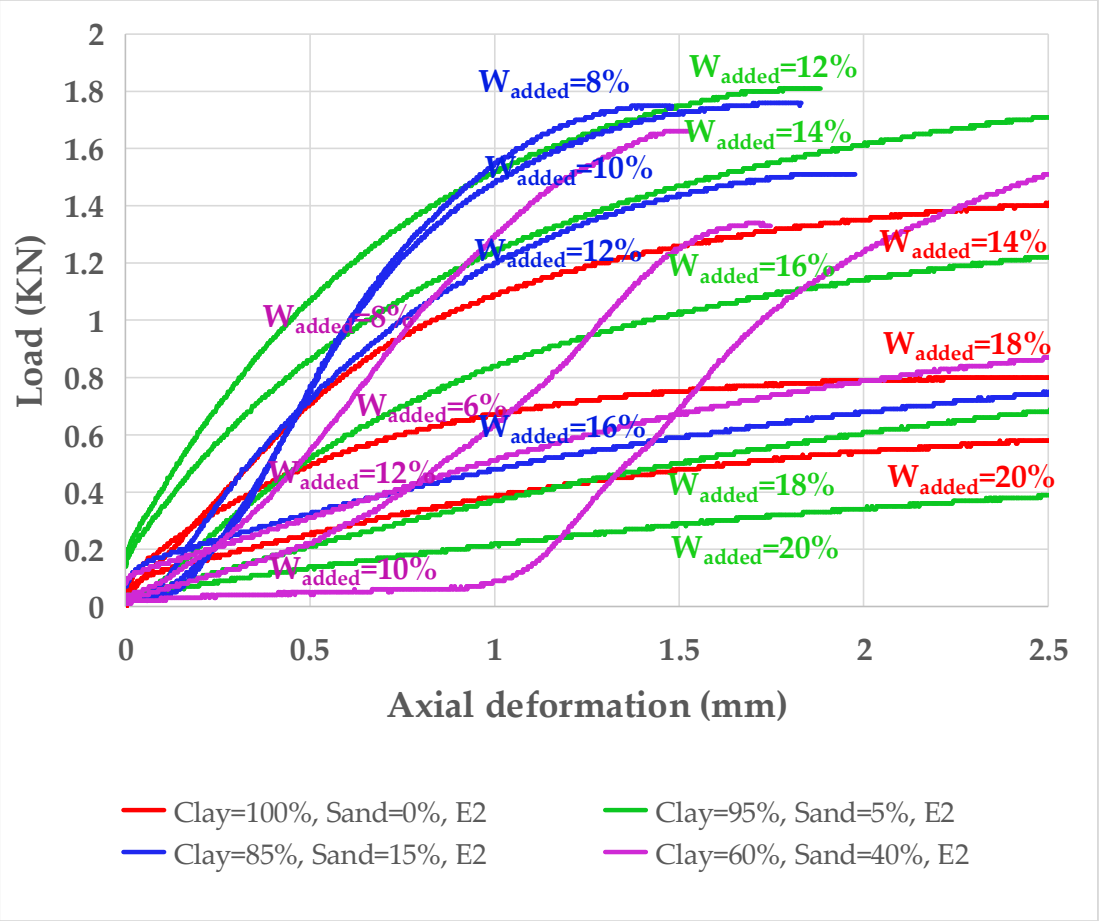

Figure 7.2. Considerable variability of Load- axial deformation along initial stages

The cohesion is one of the most widely used material parameter that reflects the behaviour of unsaturated soils, but it is not easy to obtain and a series of well-defined and complicated laboratory tests are needed. Hence, this section attempts to investigate the feasibility of contribution of uniaxial compression testing to comparative description of cohesion characteristic of rammed earth material, constituted by compacted moist earth in unsaturated state.

7.2. Methodology in current study

There are several principal properties of major interest to describe the mechanical response of a rammed earth material to applied loading. Cohesion is that important property relating strength gain and material structure changes in rammed earth materials. For these reasons, plus the fact that this property appears in many theoretical constitutive laws of material and thus, stress-strain analyses, an effort is made herein to provide a simplified procedure for its approximate qualitative determination.

The main difficulties inherent to analysis of rammed earth material are related to the diversity and complexity of stress-strain behaviour in initial stages of loading (Figure 7.2),

making the estimation of modulus of elasticity a challenging task, which may yield non-unique solutions for defining modulus of elasticity of one particular rammed earth specimen. Therefore, appropriate definition of Young's modulus is a critical issue. Based on variability of Young's modulus along whole range of applied loading on the data in Figure 7.2, one may notice the difficulty in recognition of a specific stress level or well-defined framework for Young's modulus determination, leading to an uncertainty of methodology in appropriate determination of Young's modulus, which may suggest a necessity for the establishment of a methodology, which should overcome the problem of diversity and complexity observed along initial range of loading, clearly attributed to the structure of material.

An effective way to calibrate a model employs inverse analysis, also called back analysis, techniques, minimizing the difference between experimental or field test and numerically computed results. An inverse modeling approach, by associating a finite element analysis with an optimization procedure, offer numerous advantages in the process of identification of soil material parameters of an adopted soil model from test results that produce the best fit between experimental and analytically computed results in model analysis, for any testing procedures and material model, even with no physical meaning. An inverse analysis involves calibration of a model by iteratively modifying and updating the estimates of its input parameters until a match between the numerically simulated output values and the observed experimental values, quantified by minimizing the error between computed results and experimental data, is obtained.

Generally, stress-strain , or load-deformation, curve is an extremely important indicator to represent the mechanical behaviour of soil. It is a difficult task to control many variability displayed in the form of a displacement-stress curve, which is associated with the material texture, implying load-deformation behaviour during different stages of loading, compaction, softening or hardening, dilation of soil, etc. For that reason, it is desirable to apply simplifications to experimental results. According to different kinds of load-deformation curves observed in experimentally tested specimens, as described in previous chapters, in order to overcome such above-mentioned challanges, it seems that application of inverse analysis to capture such a wide range of behaviour observed in load-deformation characteristic of rammed earth specimens require a lot of simplification having powerful adaptability. Therefore, in this study, in order to simplifying the curve into a uniform form, the stress-strain curve is equalized into an equivalent stress-strain curve, upon which the inverse analysis is mainly employed to inversely identify parameters of a material model.

Clearly, the effective simplification or equalization of information displayed in stress-strain curves can significantly improve the speed of analysis with the main aim being to obtain a uniform definition for a very wide range of stress-strain behaviour that may encounter in a very wide range of rammed earth materials.

As observed, inherited diversity and complexity of rammed earth materials has led to a complex load-deformation behaviour too. Thus, it is desired to characterize the specific behaviour of a material structure by its equivalence defined through equalization of load-deformation characteristics. Figure 7.3 shows a schematic of such equalization adopted herein.

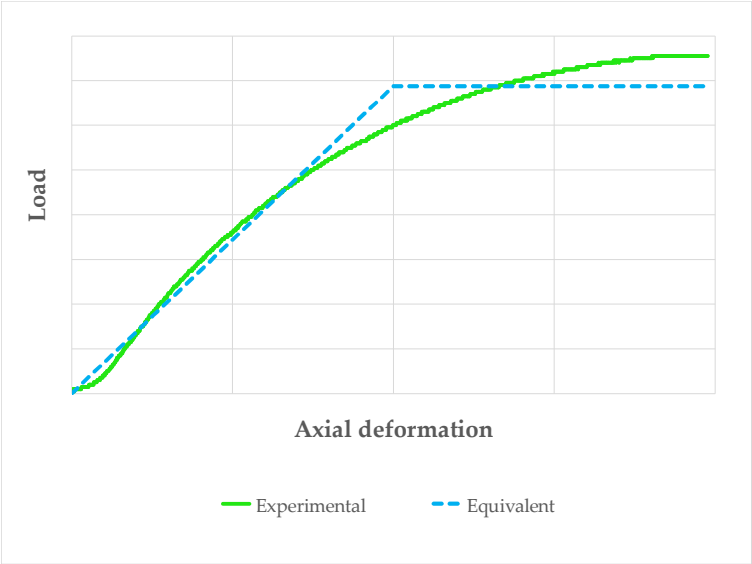

Figure 7.3. Equalization of load-deformation curve

The process of parameters identification of a rammed earth specimens considered in this study includes the following steps. The input parameter, equivalent modulus of elasticity, is initially calculated by equalizing stress-strain curve using available laboratory test results. Next, initial value for equivalent cohesion is defined and a numerical simulation of uniaxial compression test is run. The simulated load-deformation results are then compared to the equalized load-deformation curve obtained from experimentally measured data. The input parameter, equivalent cohesion, is updated and the numerical simulation is repeated until an optimal fit between load-deformation result of simulation and equalization is reached.

This approach provide solution in which the equivalent Young's modulus describes an average properties of media observed along all initial phases of loading. In order to use the result of uniaxial compression test to evaluate the cohesion characteristics of different rammed earth fabrics, this study assumes an equivalent material having equivalent Young's modulus, E_M, and equivalent cohesion, C_M, characteristics. Therefore, the equivalent Young's modulus and cohesion of rammed earth specimens can be obtained, as shown in Figure 7.3, which can then be utilized to investigate the relationship between the values of cohesion obtained by the uniaxial compression test, C_{UC} and by the analytical approach adopted herein, C_M. If a sound proportion relationship can be determined between C_{UC} and C_M of rammed earth specimens, it may be possible to develop a simple and appropriate alternative approach to characterize the cohesion characteristics using the results of uniaxial compression test.

7.3. Model development and discussion of results

In order to study the effect of structure change of material on mechanical strength gain characteristics of the rammed earth, being in an unsaturated state, a series of the two-step analytical approach described above were conducted on the specimens summarized in Figure 7.1, which have been previously described in detail in chapter 4.

Therefore, the above-mentioned equivalent load-deformation curve has been constructed for each specimen. From equivalent curve and using a finite element model, an equivalent modulus of elasticity for each specimen were obtained , with an equivalent cohesion obtained through back analysis. Figures 7.4-7.7 show equivalent behaviour obtained for four different material composition in the current investigation.

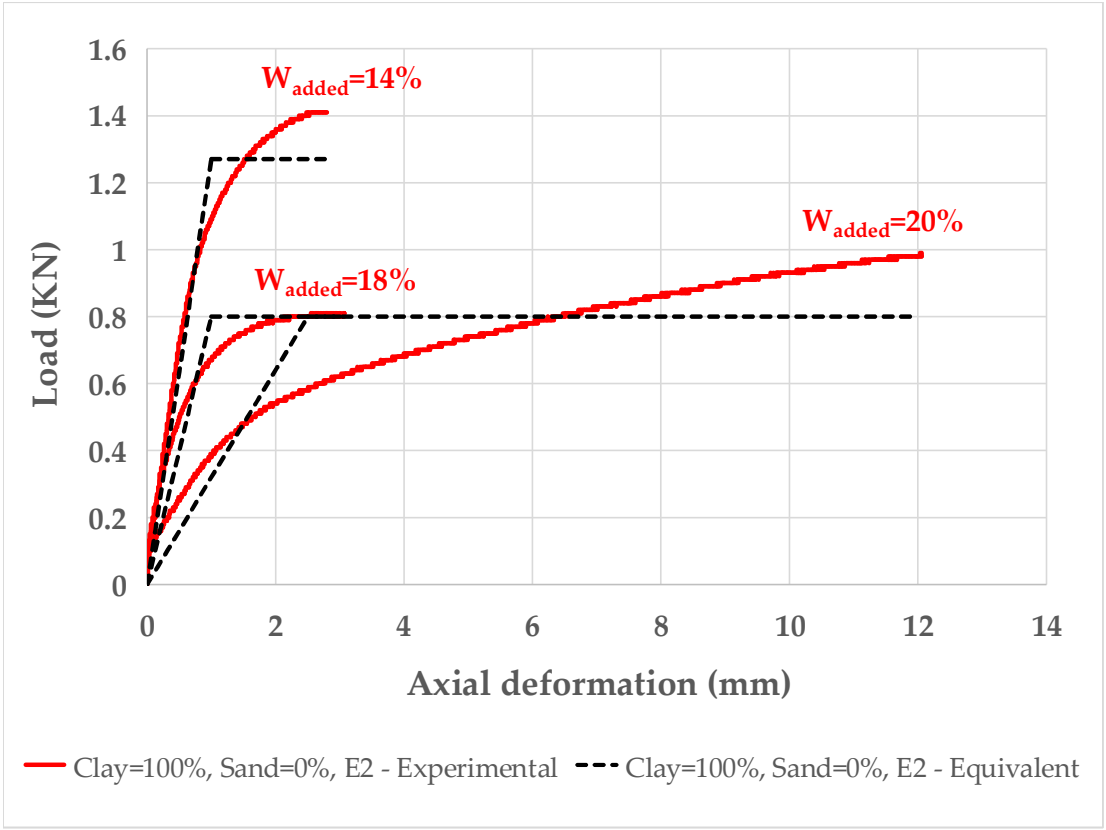

Figure 7.4. Equivalent load - axial deformation curve for clay specmens

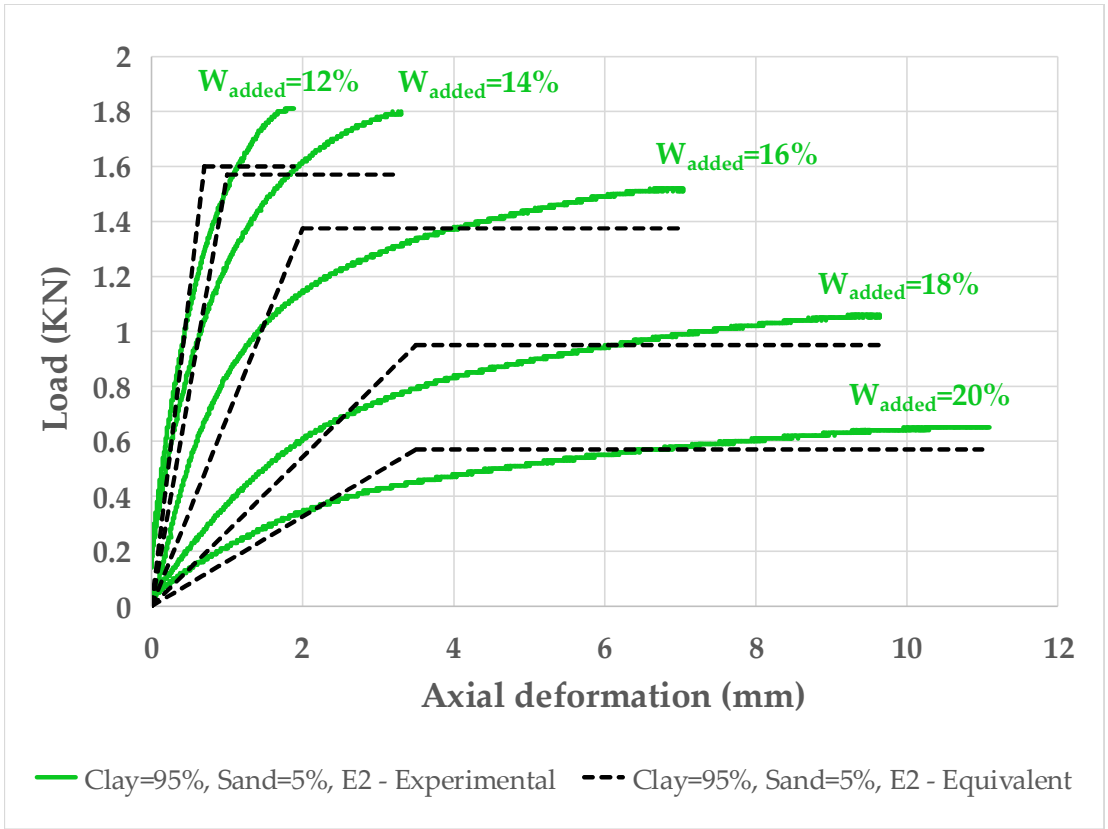

Figure 7.5. Equivalent load - axial deformation curve for clay-sand specmens with 5% sand content

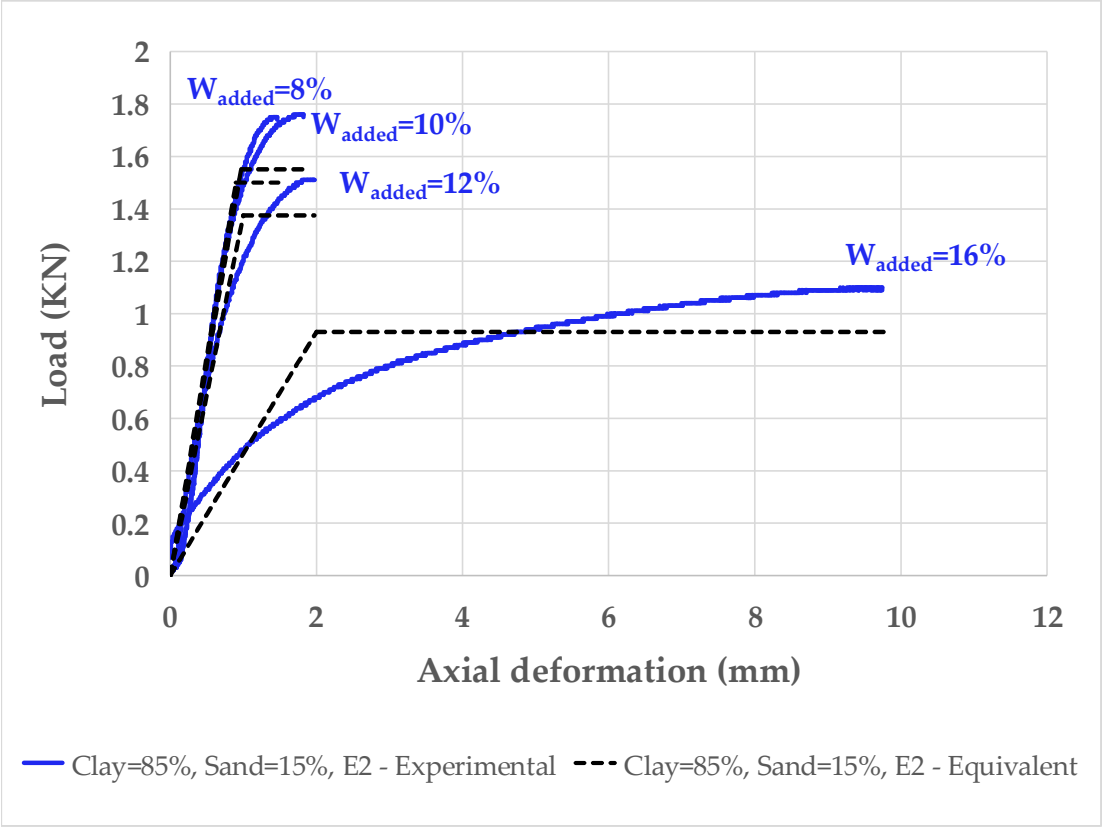

Figure 7.6. Equivalent load - axial deformation curve for clay-sand specmens with 15% sand content

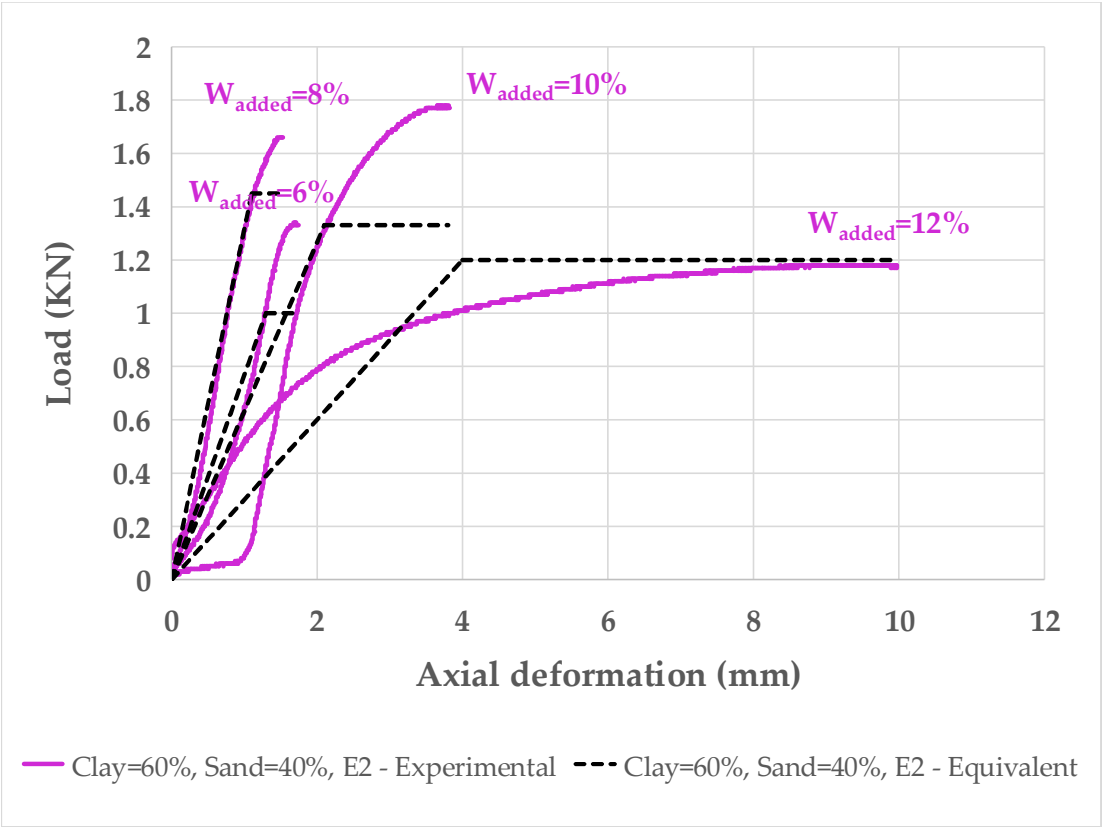

Figure 7.7. Equivalent load - axial deformation curve for clay-sand specmens with 40% sand content

The model has been created using 2D Axisymmetric Model Wizard window, with geometry being defined with the Width and the height as D/2 and H. Since the reaction force is defined at nodes, in the Definitions toolbar, Nonlocal Couplings, Integration, intop1, is defined with method being defined as summation over nodes. In the Physics toolbar, Mohr-Coulomb criterion has been attributed to Soil Plasticity. The Drucker-Prager criterion matched to a Mohr-Coulomb criterion, has been used in the modelling, with Drucker-Prager being selected to be matched at compressive meridian under plastic potential. Material data is expressed in terms of the parameters cohesion, c, and, Angle of internal friction, ϕ, defined in the Mohr-Coulomb model. The values for Angle of internal friction in modeled rammed earth specimens are defined as reported in Appendix 5. Therefore, the correlations among structure of material, the proportion of C_M and C_{UC} has been studied under the framework of the Mohr-Coulomb model combined with back analysis.

Figure 7.8 shows the relationship of the cohesion obtained from analysis (C_M) and the results derived directly from the uniaxial compression testing (C_{UC}). The analytical results show that the cohesion value is approximately in linear increasing relation to the corresponding cohesion value obtained from the uniaxial compression value. Variation of C_M/C_{UC} with respect to C_{UC} has been shown in Figure 7.9.

Based on all the results discussed above, a relationship between C_M and C_{UC} can be observed. However, because of currently insufficient amount of the laboratory data with lack of measurement of important characteristics of material, further well-defined laboratory study needs to be conducted to clarify this phenomenon and to help develop a more comprehensive approach to characterize this important parameter for practical application.

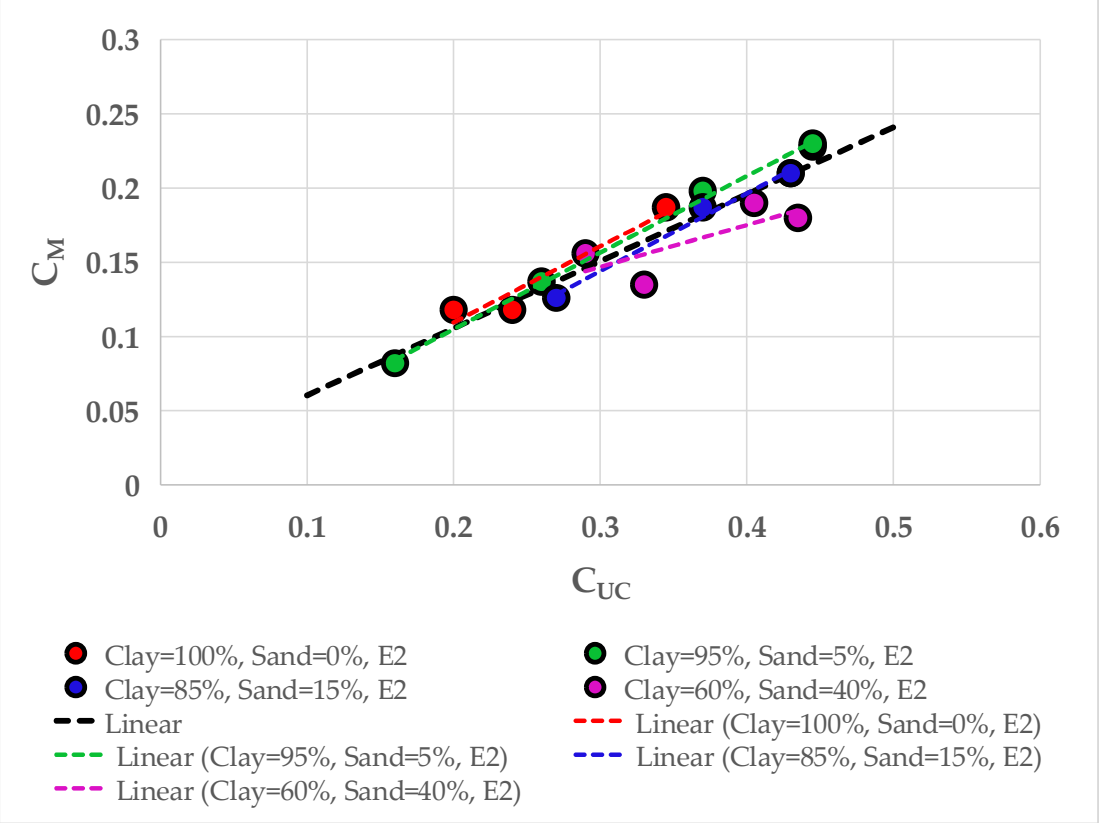

Figure 7.8. Relationship between C_M and C_{UC}

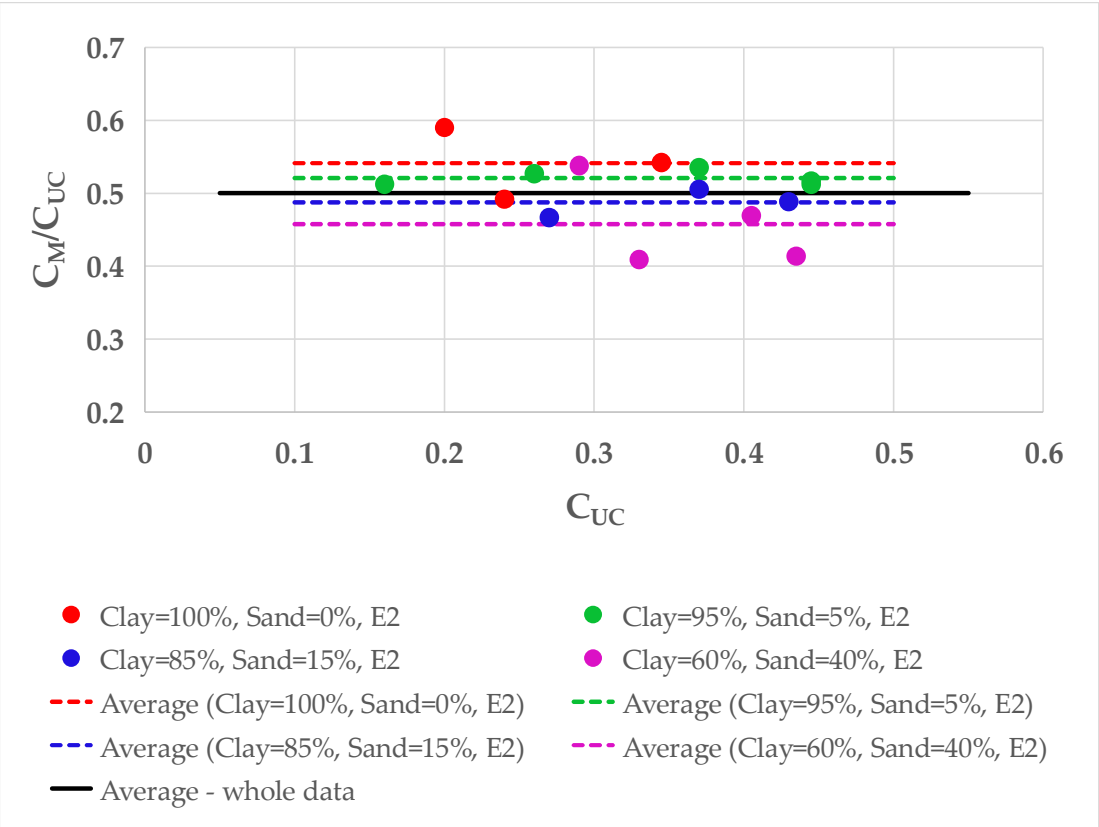

Figure 7.9. Variation of C_M/C_{UC} with respect to C_{UC}

7.4. Conclusion

It can be noticed that diversity of composition of rammed earth materials leads to complexity of structure of rammed earth materials, emphasizing a complex stress-strain behaviour too, imposing difficulty in the selection of appropriate Young's modulus of rammed earth specimens. Knowing this, equalization is indispensable for having a unique system of procedures, a well-defined and specific framework applicable for any rammed earth medium to describe and simulate the evolution of stress-strain behaviour associated with the specific material. This is the reason why it is necessary to equalize the stress-strain curve of rammed earth media to that of an equivalent media. In this respect, two main input parameters of the equivalent media, equivalent modulus of elasticity and equivalent cohesion, control the stress-strain behaviour of medium.

Thus, in the current study, a rammed earth media with stress-strain behaviour, is equalized with an equivalent continuum medium displaying an equivalent stress-strain curve. Therefore, the inverse analysis mixed with equalization introduces powerful adaptability that can provide a possibility to make use of monitored information to define the constitutive behaviour of a very wide range of rammed earth media. It can be observed that there shall be relationship between the values of parameters obtained by the uniaxial compression test and by the analytical approach adopted herein. However, because of currently insufficient amount of the laboratory data with lack of measurement of important characteristics of material, further well-defined laboratory study needs to be conducted to clarify this phenomenon and to help develop a more comprehensive approach to characterize this important parameter for practical application.

References

Baglioni, E.; Fratini, F., and Rovero, L. The characteristics of the earthen materials of the Drâa valley's architecture. J. Mater. Environ. Sci. 2016, 7(10), 3538-3547.

Benkmil, R.; Bahi, L.; Aakhssass, A., and Ouadif, L. CONTRIBUTION TO THE CHARACTERIZATION OF CONSTRUCTION MATERIALS OF HISTORICAL MONUMENTS-CASE STUDY. International Journal of Civil Engineering and Technology. 2018, 9, 1680-1688.

Cavicchioli, A.; Sant'Anna, L. G., and Perroni, M. S. Enlightening the use of materials and techniques in earthen architecture in southeast Brazil during the first coffee cycle (19th century). Journal of Cultural Heritage. 2018, 31, 208-214.

Daoudi, L.; Rocha, F.; Costa, C.; Arrebei, N., and Fagel, N. Characterization of rammed-earth materials from the XVIth century Badii Palace in Marrakech, Morocco to ensure authentic and reliable restoration. Geoarchaeology. 2018, 33(5), 529-541.

Gomes, M.I.; Gonçalves, T.D., and Faria, P. Unstabilised rammed earth: characterization of the material collected from old constructions in south Portugal and comparison to normative requirements. International Journal of Architectural heritage. 2014, 8(2), 185-212.

Jo, Y. H.; Lee, S. M., and Lee, C. H. Material characteristics and building technique for the rammed earth wall of the 13th Korean fortress in Ganghwa. Environmental Earth Sciences. 2018, 77(17), 1-15.

Keable, J. 1996. Rammed earth structure - A code of pratice. Intermediate Technology Publications. London.

Martín-del-Rio, J.J.; Flores-Alés, V.; Alejandre-Sánchez, F.J.; Blasco-López, F.J. New method for historic rammed-earth wall characterization: The Almohade ramparts of Malaga and Seville. Stud Conserv, 2019, 64(6), 363-372.

Silva, R.A.; Mendes, N.; Oliveira, D.V.; Romanazzi, A.; Domínguez-Martínez, O.; Miranda, T. Evaluating the seismic behaviour of rammed earth buildings from Portugal: From simple tools to advanced approaches. Eng. Struct. 2018, 157, 144-156.

Silva, R.A.; Domínguez-Martínez, O.; Oliveira, D.V.; Pereira, E.B. Comparison of the performance of hydraulic lime-and clay-based grouts in the repair of rammed earth. Constr Build Mater. 2018, 193, 384-394.

Wangmo, P.; Shrestha, K. C.; Miyamoto, M.; Aoki, T. Assessment of out-of-plane behavior of rammed earth walls by pull-down tests. Int. J. Archit. Heritage. 2019, 13(2), 273-287.

CHAPTER 8

Conclusion

The conservation of rammed earth heritage needs understanding of the state of material to adequately evaluate state of conservation of buildings. This dissertation provides an experimental, theoretical and analytical contribution to the understanding of rammed earth material, with the main objective being to evaluate and develop the application of destructive and non-destructive methodologies in investigating the rammed earth physical and mechanical-related properties. It consists of main parts: (i) An account of rammed earth heritage around the world and decay of rammed earth constructions; (ii) An SVM-based scheme for automatic identification of architectural line features and cracks; (iii) Assessing size effect on strength characteristics of compacted earth for the analysis of earthen buildings; (iv) Reconstruction of rammed earth material in laboratory and physico-mechanical characterization of material; (v) Interrelating non-destructive ultrasonic pulse velocity (UPV) and destructive uniaxial compression measurements for rammed earth specimens; (vi) Discussion of failure pattern development and underlying mechanisms; (vii) Identification of material parameters for rammed earth specimens.

The following conclusions can be highlighted from this work:

(i) A review of literature highlights experimental researches in which attempts have been made to investigate geotechnical properties of rammed earth materials, which are important in characterizing soil material properties, and thus the behaviour of rammed earth, including grain-size distribution, optimum water content and maximum dry density via the Proctor test, Atterberg limits and clay mineralogical composition determined by XRD. It can be indicated that, despite these important contributions, data provided by these studies does not include all of the controlling factors having influential role in characterization of rammed earth materials and thus, highlighting the difficulty in application of this data for characterization of a very wide range of rammed earth material that may be found in rammed earth heritage.
(ii) With special attention to morphological characteristics of cracks and architectural line features in surface images of earthen heritage, the current study proposes a scale-invariant SVM-based framework whose main algorithm associates with each object morphological characteristics of bidirectional bounding ellipses, namely axis length ratio, orientation ratio and length ratio, and uses a SVM classifier to create crack and architectural line feature maps. Rather than relying on the application of eight connectivity rule to combination of horizontal and vertical gradient to extract edges, features are computed on each direction, separately.
It turns out that equivalent ellipse, representing a connected component, is sufficiently good approximation for our purpose. Inclusion of three directed morphological characteristics, axis length ratio, orientation ratio and length ratio, contributes positively to the performance of crack detection algorithm for rammed earth images. The algorithm performs well on complex images, which contains the combination of different cracks and architectural line features. This approach is quite accurate at classification of horizontal texture lines, the characteristics of most rammed earth walls. Another advantage of this approach is its ability in

distinguishing severe vertical cracks, one of the most common cracks in rammed earth heritage, and vertical architectural lines. The results indicate a high degree of accuracy in producing crack and architectural feature maps.
The accuracy with very thin cracks is slightly lower than with the wider ones, but their misclassifications as architectural line features are still acceptable, since these cracks usually represent texture cracks rather than structural ones. The results of this study also indicate that the algorithm adds some true negatives in rammed earth structures with very specific texture characteristics.
(iii) This research reviews the existing experimental investigations on the influence of specimen geometry on strength characteristics of earth material. It is clarified that each group of experimental data shows the statistically significant trend associated with relationship between the uniaxial compressive strength (UCS) and the height to width ratio (H/W) of specimens. Next, using a database containing 39 series of test results gathered from the literature, which includes 20 and 19 series of cylindrical and prismatic specimens with a broad range of H/W, an analytical UCS-H/W model is introduced for compacted earth material. The present research is the very first analytical approach to size effect in characterization of mechanical strength in rammed earth materials and therefore it is, to a certain extent, bound to further investigation. In view of the very limited published experimental data available on this subject, there is a clear need for further laboratory work on the estimation of size effect in uniaxial compressive strength of rammed earth. However, in light of future research, it may be possible to examine the efficiency of the proposed formula for prediction of size effect at different water contents.
(iv) The results of this study reveals that soil structure appears to influence the mechanical behaviour of specimens. Stress-strain behaviour and uniaxial compression properties indicated a dependence on the structure of the soil and compaction characteristics. The sand content and compaction properties, such as moulding water content, has shown a significant influence on compressive strength. Increasing compactive effort on dry side of optimum has resulted in an increase in compressive strength. It should be mentioned that higher level of compaction on wet side of optimum may contribute to a lower strength value accompanied by a small decrease in strain at failure.
(v) With main objective of investigating the feasibility of using non-destructive ultrasonic pulse velocity properties to characterize rammed earth material, an investigation was performed on determination of P-wave and S-wave velocities in relation with physico-mechanical characteristics of rammed earth specimens, including compactive effort, grain-size distribution, water content, density, void ratio and saturation degree, and resulting modulus of elasticity. A strong relation between principal material parameters and ultrasonic velocities has been observed in the current study, highlighting that soil structure involves important parameters controlling the UPV of rammed earth. This research presents very first analytical formulas in interrelating non-destructive ultrasonic pulse velocities and destructive uniaxial compression characteristics for rammed earth specimens and therefore it is, to a certain extent, bound to further analytical and laboratory investigations.
(vi) In this research, which focused on the effects of soil structure on mechanical behaviour of a compacted soil incorporating cracking process, a series of uniaxial compression tests were conducted on different soil fabric, different mixture of compacted soil at different water contents and at different compactive effort. The progressive cracks induced by compression were monitored and analysed by image processing technique. Based on the obtained data, the coupling effects of physical and mechanical properties of soil on observed cracking and failure behaviour are herein analysed and discussed. Particularly, the relationship between stress-strain state of material and development of crack pattern of the soil is qualitatively characterized. The observed failure patterns indicate that rammed earth specimens can fail along inclined shear crack driven by the development of shear zones or through tensile

splitting mechanism, or through the combination of both mechanisms. The prevailing mechanism clearly depends on soil structure, which is indicative of a number of physico-mechanical structural parameters.

(vii) It can be noticed that diversity of composition of rammed earth materials leads to complexity of structure of rammed earth materials, emphasizing a complex stress-strain behaviour too, imposing difficulty in the selection of appropriate Young's modulus of rammed earth specimens. Knowing this, equalization is indispensable for having a unique system of procedures, a well-defined and specific framework applicable for any rammed earth medium to describe and simulate the evolution of stress-strain behaviour associated with the specific material. This is the reason why it is necessary to equalize the stress-strain curve of rammed earth media to that of an equivalent media. In this respect, two main input parameters of the equivalent media, equivalent modulus of elasticity and equivalent cohesion, control the stress-strain behaviour of medium.

Thus, in the current study, a rammed earth media with stress-strain behaviour, is equalized with an equivalent continuum medium displaying an equivalent stress-strain curve. Therefore, the inverse analysis mixed with equalization introduces powerful adaptability that can provide a possibility to make use of monitored information to define the constitutive behaviour of a very wide range of rammed earth media. It can be observed that there shall be relationship between the values of parameters obtained by the uniaxial compression test and by the analytical approach adopted herein. However, because of currently insufficient amount of the laboratory data with lack of measurement of important characteristics of material, further well-defined laboratory study needs to be conducted to clarify this phenomenon and to help develop a more comprehensive approach to characterize this important parameter for practical application.

It needs to note that the analytical framework presented in this dissertation is the very first approach to characterization of rammed earth materials and therefore, in view of the very limited experimental data, further laboratory and analytical investigation is necessary to examine the validity of the proposed formulas for other soils with very different material properties.

Appendix 1

Characteristics of manufactured specimens

Table 1.1 Characteristics of specimens														
	Specimen	Date	W Added %	WC %	MD (gr/cm 3)	DD(real (gr/cm3)	DD added (gr/cm3)	Weight (gr)	D (cm)	H (cm)	A (cm2)	V (cm3)	Wopt %	Wadded %
Compaction energy	Cl*	28/10/2020	0	6.30	-	-		-	-	-	-	-	-	-
	S01Sa0Si0W20E1**	28/10/2020	20	26.48	1.939	1.533	1.616	399.9	-	-	-	206.23	24.43	16-18
	S02Sa0Si0W18E1	28/10/2020	18	24.57	-	-	-	364.1	-	-	-	206.23		
	S03Sa0Si0W16E1	28/10/2020	16	22.36	1.875	1.532	1.616	386.7	-	-	-	206.23		
	S04Sa0Si0W14E1	28/10/2020	14	20.58	1.761	1.461	1.545	363.2	-	-		206.23		
	Cl		0	4.95	-	-		-	-	-	-	-	-	-
	S01Sa0Si0W20E2	03/11/2020	20	24.81	2.001	1.603	1.668	392.4	5.10	9.60	20.43	196.11	22.64	16-18
	S02Sa0Si0W18E2	03/11/2020	18	23.4	1.924	1.559	1.631	369.4	5.10	9.40	20.43	192.03		
	S03Sa0Si0W16E2	03/11/2020	16	22.02	1.987	1.628	1.713	418.0	5.10	10.30	20.43	210.41		
	S04Sa0Si0W14E2	03/11/2020	14	20.01	1.909	1.591	1.675	397.7	5.10	10.20	20.43	208.37		
	Cl	04/11/2020	0	7.74	-	-		-	-	-	-	-	-	-
	S01Sa0Si0W20E3	04/11/2020	20	26.37	1.931	1.528	1.609	408.5	5.14	10.21	20.72	211.55	21.13	14-16
	S02Sa0Si0W18E3	04/11/2020	18	24.21	1.973	1.588	1.672	419.6	5.13	10.30	20.66	212.71		
	S03Sa0Si0W16E3	04/11/2020	16	22.28	2.021	1.653	1.743	421.6	5.09	10.24	20.38	208.57		
	S04Sa0Si0W14E3	04/11/2020	14	20.25	1.984	1.650	1.740	414.3	5.10	10.22	20.43	208.85		
	S05Sa0Si0W12E3	04/11/2020	12	18.01	1.904	1.613	1.700	398.8	5.11	10.20	20.54	209.49		
Quantity of	Cl		0	6.23	-	-		-	-	-	-	-	-	-

T

Sand	S01Sa5Si0W20E2	09/11/2020	20	25.63	1.950	1.552	1.625	411.50	5.12	10.26	20.58	211.03		
	S02Sa5Si0W18E2	09/11/2020	18	23.76	1.987	1.605	1.684	417.50	5.11	10.27	20.47	210.16		
	S03Sa5Si0W16E2	09/11/2020	16	21.93	2.014	1.652	1.736	419.80	5.10	10.22	20.40	208.47	21	14-16
	S04Sa5Si0W14E2	09/11/2020	14	20.27	1.984	1.650	1.741	412.90	5.08	10.27	20.27	208.08		
	S05Sa5Si0W12E2	09/11/2020	12	17.86	1.893	1.606	1.690	399.30	5.09	10.38	20.33	210.90		
	S01Sa15Si0W16E2	11/11/2020	16	23.38	2.039	1.653	1.758	431.00	5.11	10.33	20.47	211.34		
	S02Sa15Si0W14E2	11/11/2020	14	19.28	2.056	1.723	1.803	431.00	5.08	10.36	20.25	209.67	20.7	14-16
	S03Sa15Si0W12E2	11/11/2020	12	18.52	1.997	1.685	1.783	422.00	5.10	10.34	20.45	211.33		
	CL													
	S04Sa15Si0W10E2	04/12/2020	10	15.22	1.924	1.670	1.750	401	5.10	10.20	20.43			
	S05Sa15Si0W08E2	04/12/2020	8	12.79	1.841	1.632	1.705	383	5.10	10.18	20.43			
	Cl													
	S01Sa40Si0W12E2	18/11/2020	12	16.67	2.145	1.839	1.916	450.00	5.10	10.27	20.43	209.75		
	S02Sa40Si0W10E2	18/11/2020	10	13.79	2.168	1.905	1.971	457.00	5.10	10.32	20.43	210.82	12.45	8-10
	S03Sa40Si0W8E2	18/11/2020	8	10.14	2.083	1.891	1.929	437.00	5.10	10.27	20.43	209.80		
	S04Sa40Si0W6E2	19/11/2020	6	6.82	1.939	1.815	1.829	400	5.1	10.1	20.43	206.32		
Same speciemns	S01Sa0Si0W14E2	13/11/2020	14	22.65	1.959	1.597	1.718	405.00	5.08	10.20	20.27	206.74		
	S02Sa0Si0W14E2	13/11/2020	14	23.26	1.959	1.590	1.719	405.00	5.08	10.20	20.27	206.69	-	-
	S03Sa0Si0W14E2	13/11/2020	14	21.74	1.947	1.599	1.708	405.00	5.10	10.20	20.39	208.01		
	S04Sa0Si0W14E2	13/11/2020	14	23.46	1.962	1.589	1.721	408.00	5.10	10.20	20.39	207.96		
Specimens with Optimum water content	Sa0Si0W17E2	11/12/2020	17	24.39	2.011	1.617	1.719	419	5.10	10.20	20.43	208.37	-	-
	Sa0Si0W17E2	11/12/2020	17	22.95	2.011	1.636	1.719	419	5.10	10.20	20.43	208.37	-	-
	Sa0Si0W17E2	11/12/2020	17	24.19	2.011	1.619	1.719	419	5.10	10.20	20.43	208.37	-	-
	Sa15Si0W14.7E2	14/12/2020	14.7	19.54	2.068	1.730	1.804	431	5.10	10.20	20.43	208.37	-	-
	Sa15Si0W14.7E2	14/12/2020	14.7	19.48	2.068	1.731	1.804	431	5.10	10.20	20.43	208.37	-	-
	Sa15Si0W14.7E2	14/12/2020	14.7	21.15	2.078	1.715	1.812	433	5.10	10.20	20.43	208.37	-	-

	Sa40Si0W9.2E2	15/12/2020	9.2	13.33	2.145	1.893	1.965	447	5.10	10.20	20.43	208.37	-	-
	Sa40Si0W9.2E2	15/12/2020	9.2	12.07	2.145	1.914	1.965	447	5.10	10.20	20.43	208.37	-	-
	Sa40Si0W9.2E2	15/12/2020	9.2	13.21	2.140	1.891	1.960	446	5.10	10.20	20.43	208.37	-	-

* Cl: clay

** S--Sa--Si--W--E- two digits after S: specimen number, two digits after Sa: the percentage of sand, two digits after Si: the percentage of silt, digit after water: percentage of water content, digit after E: according to table 1.

*** WC water content %, DD: dry density, D: diameter, H: height, MD: moist density, A: area of cross section, V: volume

Table 1.2 some specific measurement of weight and geometry of specimens

	WL1S	WL2S	WL3S	h1b*	h1a	h2b	h2a	h3b	h3a	Weight of Specimen
Cl60Sa40W0E0	-	-	-	-	-	-	-	-	-	288
Cl60Sa40W0E2	167	148	62	39	51	2	11	2	18	377
Cl60Sa40W0E3	166	150	67	38	53	2	13	4	19	383
Cl60Sa40W0E4	166	150	68	35	53	2	13	2	21	384
Cl60Sa40W6E2	167	-	-	43	53	2	13	13	23	400
Cl60Sa40W8E2	180	180	77	39	53	1	13	10	22	437
Cl60Sa40W10E2	183	183	91	41	55	3	14	11	24	457
Cl60Sa40W12E2	186	186	78	47	55	8	13	16	22	450

* b: before compaction, a: after compaction, WL1S: weight of the first layer of specimen, WL2S: weight of the second layer of specimen, WL3S: weight of the third layer of specimen

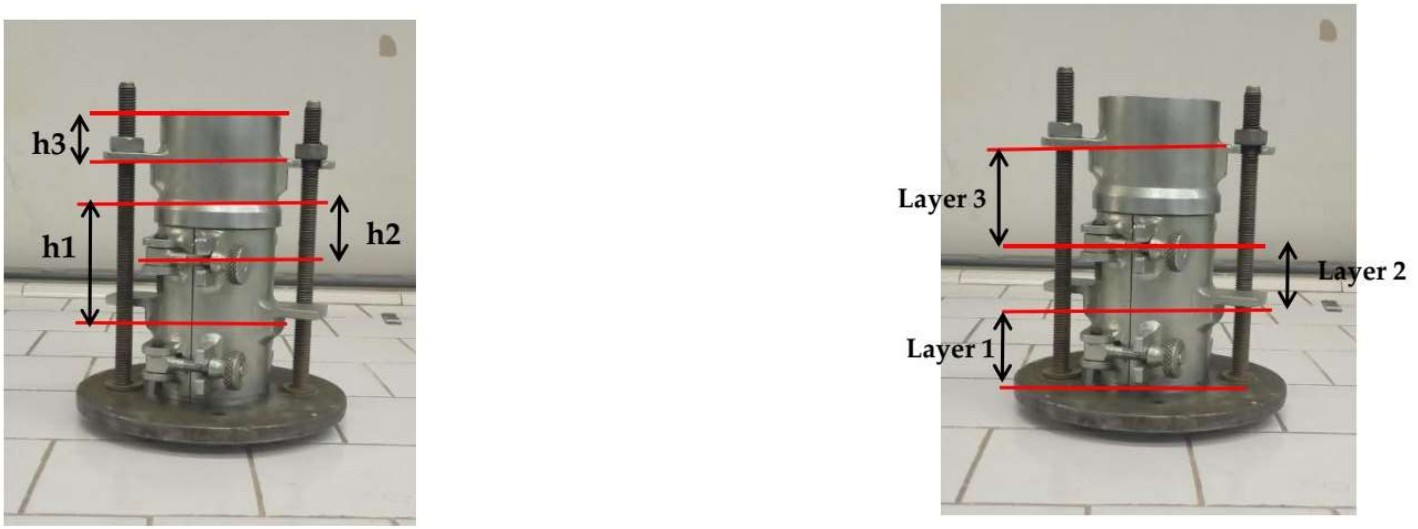

Figure 1.1 h1, h2, h3 for Table 1.2 of Appendix 1

Appendix 2

UPV measurement data

	W(%)	MD (kg/m^3)	US (MPa)	e	Sr	Vp (m/s)	Std (Vp)	Vs (m/s)	Std (Vs)	Vp/Vs	Std (Vp/Vs)	Edyn (MPa)	Etan (MPa)	$Esec_{0.5US}$ (MPa)	$Esec_{US}$ (MPa)
S01Sa0Si0W20E2	24.05	1989	0.48	0.68	0.95	436.31	6.25	276.35	0.83	1.58	0.03	353.87	128.17	14.22	3.85
S02Sa0Si0W18E2	21.93	1901	0.40	0.73	0.81	549.58	3.99	312.04	0.93	1.76	0.02	467.16	184.06	54.06	12.41
S03Sa0Si0W16E2	21.61	1980	1.86	0.66	0.89	663.54	4.53	376.59	1.94	1.76	0.02	708.95			24.16
S04Sa0Si0W14E2	19.20	1896	0.69	0.70	0.74	686.08	13.16	442.53	2.04	1.55	0.05	849.21	199.72	70.49	27.53
S01Sa0Si0W20E3	25.10	1912	0.43	0.77	0.88	349.34	3.00	242.49	0.67	1.44	0.02	232.69	32.80	11.99	3.73
S02Sa0Si0W18E3	23.35	1959	0.53	0.70	0.90	540.62	8.23	313.96	0.77	1.72	0.04	481.03	71.19	19.72	6.57
S03Sa0Si0W16E3	11.52	1844	4.65	0.63	0.49	656.43	6.44	389.40	2.17	1.69	0.03	686.83	300.76	175.98	105.87
S04Sa0Si0W14E3	19.44	1970	1.00	0.64	0.82	766.52	5.10	478.04	1.33	1.60	0.02	1064.18	208.45	115.02	30.67
S05Sa0Si0W12E3	16.83	1885	1.14	0.67	0.67	702.32	6.79	468.04	3.24	1.50	0.03	908.67	155.42	98.12	59.58
S01Sa5Si0W20E2	24.41	1931	0.32	0.74	0.89	343.17	3.53	205.44	1.25	1.67	0.03	198.97	33.22	8.69	3.25
S02Sa5Si0W18E2	22.43	1965	0.52	0.68	0.89	446.92	5.91	278.58	0.80	1.60	0.03	360.62	31.30	16.56	5.75
S03Sa5Si0W16E2	20.83	1995	0.74	0.63	0.89	621.42	8.85	362.54	2.94	1.71	0.04	651.49	93.80	44.84	11.51
S04Sa5Si0W14E2	19.13	1966	0.89	0.63	0.81	784.76	5.27	463.43	4.21	1.69	0.03	1040.38	194.89	84.92	27.86
S05Sa5Si0W12E2	16.77	1876	0.89	0.68	0.67	637.28	5.78	428.16	2.87	1.49	0.03	748.67	238.06	122.76	51.73
S01Sa15Si0W16E2	22.32	2022	0.54	0.63	0.96	548.91	23.82	297.26	2.64	1.85	0.10	461.83	157.41	21.71	6.04
S02Sa15Si0W14E2	18.17	2037		0.56	0.87	652.02	21.19	388.71	2.08	1.68	0.08				
S03Sa15Si0W12E2	17.59	1981	0.74	0.60	0.79	787.38	15.01	428.36	3.88	1.84	0.06	937.80	134.98	72.86	42.23
S04Sa15Si0W10E2	14.64	1915	0.86	0.61	0.64	787.96	13.69	472.45	8.99	1.67	0.07	1042.34	146.86	79.31	51.24
S05Sa15Si0W08E2	12.50	1836	0.86	0.65	0.52	754.88	26.25	479.91	5.30	1.57	0.09	981.98	156.03	79.27	63.78
S01Sa40Si0W12E2	15.89	2131	0.58	0.46	0.93	620.99	7.76	468.39	3.57	1.33	0.04	785.59	88.11	24.37	6.94
S02Sa40Si0W10E2	13.04	2153	0.87	0.41	0.86	1058.80	34.50	677.45	9.73	1.56	0.09	2279.92	110.96	27.21	24.03
S03Sa40Si0W8E2	9.89	2078	0.81	0.42	0.64	1015.90	7.22	628.38	2.87	1.62	0.02	1953.27	117.48	61.67	56.77
S04Sa40Si0W6E2	5.75	1919	0.66	0.48	0.32	926.23	53.92	583.71	7.85	1.59	0.14	1531.00	99.86	32.45	39.73

Appendix 3

Images of rammed earth specimens before and after uniaxial compression loading

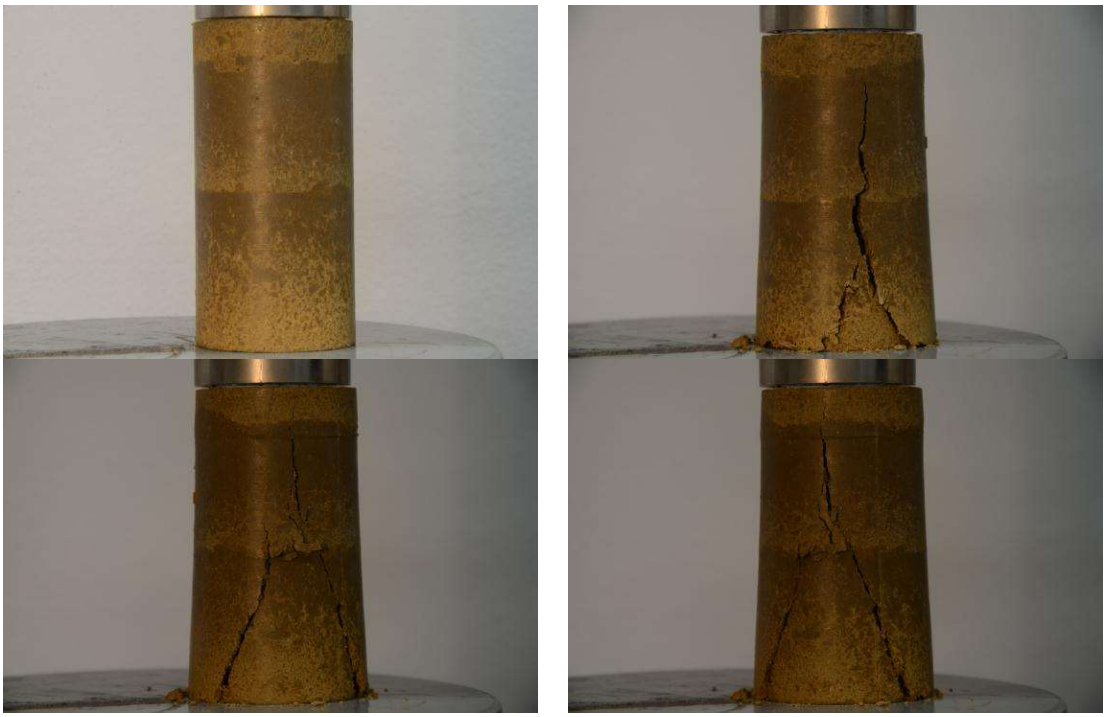

(a)

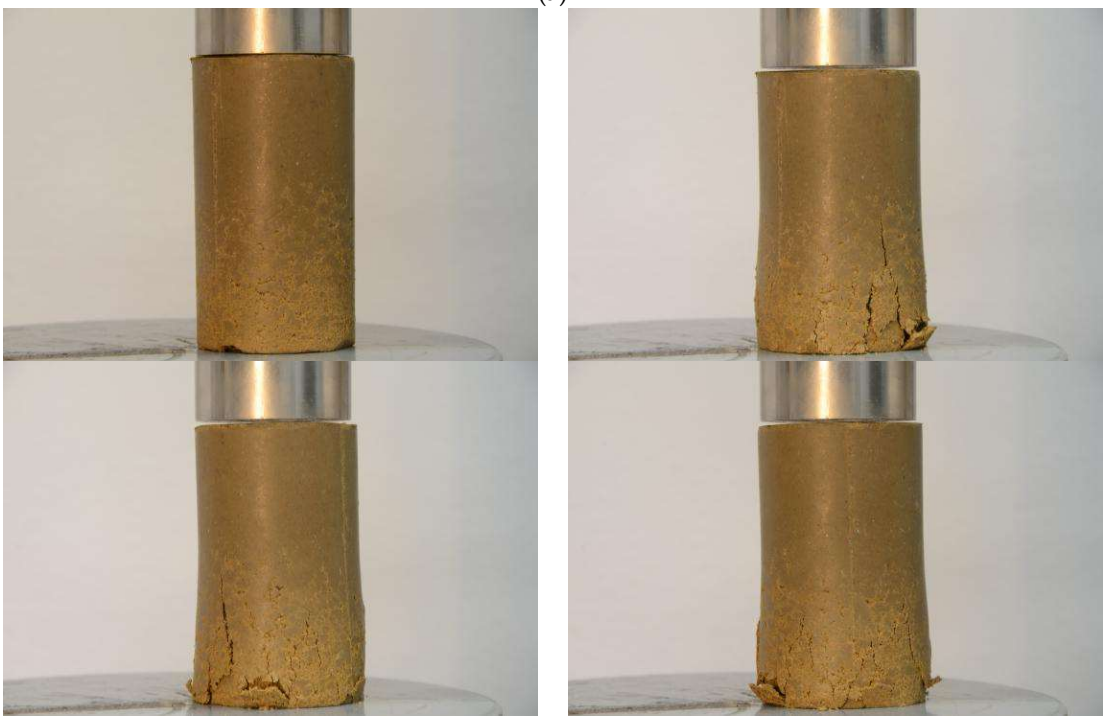

(b)

Figure 3.1. Uniaxial compression tests for specimens clay=100% and compactive effort E2 (a) S04Sa0Si0W14E2, (b) S02Sa0Si0W18E2

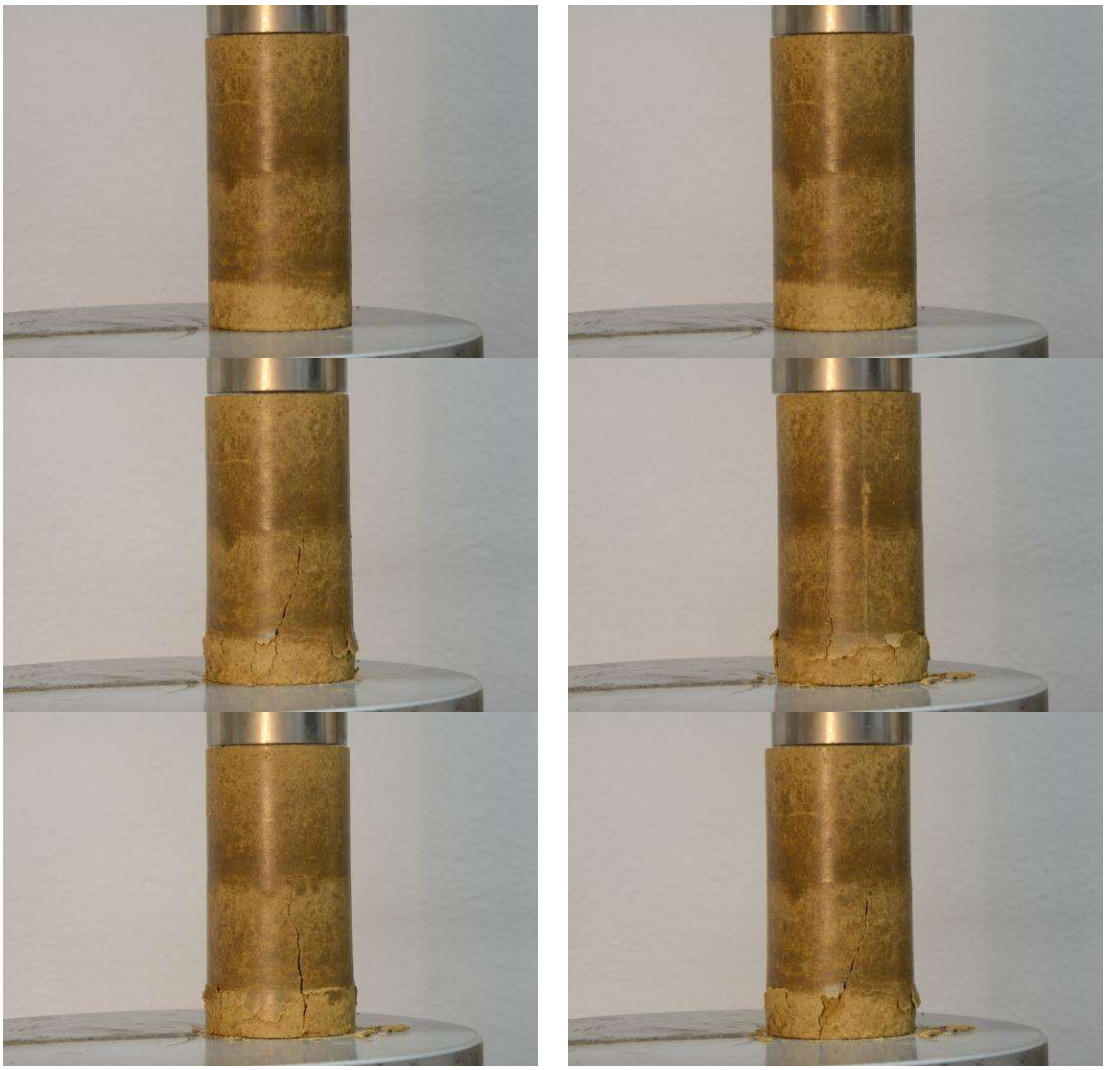

(a)

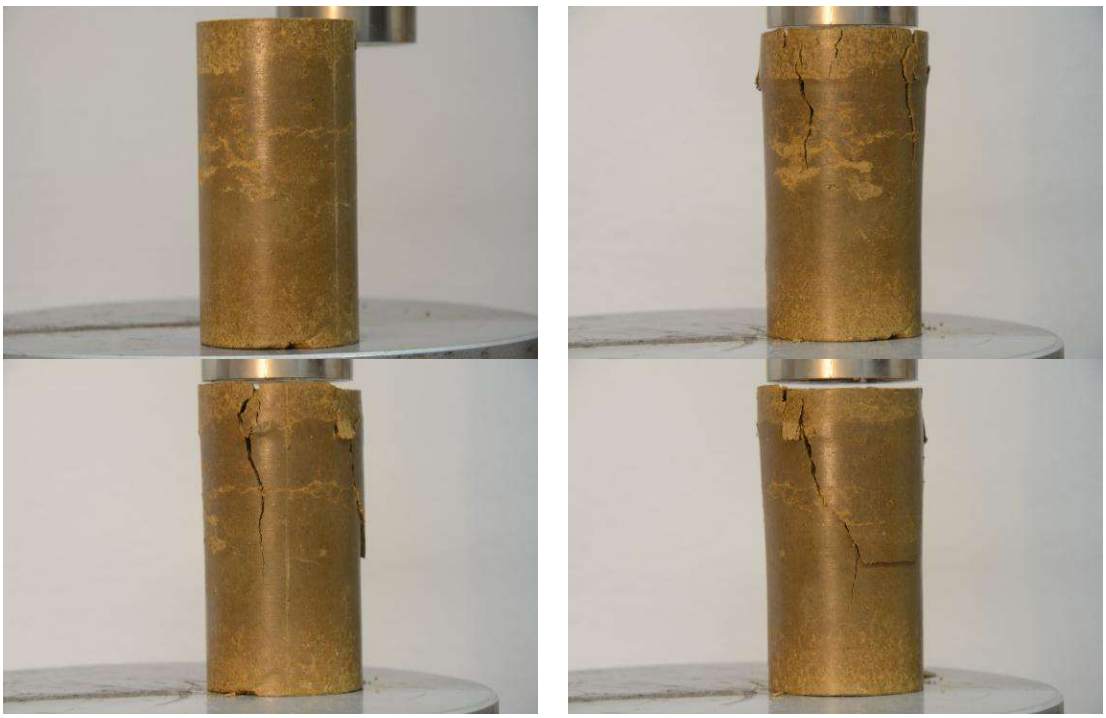

(b)

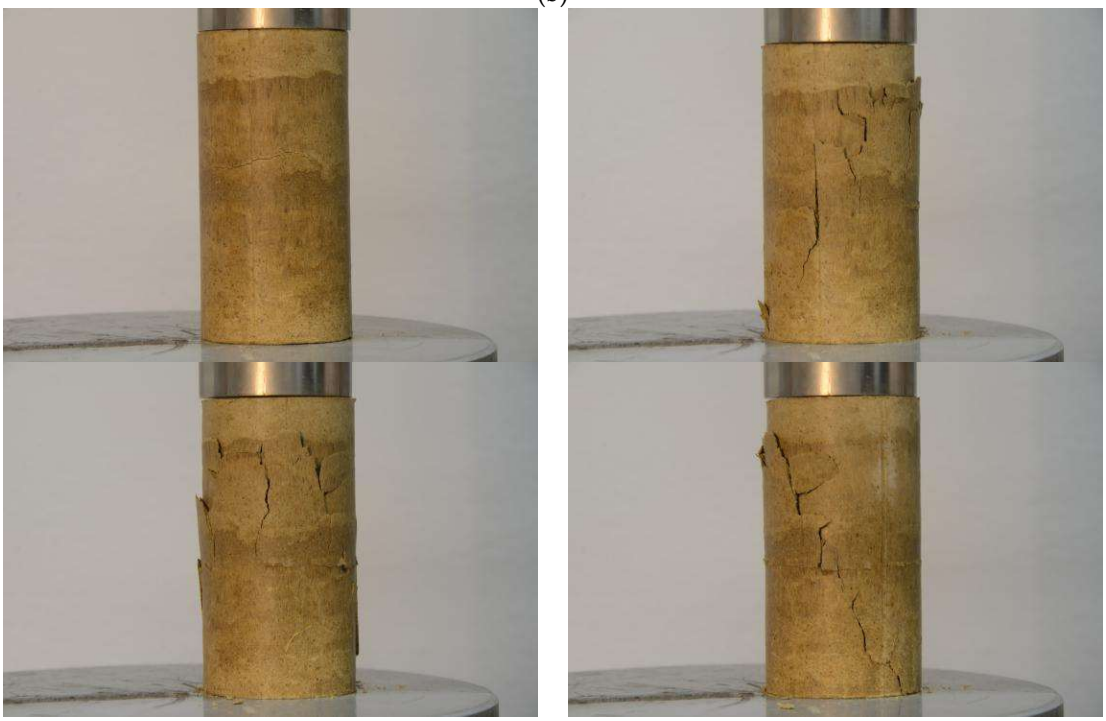

(c)

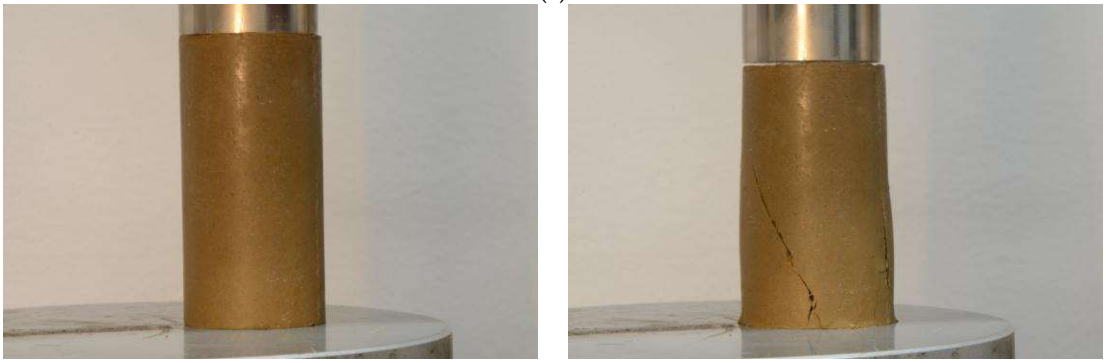

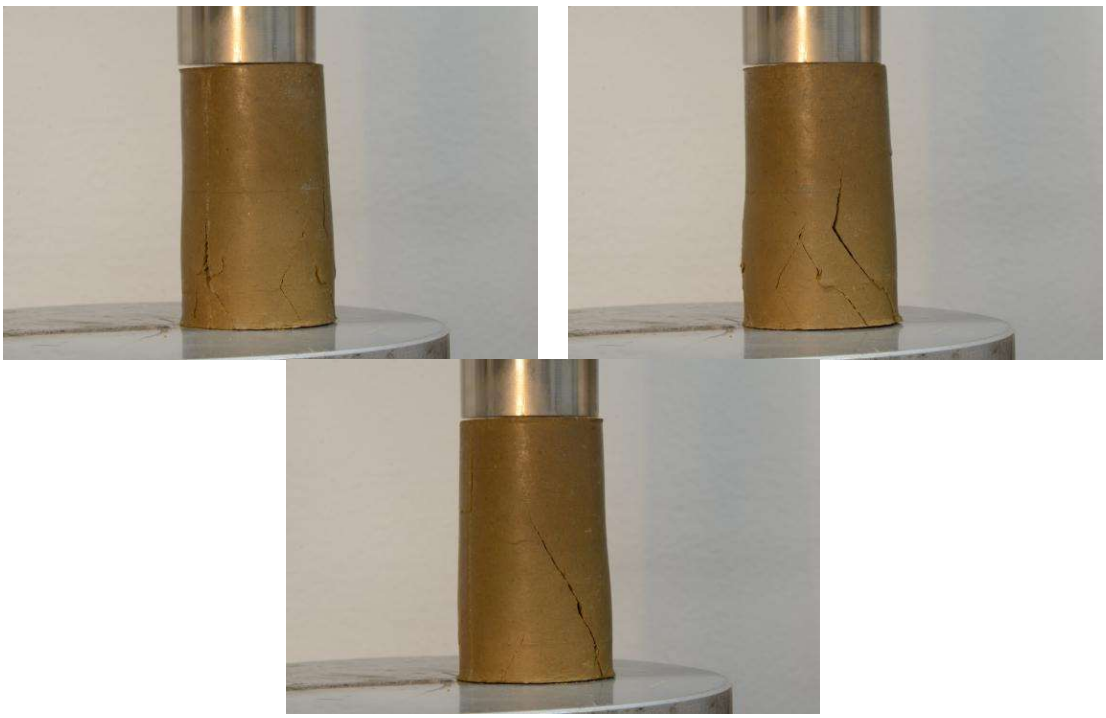

(d)

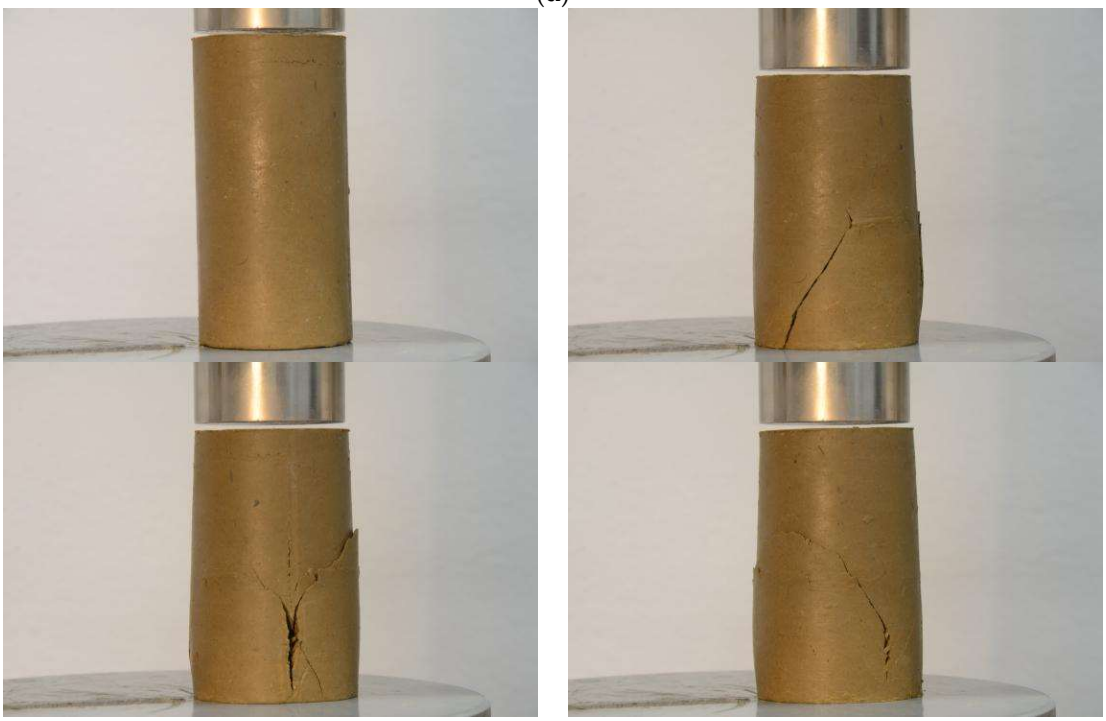

(e)

Figure 3.2. Uniaxial compression tests for different compaction energy (a) S05Sa0Si0W12E3, (b) S04Sa0Si0W14E3, (c) S03Sa0Si0W16E3, (d) S02Sa0Si0W18E3, (e) S01Sa0Si0W20E3

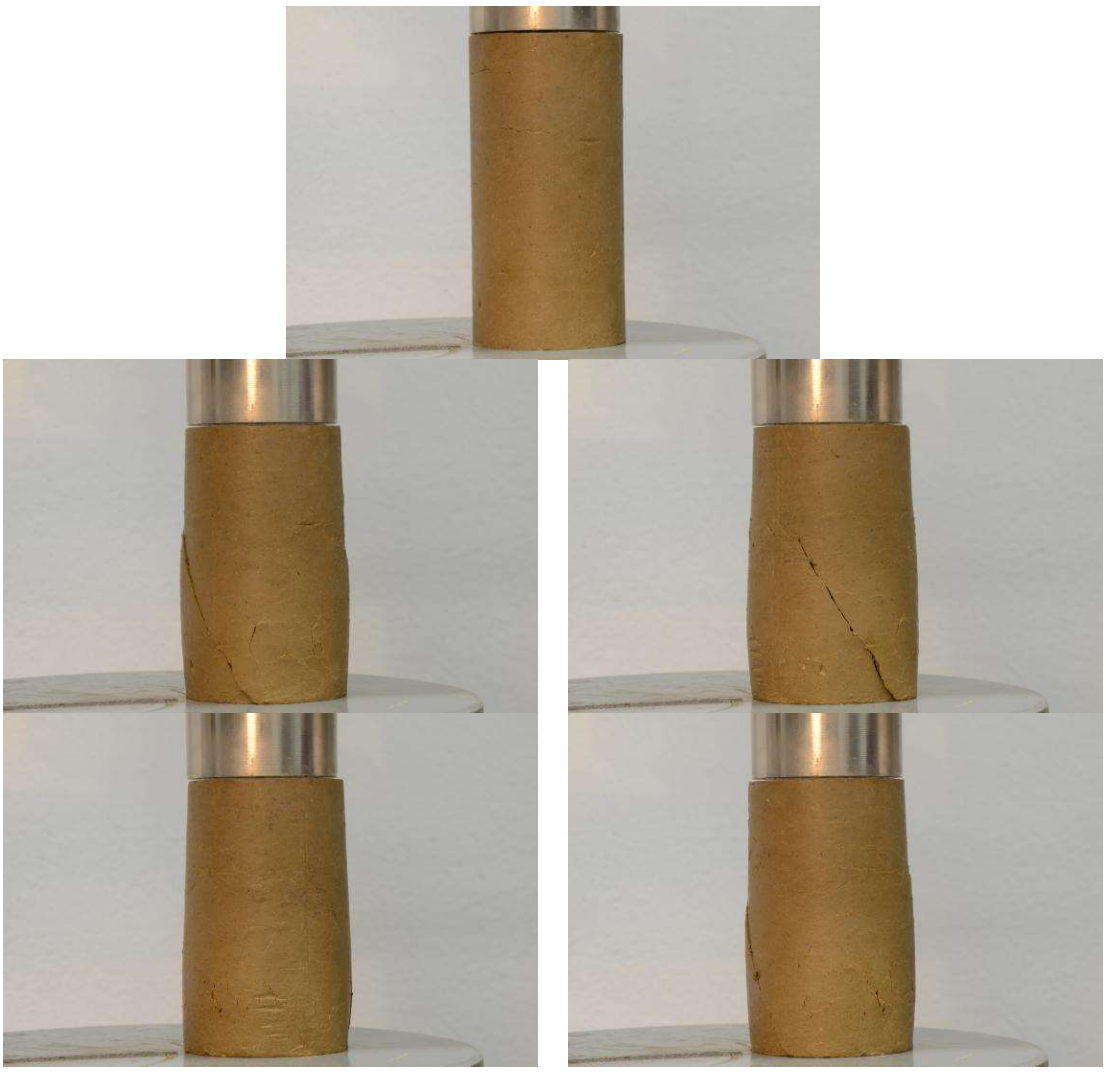

(a)

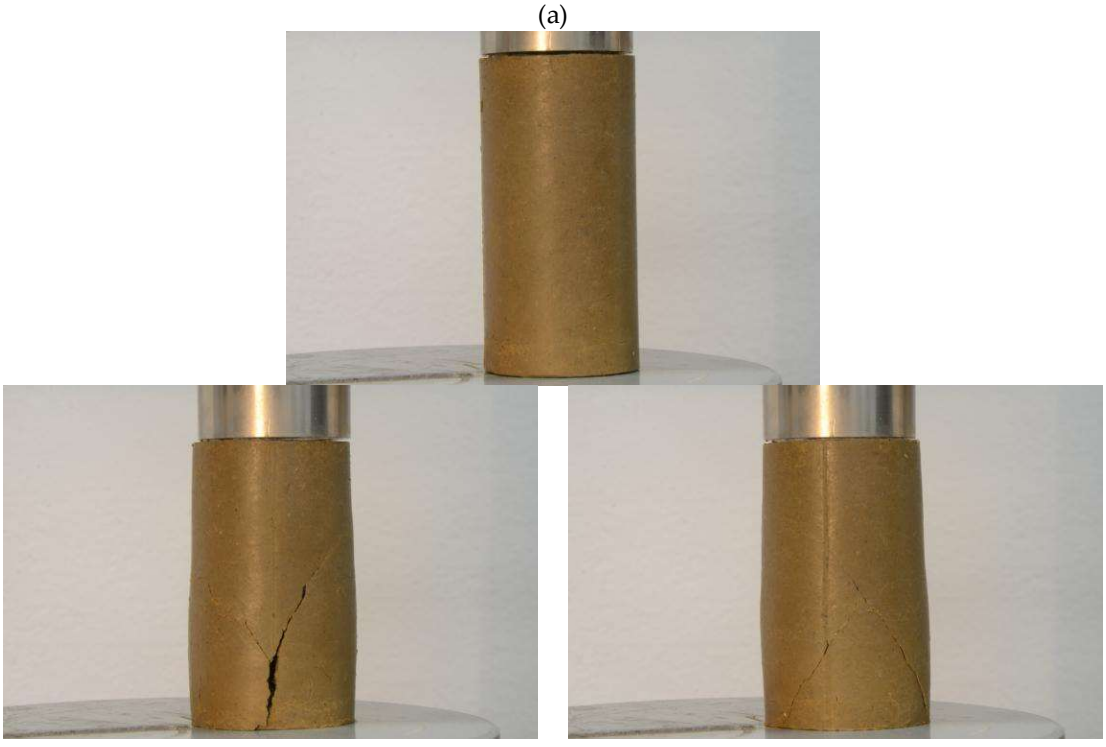

(b)

(c)

(d)

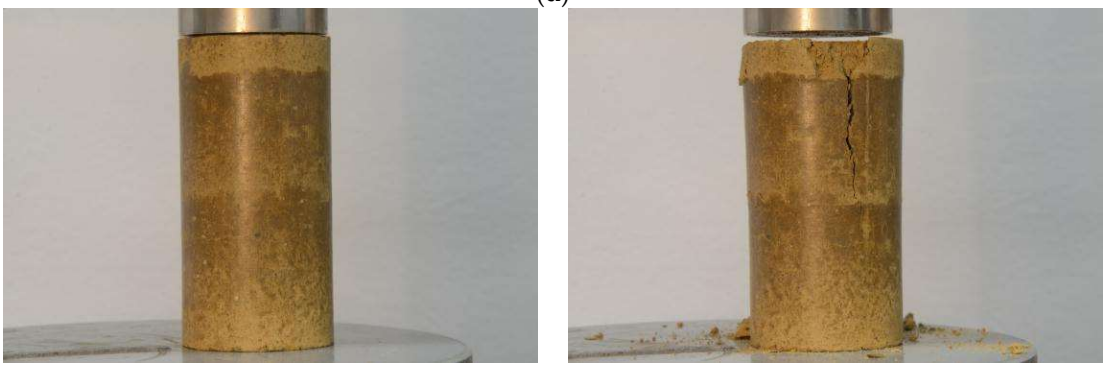

(e)

Figure 3.3. Uniaxial compression tests for specimens containing 5% sands (a) S01Sa5Si0W20E2, (b) S02Sa5Si0W18E2, (c) S03Sa5Si0W16E2, (d) S04Sa5Si0W14E2, (e) S05Sa5Si0W12E2

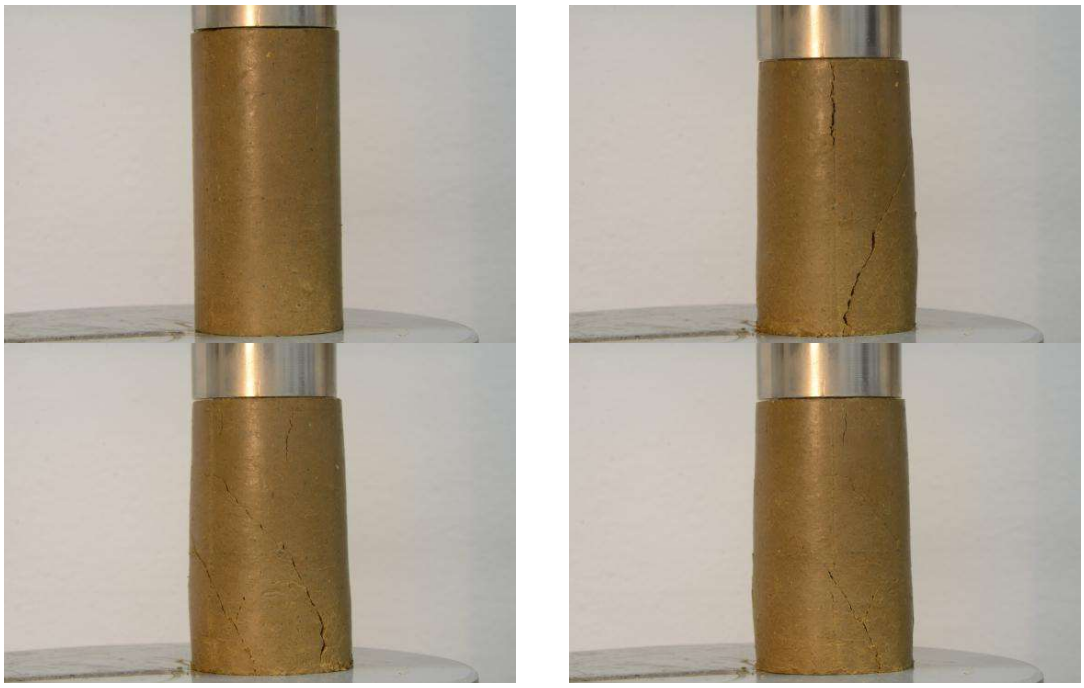

(a)

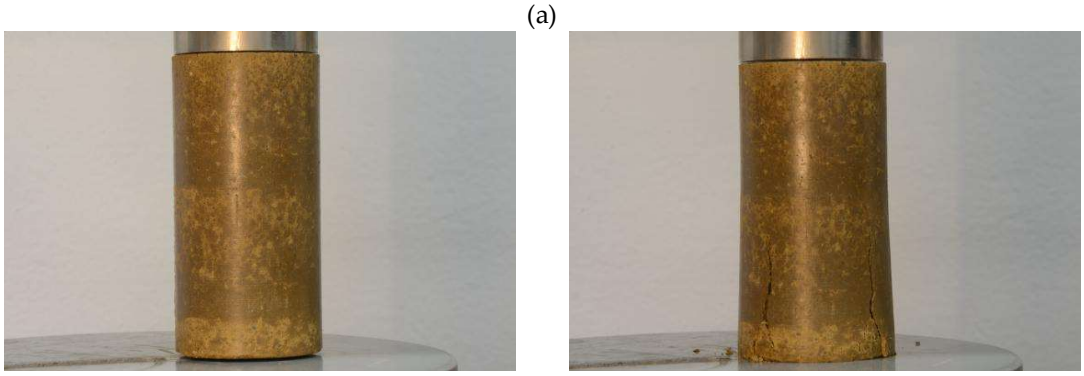

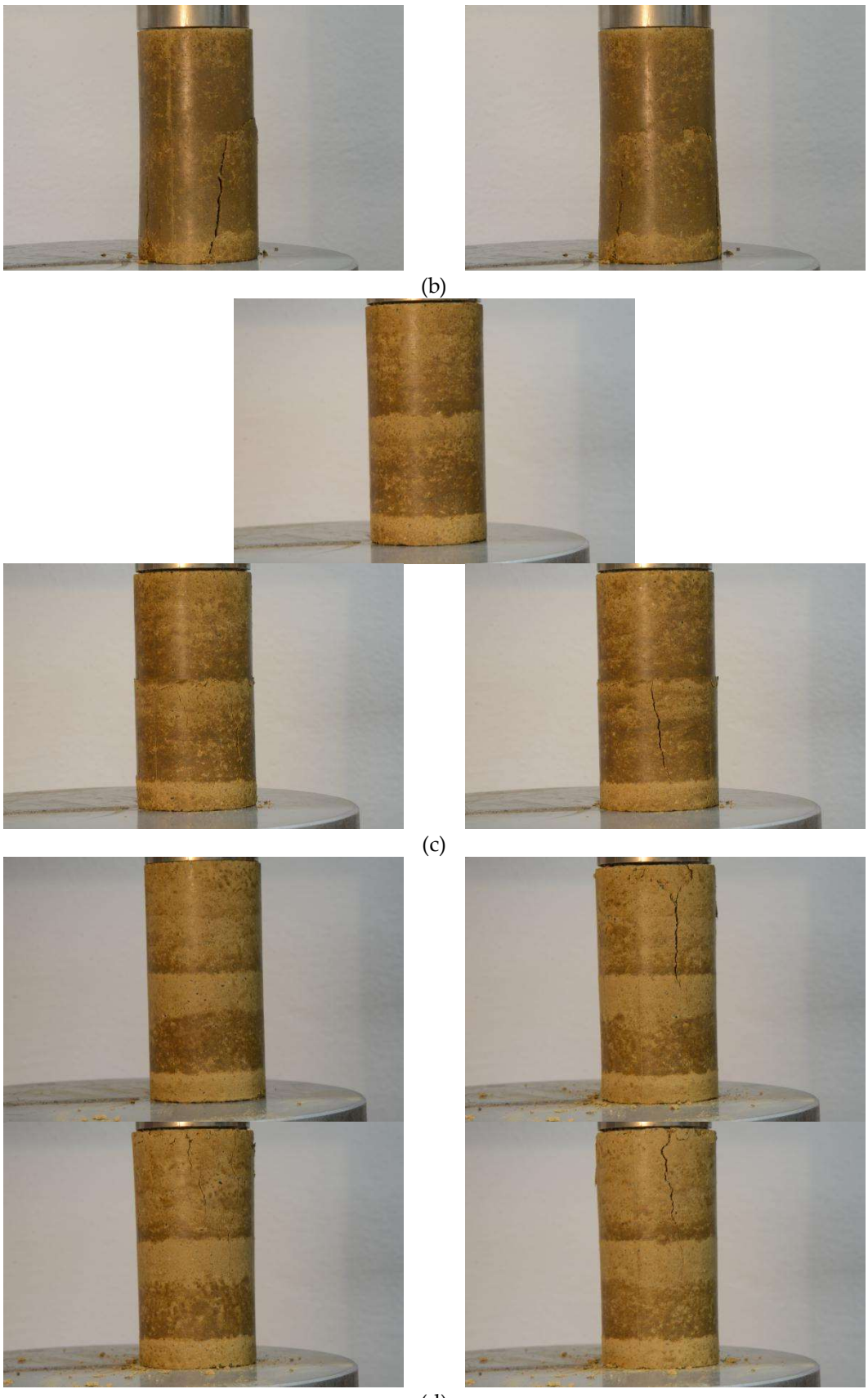

Figure 3.4. Uniaxial compression tests for specimens containing 15% sands (a) S01Sa15Si0W16E2, (b) S03Sa15Si0W12E2, (c) S04Sa15Si0W10E2, (d) S05Sa15Si0W08E2

(a)

(b)

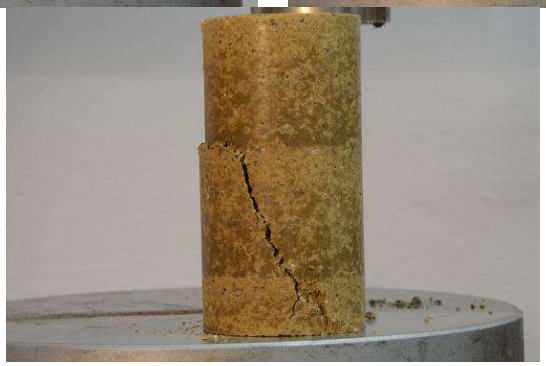

(c)

(d)

Figure 3.5. Uniaxial compression tests for specimens containing 40% sands (a) S01Sa40Si0W12E2, (b) S02Sa40Si0W10E2, (c) S03Sa40Si0W8E2, (d) S04Sa40Si0W6E2

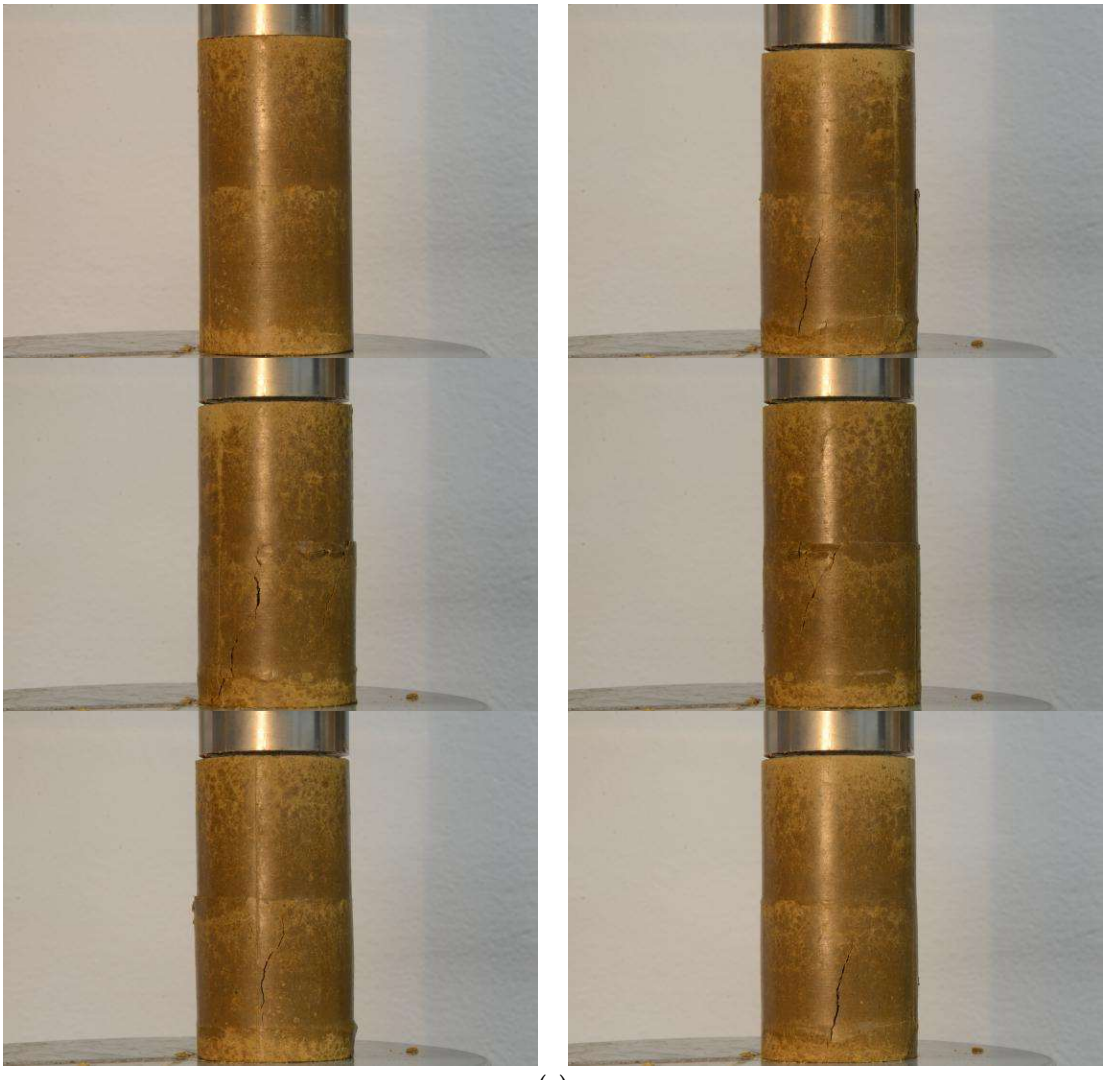

(a)

(b)

(c)

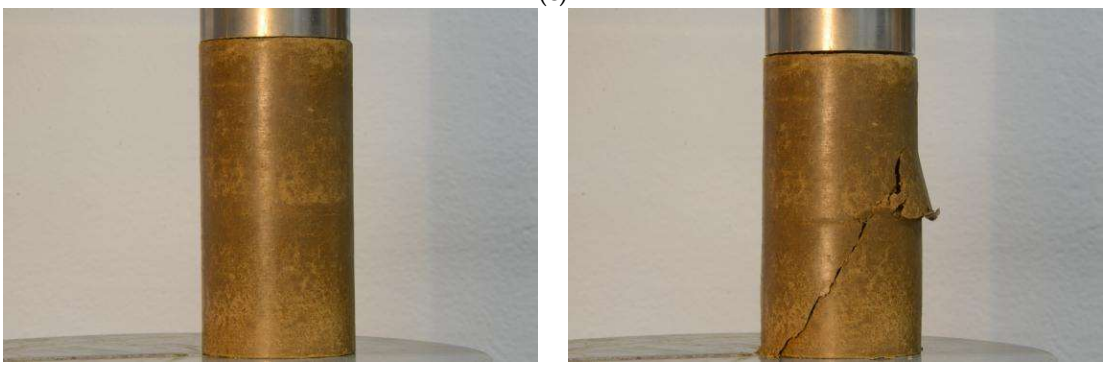

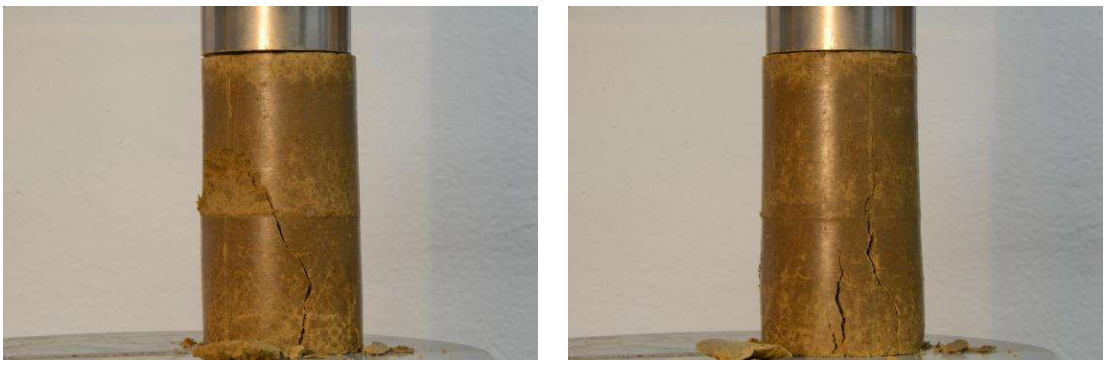

(d)

Figure 3.6. Uniaxial compression tests for specimens for loading rate (a) S01Sa0Si0W14E2-0.125mm/min, (b) S02Sa0Si0W14E2-0.25mm/min, (c) S03Sa0Si0W14E2-0.5mm/min, (d) S04Sa0Si0W14E2-1mm/min

(a)

(b)

(c)

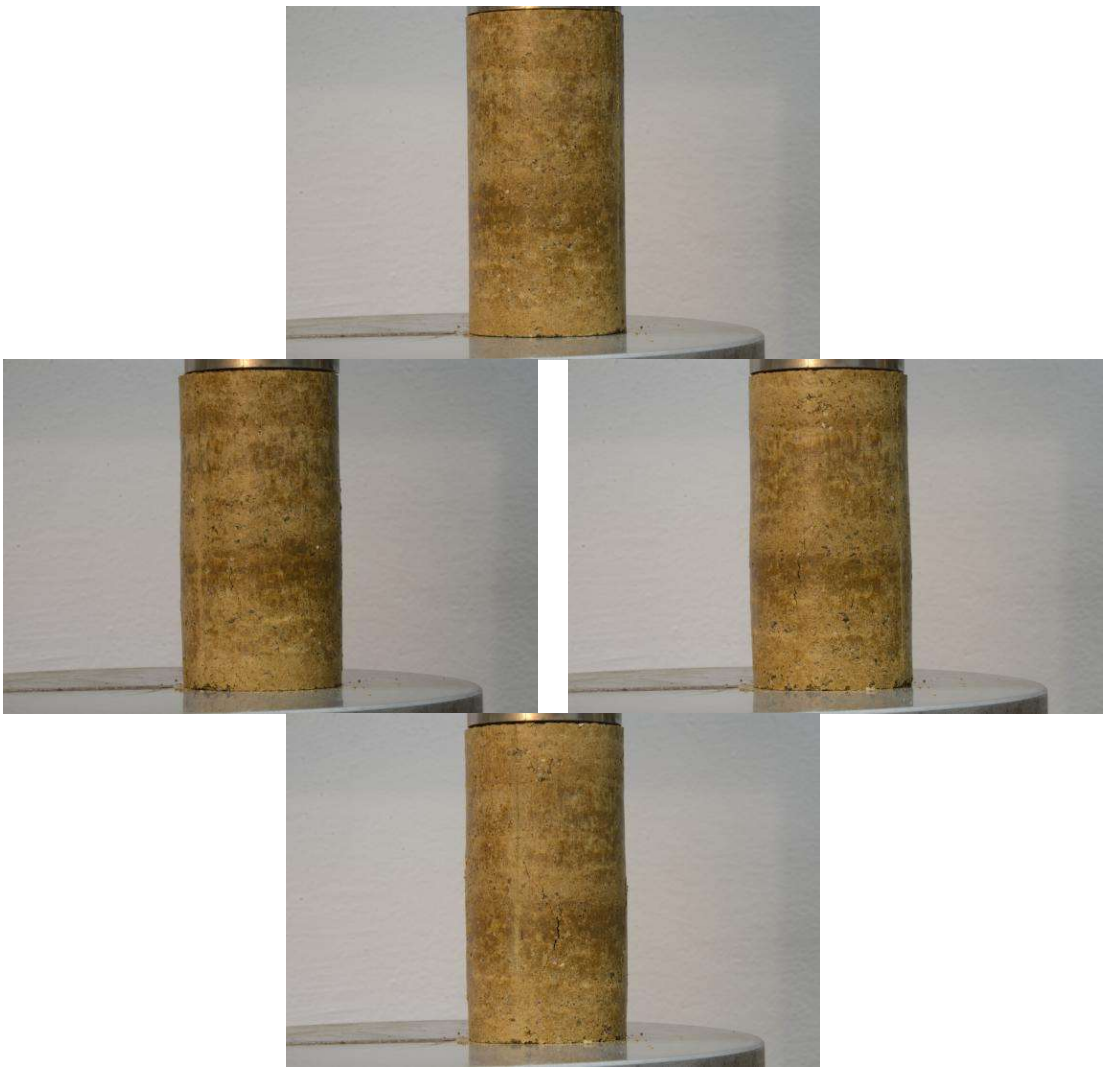

(d)

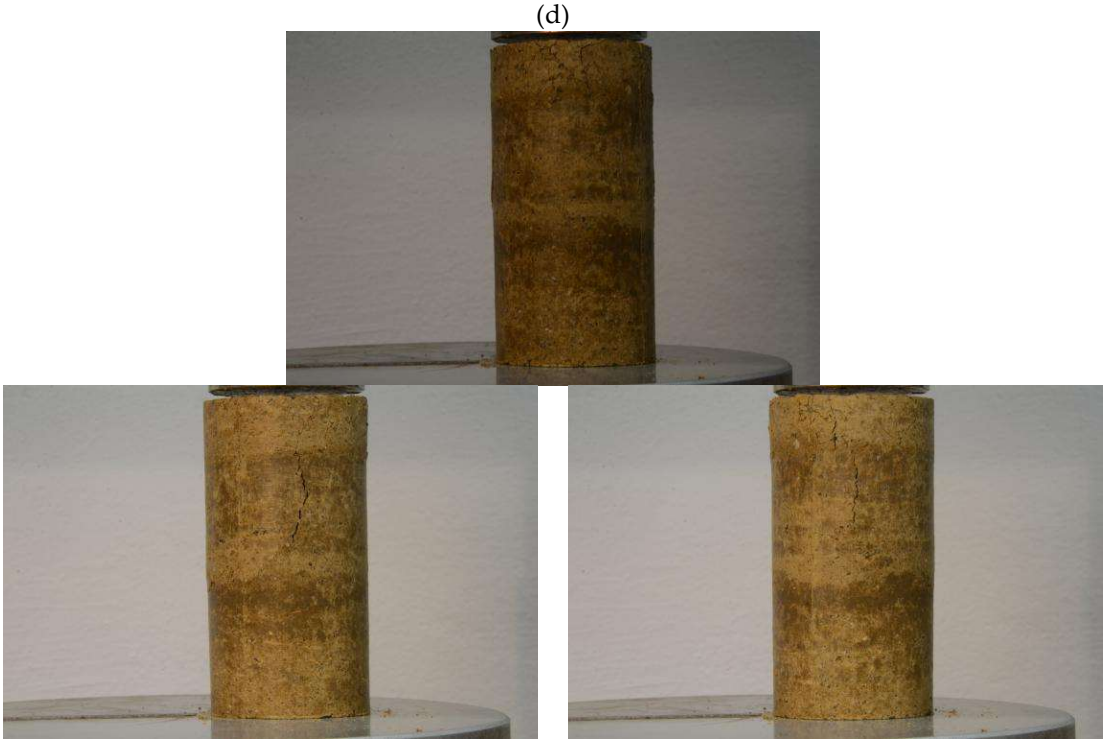

(e)

(f)

(g)

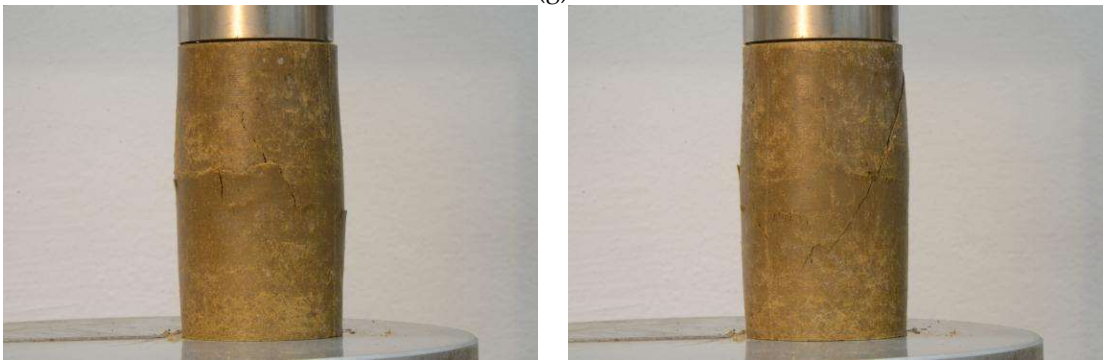

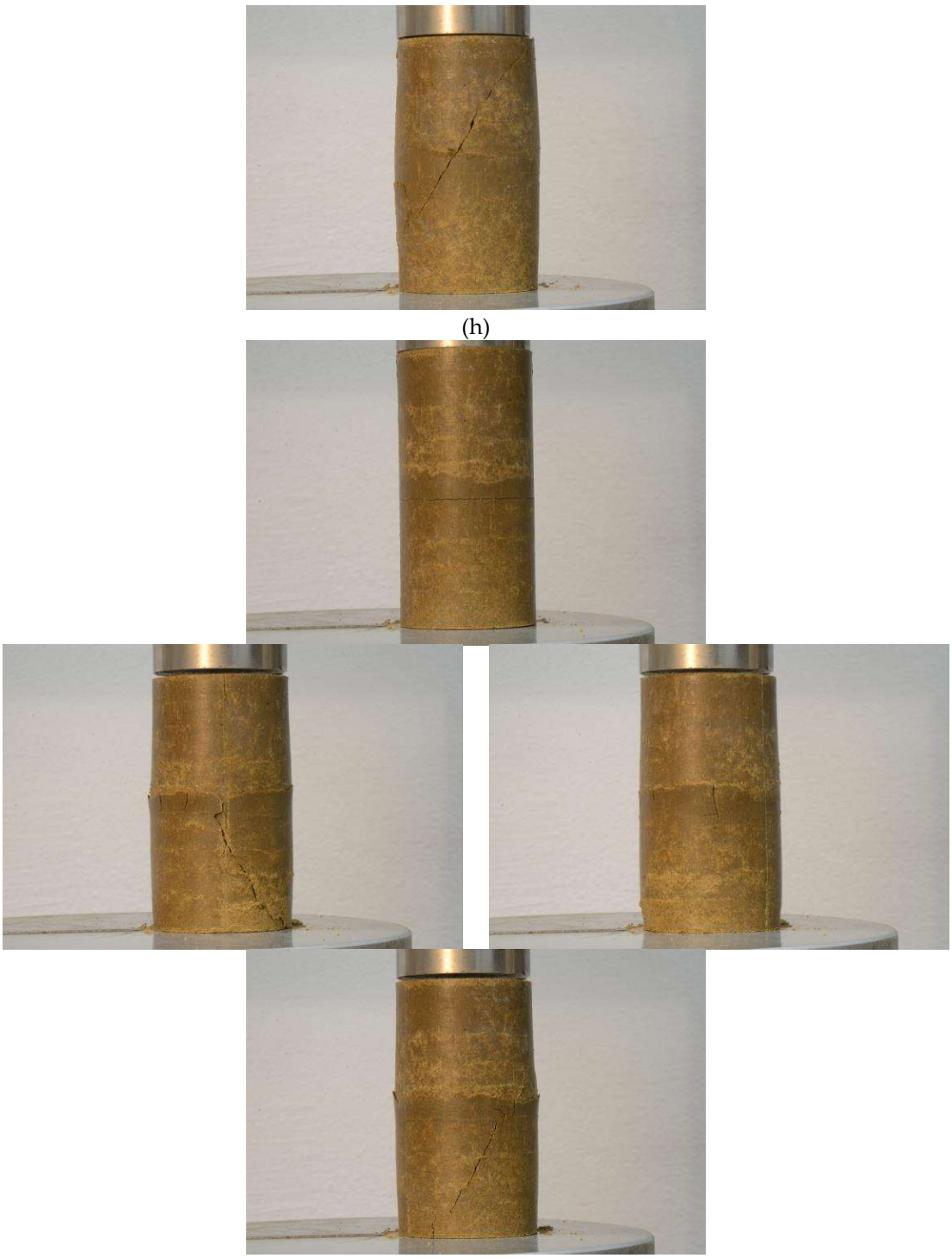

(h)

(i)

Figure 3.7. Uniaxial compression tests for specimens for specimens with optimum water content (a) S01Sa15Si0W14.7E2, (b) S02Sa15Si0W14.7E2, (c) S03Sa15Si0W14.7E2, (d) S01Sa40Si0W9.2E2, (e) S02Sa40Si0W9.2E2, (f) S03Sa40Si0W9.2E2, (g) S01Sa0Si0W17E2, (h) S02Sa0Si0W17E2, (i) S03Sa0Si0W17E2

Appendix 4

The results of DIC analysis: isolated stages of uniaxial stress-strain curves and drived stages of failure pattern in rammed earth specimens

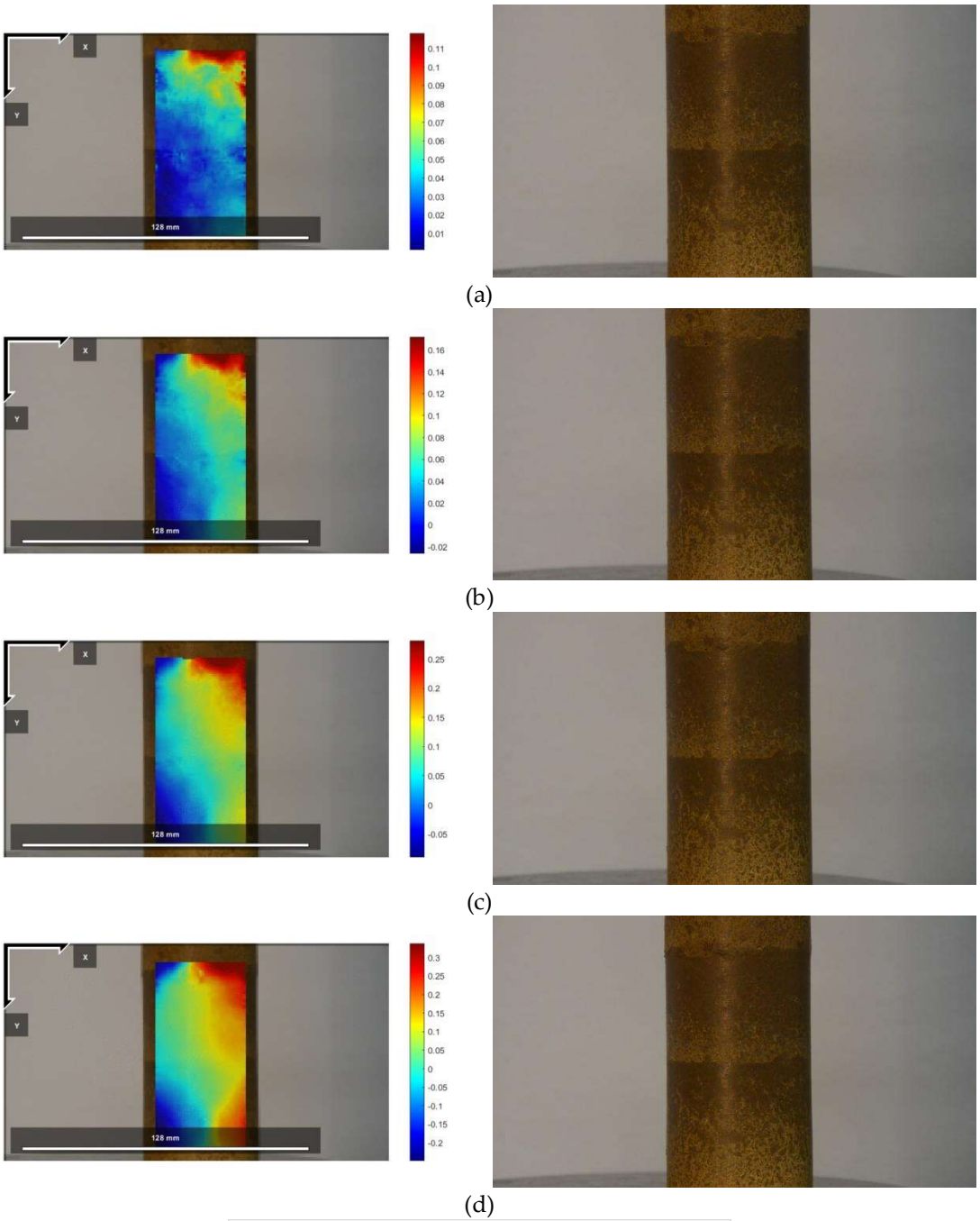

Figure 4.1. DIC Displacement in horizontal direction S04Sa0Si0W14E2, (a) 0.5*Strength, (b) 0.75*Strength, (c) 0.9*Strength, (d) Strength, (e) analysis points

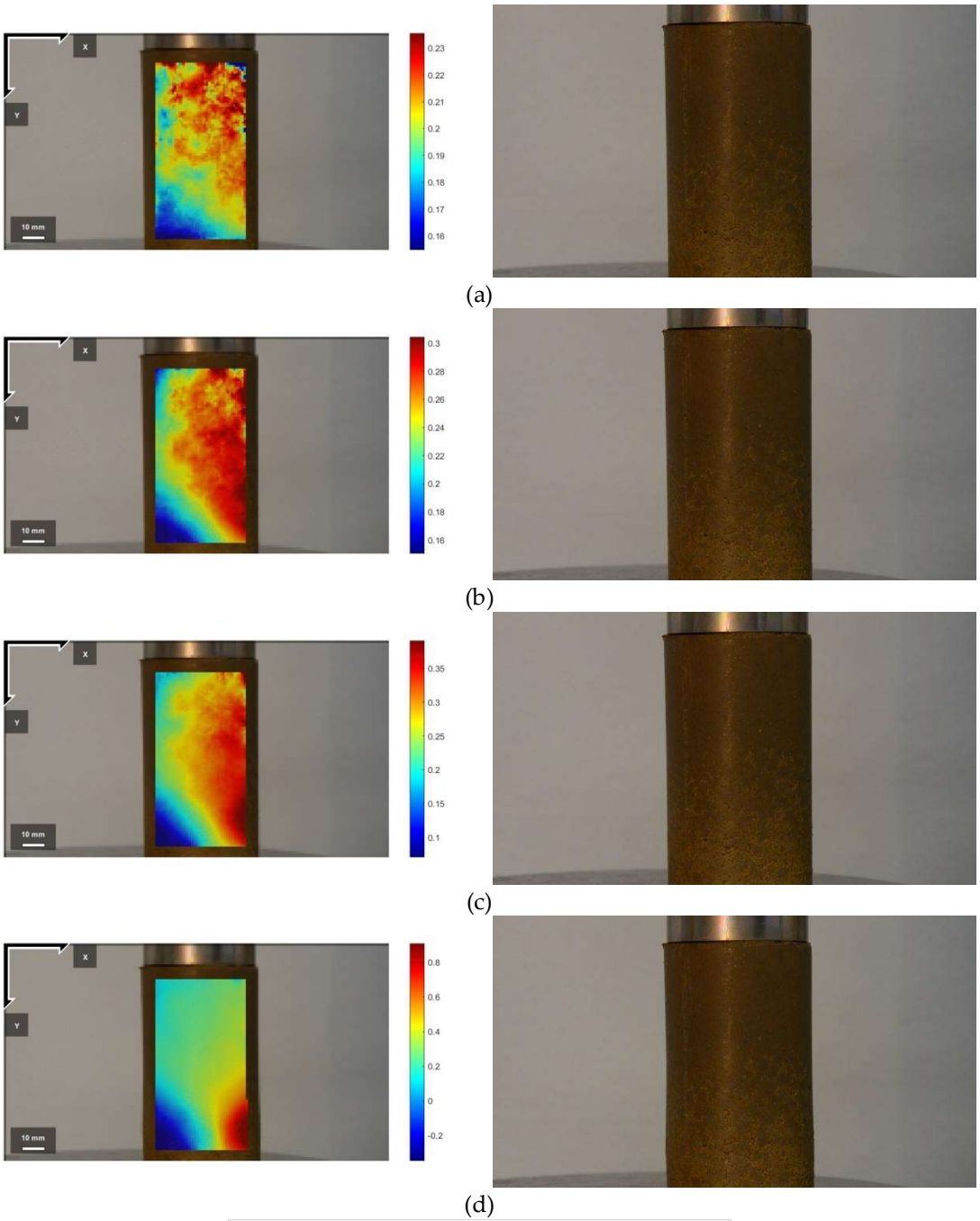

Figure4.2. DIC Displacement in horizontal direction S02Sa0Si0W18E2, (a) 0.5*Strength, (b) 0.75*Strength, (c) 0.9*Strength, (d) Strength, (e) analysis points

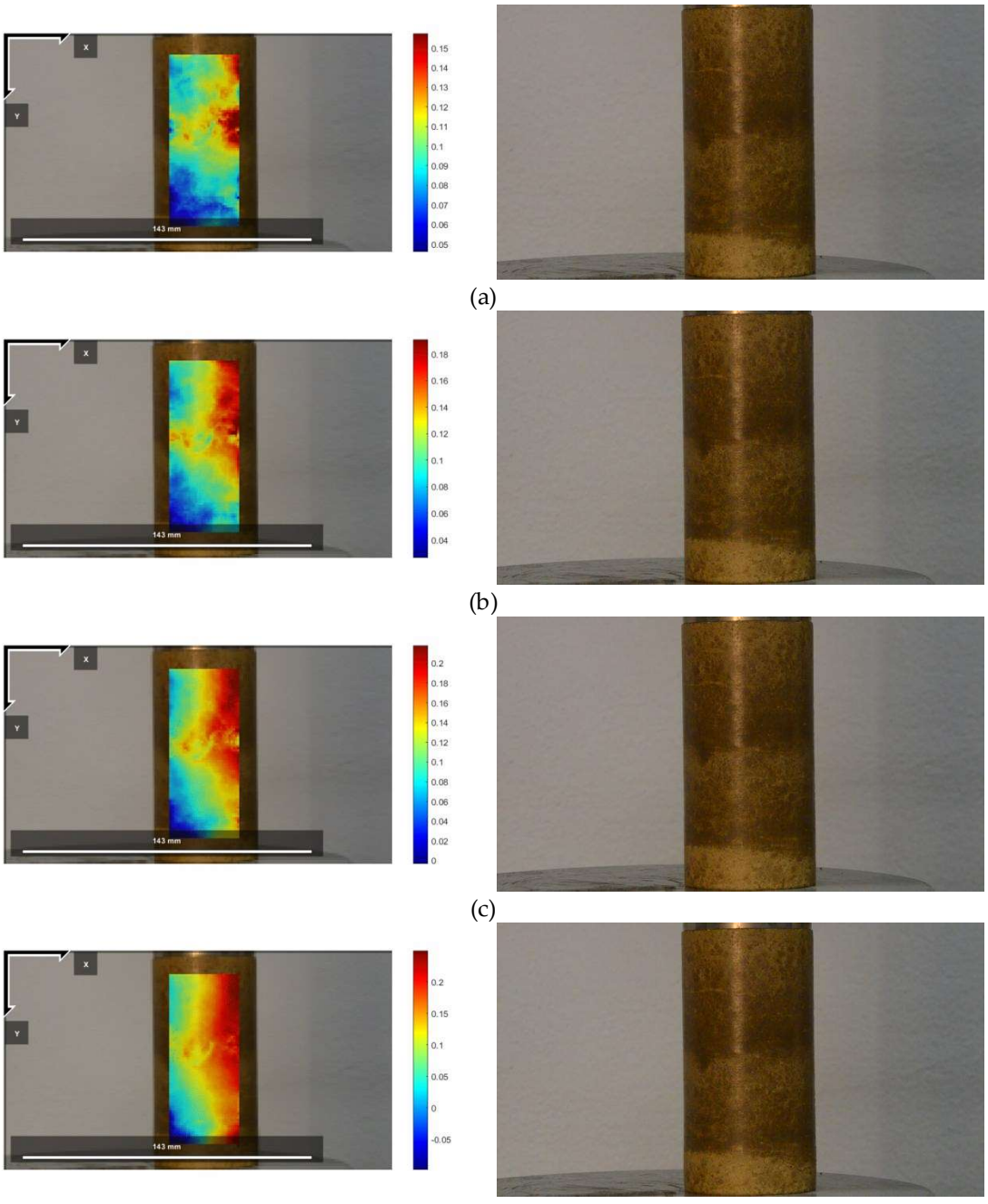

Figure 4.3. DIC Displacement in horizontal direction Sa0Si0W12E3, (a) 0.5*Strength, (b) 0.75*Strength, (c) 0.9*Strength, (d) Strength, (e) analysis points

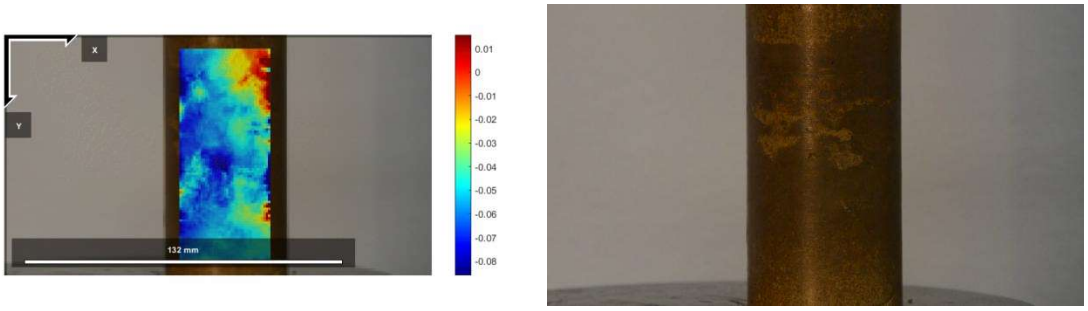

(a)

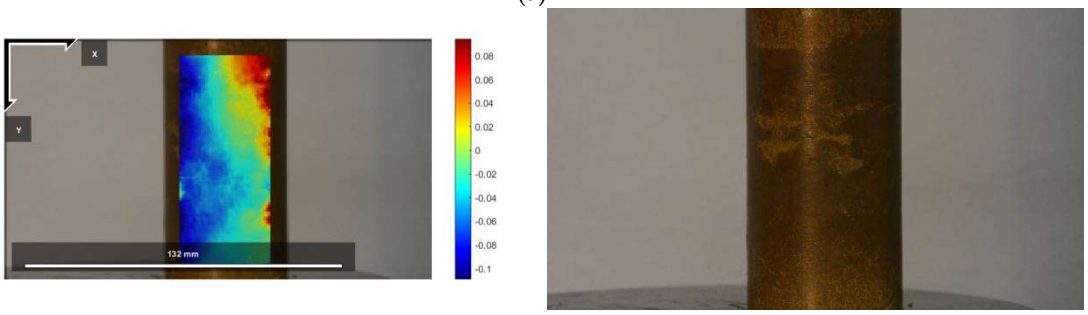

(b)

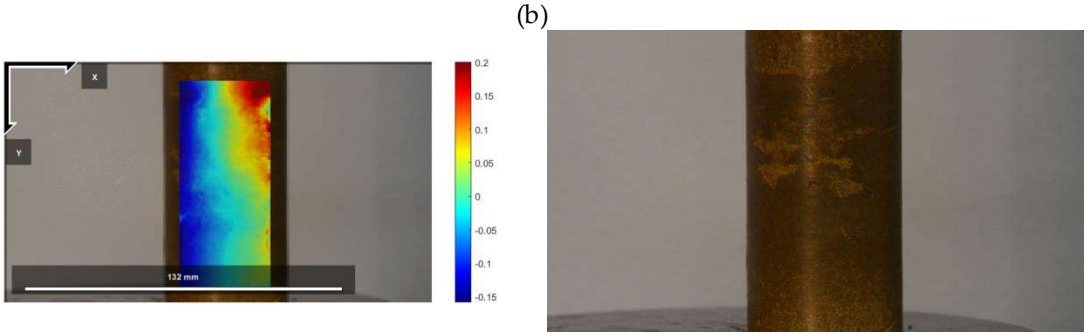

(c)

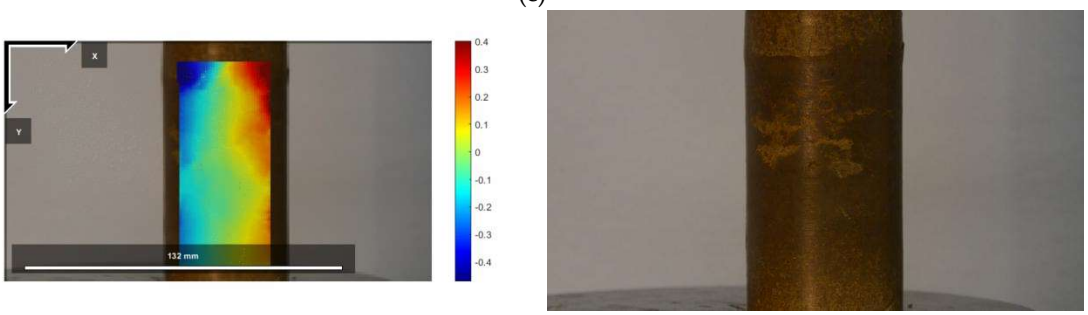

(d)

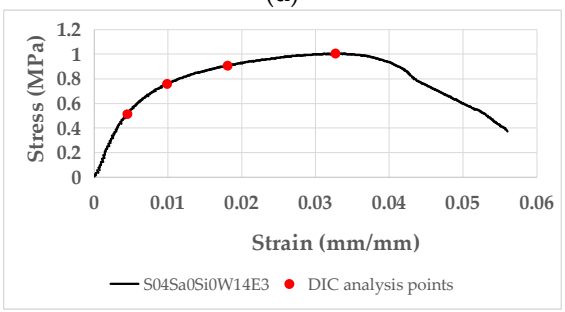

(g)

Figure 4.4. DIC Displacement in horizontal direction Sa0Si0W14E3, (a) 0.5*Strength, (b) 0.75*Strength, (c) 0.9*Strength, (d) Strength, (e) analysis points

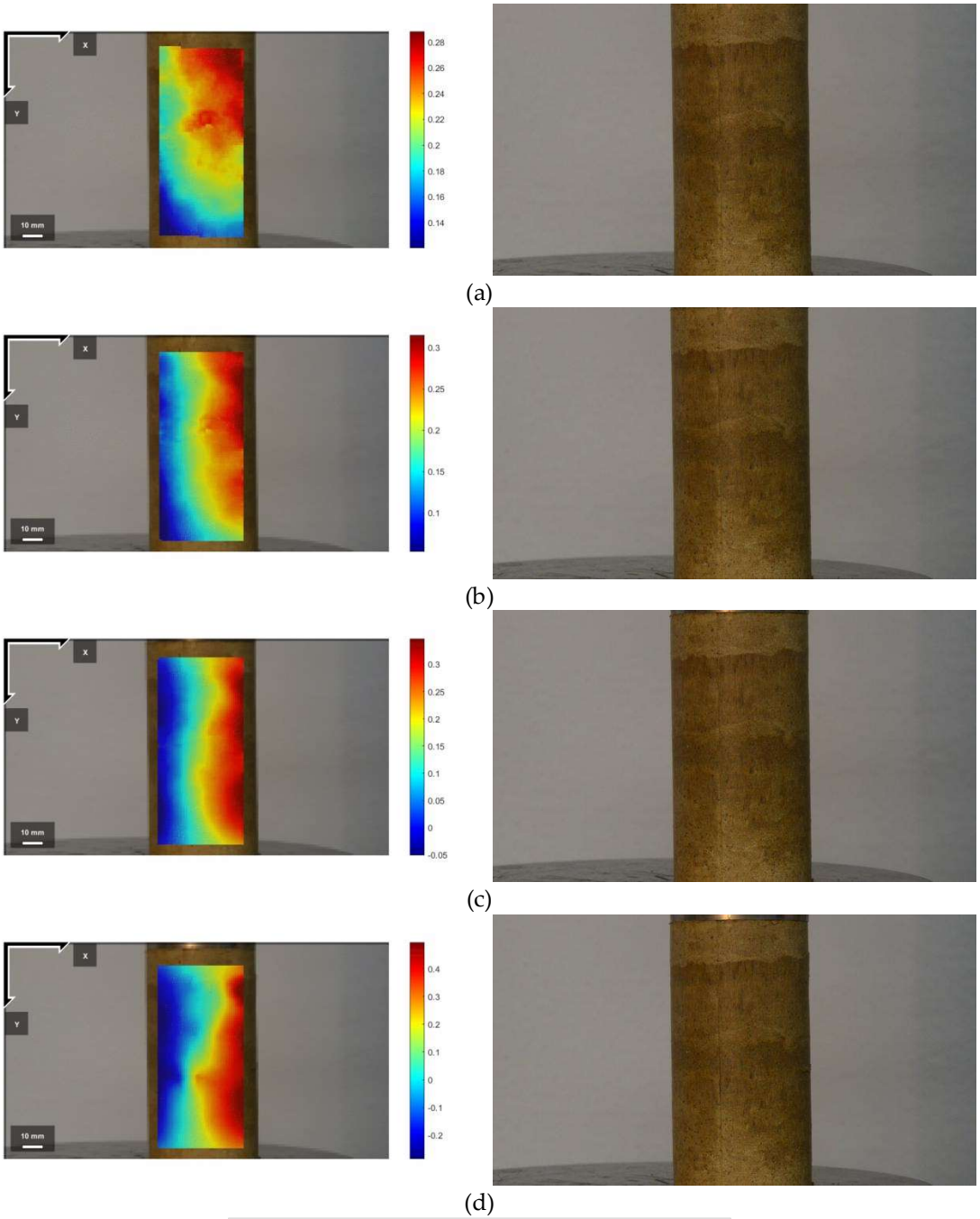

Figure 4.5. DIC Displacement in horizontal direction Sa0Si0W16E3, (a) 0.5*Strength, (b) 0.75*Strength, (c) 0.9*Strength, (d) Strength, (e) analysis points

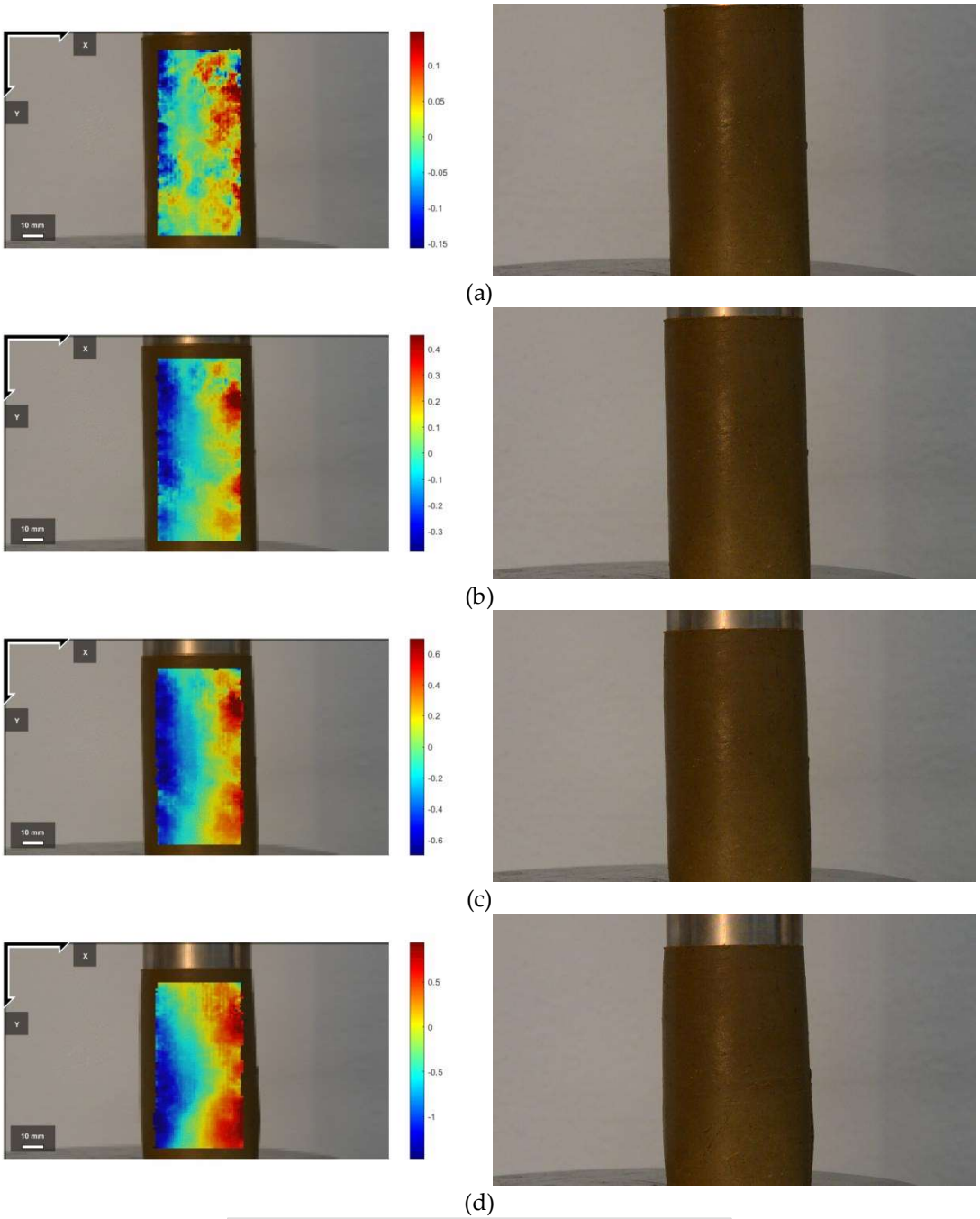

Figure 4.6. DIC Displacement in horizontal direction Sa0Si0W20E3, (a) 0.5*Strength, (b) 0.75*Strength, (c) 0.9*Strength, (d) Strength, (e) analysis points

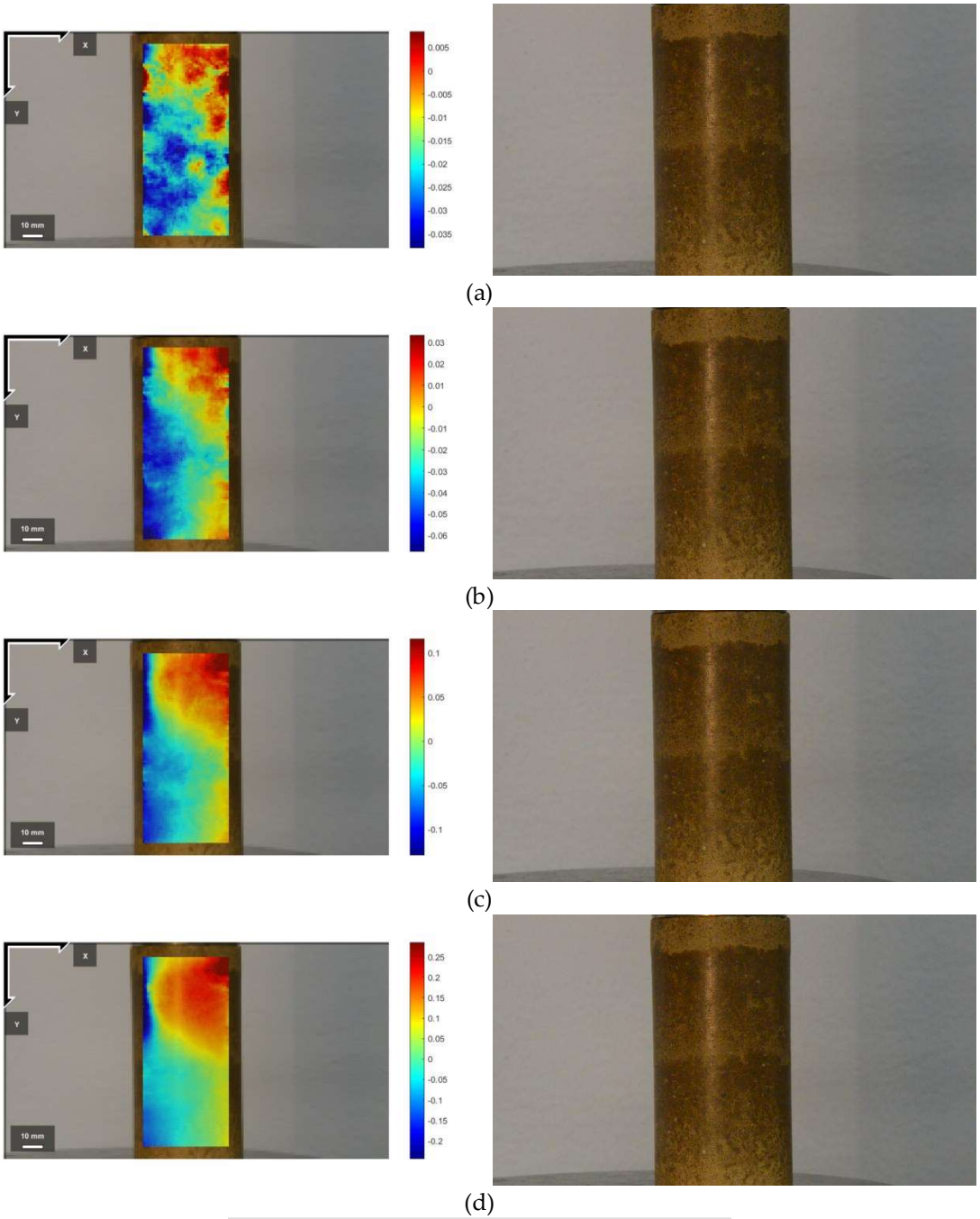

Figure 4.7. DIC Displacement in horizontal direction Sa5Si0W12E2, (a) 0.5*Strength, (b) 0.75*Strength, (c) 0.9*Strength, (d) Strength, (e) analysis points

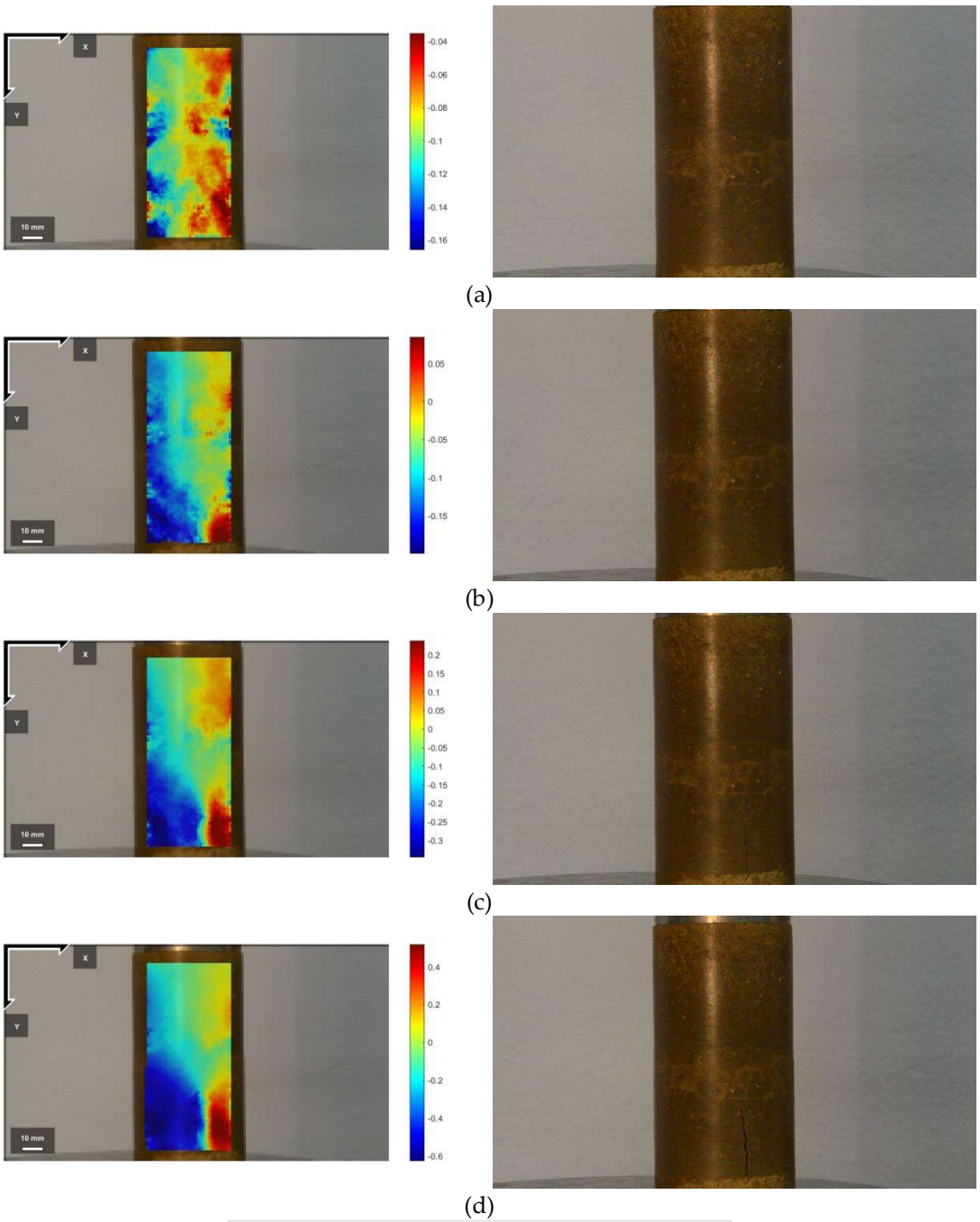

Figure 4.8. DIC Displacement in horizontal direction Sa5Si0W14E2, (a) 0.5*Strength, (b) 0.75*Strength, (c) 0.9*Strength, (d) Strength, (e) analysis points

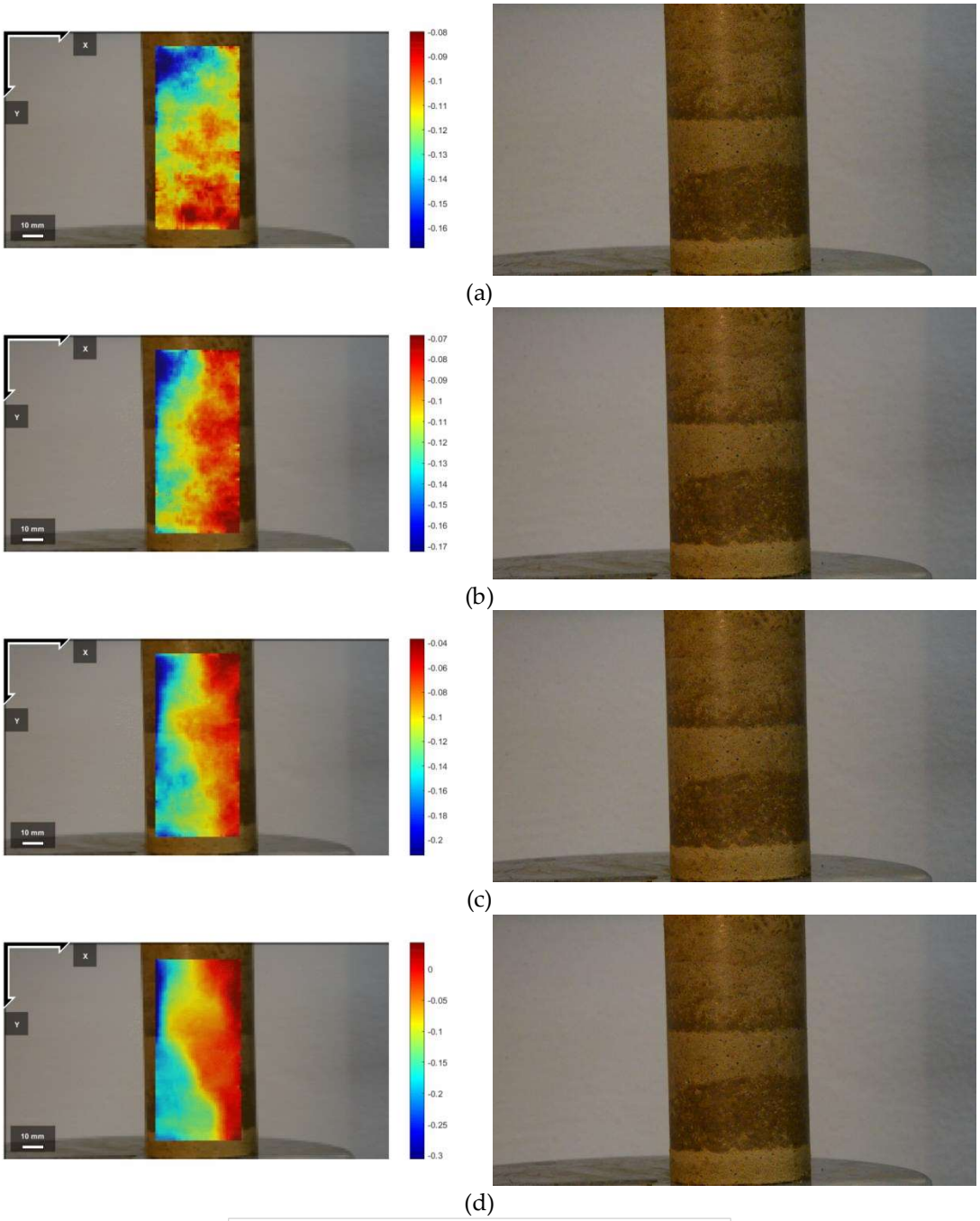

Figure 4.9. DIC Displacement in horizontal direction Sa15Si0W08E2, (a) 0.5*Strength, (b) 0.75*Strength, (c) 0.9*Strength, (d) Strength, (e) analysis points

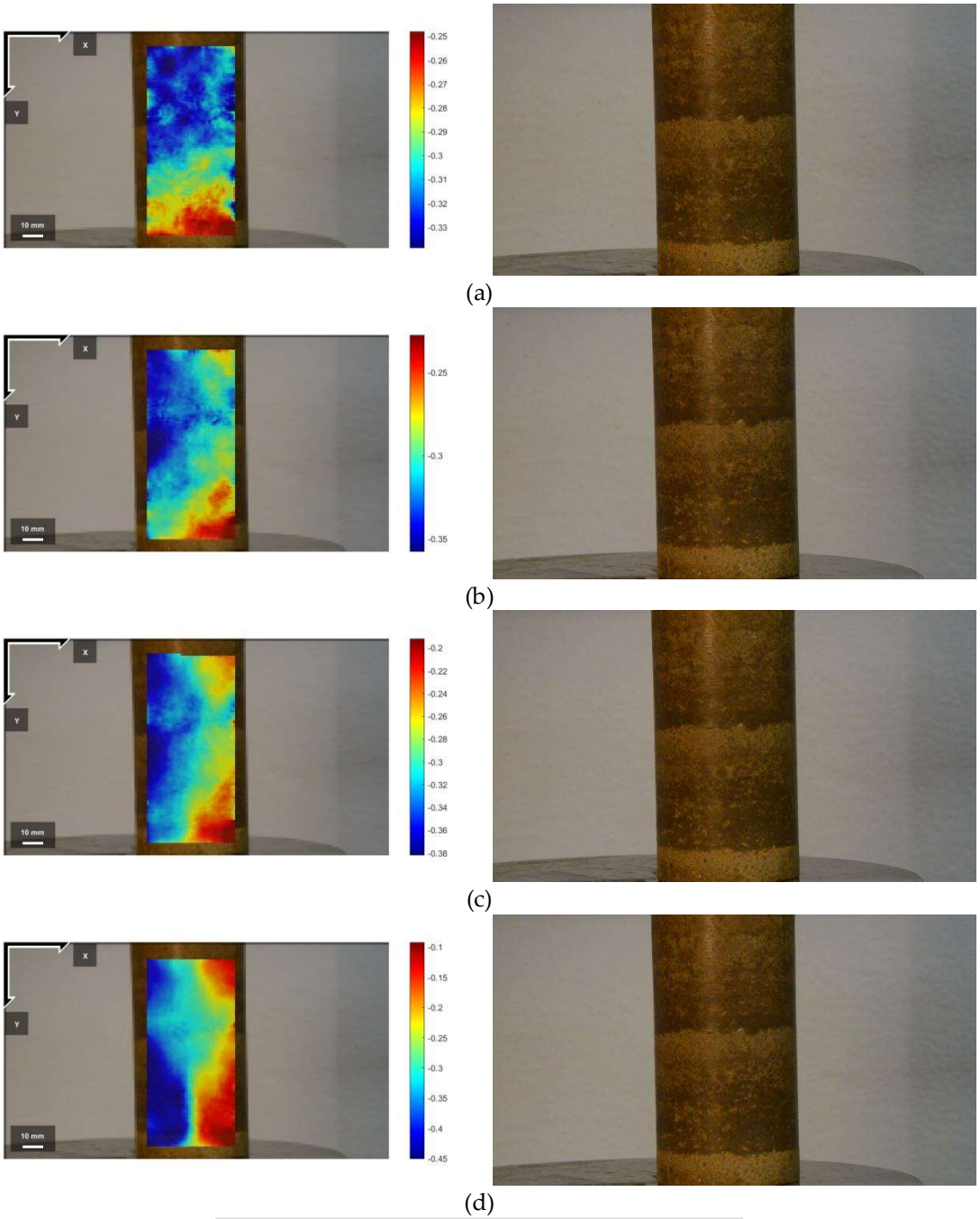

Figure 4.10. DIC Displacement in horizontal direction Sa15Si0W10E2, (a) 0.5*Strength, (b) 0.75*Strength, (c) 0.9*Strength, (d) Strength, (e) analysis points

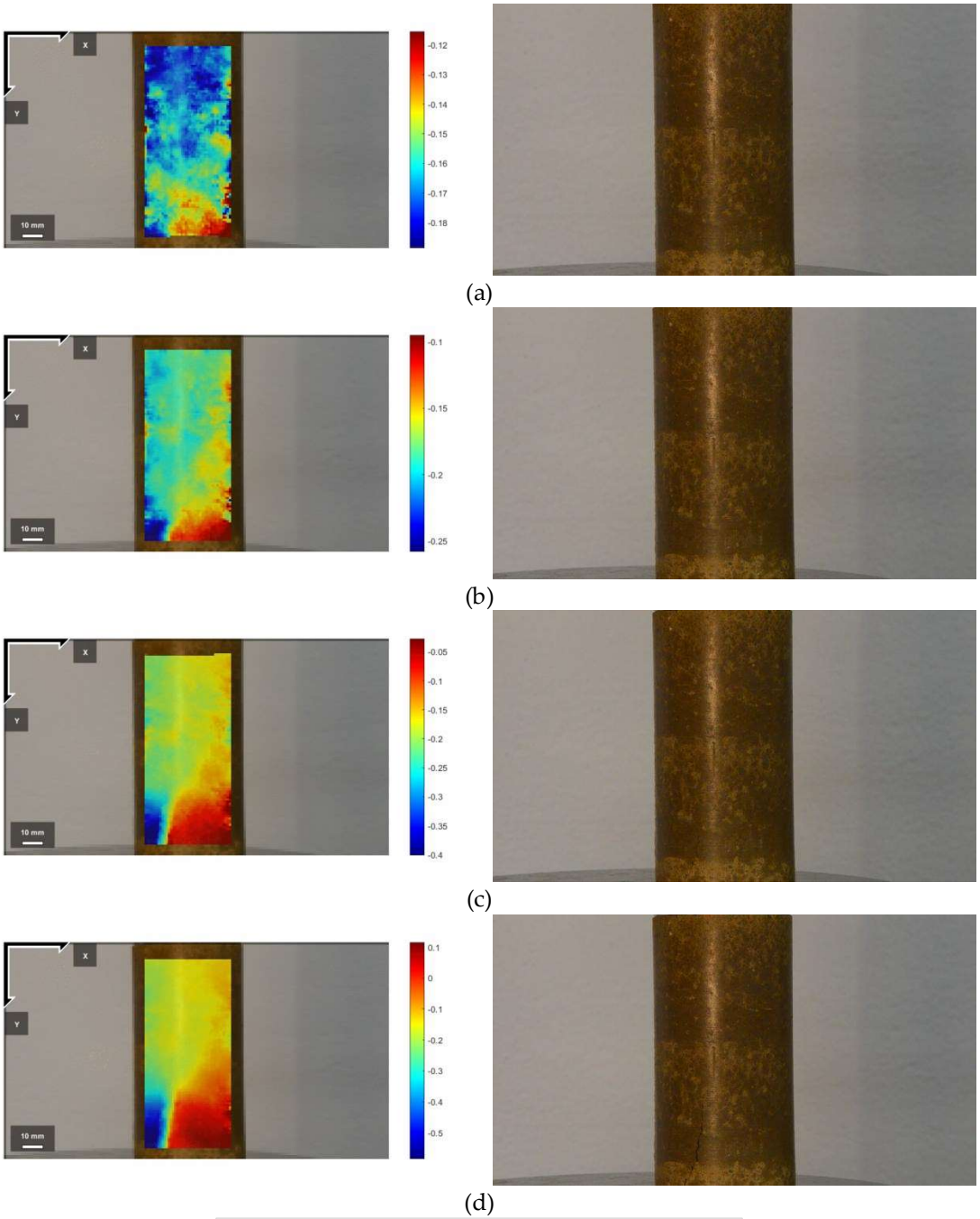

Figure 4.11. DIC Displacement in horizontal direction Sa15Si0W12E2, (a) 0.5*Strength, (b) 0.75*Strength, (c) 0.9*Strength, (d) Strength, (e) analysis points

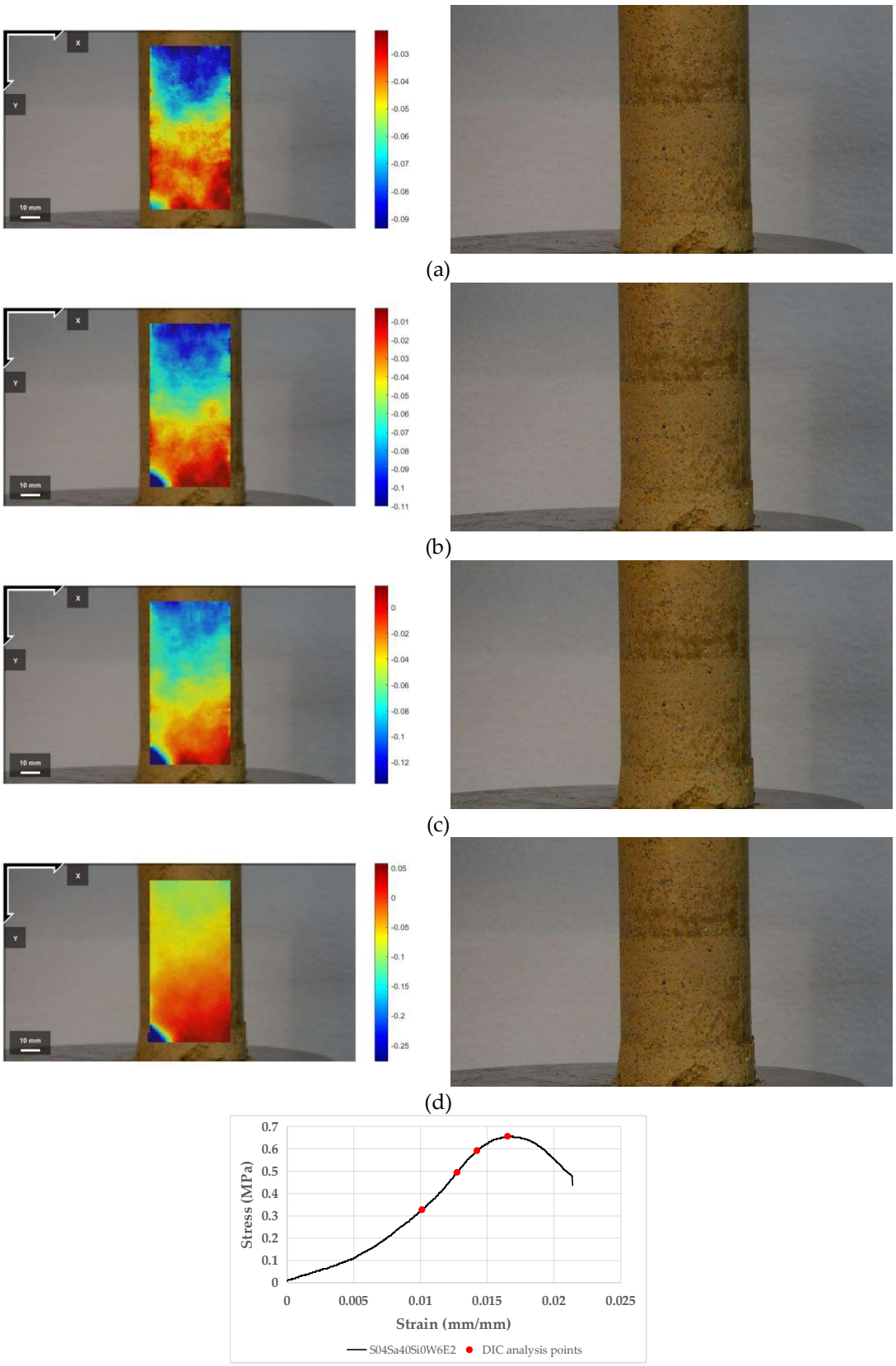

Figure 4.12. DIC Displacement in horizontal direction Sa40Si0W06E2, (a) 0.5*Strength, (b) 0.75*Strength, (c) 0.9*Strength, (d) Strength, (e) analysis points

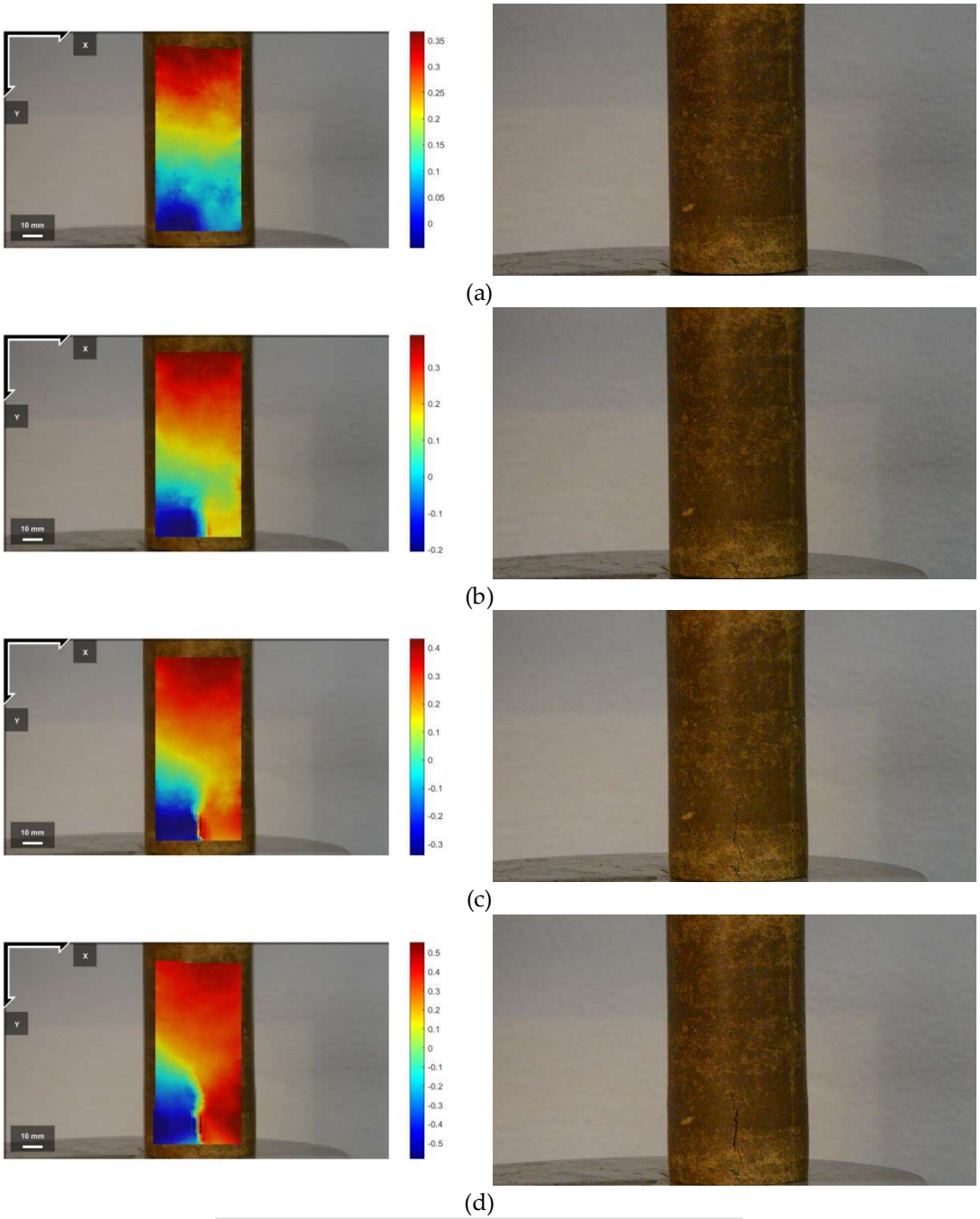

Figure 4.13. DIC Displacement in horizontal direction Sa40Si0W10E2, (a) 0.5*Strength, (b) 0.75*Strength, (c) 0.9*Strength, (d) Strength, (e) analysis points

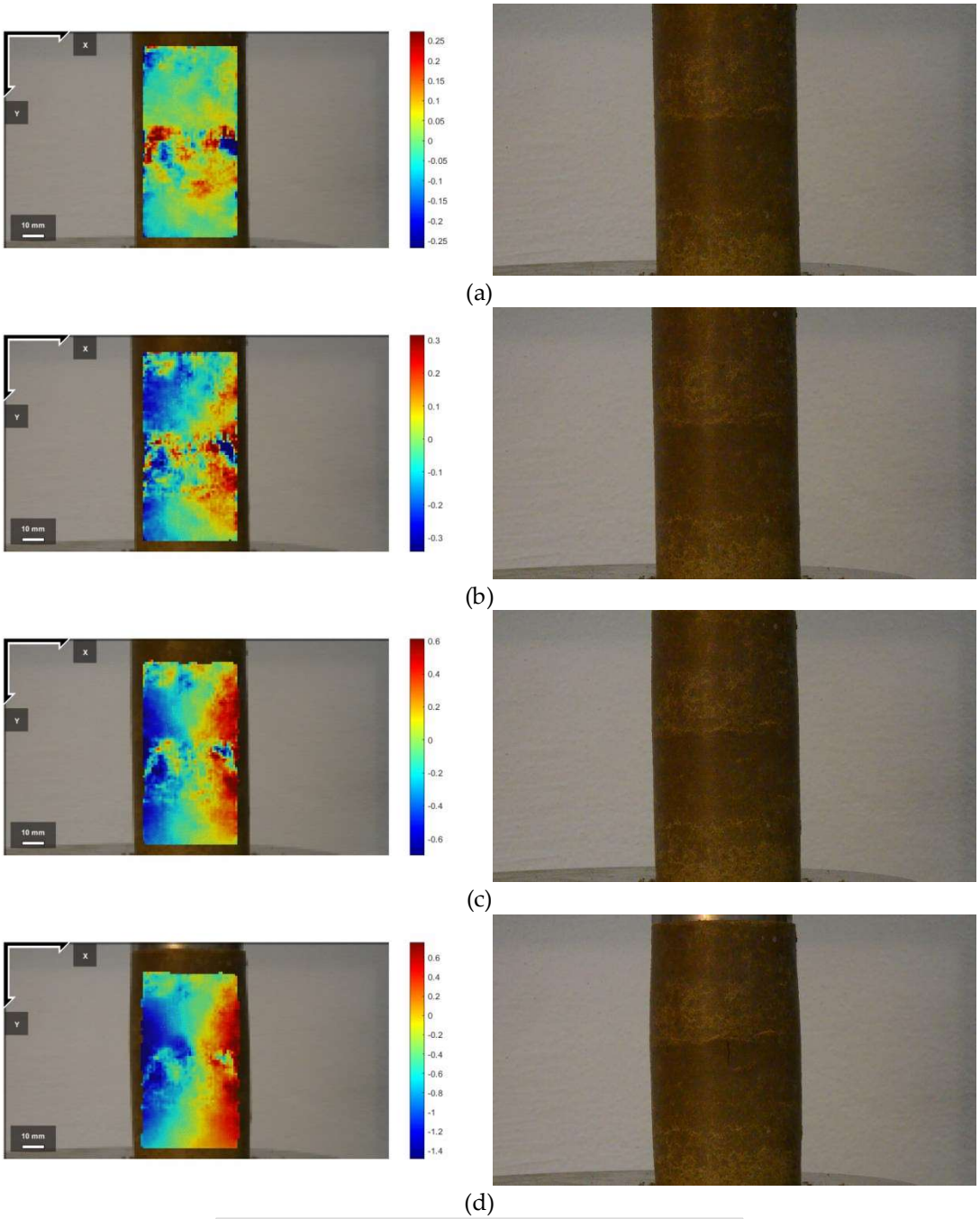

Figure 4.14. DIC Displacement in horizontal direction S02Sa0Si0W17E2, (a) 0.5*Strength, (b) 0.75*Strength, (c) 0.9*Strength, (d) Strength, (e) analysis points

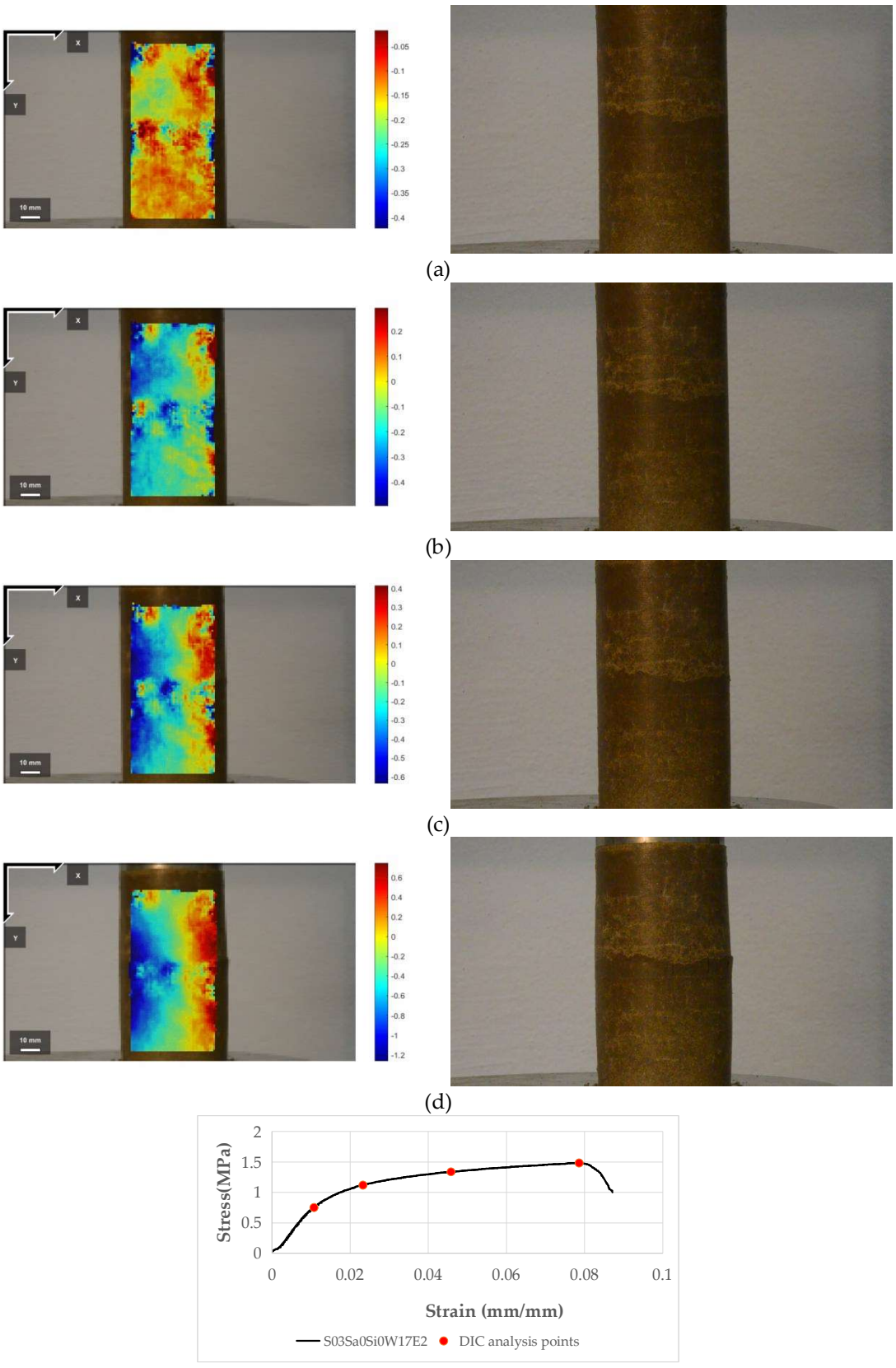

Figure 4.15. DIC Displacement in horizontal direction S03Sa0Si0W17E2, (a) 0.5*Strength, (b) 0.75*Strength, (c) 0.9*Strength, (d) Strength, (e) analysis points

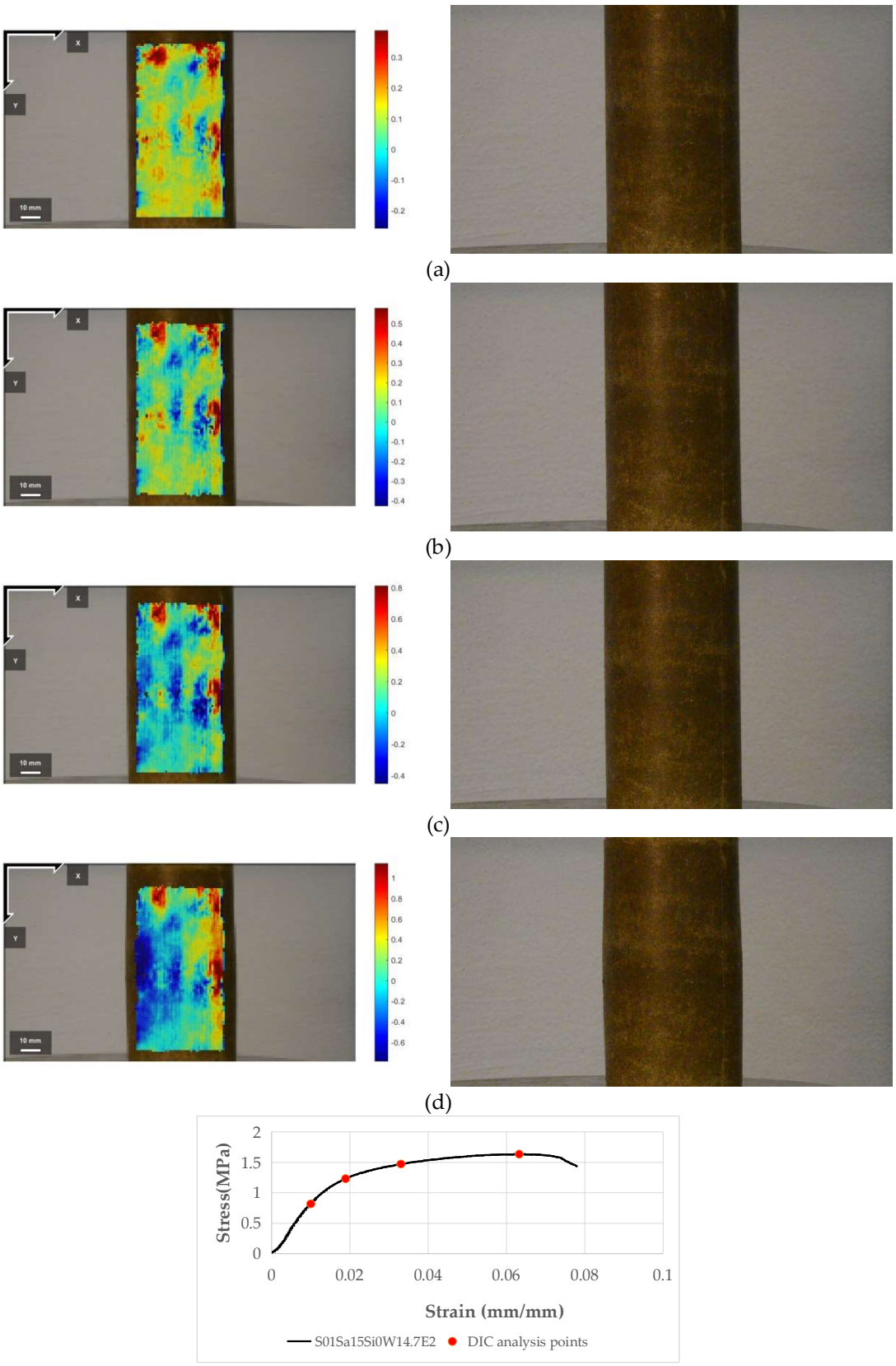

Figure 4.16. DIC Displacement in horizontal direction S01Sa15Si0W14.7E2, (a) 0.5*Strength, (b) 0.75*Strength, (c) 0.9*Strength, (d) Strength, (e) analysis points

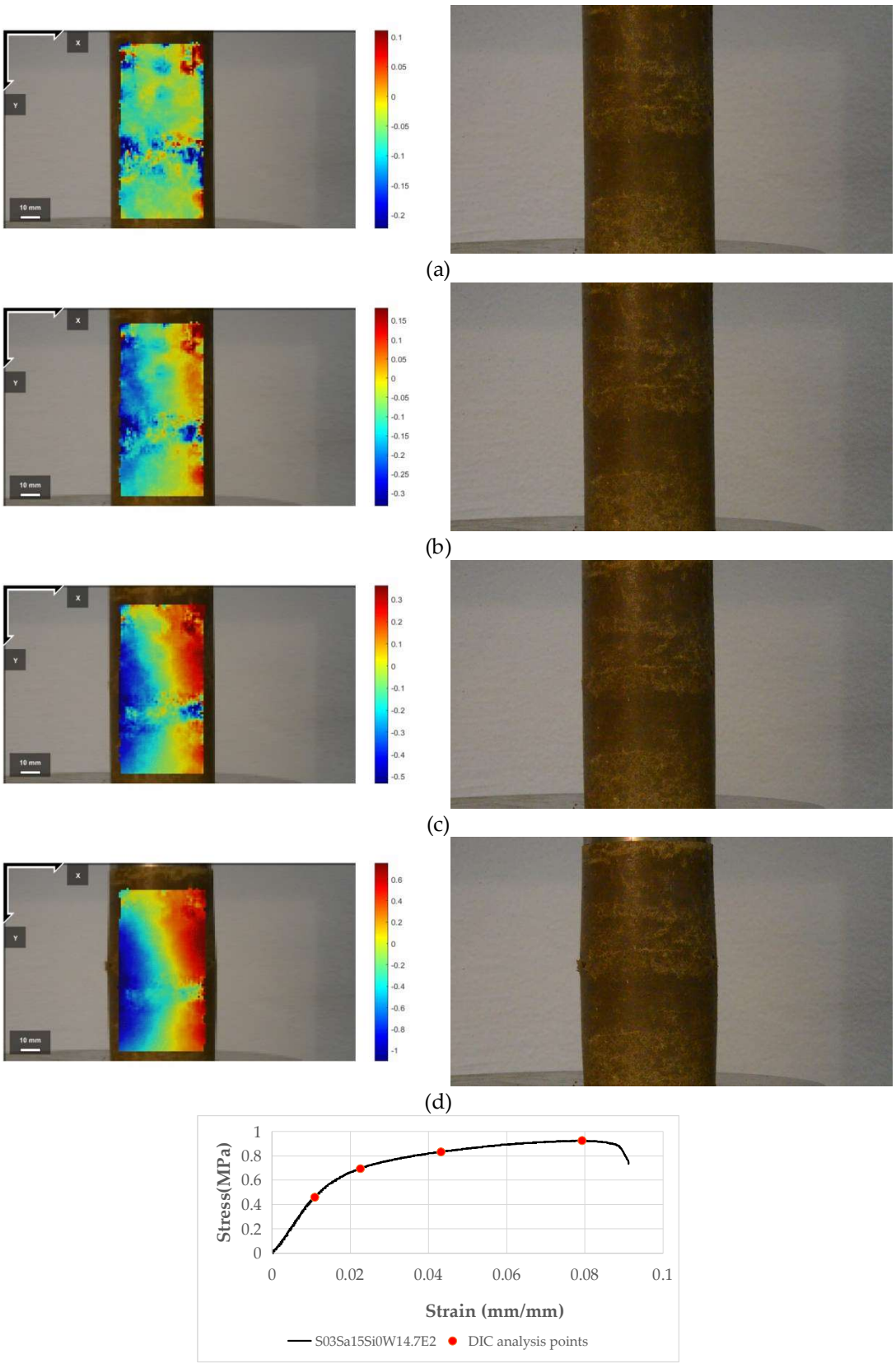

Figure 4.17. DIC Displacement in horizontal direction S03Sa15Si0W14.7E2, (a) 0.5*Strength, (b) 0.75*Strength, (c) 0.9*Strength, (d) Strength, (e) analysis points

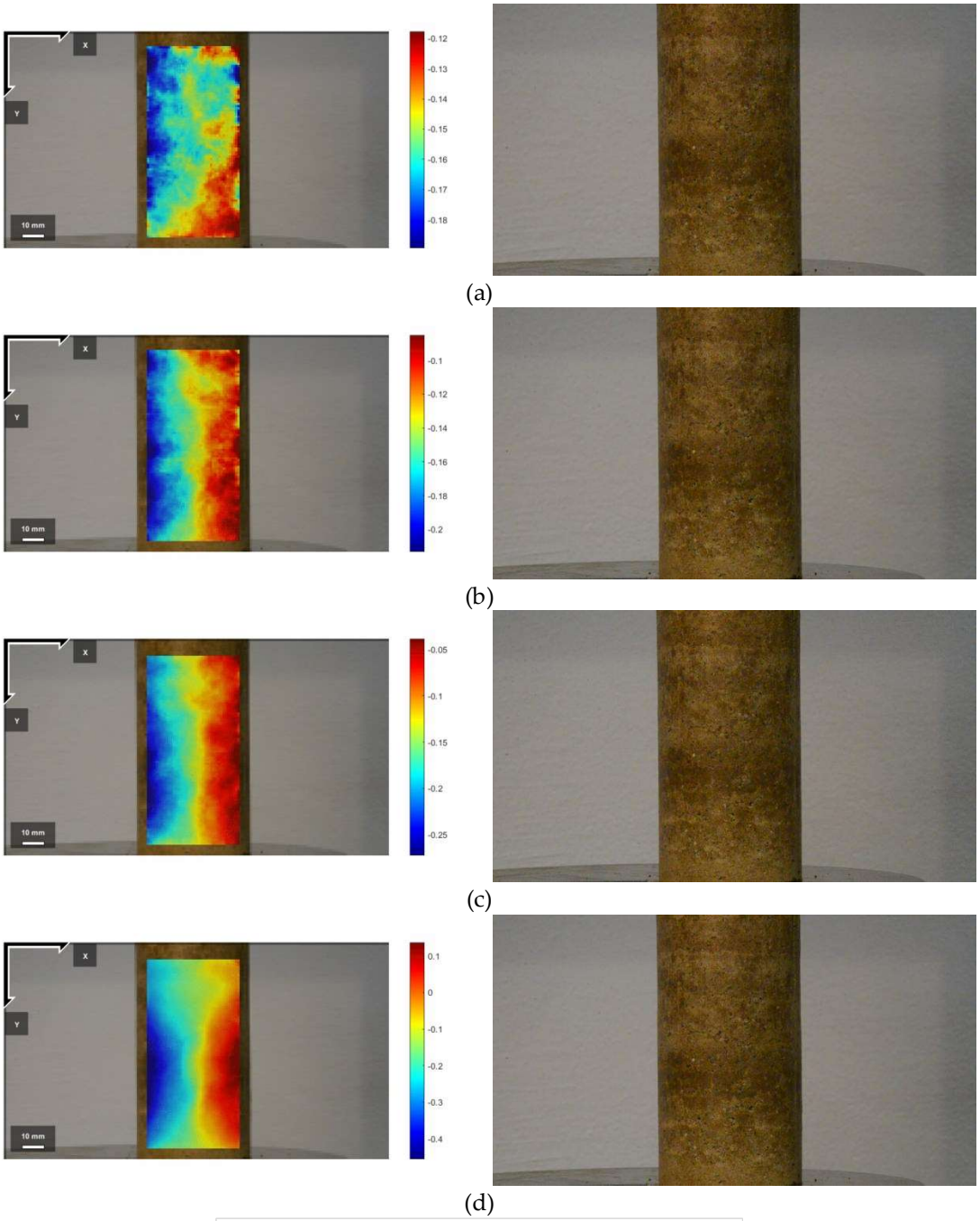

Figure 4.18. DIC Displacement in horizontal direction S01Sa40Si0W9.2E2, (a) 0.5*Strength, (b) 0.75*Strength, (c) 0.9*Strength, (d) Strength, (e) analysis points

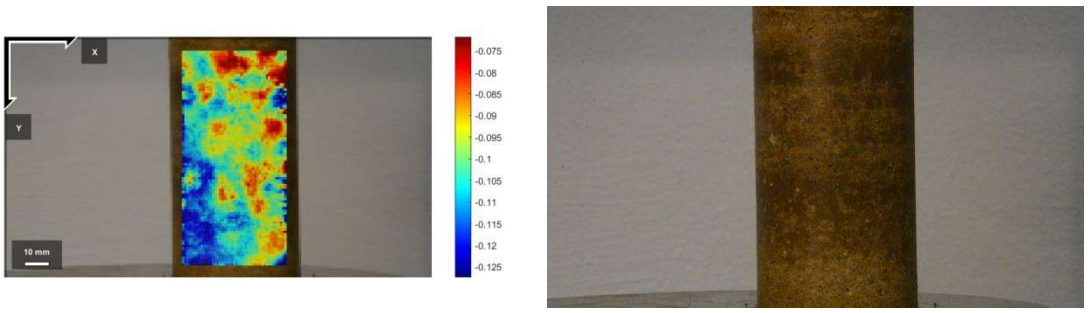

(a)

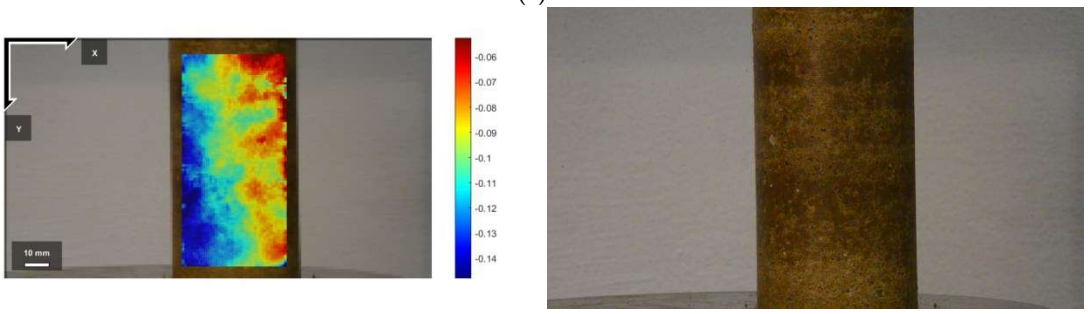

(b)

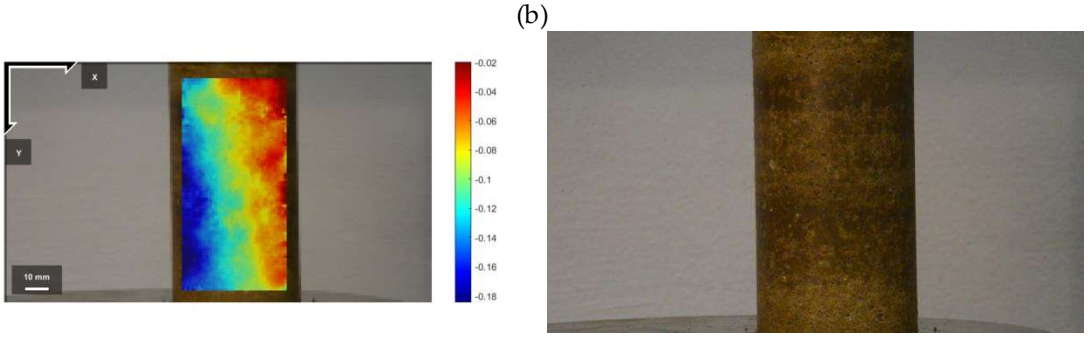

(c)

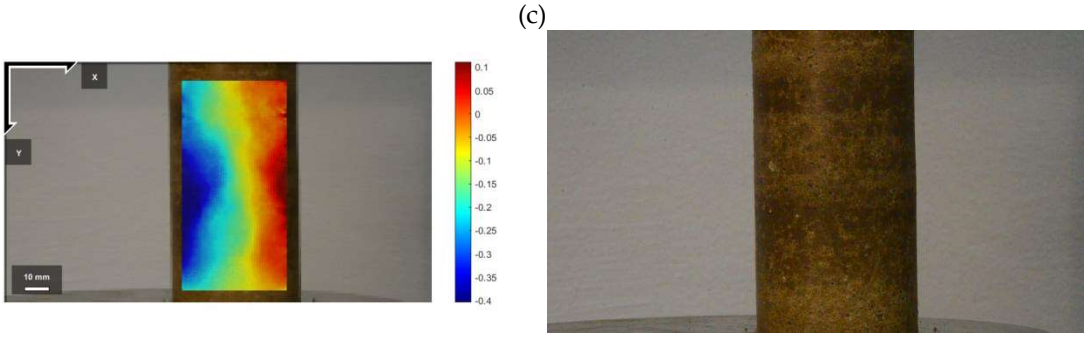

(d)

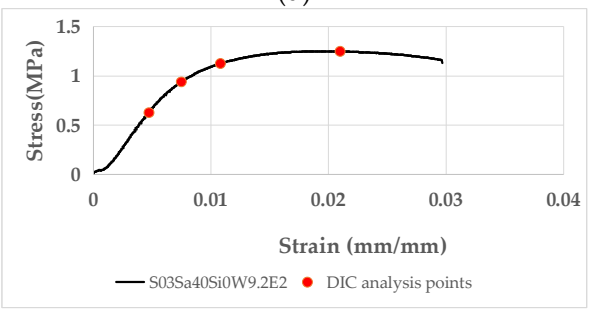

(e)

Figure 4.19. DIC Displacement in horizontal direction S03Sa40Si0W9.2E2, (a) 0.5*Strength, (b) 0.75*Strength, (c) 0.9*Strength, (d) Strength, (e) analysis points

Appendix 5

Material parameters of rammed earth specimens

	Angle of internal friction (deg)	Equivalent Young's modulus (Pa)	Equivalent Cohesion (Pa)	Density (kg/m3)	UCS (MPa)
S01Sa0Si0W20E2	28	15030000	118000	1989	0.48
S02Sa0Si0W18E2	28	36810000	118000	1901	0.40
S04Sa0Si0W14E2	28	63410000	187000	1896	0.69
S01Sa5Si0W20E2	29	8150000	82000	1931	0.32
S02Sa5Si0W18E2	29	13630000	137000	1965	0.52
S03Sa5Si0W16E2	29	34320000	198000	1995	0.74
S04Sa5Si0W14E2	29	79780000	228000	1966	0.89
S05Sa5Si0W12E2	29	115700000	230000	1876	0.89
S01Sa15Si0W16E2	32	23350000	126000	2022	0.54
S03Sa15Si0W12E2	32	69320000	187000	1981	0.74
S04Sa15Si0W10E2	32	79780000	210000	1915	0.86
S05Sa15Si0W08E2	32	83210000	210000	1836	0.86
S01Sa40Si0W12E2	34	15120000	156000	2131	0.58
S02Sa40Si0W10E2	34	31930000	180000	2153	0.87
S03Sa40Si0W8E2	34	66460000	190000	2078	0.81
S04Sa40Si0W6E2	34	38030000	135000	1919	0.66